Lecture Notes in Physics

277

Molecular Dynamics and Relaxation Phenomena in Glasses

Proceedings of a Workshop
Held at the Zentrum für interdisziplinäre Forschung
Universität Bielefeld, Bielefeld, FRG
November 11–13, 1985

Edited by Th. Dorfmüller and G. Williams

Springer-Verlag
Berlin Heidelberg New York London Paris Tokyo

Editors

Thomas Dorfmüller
Lehrstuhl für Physikalische Chemie, Universität Bielefeld
Postfach 8640, D-4800 Bielefeld 1, FRG

Graham Williams
Edward Davies Chemical Laboratories
University College of Wales, Aberystwyth, UK

ISBN 3-540-17801-5 Springer-Verlag Berlin Heidelberg New York
ISBN 0-387-17801-5 Springer-Verlag New York Berlin Heidelberg

Printing: Druckhaus Beltz, Hemsbach/Bergstr.;
Bookbinding: J. Schäffer GmbH & Co. KG., Grünstadt
2153/3140-543210

PREFACE

The "Zentrum für interdisziplinäre Forschung" of the University of Bielefeld (ZiF) is supporting a project on "Complex Liquids". Under the auspices of this project a Workshop was held 11-13 November 1985 at the ZiF which was concerned with glass-forming liquids, secondary relaxations and physical ageing. This volume is a documentation of the lectures held at this Workshop.

Although glasses are often considered to be solids rather than liquids, the limits separating glasses from both extreme states of matter is unclear, partly due to the fact that the definition of a liquid is to some extent ambiguous and vague. The reason is that the properties normally attributed to liquids may not apply to particular systems and the decision of which property is necessary to define a liquid becomes a matter of choice. Thus we usually think of a liquid as being a condensed disordered state of matter displaying a large mobility as compared to solids. In saying mobility we mean the macroscopic flow properties as well as molecular mobility, but these are, to some extent, connected. The situation becomes even more unclear if we consider molecules which are highly anisotropic in shape, such as rod-like molecules, or molecules which interact by anisotropic forces, as in the case of hydrogen bonding, or which have significant internal mobility, like macromolecules. Liquids whose properties are significantly influenced by these factors are usually termed "complex liquids".

When a liquid is cooled, molecular mobility decreases as a consequence of the decrease in the thermal energy kT. The sudden onset of crystallization at a well-defined temperature marks a cooperative process, usually involving heterogeneous nucleation in which molecular translational and rotational degrees of freedom are normally lost, leaving only vibrational degrees of freedom (inter and intra) in the crystalline solid. From the kinetic point of view the potential energy surface of a "simple" liquid near its freezing point is rather smooth, displaying localized and well-defined potential minima easily accessible by the rapid ($< 10^{-9}$s) random thermal motions of the molecules. However, for many complex liquids the situation is very different, mainly because the shape or internal conformational states of the molecules, their flexibility and/or interactions lead to complicated energy surfaces creating regions accessible only by large-scale cooperative rearrangements. Thus the crystalline state is achieved only at the expense of a very high value of the apparent Gibbs free energy of activation $\Delta G^{\neq}$. In this case the process of crystallization may be so slow that on cooling the liquid there is an eventual immobilization of non-equilibrium structures, the material "freezes" and in this sense becomes a glass below an apparent glass transition temperature T_g.

Despite its intuitive appeal, this picture is too simple in many respects. Thus, it does not differentiate between the many degrees of freedom of complex liquids. While some degrees of freedom of some molecules become immobilized by cooling a complex liquid into a glass, others may retain their mobility even below the glass temperature. The occurrence of molecular motion in the glassy state, and its variation with temperature, confers on glasses a variety of mechanical and electrical phenomena. Probing the dynamics of the material down to and below its T_g often results in the observation of several broad relaxation regions, each with its own characteristic relaxation function and temperature dependence. The glass point is characterized operationally in different ways, one being the asymptotic increase of the average relaxation time for structural relaxation (dielectric, mechanical) with decreasing temperature. Vitrification is intimately connected with the structural relaxation time becoming long with respect to normal time scales of measurement. Secondary relaxation processes observed in the glassy state are very broad and have a lower apparent activation energy than that for the structural (or α) relaxation process. One can take the view that a glass is a solid with respect to deformation or flow involving the α process. The questions of the origins of the structural relaxation and secondary relaxation processes are some of the most important in condensed matter physics and their consideration in this ZiF Workshop raises several fundamental and largely open questions in glassy-state

chemical physics. The second topic "ageing" is connected with the observation that glasses, being non-equilibrium materials, change their physical properties (e.g. electrical, mechanical) and apparent thermodynamic properties with time as they seek to achieve thermodynamic equilibrium. The conditions under which such changes are observed, their mechanism, and the implications of physical ageing for the use of glasses as industrial materials and as materials for high technology justify the focus which was placed on this phenomenon at the ZiF Workshop.

It is well known that non-crystallizable materials form glasses on cooling from the molten (or liquid) state to below T_g. Examples are inorganics such as borosilicate glasses, polymers such as atactic polystyrene and liquids composed of flexible molecules such as di-n-butyl phthalate. However, glasses may be formed from crystallizable materials such as stereoregular polymers, metallic solutions and even simple organic liquids such as cyclohexane if the cooling from the molten state is sufficiently rapid. Also rotator-phase molecular crystals and nematic, smectic and cholesteric liquid crystals form "glasses" when they are quenched rapidly from the melt to below their effective T_g. In all cases, irrespective of the chemical structure or the method of preparation, the cooperative long-range diffusional and reorientational motions of molecules or atoms (for metallic glasses) are effectively frozen-in in the glass with respect to normal time scales of measurement. Such glasses are in a non-equilibrium state thermodynamically and also possess a memory of the thermal/temporal path used for their preparation. These features ensure that glasses exhibit unusual properties, such as physical ageing, and present the experimentalist and theorist alike with a wide variety of phenomena for study, interpretation and application. In recent years substantial advances have been made with regard to the fundamental properties of glass-forming materials. Some of these are presented in this volume which gives the papers presented at the ZiF Workshop. Systems of very different chemical structures are investigated using a variety of equilibrium and thermodynamic methods. These studies are complementary and will be of interest not only to scientists concerned with the fundamental properties of glass-forming materials but also to applied scientists, chemists, physicists, theorists, electrical, optical and mechanical engineers, materials scientists, polymer scientists and glass technologists, who have an interest in the amorphous state, relaxation phenomena, and mechanical optical and electrical properties of solids. The new research described here will be of interest to scientists concerned with modern applications of organic and inorganic glasses in optics and electronics, as optical fibres and semi-conducting materials, and as special components in optical devices, where the understanding of the physical properties and the control of the physical state of the material is essential for their application.

Experimental studies of the electrical, dielectric, mechanical and NMR properties of glass-forming materials both above and below T_g have shown that the relaxation behaviour cannot be described by a single decay rate. The relaxations appear to obey an empirical "stretched-exponential" function known as the Kohlrausch-Williams-Watts empirical relaxation function. This equation gives a very satisfactory representation of the dielectric, mechanical and NMR relaxations of a variety of systems studied under isothermal conditions both above T_g and in the glass-transition region. This success has led to its further application to non-linear behaviour and to non-isothermal experiments, as occur for example in volume relaxation in the glass-transition region and for materials cycled in that region. The success of these applications of the KWW function has prompted many recent theoretical studies which seek to provide a mechanistic or molecular basis for this function for relaxation in the glass-transition region. In addition it is found that molecular motions occur at a local level in the glassy state and that these may be investigated by dielectric, electrical, mechanical, NMR and optical relaxation methods. Again there is much interest in establishing a mechanistic or molecular basis for local motions which would satisfy the experimental results. The lectures presented at this Workshop give new experimental data in these areas and seek unified interpretations of the behaviour. The various model theories which lead to KWW behaviour are discussed by Blumen, while molecular mobility and volume relaxation and enthalpy relaxation in the glass transition region are formulated in the papers by Kovacs and Hutchinson in terms of double box distributions of relaxation times. These authors show how their KAHR model is able to account for all the features of volume relaxation data and of the complicated curves obtained in differential scanning calorimetry experiments when materials are subjected to dif-

ferent thermal histories. Thermodynamic recovery phenomena, structural relaxation and volume relaxation in the glass-transition region are described by Matsuoka, and the Adam-Gibbs theory, which relates structural relaxation to configurational entropy, is shown to provide an improved basis for the rationalization of the experimental data (c.f. Kovacs and Hutchinson). The α and β relaxations in polyalkyl methacrylates and their complementarity in forming the merged $\alpha\beta$ process, as observed by photon correlation spectroscopy, is outlined by Meier who has also shown how the distribution function for optical relaxation times may be determined from data covering a very wide range of time ($\sim 10^7$s). It is shown that NMR methods provide detailed information on molecular motion in the glassy state of amorphous polymers (Monnerie) and of simple small molecule glasses (Rössler), while Raman spectroscopy is used by Dorfmüller to characterize phenyl-ring mobility in polystyrene. Johari shows that localized motions of groups of atoms or molecules are generally observed, using dielectric and mechanical relaxation spectroscopy, in the glassy state formed by liquids, liquid crystals and molecular rotator-phase crystals, and he makes it clear how the dynamic disorder in the glass is related to the thermodynamic behaviour, to physical ageing and to densification.

The classic mechanical relaxation data of Heijboer for glassy polymers containing cyclohexyl groups in the side chains are re-examined by Struik. He shows that the two-site model previously used to explain the data only partially agrees with experiment and a new model is proposed which involves a coupling of the cyclohexyl group to its glassy environment and which correctly describes the experimental data and explains the paradox that strong coupling is not in contradiction with the data, i.e. the activation parameters are almost independent of the environment of the ring. Dynamic mechanical and creep relaxation data for polymethyl methacrylate are presented by Read in a study which covers fourteen decades of frequency. He demonstrates that the β relaxation in this polymer does not obey time-temperature superposition and also shows how the α and β processes are involved in the room-temperature creep relaxation and in physical ageing of this polymer.

Inorganic glasses are considered in the lectures of Moynihan and of Angell. Structural (enthalpic) relaxation of ZrF_4-based glasses used in new optical fibres is described by Moynihan who shows that structural relaxation effects will be small over periods of tens of years for these glasses when suitably prepared. Primary and secondary relaxations (electrical and mechanical) for a fast-cation conductor and for a fast-anion conductor in their glassy states are described by Angell and the forms of the frequency functions are compared and discussed for data covering exceptionally wide ranges of frequency and temperature. Finally, Woodcock describes a large scale numerical simulation of the thermodynamic properties and flow behaviour of model liquids composed of hard or soft spheres, and all the usual non-Newtonian flow phenomena such as dilatancy, shear thickening and thinning, structural ordering, shear flocculation, normal pressure effects and time-dependent viscoelasticity are shown to arise, dependent on the parameters of the model and the packing density.

A feature of these lectures is that they are all complementary and seek unifying interpretations which may apply to all glass-forming materials. Thus a scientist primarily concerned with relaxation phenomena in inorganic glasses will find similar analyses being made for polymer glasses and vice versa, suggesting that common interpretations apply (Occam's razor). Also many new results are presented and modern interpretations are applied which represent state-of-the-art knowledge about the unusual physical properties of these chemically diverse glass-forming materials. This volume should be of interest to specialists in the subject, to polymer scientists, glass technologists and materials scientists, and, most importantly, to research scientists and teachers who wish to be informed about some of the most recent fundamental research on glass-forming materials.

In preparing this volume for publication, we wish to express our gratitude to the ZiF of the University of Bielefeld for providing the financial support for the project on "Complex Liquids". We are grateful to the staff of the ZiF, in particular to Ms. Hoffmann who expertly handled the organization of the meeting. We are also very pleased to acknowledge the expert assistance of Mrs. L. Jegerlehner in the preparation of this volume and for her excellent typing of the manuscript.

Bielefeld, January 1987

Thomas Dorfmüller
Graham Williams

CONTENTS

MODELS FOR DYNAMICS OF RELAXATION IN GLASSES

A. Blumen
Max-Planck Institut für Polymerforschung, D-6500 Mainz
and
Physikalisches Institut der Universität
D-8580 Bayreuth, FRG

Summary

Wide classes of disordered materials display relaxations which cannot be expressed in terms of a single decay rate. The analysis of experimental data often leads to the Kohlrausch-Williams-Watts stretched exponential $\exp[-(t/\tau)^{\beta}]$ or to algebraic time dependences C/t^{γ}. In this article, we show how such decay patterns may arise from quite different microscopic dynamics. Possible candidates for modelling disorder are (a) self-similar spatial distributions of sites (fractal geometries), (b) distributions of waiting times and (c) self-similar distributions of energy barriers (ultrametric spaces). For each of these models one may obtain under certain conditions stretched exponential or algebraic decays, although the microscopic relaxation dynamics differ in every case.

1. Introduction

In recent years, the theory of the glassy state has seen an upsurge of interest in the stretched exponential form:

$$\Phi(t) = \exp[-(t/\tau)^{\beta}] \qquad (0 < \beta < 1). \qquad (1)$$

This form has been discussed by Williams and Watts in the framework of dielectric relaxation [1,2], but it also was suggested by earlier works such as Kohlrausch's [3] which were concerned with dynamical processes in complex materials with slow relaxations. The Kohlrausch-Williams-Watts (KWW) function seems to be of quite common occurrence, as witnessed by the large number of materials which display it [3-5]. As examples, the KWW-form has been used with much success in fitting dielectric [1], NMR [6] and dynamical light-scattering data [7-9]. The KWW-expression was observed in measurements of optical bleaching of the reversible transformation of spiropyran into merocyanine in a polymer matrix [10]. The same form also appears in the abstraction of hydrogen atoms from glassy matrices [11].

One should stress, however, that Eq. (1) is only one of a whole class of relaxation patterns which show non-Debye (nonexponential) decay behavior. Other patterns of slow decay at long times are given by exponential logarithmic dependences:

$$\Phi(t) = \exp[-\gamma \ell n^{\delta} (t/\tau)] \tag{2}$$

valid for $t > \tau$.

Special cases of Eq. (2) are of quite common occurrence. Thus electron transfer rates in glasses, measured by pulsed radiolysis and optical detection [12,13], could be fitted to Eq. (2), with $\delta = 3$. For small values of γ in Eq. (2), the exponential may be expanded in a series, and yields as first terms:

$$\Phi(t) \simeq 1 - \gamma \ell n^{\delta} (t/\tau) \ . \tag{3}$$

The recovery after hole-burning of quinizarin embedded in ethanol-methanol glass follows a logarithmic pattern with $\delta = 1$, as determined by Friedrich and Haarer [14].

For small γ the domain of validity of Eq. (3) may be very wide, as discussed in Ref. [15]. For general γ and $\delta = 1$, Eq. (2) reverts to the algebraic behavior:

$$\Phi(t) = \exp[-\gamma \ell n(t/\tau)] = (t/\tau)^{-\gamma} \ . \tag{4}$$

Both Eq. (2) and Eq. (4) make sense only at longer times, say $t > \tau$. Forms related to Eq. (4) have been reported for the relaxation of photogenerated carriers in amorphous Si:H [16] and in carrier diffusion through xerographic films [17,18].

In this work we will concentrate mostly on the KWW-form, Eq. (1), and we will show how several dynamical models lead to it. Recent investigations suggested a dichotomy between parallel and sequential channels in the explanation of nonexponential relaxations [19]. In former works, summarized in Ref. [20], we have shown how KWW-forms may arise from parallel schemes; these contain centers, which are independent of each other and which, due to fluctuations in the local environments, relax on widely distinct time-scales. Here we center on random-walk models of mixed (parallel and sequential) type, whose relaxation is of KWW-form. Of interest is the finding that models of very different microscopic dynamics lead to strikingly similar decay patters. A fact which appears to be basic to our investigations is that our models must involve some disorder facet in order to lead to the KWW-form. Such a facet may be structural, temporal or energetic. In this presentation, we will use fractals to model the structural disorder [21,22], continuous-time random-walks (CTRW) for the temporal disorder [17,18,23] and ultrametric spaces for the energetic disorder [24,25]. In so doing we will follow the main lines of our more extensive analysis [26,27] which were concerned with chemical kinetics in the presence of randomness.

2. Dynamical Models

Models of the glassy state may be related to features pertaining to thermodynamics and to stochastic processes. Arguments in favour of the thermodynamic picture have been pertinently summarized by DiMarzio in his review of the equilibrium theory of glasses [28]. The drawback of such descriptions is that glasses are inherently not in equilibrium and may be far from it, so that extensions of ideas based on thermodynamics of homogeneous systems to disordered, metastable objects soon become very hard to control. On the other hand, descriptions of glasses on a purely microscopic level demand molecular-dynamics (MD) computations, which soon get quite complex [29-31]. As a compromise between these extremes one can investigate simplified stochastic models in which certain aspects of the disordered-glassy state are built-in. Then the analysis may be pushed quite far without having to fulfill the numerical demands of MD-computations, while being able to assess the importance of specific disorder types one-by-one.

Such a stochastic model was proposed by Glarum [32]. The main feature of the model is that a component of the structure (spin, dipole, side-chain) may relax when another component (mostly a so-called "free-volume") passes-by. The model combines thus a dynamical ingredient (the random-walk of the free volume) with a parallel component (namely the ensemble average over all the relaxing centers). In its approach the Glarum model is thus of reaction-diffusion type and is related to chemical models in which the species react only at short distances, so that for an elementary reaction to occur it is necessary that the reactants first get together. Extensions of the Glarum model in the CTRW framework have been worked out by Shlesinger, Montroll and Bendler [33,34].

At this point, we should stress that disorder is fundamental in obtaining the KWW stretched exponential, Eq. (1) and the general algebraic decay, Eq. (4). The reason for this is that a simple kinetic scheme is unable to give these expressions. Viewing namely the relaxation as corresponding to the reaction:

$$A + B \xrightarrow{k} 0 \tag{5}$$

one readily obtains the solution of the corresponding kinetic equation. The time development $A(t)$ of the A-species is given in implicit form [26] through:

$$[1 + C/A(t)]/[1 + C/A_0] = \exp(Ckt). \tag{6}$$

Here $A_0 \equiv A(0)$ and $B_0 \equiv B(0)$ are the initial number of molecules, and $C = B_0 - A_0$. If one of the species is in excess, say $B_0 >> A_0$, then the reaction has pseudounimolecular character, and:

$$A(t) \approx A_0 \exp[-B_0 kt] \ . \tag{7}$$

On the other hand, if the number of particles is equal at start $A_0 = B_0$, then it stays equal throughout the reaction, and one has at longer times:

$$A(t) = B(t) \sim 1/kt \ . \tag{8}$$

Hence the kinetic reaction scheme leads only to the very special cases $\beta = 1$ in Eq. (1) and $\gamma = 1$ in Eq. (4).

To obtain more general expressions, with $\beta \neq 1$ and $\gamma \neq 1$, one has to take disorder aspects into account. As pointed out in Ref. [26], the failure of the kinetic scheme is due to the implicit assumption of a "well-stirred reactor", so that the particle distribution is taken as being homogeneous throughout the sample at all times.

Nonhomogeneities are best seen when the underlying space over which the motion of the particles takes place is already discrete. We will therefore model the dynamics through random walks over discrete structures.

3. Target Annihilation and Trapping

Let therefore two types of particles A (the relaxing center) and B (say, the free volume) perform a random-walk motion over preassigned, discrete geometries. In the pseudounimolecular scheme the number of A-particles is considerably less than that of the B, so that one may consider a single A-center immersed in a swarm of B-particles. For simplicity, we furthermore take the A-particle to relax instantaneously and completely at the first encounter of a B (this is the so-called first-passage approximation).

We may distinguish between the models, depending on which of the species performs the motion. If only the A move whereas the B are static, one speaks of the trapping-model [35-37]; in the opposite case, when the B move and the A play the role of immobile targets, one has the target annihilation problem [33,38,39]. The relaxation of the A-centers is evaluated by ensemble averaging the corresponding decay behavior over all possible particle distributions and motions.

Interestingly, as we have recently demonstrated, the target annihilation problem admits an exact solution for walks performed on regular (translationally invariant) lattices [39]. The solution is valid for lattices in spaces of arbitrary dimensions and involves S_n, the mean number of distinct sites visited in n-steps. Thus, in the target problem the dependence on dimensionality enters through S_n. As a reminder, for not-too-small n one has for nearest-neighbor-random walks:

$$S_n \sim \begin{cases} \sqrt{n} & d = 1 \\ n/\ell n(n) & d = 2 \\ n & d \geq 3 \end{cases} \quad . \tag{9}$$

The simplest form for the relaxation in the target annihilation problem obtains for B-particles which were initially Poisson-distributed on the lattice, and which move independently of each other. The ensemble averaged relaxation pattern has then the form:

$$\Phi_n = \exp[-p(S_n - 1)] \tag{10}$$

where p is the number density of B-particles. In this expression the time is given implicitly, through the number of steps. Usually one takes the steps to occur at fixed, equally-spaced time intervals, so that for all practical purposes the time and the number of steps depend linearly on each other. Inserting now Eq. (9) into Eq. (10) one finds that the target-annihilation is exponential in $d = 3$, but that it shows a KWW-form (Eq. (1)), with $\beta = 1/2$ for relaxations in $d = 1$.

Paradoxically, the relaxation in the trapping-model, in which only the A-center moves, whereas the B-particles are immobile is considerably harder to solve. Fortunately, however, for the glassy state the trapping-model is physically less realistic than the target-annihilation. The situation is different in the energy and carrier-transport fields, in which the trapping model is fundamental. For the sake of completeness we like to mention that for trapping an exact expression for the relaxation Φ_n is known [36] only in $d = 1$. Thus in the general case one has to consider approximating schemes and to resort to simulations [35,37]. In the short time domain the relaxation due to trapping may be expressed as an expansion in the cumulants $K_{j,n}$ of the distribution of visited sites. Setting $\lambda = -\ell n(1 - p)$, where p is again the number density of B-particles (traps), and considering now a binomial distribution of traps, one has [35,36]:

$$\tilde{\Phi}_n = \exp[\lambda + \sum_{j=1}^{\infty} K_{j,n} (-\lambda)^j/j!] \quad . \tag{11}$$

Taking into account only the first two terms in the exponent of Eq. (11), one obtains:

$$\tilde{\Phi}_n = \exp[-\lambda(S_n - 1)] \exp[+(\lambda^2/2)\sigma_n^2)] \tag{12}$$

where σ_n^2 is the variance in the distribution of distinct sites visited, and depends on dimension. Comparison of Eqs. (10) and (12) shows that the KWW-behavior is modified by the multiplication with a new, σ_n^2-dependent term.

The asymptotic (large n) behaviour of $\tilde{\Phi}_n$ is [37]:

$$\tilde{\Phi}_n \sim \exp[-C\lambda^{2/(d+2)}n^{d/(d+2)}]. \qquad (13)$$

This is again a KWW-form, with $\beta = d/(d+2)$. Eq. (13) holds for arbitrary d, but its domain of validity (extremely large n) renders quite problematic its use in the interpretation of experimental data.

The above expressions and also the numerical analysis of simulations of random-walks display clearly that at long times the relaxation behavior for target annihilation Φ_n, and for trapping, $\tilde{\Phi}_n$, are qualitatively distinct, and that they lead to different exponents of β in the KWW-form. The relaxation depends therefore on which of the species (the majority or the minority) moves. As we already discussed [27,40], this finding is at variance with classical chemical-kinetic views which are based on pair-approximations, and which suggest that a reaction depends only on the sum $D = D_A + D_B$ of the diffusion coefficients of the reactants, but not on D_A and D_B separately.

The basic finding of this Section is that, distinct from the kinetic scheme of Sec. 2, random-walks on regular lattices already display KWW-behaviour, e.g. Eqs. (10), (12) and (13). Note that this is due to the introduction of stochastic aspects, both through the initial particle distributions and through the different realizations of random-walks. Further progress can be made by also accounting for structural, temporal and energetic disorder aspects, as we proceed to show in the next Sections.

4. Fractals and the Loss of Translational Symmetry

The term fractal has been coined by Mandelbrot to describe objects which display scale-invariance: the patterns are self-similar, i.e. basically unchanged under dilatation operations [21]. Topological investigations of some simple fractals were already performed early in this century [21,22] but it is the merit of Mandelbrot to have pointed out the overall presence of fractals in Nature. In fact, many stochastically disordered systems, like polymers, porous glasses and catalytically active surfaces have been characterized as being self-similar under length-scaling. Also some model structures, such as percolation clusters at criticality and difussion-limited aggregates were found to be fractal. For a summary of such patterns, including "state of the art" pictorial renderings, see Ref. [41]. Deterministically-built fractals are the Sierpinski-gaskets, whose generators (in the d-dimensional Euclidean space) are hypertetrahedrons consisting of $d+1$ hypertetrahedra of half the original sidelength [21]. Using other generators a plethora of deterministic fractals may be constructed: we have presented several classes of different fractals, obtained by taking other scaling factors than 2 and by varying the coverage of the original hypertetrahedron [42,43].

Since dilatational symmetry is a weaker requirement than translational symmetry, most fractals are not translationally invariant: this renders them particularly suitable

to describe features related to the loss of translational order.

A fractal object may be characterized by several parameters which play roles similar to the Euclidean dimension d for regular lattices. Using the fact that a fractal scales with distance, one defines the fractal (Hausdorff) dimension $\bar{d}$ through the scaling exponent [21]. Interestingly, dynamical processes on fractals are not determined solely through $\bar{d}$; in a by now classic work [44], Alexander and Orbach have shown that the "fracton" or spectral dimension $\tilde{d}$ is fundamental for the Laplace equation on the fractal. That $\bar{d}$ and $\tilde{d}$ do not coincide is a new feature for fractals, an aspect which is not found in translationally-invariant lattices. The parameters $\tilde{d}$ and $\bar{d}$ are not necessarily restricted to integers, but may take arbitrary positive values (hence the name "fractals", from "fractional", for the geometrical objects).

For the target and trapping problems $\tilde{d}$ is the fundamental quantity, as will become clear from the equations which now follow.

Let us again start with S_n, the average number of distinct sites visited in n steps. From analytical work and numerical simulations one obtains [37, 42-44]:

$$S_n \sim \begin{cases} n^{\tilde{d}/2} & \text{for } \tilde{d} < 2 \\ n & \text{for } \tilde{d} > 2 \,. \end{cases} \tag{14}$$

Comparison of Eqs. (9) and (14) shows that the behavior on fractals interpolates smoothly between that for regular lattices. Furthermore, Eq. (14) renders clear the marginal role played by the dimension $\tilde{d} = 2$.

What is now the relaxation in the target problem? The result is here less straightforward than for regular lattices, since sites on fractals are in general not equivalent to each other, and the relaxation depends on the position of the target. One needs therefore, additional to the averaging procedures required for regular lattices, also an average over the different target positions. For relatively homogeneous fractals, such as the Sierpinski-gaskets, one finds that the decay due to target annihilation is still well-represented through Eq. (10), which now, however, is only approximate. Inserting Eq. (14) into Eq. (10) converts it to a KWW-form for $\tilde{d} < 2$ and to a simple exponential for $\tilde{d} > 2$. Here we find $\beta = \tilde{d}/2$ for $\tilde{d} < 2$, which is no longer restricted to the single value $\beta = 1/2$, but which may vary considerably. Given the observation that experimentally values $\beta \neq 1/2$ are the rule, fractals may be one of the means to describe such a behavior.

The interpolating character of fractals is also evident from an analysis which centers on trapping. For trapping one finds the same short time relaxation behavior as in

Eqs. (11) and (12), where S_n is now given by Eq. (14). The correction terms to the KWW-behavior are thus again multiplicative. The asymptotic regime (large n) has the form [37]:

$$\tilde{\Phi}_n \sim \exp[-c^{2/(\tilde{d}+2)} n^{\tilde{d}/(\tilde{d}+2)}] \tag{15}$$

which is nothing else but Eq. (13), with d replaced by $\tilde{d}$. The KWW-parameter β in the long-time regime is $\beta = \tilde{d}/(\tilde{d}+2)$. Note, however, that for the application of Eq. (15) to the data the same provisos as mentioned after Eq. (13) apply.

5. Temporal Randomness: Continuous-Time Random Walks (CTRW)

Relaxing the condition that changes, such as the steps of a walker, occur only at predetermined times leads to processes in continuous time. One introduces therefore a waiting-time distribution $\psi(t)$, which gives the probability density that the time between stops equals t. This method has been used in a classic CTRW-work by Montroll and Weiss, who included [45] with the help of $\psi(t)$ continuous temporal aspects into the generating-function formalisms for simple random walks. The approach was elaborated later by Scher and Lax [23] and Scher and Montroll [17], who applied the CTRW to transport in disordered systems. Shlesinger and Montroll [33] and Bendler and Shlesinger [34] have used the CTRW-formalism to extend the Glarum model to continuous time, and were the first to point out that such a formalism allowed to find KWW-forms with arbitrary values of the parameter β, i.e. $0 < \beta < 1$. In this Section, we follow the ideas put forth by these authors.

Consider first the waiting-time distribution $\psi(t)$. In the simplest situation the probability of remaining at a given site during a time interval t is exponential:

$$\tilde{\psi}(t) = b \exp(-bt). \tag{16}$$

This distribution gives rise to a Poisson process. A more general waiting-time distribution may be envisaged to be a linear combination of Poisson processes with different b-values.
Consider for instance the form:

$$\psi(t) = \frac{1-q}{q} \sum_{j=1}^{\infty} q^j b^j \exp(-b^j t) \tag{17}$$

with $q < 1$ and $b < 1$. Then it is a simple matter to show that at long times $\psi(t)$ obeys

$$\psi(t) \sim 1/t^{1+\gamma} \tag{18}$$

where $\gamma = \ell nq/\ell nb$. Hence $\psi(t)$ scales with time and the authors of Refs. [33] and [34] use the expression "fractal time" to describe this situation.

Note that for $\gamma < 1$, i.e. for $b < q$, Eq. (18) has no first moment since the corresponding integral diverges. In this case the properties of the CTRW differ qualitatively from those displayed by random walks with constant waiting intervals between steps. As an example, $S(t)$, the mean number of distinct sites visited during the time interval t depends on whether or not the first moment of $\psi(t)$ exists. If the first moment exists, the behavior of $S(t)$ parallels that of S_n, Eqs. (9) and (14). To be general, we use the fractal notation, and have

$$S(t) \sim \begin{cases} t^{\tilde{d}/2} & \text{for } \tilde{d} < 2 \qquad (19a) \\ t & \text{for } \tilde{d} > 2 \ . \qquad (19b) \end{cases}$$

On the other hand, when the first moment of $\psi(t)$ is infinite ($\gamma < 1$) the behavior of $S(t)$ changes qualitatively to:

$$S(t) \sim \begin{cases} t^{\gamma\tilde{d}/2} & \text{for } \tilde{d} < 2, \ \gamma < 1 \qquad (20a) \\ t^{\gamma} & \text{for } \tilde{d} > 2, \ \gamma < 1 \ . \qquad (20b) \end{cases}$$

Interestingly, in the first equation of (20) the geometrical and the temporal scaling aspects, exemplified by $\tilde{d}$ and by γ, combine multiplicatively. Hence the two aspects subordinate in $S(t)$ [37,46].

The derivation of the relaxation of targets in the CTRW-framework [27] leads to an expression which again involves only $S(t)$, the mean number of sites visited:

$$\Phi(t) = \exp[-pS(t)] \ . \qquad (21)$$

Inserting Eqs. (19) or (20) into Eq. (21) lets us recover KWW-stretched exponential behavior. Now the parameter β may take any value between 0 and 1, if only γ is chosen accordingly. This holds also for regular lattices in arbitrary dimensions (and not only for fractals). It is this fact which, as mentioned, was remarked by Shlesinger and Montroll [33], and which is the basis of their extension of the Glarum model of spin relaxation in glasses.

From a theoretical point of view, the subordination displayed by Eq. (20), and discussed by us in Ref. [46] is most intriguing. When both spatial and temporal scaling aspects are present, such as to have simultaneously $\tilde{d} < 2$ and $\gamma < 1$, the knowledge of β alone ($\beta = \gamma\tilde{d}/2$) is not sufficient for unraveling the temporal disorder from the spatial one: There exist an infinity of $(\gamma, \tilde{d}/2)$ pairs which lead to the same

value of β. Then additional quantities have to be determined in order to differentiate between the two types of disorder.

Remarkably, the situation is clearer in the trapping case. There the short-time behavior may be again expressed as a cumulant expansion. Its first term is akin to Eq. (21), and leads to the β-parameter. The long-time behavior, on the other hand, is dominated (for not too large spatial disorder) by the temporal aspects. As shown by us in Ref. [46], for $\gamma < 1$ one has at longer times an algebraic decay:

$$\tilde{\Phi}(t) \sim t^{-\gamma} \tag{22}$$

whose time-development does no longer depend on the dimension of the underlying grid. Thus Eq. (22) is not of KWW-type, but follows the pattern of Eq. (4). The fact that the relation (22) depends directly on γ allows to assess the temporal disorder unhampered by spatial considerations; the spatial aspect is then retrievable from the short-time behavior of $\tilde{\Phi}(t)$.

6. Energetic Randomness: Ultrametric Spaces

As a consequence of the geometric randomness of glasses, one also finds that the microscopic processes depend on the site where they take place. We have already encountered this effect in fractals and it leads to a dispersion in the local temporal patterns. For tunnelling processes one may view this dispersion as arising from a distribution of energy barriers. A whole series of models of the glassy state is based on this idea of energy barriers of different kinds, see the works of Anderson [47] and Jäckle [48] or the models put forth by Rosato and Williams [49] and by Johari [50].

In the models considered by us so far all steps to neighboring sites were taken to be equivalent. The presence of a distribution of energy barriers changes drastically this picture. If the height of the energy barriers is random, then a given activation energy allows a walker to visit only a subset (cluster) of sites in the neighborhood of the starting point. The barriers whose energy is higher than the one provided to the walker hinder it to pass over them, and can restrict it to a rather small spatial region. Given an origin of the walk, it becomes then possible to classify the other sites through the minimal activation energy required to reach them: the topological equivalent of such a classification, carried through for all sites is a dendrogram, i.e. an ultrametric space [24,25,51].

Ultrametric spaces (UMS) have been used to model the energetic disorder in spin-glasses. A recent growth of interest has been evidenced in the study of dynamical processes, such as diffusion and trapping on UMS [52-55]. We will follow the steps of Ref. [52]

in describing the solutions of the Glarum model and of the trapping model on UMS.

The set of tips of a finite Bethe-lattice provides a simple UMS-picture. Evidently, the Bethe-lattice itself is tree-like, and we will focus on the simple case that exactly z-branches sprout forth from any branch of the preceding level: each internal site is then the meeting place of $z+1$ branches. Now only the tips of the lattice belong to the UMS and the rest of the structure allows to define a generalized distance: one counts the minimal number of branches one has to walk along the tree in order to reach, say, site x when starting from site y. It is a simple matter to verify that this number d has all the properties of a distance, e.g. symmetry: $d(x,y) = d(y,x)$, positiveness: $d(x,y) \geq 0$, and $d(x,y) = 0$ only if x is identical to y. Furthermore, the triangle inequality is fulfilled: d obeys the even more restrictive ("ultra") condition:

$$d(x,y) \leq \max(d(x,z), d(y,z)) \tag{23}$$

for all sites x,y,z of the UMS. In fact, it is condition (23) which allows to call the space under the distance $d(x,y)$ "ultrametric".

One may now associate to the distance the physical meaning of an energy required to get from one site to the other. One obtains then the partition mentioned previously: specifying a value for the activation energy of a particle partitions the UMS into disjoint clusters, whereby the particle starting from one site of a cluster may visit all cluster sites, but no sites outside the cluster. This fact may be proven rigorously by using the properties of the distance, see for instance Refs. [24] and [25], and for the Bethe-lattice it may be simply verified. For simplicity we will take all branches to be of equal length and we assume a linear relationship between this length and the energy. The barrier heights are then hierarchically distributed, so that all consecutive energy levels differ by a constant amount, say Δ. (Evidently, more sophisticated models may be envisaged, where both Δ and z are allowed to vary over the structure.)

A qualitative argument allows now to determine $S(t)$, the mean number of distinct sites visited during t [52]. For thermally activated jumps, the intersite transition rates are given by $w \exp(-j\Delta/kT)$, where $j\Delta$ is the barrier height to be surmounted, T the temperature, and w a unit rate. During the time interval

$$e^{j\Delta/kT} \leq wt_j < e^{(j+1)\Delta/kT} \tag{24}$$

z^j points of the UMS are accessible to the walker. Hence

$$z^j \sim z^{(kT/\Delta)\ln(wt_j)} = (wt_j)^{\gamma} \tag{25}$$

where we set

$$\gamma \equiv (kT/\Delta)\ell nz \ . \tag{26}$$

For $\gamma < 1$, z^j increases more slowly than t_j and the walker explores practically all accessible points. Therefore, using this idea of compact exploration [56]

$$S(t) \simeq (wt)^\gamma \sim t^\gamma \qquad (\gamma < 1). \tag{27}$$

For $\gamma > 1$, on the other hand, the increase of z^j is more rapid than that of t_j, so that the average number of distinct sites visited increases linearly with the time. Thus

$$S(t) \sim t \qquad (\gamma > 1). \tag{28}$$

A quick comparison of Eqs. (27) and (28) with the CTRW results, Eqs. (20b) and (19b), shows a remarkable parallelity between UMS and CTRW. This parallelity prompted us to use the letter "γ" for the definition of the quotient $(kT/\Delta)\ell nz$ in Eq. (26). Another remarkable similarity exists between UMS and fractals, as witnessed by Eqs. (27) and (28) on one hand and Eq. (14) on the other. One may namely identify γ with $\tilde{d}/2$, and call 2γ an effective spectral dimension [55]. Note, however, that γ depends on the temperature, so it is not a measure of the underlying structure only.

In Ref. [52] we have established through numerical simulations that Eqs. (27) and (28) are well-fulfilled. Furthermore, such calculations allowed us to determine the relaxation for the Glarum (target-) model and for trapping.

As may by now be expected, the analogy between UMS, CTRW and fractals carries through. The target decay is exactly:

$$\Phi_n = \exp[-p(S_n - 1)] \tag{29}$$

and it has, using Eq. (27) a KWW-form. The parameter β in Eq. (1) is for UMS a function of temperature. Thus, depending on T one has a crossover from stretched exponential forms at low temperatures $(kT\ell nz < \Delta)$ to purely exponential decays at high temperatures $(kT\ell nz > \Delta)$. For experimental purposes this finding is remarkable, since a simple change in temperature leads to a qualitative change in the KWW-behavior: this offers the possibility to decide experimentally whether for a given material the energetic disorder is basic or not.

The relaxation due to trapping again admits a cumulant expansion at short times, whose leading term is similar to Eq. (29), with p being replaced by $\lambda = -\ell n(1-p)$.

The higher terms of this short-time expansion display clearly the parallelity between UMS and fractals, which we discussed before. This aspect is also evident from the long-time relaxation due to trapping:

$$\tilde{\Phi}(t) \sim \exp[-C\lambda^{1/(\gamma+1)}{}_n\gamma/(\gamma+1)]. \qquad (30)$$

This equation is identical to Eq. (15) with $\tilde{d}$ being replaced by 2γ. Of course, the applicability of Eq. (30) to experimental data is restricted in the same way as discussed after Eq. (13).

6. Conclusions

In this work we have considered several models for randomness, such as fractals for systems lacking translational invariance, walks in continuous time for temporally-disordered processes and ultrametric spaces for the random distribution of energy barriers. All these models are characterized by some scaling (they are hierarchical), and this feature facilitates their analytical study. In the mathematical literature the topological aspects of fractals and UMS are well-studied. The new interest in these objects centers in the properties of dynamical processes over them.

Remarkably, we have shown in many instances that the relaxation of excited centers follows a KWW-form. Since this form is so widespread, one needs additional information in order to specify in a given experimental set-up the microscopic mechanisms which lead to KWW-behavior. Examples for such additional information may be the temperature and pressure (density) dependence of the relaxation or some insight into the microscopic structure of the material under investigation.

Acknowledgements

Most of the results presented here were found and investigated in collaboration with Dr. J. Klafter and Dr. G. Zumofen, and I am very thankful for their continuous encouragement and support. To Dr. B. Ewen I am much indebted for his gracious, unrelenting help. Research grants from the Deutsche Forschungsgemeinschaft and from the Fonds der Chemischen Industrie are gratefully acknowledged.

References

[1] G. Williams and D.C. Watts, Trans. Faraday Soc. 66, 80 (1970)

[2] G. Williams, Adv. Polym. Sci. 33, 59 (1979)

[3] A.K. Jonscher, Nature 267, 673 (1977)

[4] K.L. Ngai, Comments Solid State Phys. 9, 127 (1979); 9, 141 (1980)

[5] See "Relaxation in Complex Systems", K.L. Ngai and G.B. Wright eds. (Natl. Techn. Inform. Service, U.S. Govt. Printing Office, 1985)

[6] A.A. Jones, J.F. O'Gara, P.T. Inglefield, J.T. Bendler, A.F. Yee and K.L. Ngai, Macromolec. 16, 658 (1983)

[7] G.D. Patterson, Adv. Polym. Sci. 48, 125 (1983)

[8] G. Fytas, Th. Dorfmüller and C.H. Wang, J. Phys. Chem. 87, 5041 (1983)

[9] G. Fytas, A. Patkowski, G. Meier and Th. Dorfmüller, J. Chem. Phys. 80, 2214 (1984), see also the contribution of G. Meier in this volume; G. Fytas, C.H. Wang, G. Meier and E.W. Fischer, Macromolecules 18, 1492 (1985); G. Meier, G. Fytas and Th. Dorfmüller, Macromolecules 17, 952 (1984)

[10] R. Richert and H. Bässler, Chem. Phys. Lett. 118, 235 (1985)

[11] V.L. Vyazovkin, B.V. Bol'shakov and V.A. Tolkatchev, Chem. Phys. 75, 11 (1983)

[12] J.R. Miller, Chem. Phys. Lett. 22, 180 (1973)

[13] J.V. Beitz and J.R. Miller, J. Chem. Phys. 71, 4579 (1979)

[14] J. Friedrich and D. Haarer, Angew. Chemie, Int. Engl. Ed. 23, 113 (1984)

[15] J. Friedrich and A. Blumen, Phys. Rev. B32, 1434 (1985)

[16] J. Tauc, Semicond. and Semimetals 21B, 299 (1984)

[17] H. Scher and E.W. Montroll, Phys. Rev. B7, 4502 (1973)

[18] G. Pfister and H. Scher, Adv. Phys. 27, 747 (1978)

[19] R.G. Palmer, D.L. Stein, E. Abrahams and P.W. Anderson, Phys. Rev. Lett. 53, 958 (1984)

[20] A. Blumen, Nuovo Cimento B63, 50 (1981)

[21] B.B. Mandelbrot, "The Fractal Geometry of Nature", W.H. Freeman and Co., San Francisco (1982)

[22] K.J. Falconer, "The Geometry of Fractal Sets", Cambridge Univ. Press (1985)

[23] H. Scher and M. Lax, Phys. Rev. B7, 4491; 4502 (1973)

[24] N. Bourbaki, "Eléments de mathématique, Topologie générale", Chap. IX, CCLS, Paris (1974)

[25] W.H. Schikhof, "Ultrametric Calculus", Cambridge Univ. Press (1984)

[26] G. Zumofen, A. Blumen and J. Klafter, J. Chem. Phys. 82, 3198 (1985)

[27] A. Blumen, J. Klafter and G. Zumofen, "Models for Reaction Dynamics in Glasses", in: "Optical Spectroscopy of Glasses", I. Zschokke-Gränacher ed., Reidel, Dordrecht, Holland (1986) p. 199

[28] E.A. DiMarzio, "Equilibrium Theory of Glasses", in "Structure and Mobility in

Molecular and Atomic Glasses", J.M. O'Reilly and M. Goldstein eds., Ann. N.Y. Acad. Sci. 371, 1 (1981)

[29] C.A. Angell, Ann. N.Y. Acad. Sci. 371, 136 (1981)

[30] L.V. Woodcock, Ann. N.Y. Acad. Sci. 371, 274 (1981)

[31] C.A. Angell, J.H.R. Clarke and L.V. Woodcock, Ann. Rev. Phys. Chem. 48, 397 (1981)

[32] S.H. Glarum, J. Chem. Phys. 33, 1371 (1960)

[33] M.F. Shlesinger and E.W. Montroll, Proc. Natl. Acad. Sci. USA 81, 1280 (1984)

[34] J.T. Bendler and M.F. Shlesinger, in: "Relaxation in Complex Systems", Ref. [5], p. 261

[35] G. Zumofen and A. Blumen, Chem. Phys. Lett. 88, 63 (1982)

[36] G.H. Weiss and R.J. Rubin, Adv. Chem. Phys. 52, 363 (1983)

[37] J. Klafter, A. Blumen and G. Zumofen, J. Stat. Phys. 36, 561 (1984)

[38] S. Redner and K. Kang, J. Phys. A17, L 451 (1984)

[39] A. Blumen, G. Zumofen and J. Klafter, Phys. Rev. B30, 5379 (1984)

[40] A. Blumen, J. Klafter and G. Zumofen, in: "Transport and Relaxation Processes in Random Materials", J. Klafter et al. eds., World Scientific, Singapore (1986)

[41] F. Family and D.P. Landau eds., "Kinetics of Aggregation and Gelation", North-Holland, Amsterdam (1984)

[42] R. Hilfer and A. Blumen, J. Phys. A17, L 537 (1984)

[43] R. Hilfer and A. Blumen, J. Phys. A17, L 783 (1984)

[44] S. Alexander and R. Orbach, J. Physique Lett. 43, L 625 (1982)

[45] E.W. Montroll and G.H. Weiss, J. Math. Phys. 6, 167 (1965)

[46] A. Blumen, J. Klafter, B.S. White and G. Zumofen, Phys. Rev. Lett. 53, 1301 (1984)

[47] P.W. Anderson, in "Ill-Condensed Matter", R. Balian, R. Maynard and G. Toulouse eds., North-Holland, Amsterdam (1979) p. 162

[48] J. Jäckle, in: "Amorphous Solids", W.A. Phillips ed., Topics in Current Phys. 24, 135 (1985) Springer Verlag, Berlin, and Reports on Progress in Physics (1986), to be published

[49] V. Rosato and G. Williams, Adv. Molec. Relax. and Interact. Processes 20, 233 (1981)

[50] G.P. Johari, in: "Plastic Deformation of Amorphous and Semicrystalline Materials", Les-Houches Lectures (Editions de Physique, 1982)

[51] A.D. Gordon, "Classification", Chapman and Hall, London (1981)

[52] A. Blumen, J. Klafter and G. Zumofen, J. Phys. A19, L 77 (1986)

[53] B.A. Huberman and M. Kerszberg, J. Phys. A18, L 331 (1985)

[54] A.T. Ogielski and D.L. Stein, Phys. Rev. Lett. 55, 1634 (1985)

[55] S. Grossmann, F. Wegner and K.H. Hoffmann, J. Physique Lett. 46, L 575 (1985)

[56] P.D. deGennes, Compt. Rendus Acad. Sci. (Paris), Sér. II, 296, 881 (1983)

SUB-Tg RELAXATIONS IN HEAVY METAL FLUORIDE GLASSES

C.T. Moynihan, S.M. Opalka, R. Mossadegh,
S.N. Crichton and A.J. Bruce

Center for Glass Science and Technology
Materials Engineering Department
Rensselaer Polytechnic Institute
Troy, NY 12180-3590, USA

Abstract

Structural relaxation studies during annealing of a series of ZrF_4-based glasses below the glass transition temperature have been carried out. Indications are that no property changes due to structural relaxation are likely to occur at ambient temperature over periods of tens of years. Some of the lower Tg glasses, however, did exhibit detectable structural relaxation on annealing at temperatures as low as 100°C over roughly a one year time period.

1. Introduction

Heavy metal fluoride glasses (HMFG) are a fairly new class of materials which are currently receiving much attention because of potential uses as optical materials in the mid-IR [1,2]. Depending on composition, their IR transparency extends out to 6-9 μm, much further than silicate glasses, whose IR transparency stops at around 2-3 μm. The most widely characterized of the HFMG are those whose main component is ZrF_4. ZrF_4-based HMFG compositions, which are typical for these materials and which were characterized in this study, are listed in Table I, along with their glass transition temperatures Tg measured by differential scanning calorimetry (DSC) at a 10 K/min heating rate.

Table I: HMFG compositions (mol%) and glass transition temperatures

Glass	ZrF_4	BaF_2	LaF_3	AlF_3	NaF	LiF	PbF_2	Tg(K)
ZBL	62	33	5	-	--	--	--	574
ZBLA	58	33	5	4	--	--	--	584
ZBLAN	56	14	6	4	20	--	--	536
ZBLALi	51	21	5	3	--	20	--	523
ZBLALiPb	50	17	5	3	--	20	4	513

Tg's for these glasses are fairly low - 240 to 311°C - with the alkali fluoride containing glasses having the lower Tg's. There thus exists the possibility that at ambient temperatures structural relaxation or physical aging of these glasses might cause their properties to drift over long periods of time. (See Refs. [3-10] for some recent articles on structural relaxation in glasses.) Slight changes in, for instance, refractive index over a period of years could lead to unacceptable changes in optical properties of extremely long fiber optic waveguides made from these materials. Such considerations prompted our studies of sub-Tg structural relaxation in HMFG.

2. Sub-Tg Annealing Experiments

Our experimental approach has been described in detail in a report of some early results [9] and is illustrated schematically in Fig. 1. Briefly, samples of the glasses were rated cooled on the DSC at 10 or 100 K/min from above to well below the glass transition region. The samples were then annealed isothermally at temperature T_A well below Tg for times t_A ranging up to over one year. Following the isothermal anneal, the specific heats Cp were measured on the DSC at 10 K/min while reheating through the glass transition region. During this reheat the glass regains any enthalpy lost due to the earlier sub-Tg anneal, so that the Cp curves measured during reheating can be used to monitor the progress of enthalpy changes due to structural relaxation during sub-Tg annealing.

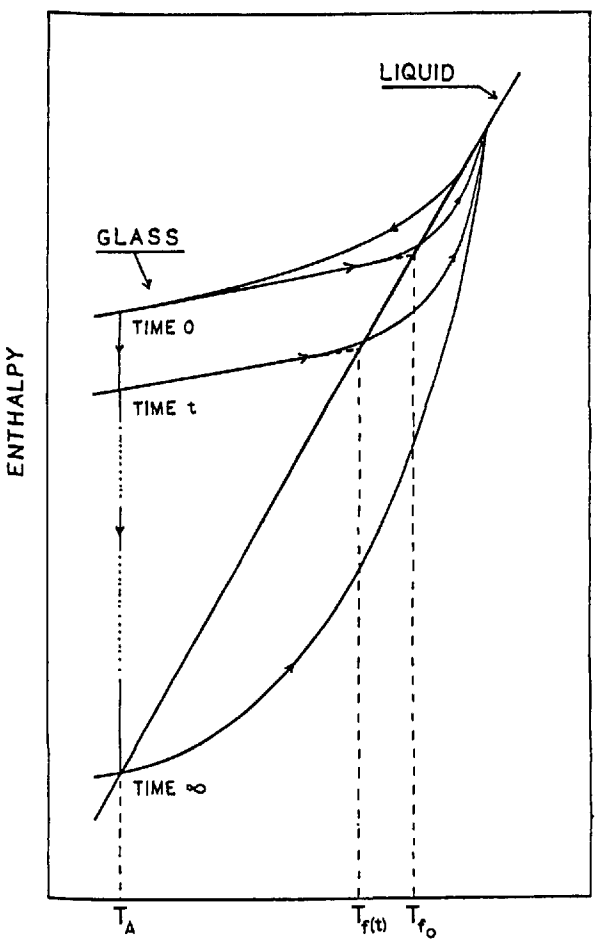

Fig. 1: Schematic representation of the variation of enthalpy and fictive temperature during rate cooling through the glass transition region, sub-Tg annealing and rate heating through the glass transition region

Typical DSC results are shown in Figs. 2 and 3. Figure 2 is characteristic of anneals carried out at temperatures a moderate distance (10-60 K) below Tg. The effect of annealing is to increase the magnitude of the Cp

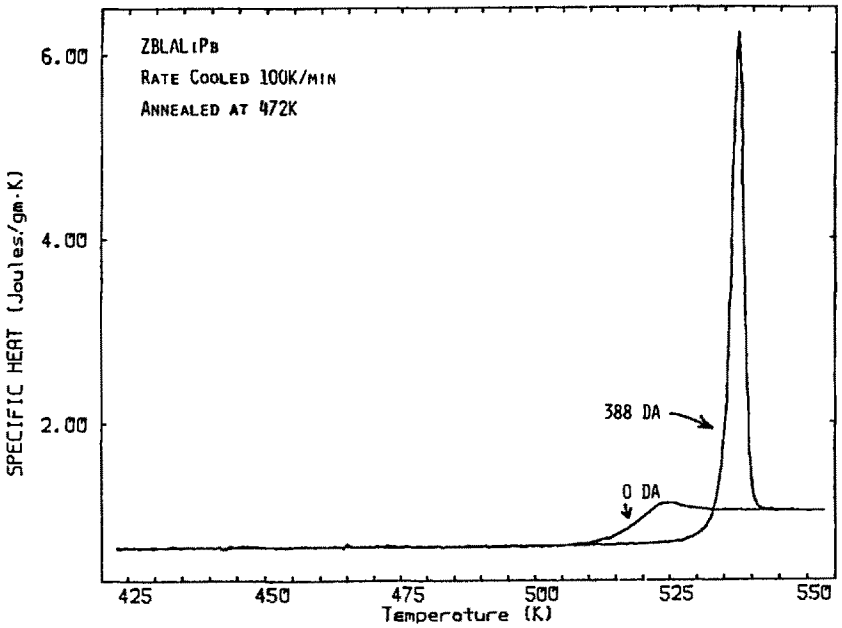

Fig. 2: Specific heat measured at 10 K/min heating rate for ZBLALiPb glass following rate cool and sub-Tg anneal for times shown in figure

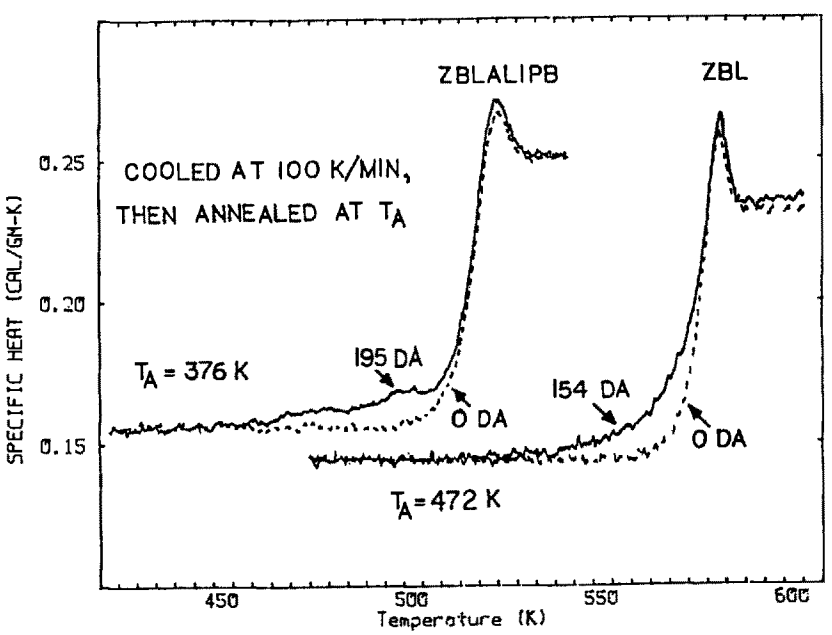

Fig. 3: Specific heat measured at 10 K/min heating rate for ZBL and ZBLALiPb glasses following rate cool and sub-Tg anneal for times shown in figure

maximum in the main glass transition region and shift it to higher temperature. Figure 3 is characteristic of anneals carried out a fairly large distance (100-140 K) below Tg. Here the effect of annealing shows up as an increase in Cp or even a small, extra Cp peak in the sub-Tg region just below the main glass transition region. Both of these results are in accord with predictions of the standard Tool-Narayanaswamy kinetic model for structural relaxation [3-10], which assumes that the relaxation process is non-linear and is controlled by a monotonic, single-peaked spectrum of relaxation times. The appearance of two peaks in the Cp reheating curve does not require a double-peaked spectrum of relaxation times and does not imply that there are two distinct relaxation mechanisms in the glass [6,7].

For purposes of analysis it is convenient to express the changes in enthalpy due to structural relaxation in terms of the time dependence of the fictive temperature T_f. T_f may be thought of as a measure of the average configurational enthalpy of the glass and is defined such that $T = T_f$ for a glass in the equilibrium state at temperature T (see Fig. 1). T_f is calculated from the experimental Cp data obtained during reheating via the following expression [3]:

$$T_f = T^* + \int_{T^*}^{T<<Tg} [(Cp-Cpg)/(Cpe-Cpg)]dT \qquad (1)$$

where T^* is a temperature above the glass transition region and Cpg and Cpe are respectively the glass and equilibrium liquid heat capacities. This calculation is illustrated in Fig. 4 for a ZBLA glass sample. T_f in this case is the fictive tem-

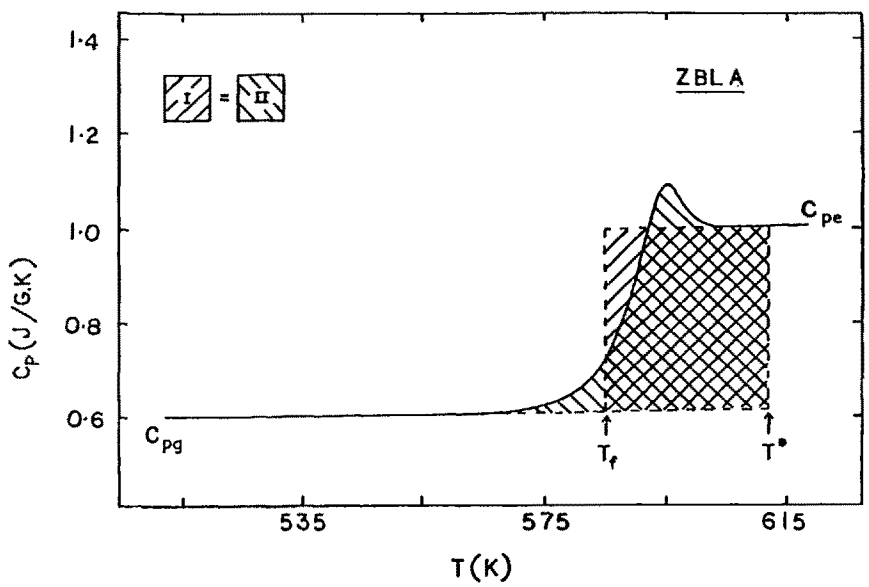

Fig. 4: Illustration of fictive temperature calculation for ZBLA glass heat capacity data measured at a 10 K/min heating rate immediately following a 100 K/min rate cool through the transition region

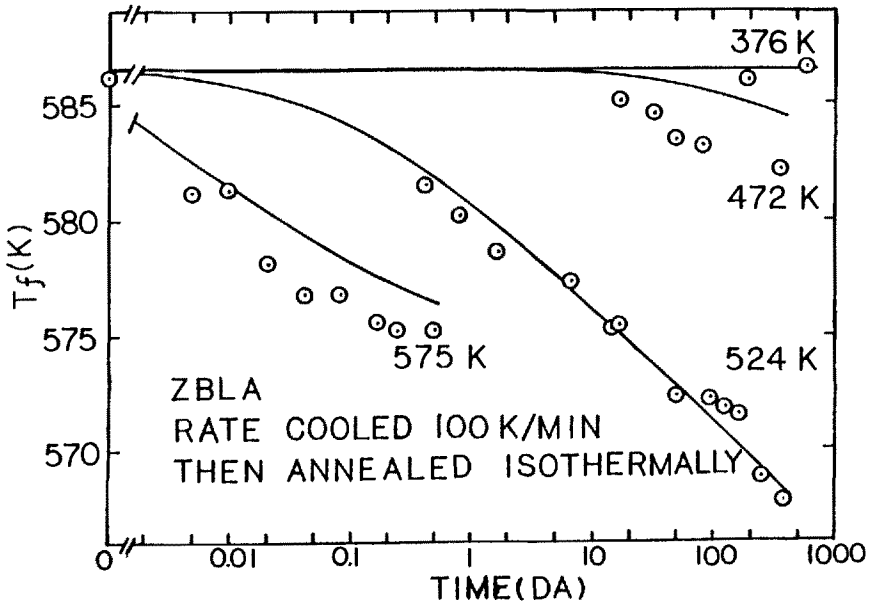

Fig. 5: Evolution of fictive temperature of ZBLA glass during sub-Tg annealing following a rate cool at 100 K/min. Solid lines are calculated from parameters in Table III as described in text

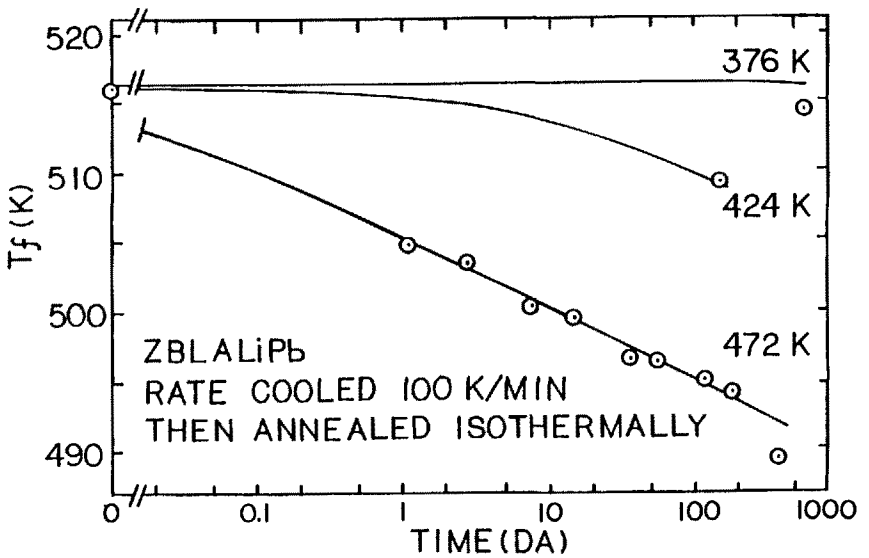

Fig. 6: Evolution of fictive temperature of ZBLALiPb glass during sub-Tg annealing following a rate cool at 100 K/min. Solid lines are calculated from parameters in Table III as described in text

perature reached by the glass immediately after cooling at 100 K/min through the transition region and would correspond to T_{fo} in Fig. 1.

3. Results of Sub-Tg Annealing Experiments

Figure 5 shows typical results for ZBLA glass for the evolution of T_f with time during sub-Tg annealing at several temperatures T_A. Note from Fig. 4 that the initial fictive temperature at time t = 0 obtained immediately after rate cooling through the glass transition region is approximately equal to Tg. For the sub-Tg anneal at the highest temperature the sample comes to equilibrium ($T_f = T_A$ = 575 K) within one day. For annealing at the next two lower temperatures (T_A = 472 and 524 K) relaxation is slower but appreciable over a one year time period. However, the samples are still very far from equilibrium after one year. At the lowest temperature (T_A = 376 K) some 210 K below Tg no detectable relaxation has occurred in nearly two years. Similar results are shown in Fig. 6 for ZBLALiPb glass. Note that with this glass a small but detectable change in T_f does occur on annealing for several months or longer at 376 K, as is also indicated directly in Fig. 3 by the effect of annealing on the Cp curves. Figure 7 compares the rates of sub-Tg relaxation following a 100 K/min cool of all five glasses of Table I at a common temperature T_A = 472 K. As expected, the glasses with the lowest Tg relax most rapidly.

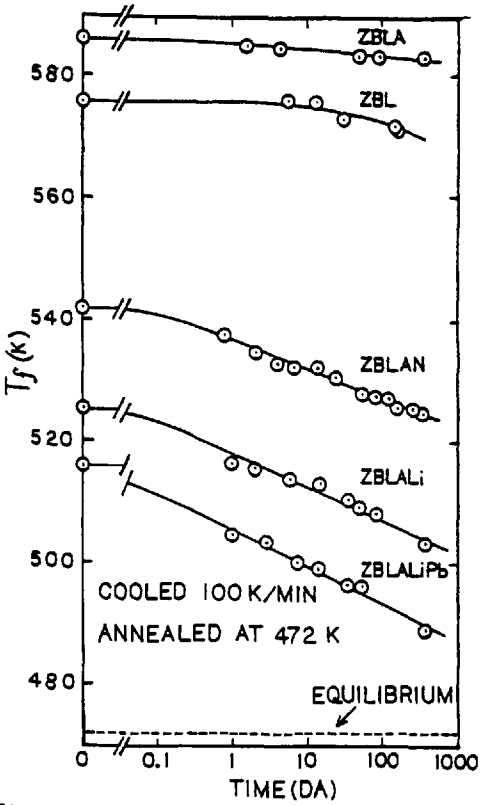

Fig. 7: Evolution of fictive temperature of five glasses during sub-Tg annealing at 472 K following a rate cool. Solid lines are smooth curves drawn through data points

4. Analysis of Sub-Tg Relaxation Curves

The Tool-Narayanaswamy model [3-10] for structural relaxation during isothermal annealing at temperature T_A gives for the time dependence of fictive temperature:

$$T_f(t) = T_A + \sum_{i=1}^{n} g_i[T_{fi}(0) - T_A] \exp[-\int_0^t dt/\tau_i(t)] \qquad (2)$$

where the relaxation process is assumed to involve n relaxing order parameters,

the contribution of each of which is governed by a weighting coefficient g_i and a relaxation time τ_i. A fictive temperature $T_{fi}(t)$ is associated with each of the order parameters, and the experimental fictive temperature $T_f(t)$ is the weighted average of these:

$$T_f(t) = \sum_{i=1}^{n} g_i \, T_{fi}(t) \; . \tag{3}$$

$T_{fi}(0)$ in Eq. (2) is the initial fictive temperature (i.e., immediately after rate cooling) associated with the i-th order parameter. The relaxation is non-linear, so that the relaxation times depend both on actual temperature T and average fictive temperature $T_f(t)$:

$$\tau_i(t) = A_i \exp[x\Delta H^*/RT + (1-x)\Delta H^*/RT_f(t)] \tag{4}$$

where A_i is a pre-exponential constant, ΔH^* the activation energy for structural relaxation, $x(0 \leq x \leq 1)$ the non-linearity parameter and R the ideal gas constant. The activation energy ΔH^* can be determined from the dependence of the fictive temperature T_{fo} obtained immediately after rate cooling the glass on the cooling

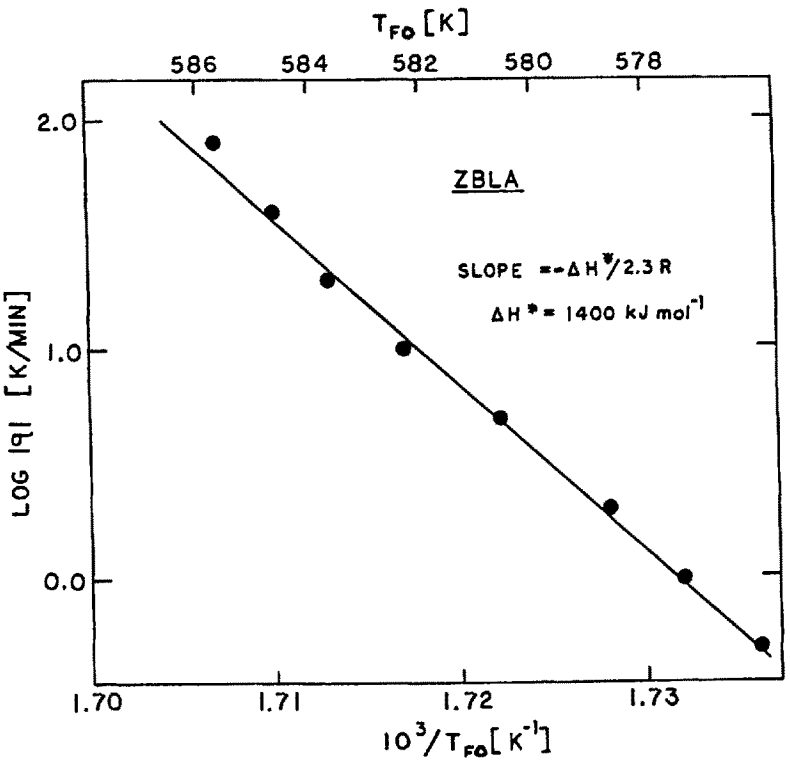

Fig. 8: Logarithm of cooling rate $|q|$ vs. reciprocal of fictive temperature T_{fo} for ZBLA glass

rate q [3,11]:

$$d\ell n|q|/d(1/T_{fo}) = -\Delta H^*/R \ . \qquad (5)$$

This is illustrated in Fig. 8 for ZBLA glass. In Table II are listed the structural relaxation activation energies obtained in this fashion for the glass samples of the present study. ΔH^* is generally found to be the same or very nearly the same as the activation energy ΔH^*_η for shear viscosity in the glass transition region [3].

Table II: Activation energies ΔH^* for structural relaxation obtained from Eq. (5) and activation energies ΔH^*_η for viscous flow in the glass transition region

Glass	ΔH^*(kJ/mol)	ΔH^*_η(kJ/mol)
ZBL	1430	-
ZBLA	1400	1150
ZBLAN	930	870
ZBLALi	1100	-
ZBLALiPb	1030	-

We have also listed in Table II values of ΔH^*_η obtained from beam bending measurements in our laboratory for two of the glasses. The agreement between ΔH^* and ΔH^*_η is within or nearly within experimental error. An apparent large discrepancy between ΔH^* and ΔH^*_η for ZBLA glass reported by Shelby et al. [12] has been found probably to be due to differences between their viscosity samples and our DSC samples [13]. It has been suggested [11,14] that the decrease in ΔH^* or ΔH^*_η that occurs when alkali fluoride is incorporated into ZrF_4-based glasses is largely responsible for the improved stability of the alkali fluoride-containing compositions against devitrification.

ΔH^* for the HMFG is extremely large, so that at equilibrium ($T_f = T$) the relaxation times would change by an order of magnitude roughly every 5 K. That extensive relaxation can be observed in these glasses very far below Tg thus indicates that the relaxation is highly non-linear, i.e., that the relaxation times depend very strongly on T_f and that x in Eq. (4) is relatively small. (Hodge [7] has noted and rationalized a correlation between large ΔH^* and small x.) This high degree of non-linearity is apparent in the data of Figs. 5, 6 and 7. For example, during the ZBLA glass anneal at 524 K shown in Fig. 5 the relaxation is initially fairly rapid, and T_f drops about 6 K in the first day. Once this has occurred, however, the relaxation

times via Eq. (4) are greatly increased, and a subsequent 6 K drop in T_f takes much longer - about 30 days.

A fit of the data in Figs. 5 and 6 along with analogous data for relaxation of ZBLA and ZLALiPb glasses initially cooled at 10 K/min to Eq. (2) was carried out. The (g_i, τ_i) pairs in Eq. (2) were chosen to correspond to the well-known KWW or stretched exponential relaxation function $\exp[-(t/\tau_0)^{\beta}]$ [8,15]. Hence a fit to Eq. (2) requires the use of four adjustable parameters - β, A_0, ΔH^* and x. The last three of these determine the value of KWW relaxation time τ_0 for non-linear relaxation [4-6]:

$$\tau_0(t) = A_0 \exp[x\Delta H^*/RT + (1-x)\Delta H^*/RT_f(t)] \ . \qquad (6)$$

The values of A_0 and ΔH^* are fixed by the slope and intercept of the best fit line through the $\ell n|q|$ vs. $1/T_{f0}$ plot [4,5] (see Fig. 8), so that to fit data such as that in Figs. 5 and 6 one need only iterate on two parameters, x and β.

The fit to the sub-Tg annealing T_f vs. t data for ZBLA and ZBLALiPb glasses was carried out using procedures similar to those employed previously [4-6,8]. The structural relaxation parameters are listed in Table III, and the solid curves in Figs. 5 and 6 were calculated from these parameters via Eq. (2). (That β and x are the same for the ZBLA and ZBLALiPb glasses may be fortuitous.) Hodge [7] has compared the relaxation parameters A_0, β, ΔH^* and x for a variety of polymeric, organic and inorganic glasses and showed that there appear to be correlations among them, e.g., a high ΔH^* is generally associated with low values of ℓnA_0, β and x. Interestingly, the values of the relaxation parameters for the HMFG glasses in Table III fall fairly closely on Hodge's correlation lines.

Table III: Best fit structural relaxation kinetic parameters for T_f vs. t curves obtained during sub-Tg annealing of ZBLA and ZBLALiPb glasses following rate cools at 10 and 100 K/min

Glass	A_0(s)	ΔH^*(kJ/mol)	β	x
ZBLA	4.1×10^{-124}	1400	0.54	0.28
ZBLALiPb	2.8×10^{-103}	1030	0.54	0.28

The best fits to the data using the Tool-Narayanaswamy model are in general not within experimental error, as is particularly clear from Fig. 5 in which a wide range of sub-Tg annealing temperatures is covered. This is not surprising. Scherer [16], for instance, has recently analyzed sub-Tg annealing data for a soda-lime silicate glass and found that structural relaxation rates for rapidly cooled specimens at temperatures far below Tg were considerably faster than were predicted from fits to data at higher temperatures closer to Tg. Improvements in the semi-empirical Tool-Narayanaswamy model to allow accurate modelling and prediction of rates of structural relax-

ation over a wide range of times and temperatures is a currently active research area both at our laboratory and elsewhere.

5. Conclusions

In this study we have investigated the change in enthalpy H of HMFG during sub-Tg annealing. Of interest for fiber optic applications are changes in index of refraction. Refractive index n, which generally correlates linearly with density, does not and is not expected to relax at exactly the same rate as enthalpy [4,5,8]. However, judging from results on oxide glasses [4,5,8], differences in the rates of relaxation of H and n appear to be relatively small - no more than a factor of 2 in the relaxation times. Hence one may conclude that any substantial drifts in enthalpy due to structural relaxation will be accompanied by substantial drifts in refractive index.

Lacking at the moment a good kinetic model for extrapolating rates of structural relaxation to low temperatures and long times, we can only make qualitative predictions based on the actual data of rates of drift of properties at use temperatures envisioned for HMFG. Inspection of the data for annealing at 376 K (= 103°C) indicates only minor structural relaxation over times of the order of a year for the lowest Tg, fastest relaxing glass - ZBLALiPb (see Figs. 3 and 6). Indications are thus that negligible long term structural relaxation and change of properties at ambient temperature are expected for any of the glasses of the present study. Given that more rapidly quenched glasses, e.g., optical fibers, relax more quickly than slowly cooled glasses [9,16], however, some of the low Tg HMFG might show some perceptible long term property drifts if use temperatures range up to the 100°C region. Likewise, IR transmitting glasses with substantially lower Tg's ($\leq$about 200°C) than those considered here are very apt to suffer from long term ambient temperature structural relaxation.

Acknowledgements

The studies reported here were supported by Contract No. F19628-83-C-0016 from the Air Force Electronic Systems Division, USAF and Grant No. DMR85-10617 from the National Science Foundation. The authors are grateful to Dr. G.W. Scherer for sharing with them his versatile computer program for analysis of structural relaxation.

References

[1] Drexhage, M.G., in "Treatise on Materials Science and Technology", Vol. 26, M. Tomozawa and R.H. Doremus, Eds., Academic Press, New York, 1985, pp. 151-243

[2] Tran. D.C., Sigel, G.H. and Bendow, B., J. Lightwave Tech. LT-2, 566 (1984)

[3] Moynihan, C.T., Easteal, A.J., DeBolt, M.A. and Tucker, J., J. Am. Ceram. Soc. 59, 12 (1976)

[4] DeBolt, M.A., Easteal, A.J., Macedo, P.B. and Moynihan, C.T., J. Am. Ceram. Soc. 59, 16 (1976)

[5] Moynihan, C.T. et al., Ann. NY Acad. Sci. 279, 15 (1976)

[6] Hodge, I.M. and Berens, A.R., Macromolecules 15, 762 (1982)

[7] Hodge, I.M., Macromolecules 16, 898 (1983)

[8] Scherer, G.W., J. Am. Ceram. Soc. 67, 504 (1984)

[9] Moynihan, C.T., Bruce, A.J., Gavin, D.L., Loehr, S. R., Opalka, S.M. and Drexhage, M.G., Polym. Engin. and Sci. 24, 1117 (1984)

[10] Rekhson, S.M., J. Non-Cryst. Solids 73, 151 (1985)

[11] Moynihan, C.T., Gavin, D.L., Chung, K.-H., Bruce, A.J., Drexhage, M.G. and El Bayoumi, O.H., Glastechn. Ber. 56K, 862 (1983)

[12] Shelby, J.E., Pantano, C.G., and Tesar, A.A., J. Am. Ceram. Soc. 67, C-164 (1984)

[13] Shelby, J.E., private communication

[14] Bansal, N.P., Bruce, A.J., Doremus, R.H. and Moynihan, C.T., J. Non-Cryst. Solids 70, 379 (1985)

[15] Moynihan, C.T., Boesch, L.P. and Laberge, N.L., Phys. Chem. Glasses 14, 122 (1973)

[16] Scherer, G.W., J. Am. Ceram. Soc. 69, 314 (1986)

MECHANICAL RELAXATION IN SOLID POLYMERS: PROPOSAL FOR A NEW APPROACH AND A SOLUTION OF HEIJBOER'S PROBLEM

L.C.E. Struik

Plastics and Rubber Research Institute TNO
P.O. Box 71, 2600 AB Delft
The Netherlands

Contents

Summary

This paper deals with the application of the two-potential-well model for the description of secondary relaxation in glassy polymers. The model is outlined and it is shown that the theoretical predictions do not, or only partially, agree with experiment. It is also shown that the model contains some serious inconsistencies, the most important one being the fact that the coupling of the molecule responsible for relaxation and its immediate environment is neglected. A new model is proposed in which this coupling is taken into consideration. The exact way of coupling is found by considering the fact that the glassy environment has once been prepared by cooling the polymer from the molten state above Tg to the glassy state below Tg. The new model works satisfactorily and can explain the paradoxical situation that strong coupling with the environment is not in contradiction with the experimental finding that, at least for the chair-chair relaxation of cyclohexyl rings, the activation parameters are almost independent of the environment of the ring.

1. Introduction

Usually, relaxation in solid polymers is described by the two-(or more) potential-well model. The molecule responsible for relaxation is assumed to have two (or more) stable states (energy wells) separated by high energy barriers. The distribution over the different states depends on their energy levels and these levels are supposed to change with an applied electrical field or mechanical stress. A change in field or stress thus induces a change in distribution: because of the high energy barriers, this change takes time and, macroscopically, we observe relaxation. A brief description of the model for two states is given in Section 2, more details can be found in [1]; an example of a multi-state barrier model can be found in [2].

In 1972, Heijboer [3] reported experimental data on polymers containing cyclohexyl rings and definitely showed that the two-potential-well model in its usual form is inadequate, qualitatively as well as quantitatively, to describe mechanical relaxation. A summary of Heijboer's findings is given in Section 3. A discussion of the underlying inconsistencies in the usual model is given in Section 4. It will be shown that the basic problem in this model is that the mechanical coupling of the (moving) molecule with its environment is not taken into account properly.

A proposal for a refined theory is given in Section 5. As other authors did (see e.g. [4]), we assumed that the moving molecule is firmly coupled (mechanically) to its environment. To find how the molecule exactly fits in its environment, we take into account that this environment has once been formed by transforming the liquid polymer into a glass (cooling from above to below glass-temperature Tg). Also resolved is the apparent paradox between the theoretical assumption of firm mechanical coupling

of the molecule to its environment and Heijboer's [3] experimental finding that the relaxation parameters (activation energy, relaxation time, relaxation strength) of the cyclohexyl ring process hardly depend on the environment of the cyclohexyl ring. That the new theory properly describes Heijboer's data is shown in Section 5.8.

2. The Usual Two-Potential-Well Model [1], [3]

The potential energy curve of the molecule is depicted in Fig. 1A. There are two 'stable' conformations, labelled I and II, with an energy barrier in between. In almost all representations of the theory, the curve is approximated as shown in Fig. 1B. The energies of the square wells are U_1 and U_2, and the conformational energy difference U_2-U_1 is denoted by ΔU. Entropy effects are neglected (cf. [3]); further the barrier is assumed so high that the fraction of the molecules at the top of the barrier can be neglected also.
Application of a mechanical stress σ is supposed to change the $U(x)$ curve (see Fig. 1). What counts is the change in ΔU; for small stresses we write:*)

$$\Delta U = \Delta U_0 + b\sigma . \tag{2.1}$$

This assumption stems from the fact that the σ acts in a certain direction and makes one of the two states more favourable. Of course, parameter b in (2.1) depends on the orientation of the molecule in the stress field and therefore b will vary from molecule to molecule. In view of this, we first consider an assembly of n molecules with b-values between b and $b+db$ and perform an integration over all possible b-values later on. For this assembly, we have populations n_{10} and n_{20} in the stress-free state ($\sigma = 0$) and populations n_1 and n_2 in the stressed state. Using Boltz-

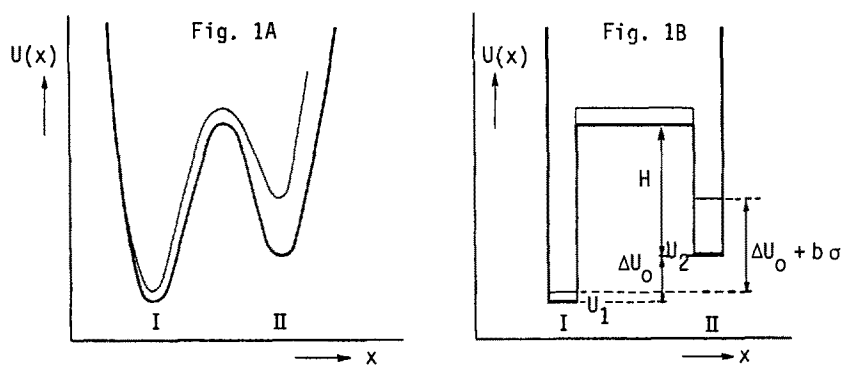

Fig. 1. Illustration of the two-potential-well model; potential energy curve $U(x)$ is given for zero stress (▬) and for stress $\sigma \neq 0$ (——). Fig. 1A shows the actual $U(x)$ curve, Fig. 1B a rectangular approximation

*) All energies are expressed per mol, not per particle.

mann's formula and neglecting the population at the top of the barrier, we find with (2.1):

$$n_{10} = n/[1 + \exp.(-\Delta U_0/RT)] \tag{2.2}$$

$$n_{20} = n - n_{10} \tag{2.3}$$

$$n_1 = n/[1 + \exp.(-(\Delta U_0 + b\sigma)/RT)] \tag{2.4}$$

$$n_2 = n - n_1 \tag{2.5}$$

where R and T have their usual meaning (gasconstant and absolute temperature). For infinitely small σ-values (linear viscoelastic behaviour) we can write:

$$e^{-(\Delta U_0 + b\sigma)/RT} \equiv e^{-\frac{\Delta U_0}{RT}} (1 - \frac{b\sigma}{RT}); \qquad b\sigma << RT. \tag{2.6}$$

With (2.2) and (2.4) this yields

$$n_1 - n_{10} = \frac{n}{4} \frac{b\sigma}{RT} \cosh^{-2} (\frac{\Delta U_0}{2RT}) . \tag{2.7}$$

So the result of applying stress σ is that $n_1 - n_{10}$ molecules 'move from one well into the other' (if $b > 0$ from II to I, see Fig. 1). Each molecule doing so absorbs an energy $b\sigma$ from the mechanical stress field (Eq. (2.1)). The total work thus equals:

$$w(\sigma) = (n_1 - n_{10})\, b\sigma = \frac{n}{4} \frac{b^2\sigma^2}{RT} \cosh^{-2} (\frac{\Delta U_0}{2RT}) . \tag{2.8}$$

We now have to integrate over all possible b values between $-\infty$ and $+\infty$. Let N be the total number of molecules per unit volume and $n(b)db$ the number of molecules with b values between b and $b + db$ (the assembly considered above). Writing:

$$B = \int_{-\infty}^{+\infty} \frac{n(b)b^2}{N}\, db \tag{2.9}$$

the total work performed by the stress per unit volume is then found as:

$$W(\sigma) = \frac{NB\sigma^2}{4RT} \cosh^{-2} (\frac{\Delta U_0}{2RT}) . \tag{2.10}$$

Another formula for $W(\sigma)$ can be found from the linear viscoelastic theory [5], [6]. Suppose that the constant stress σ is applied at time $t = 0$. The instantaneous elastic energy is not contained in $W(\sigma)$ since this quantity pertains to the delayed change of the distribution of the molecules over the two wells. So, $W(\sigma)$ is equal to the

mechanical work per unit volume performed between $t = 0^+$ and $t = \infty$, i.e.:

$$W(\sigma) = \sigma^2 \, \Delta J \tag{2.11}$$

where:

$$J(t) = \text{creep compliance} \tag{2.12}$$

$$\Delta J = J_\infty - J_0 = \text{retardation strength} \tag{2.13}$$

$$J_\infty = J(t = \infty); \; J_0 = J(t = 0). \tag{2.14}$$

Combining (2.10) and (2.11) we find:

$$\Delta J = \frac{NB}{4RT} \cosh^{-2} \left(\frac{\Delta U_0}{2RT}\right) . \tag{2.15}$$

In the subsequent sections, we will often deal with the relaxation strength ΔG defined by:

$$\Delta G = G_0 - G_\infty \tag{2.16}$$

$$G(t) = \text{stress relaxation modulus} \tag{2.17}$$

$$G_0 = G(t = 0); \; G_\infty = G(t = \infty) . \tag{2.18}$$

Because [5], [6]:

$$G_0 = 1/J_0 ; \; G_\infty = 1/J_\infty \tag{2.19}$$

we have:

$$\Delta G = G_0 \, G_\infty \, \Delta J . \tag{2.20}$$

For weak relaxations, we have:

$$\Delta J \ll J_0 . \tag{2.21}$$

This yields:

$$J_0 \sim J_\infty ; \; G_0 \sim G_\infty \tag{2.22}$$

$$\Delta G \sim G_0^2 \, \Delta J = \frac{NBG_0^2}{4RT} \cosh^{-2} \left(\frac{\Delta U_0}{2RT}\right) . \tag{2.23}$$

Consequently, the strong dependence on T and ΔU_0 due to the $\cosh^{-2} (\Delta U_0/2RT)$ term in Eqs (2.15) and (2.23) will similarly be found in ΔG and ΔJ. Both quantities are proportional to each other (for weak relaxations).

In the sequel, we also require a formula for the relaxation time τ of the process. As usual, we write:

$$\frac{dn_1}{dt} = -n_1 k_{12} + n_2 k_{21} \tag{2.24}$$

where n_1 and n_2 are the populations in wells I and II, respectively, and k_{12} and k_{21} the transition probabilities. Using:

$$n_1 + n_2 = n = \text{constant} \tag{2.25}$$

we find:

$$\frac{dn_1}{dt} = -n_1 (k_{12} + k_{21}) + nk_{21} . \tag{2.26}$$

In equilibrium $(t \to \infty)$ we have $dn_1/dt = 0$. For the equilibrium value $n_{1\infty}$ of n_1 we thus have:

$$n_{1\infty} = n \frac{k_{21}}{k_{12} + k_{21}} . \tag{2.27}$$

Combining (2.26) and (2.27), we obtain:

$$\frac{d(n_1 - n_{1\infty})}{dt} = - \frac{n_1 - n_{1\infty}}{\tau} \tag{2.28}$$

where:

$$\tau = 1/(k_{12} + k_{21}) . \tag{2.29}$$

According to Fig. 1B, we have:

$$k_{12} = \nu_0 e^{-(H + \Delta U_0)/RT} \tag{2.30}$$

$$k_{21} = \nu_0 e^{-H/RT} \tag{2.31}$$

where ν_0 is some frequency factor.

Combining (2.29) - (2.31), we find:

$$\tau = \tau_0 e^{+H/RT} / [1 + e^{-\Delta U_0/RT}] \tag{2.32}$$

$$\tau_0 = 1/\nu_0 . \tag{2.33}$$

Eq. (2.32) shows that τ hardly depends on the energy difference ΔU_0. When ΔU_0

varies from 0 to ∞, the resulting change in τ is a factor of 2 only. Such a change is small compared to the many-order-of-magnitude changes in τ produced by changes in temperature. Consequently, we can approximate Eq. (2.32) by:

$$\tau \sim \tau_0 \, e^{H/RT} \tag{2.34}$$

which shows that τ is determined by the energy level of the highest well (see Fig. 1).

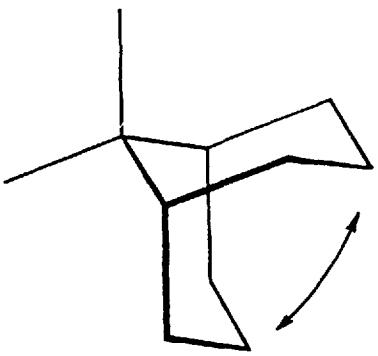

Fig. 2. The chair-chair transition of the cyclohexylgroup

3. Heijboers Problem [3]

Heijboer studied the mechanical relaxation due to the chair-chair transition of cyclohexyl rings (see Fig. 2). The rings were 'embedded' in the polymer matrix in different ways: as side groups on polymer chains of different types (e.g. as polycyclohexylmethacrylate) or as part(s) of plasticizer molecules in different polymeric matrices (e.g. dicyclohexylphthalate in polymethylmethacrylate). Low molecular weight liquids such as cyclohexanol were also considered. So, the study embraced a wide variation of the immediate environment of the relaxing molecule (cyclohexyl group, further abbreviated as CH-group).

A second variable considered was the concentration of CH-groups per unit volume. This was achieved by varying the concentration of the CH-containing plasticizer or by copolymerization of CH-containing monomers with other monomers in different ratios.

The third variable considered was the conformational energy difference ΔU_0 (see Fig. 1 and Eq. (2.15)). This was achieved by varying the chemical structure of the substituents to the ring; the range for ΔU_0 was from 0 to 14 kJ/mol. The ΔU_0 values were obtained from NMR measurements on the corresponding small molecules.

The fourth variable considered was the 'size' of the moving group; by adding substituents, the 'sweeping volume' connected to the chair-chair transition could be varied over a wide range.

The relaxation was measured mechanically; the parameters obtained were relaxation strength ΔG, activation energy ΔH_0, and relaxation time τ, all as functions of temperature and frequency. In some cases the frequency was varied over more than 10 orders of magnitude (10^{-4} Hz to 10^{6} Hz). An example of the data for one particular polymer is given in Fig. 3.

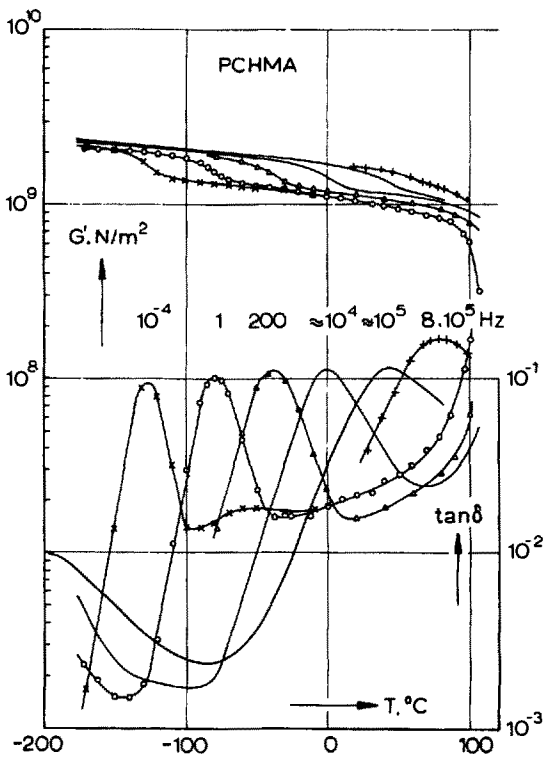

Fig. 3. Shear modulus G' and damping tan δ as functions of temperature at six frequencies for polycyclohexylmethacrylate (after [3])

The main conclusions from Heijboer's work were the following:

1. Relaxation strength ΔG is simply proportional to the number of CH-groups per unit volume (see Fig. 4) and independent of the local environment of the group. As shown in Fig. 4, it does not matter whether the CH-group is part of a plasticizer molecule or part of the side chain in a plasticized or non-plasticized polymer.
2. The plot of frequency of maximum loss (cf. Fig. 3) vs. 1/T is insensitive to the local environment of the CH-group. An example is given in Fig. 5; obviously it does not matter whether the CH-group is part of the methacrylate polymer, the acrylate polymer (much lower Tg than the first) or even *liquid* cyclohexanol.

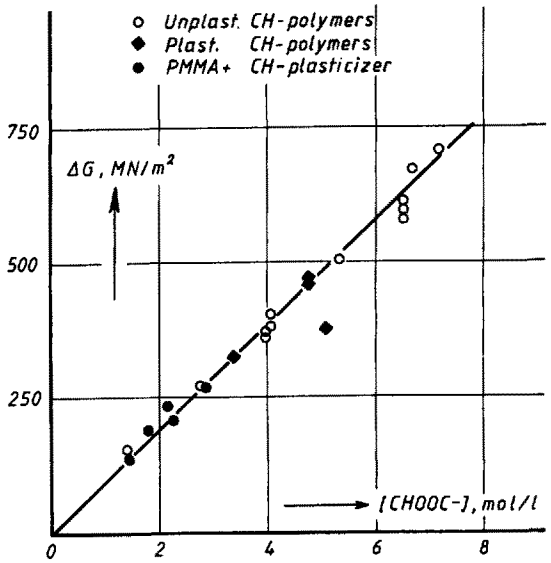

Fig. 4. Relaxation strength of cyclohexylmotion vs. CH-concentration for polymers containing the cyclohexyloxycarbonyl group in the polymer or in the plasticizer. For details and data see [3]. For all materials, ΔU_0 was the same (0.7 kcal/mol)

3. In the framework of the theory of Section 2, conclusion 1 implies that ΔU_0 is independent of the local environment of the CH-group (Eq. (2.23) tells that the relaxation strength strongly depends on ΔU_0). Further, conclusion 2 implies that the parameters τ_0 and H in Eqs (2.23) - (2.34) are also independent of the local environment of the CH-group. In the square well model used in Section 2, the potential energy curve is completely specified by ΔU_0 and H (see Fig. 1B). So, the inevitable conclusion follows that the potential energy curve is independent of the local environment and thus a (intramolecular) property of the molecule itself (at least this follows if we use the theory of Section 2 for the interpretation of Heijboer's data).

4. If the potential energy curve is a property of the CH-group itself, it can be determined by e.g. NMR measurements on the corresponding low-molecular weight substances. This has been done, and so, Heijboer could obtain the ΔU_0 values for his polymeric materials (cf. Table 7.1 of [3]). The range of variation of ΔU_0 was from 0 to 14 kJ/mol.

5. According to Eq. (2.23), the relaxation strength has to decrease strongly with increasing ΔU_0 ($\cosh^{-2}$ term). A comparison between theory and experiment is shown in Fig. 6. Obviously, the agreement between theory and experiment is only qualitative; the actual decrease in ΔG is much less than the predicted one.

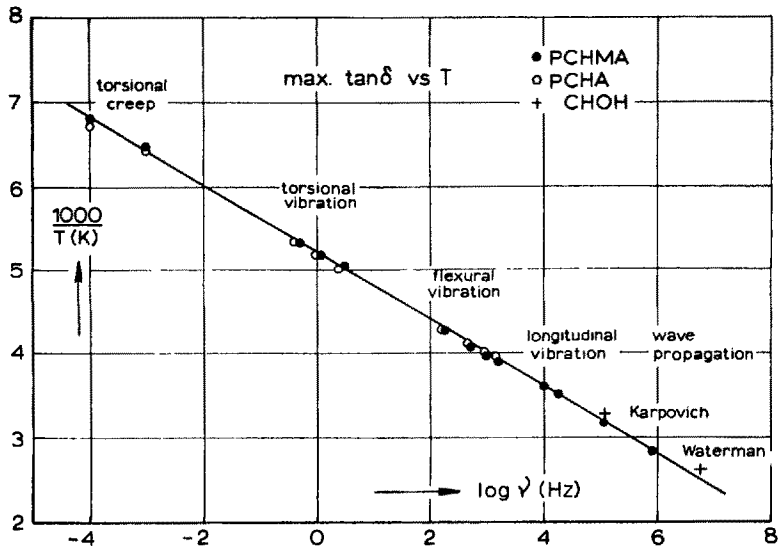

Fig. 5. Arrhenius plot for the frequency ν of maximum loss (tan δ) in polycyclohexylmethacrylate (PCHMA), polycyclohexylacrylate (PCHA) and cyclohexanol (CHOH). After [3]

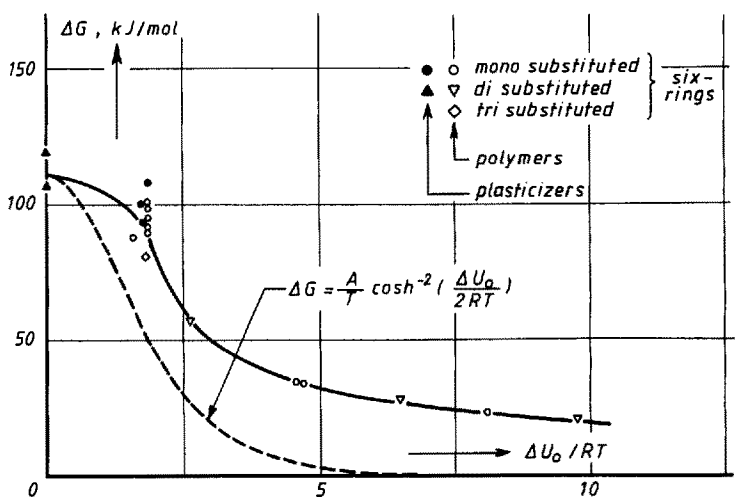

Fig. 6. Relaxation strength ΔG per mol CH-groups at 1 Hz as a function of $\Delta U_o/RT$. For details see [3]

6. A much more serious disagreement between theory and experiment is obtained when we consider the temperature dependence of ΔG (experimentally, this is done by measurements at widely different frequencies, cf. Fig. 3). Eq. (2.23) tells us that for ΔU_o values differing from 0, ΔG will (strongly) depend on temperature. A plot of the function of Eq. (2.23) is given in Fig. 7. It is quite clear that for ΔU_o values of 1-4 kcal/mol ($\sim$4-16 kJ/mol), ΔG should strongly

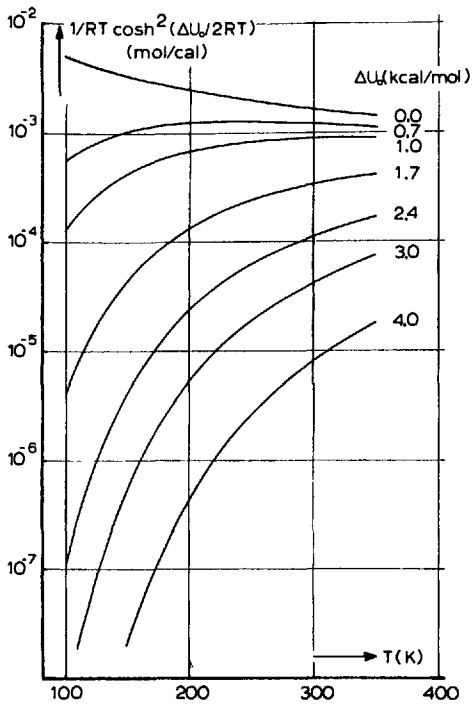

Fig. 7. Plot of relaxation strength vs. temperature for various ΔU_0 values; formula according to Eq. (2.23). After [3]

increase with temperature. Nothing of such an effect has been found, however. Fig. 8 shows ΔG vs. T for ΔU_0 values between 0.6 and 2.4 kcal./mol. In all cases, ΔG slowly decreases with temperature and for all polymers in about the same way.

So, the final conclusion must be that in some basic aspects the model of Section 2 is in partial or complete disagreement with experiment.

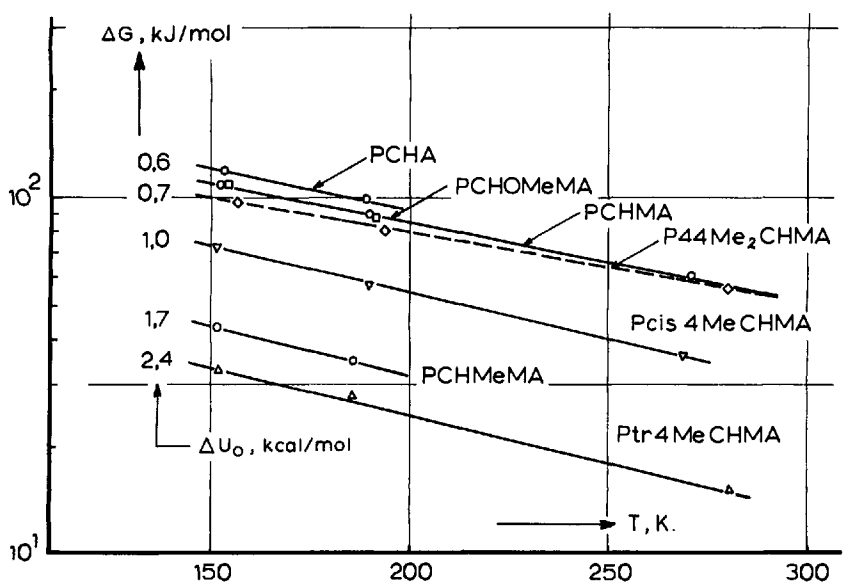

Fig. 8. Relaxation strength ΔG vs. temperature for cyclohexyl rings with different ΔU_0 values. After [3]

4. Inconsistencies in the Usual Two-Potential-Well Model

That Heijboer encountered the problems described at the end of Section 3 is not surprising. The model of Section 2 and particularly the way in which it was used in Section 3 is so inconsistent that it is, in fact, surprising that still some agreement is found with experiment. To understand this, we return to point 3 in Section 3. It was concluded that the potential energy curve was independent of the local environment of the CH-group. This conclusion, however, cannot be maintained. If $U(x)$ is independent of the local environment, there is no coupling between the CH-group and its environment and there will be no mechanical relaxation at all. So the conclusion drawn at the end of point 3 has 'blown up' the whole theory; if we neglect this, as was done in Section 3, we should not be surprised that we encounter serious problems (points 5 and 6 of Section 3).

It should be realized that without (mechanical) coupling, the $b\sigma$ term in Eq. (2.1) loses its physical meaning. If it is maintained, as is usally done, we implicitly assume that mechanical stresses act as electrical fields, i.e. from a distance through vacuum.

Further, the whole idea of no (strong) mechanical coupling with the environment is unrealistic. Only in two cases coupling can be neglected:

a) if the environment rearranges much faster than the CH-group, the populations over wells I and II will be determined by the intramolecular potential only. But, in the glassy state we have exactly the opposite situation: the CH-group rearranges rapidly and the environment is very slow (glassy);

b) if the CH-group has a free-volume package around it so large that it can move freely. The required free-volume can be estimated as 50 cm^3/mol. For polycyclohexylmethacrylate, this would imply some 300 cm^3/kg. On the basis of density-values, this is a highly unrealistic assumption.

So, we have to accept a (strong) mechanical coupling of the relaxing group with its environment and our real problem is to harmonize this with the experimental findings (conclusions 1-3 of Heijboer) which apparently point in exactly the opposite direction. A proposal to solve this problem is given in Section 5.

It should finally not be forgotten that the theory of Section 2 is limited in still another way. It is a 'dilute solution theory' in which interactions between different relaxing groups are ignored. We will not consider this point in the present paper.

5. Proposal for a New Model

5.1. Interaction of the relaxing group with its environment

We assume that the molecule responsible for relaxation is mechanically coupled with its environment; actually, that it is fixed to and embedded in an elastic matrix. A transition from state I to state II results in a deformation/shearing of the matrix. Most of the stress field is localized, just as around point defects in crystalline solids.

The stress pattern due to a change from state I to II is denoted by $\Delta\sigma_{ij}(x,y,z)$. It is completely determined by the geometrical changes connected to the transition I → II and by the elastic constants of the matrix (we assume that the matrix behaves linearly elastic). The geometrical changes being known from molecular models, the elastic constants being known from measurements, $\Delta\sigma_{ij}$ can be calculated (e.g. by finite element methods).

Localized stress fields are not only generated by the transition from I to II, they will also exist in the states I and II. We denote these stress fields by $\sigma_{ij1}(x,y,z)$ and $\sigma_{ij2}(x,y,z)$; obviously quantity $\Delta\sigma_{ij}$ discussed above is given by:

$$\Delta\sigma_{ij} = \sigma_{ij2} - \sigma_{ij1} \,. \tag{5.1}$$

The stresses σ_{ij1} and σ_{ij2} depend on the exact way in which the relaxing molecule is packed in the matrix in states I and II, respectively. Therefore, σ_{ij1} and σ_{ij2} are not obtained as easily as $\Delta\sigma_{ij}$; to find σ_{ij1} and σ_{ij2} we have to consider the history of the glassy environment and the way in which this environment has been formed (Section 5.4).

Stress σ_{ij1} will be zero when the molecule exactly fits in its environment in state I; σ_{ij2} is then non-zero. Similarly, σ_{ij2} will be zero for perfect fitting in state II. Obviously, only one of the two stresses can be zero, and for generality we assume that both are non-zero.

The stress fields σ_{ij1} and σ_{ij2} give rise to deformation energies E_1 and E_2 in the matrix. For state I, the deformation energy is denoted by E_1, for II by E_2. These energies can be found from the stress fields [7]:

$$\text{Energy} = \iiint \left\{ \frac{1}{2E}\left(\sigma_x^2+\sigma_y^2+\sigma_z^2\right) - \frac{\nu}{E}\left(\sigma_x\sigma_y+\sigma_y\sigma_z+\sigma_x\sigma_z\right) + \right. \\ \left. + \frac{1}{2G}\left(\tau_{xy}^2+\tau_{xz}^2+\tau_{yx}^2\right)\right\} dx\,dy\,dz \tag{5.2}$$

where: E = Young's modulus of matrix*)

G = shear modulus

ν = Poisson ratio

σ_x, σ_y, σ_z, τ_{xy}, etc., are the components of σ_{ij} .

The integration should be performed over the whole sample. To find E_1 , we have to substitute σ_{x1}, σ_{y1}, σ_{z1}, etc., to find E_2 we substitute σ_{x2}, σ_{y2}, σ_{z2}, etc.

Since σ_{ij1} and σ_{ij2} are not (a priori) known, E_1 and E_2 are unknown also (see Section 5.4 - 5.7). A quantity that can, however, be calculated directly is the energy parameter ΔE defined as $E_2 - E_1$ for the *special case* that state I is stress free. We then have $E_1 = 0$ and to calculate $E_2 = \Delta E$ we can substitute the (known) stress components $\Delta\sigma_{ij}$ in the integral of Eq. (5.2). This parameter ΔE plays an important role in the sequel, we therefore first try to find an estimate for ΔE .

For the chair-chair transition of the cyclohexylring (Fig. 9) we assume that a volume a^3 is sheared by 100%; a will be of the order of 0.4 nm. This value exceeds the values of 0.22 and 0.25 nm given in Fig. 9 because also part of the environment will be sheared strongly. With $G = 2 \times 10^9$ N/m^2 and $N_A = 6 \times 10^{23}$/mol we find:

$$\Delta E = \frac{1}{2} G a^3 N_A = 38 \text{ kJ/mol}. \qquad (5.3)$$

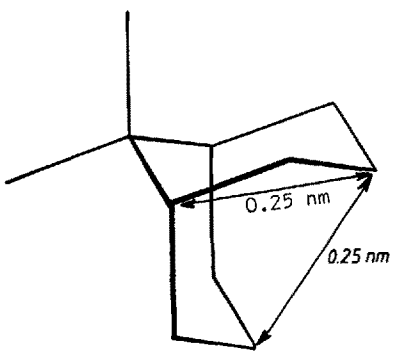

Fig. 9. On the calculation of ΔE for the cyclohexylring (for details, see text)

This value for ΔE is a very crude approximation, but it can be used for an order-of-magnitude comparison with other energy values. In Heijboer's tests, T varied between 150 and 300 K. So, RT varied between 1.3 and 2.5 kJ/mol, thus:

$$\Delta E >> RT . \qquad (5.4)$$

*) We use symbol E both for energy and Young's modulus. This will not give rise to confusion, the meaning will be clear from the context.

Further, Heijboer's ΔU_0 varied between zero and 14 kJ/mol. So, we have:

$$\Delta E > \text{ or } >> \Delta U_0 \ . \tag{5.5}$$

Finally, the experimental activation energy ΔH for the chair-chair transition was found to be 47 kJ/mol. Consequently:

$$\Delta E \sim \Delta H \ . \tag{5.6}$$

So, we learn that the coupling energy is of the order of the activation energy, much greater than RT and greater or much greater than ΔU_0 .

5.2 Description of the relaxation process

To describe the relaxation of the molecule, we add the deformation energy to the intramolecular potential $U(x)$. An illustration is given in Figs 10 and 11. For the cyclohexylrelaxation we take as 'reactioncoordinate' x the position of the tip of the ring; it is x_1 in state I and x_2 in state II (Fig. 10). The deformation energy continuously varies with x and is written as $E(x)$. It can be calculated with (5.2) if the stress field (also a function of x) is known. The total energy $F(x)$ is the sum of the intra-molecular energy $U(x)$ and the coupling energy $E(x)$:

$$F(x) = U(x) + E(x) \ . \tag{5.7}$$

The energy curves are given in Fig. 11 which is comparable to Fig. 1. Fig. 11A gives the continuous curves, Fig. 11B gives the square well approximation. In the latter approximation, the energies in states I and II are:

$$F_1 = U_1 + E_1 \tag{5.8}$$

$$F_2 = U_2 + E_2 \tag{5.9}$$

$$\Delta F = F_2 - F_1 = \Delta U + (E_2 - E_1). \tag{5.10}$$

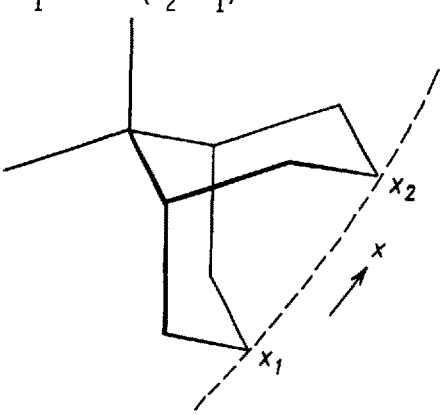

Fig. 10. Chair-chair transition of cyclohexylring, definition of coordinate x

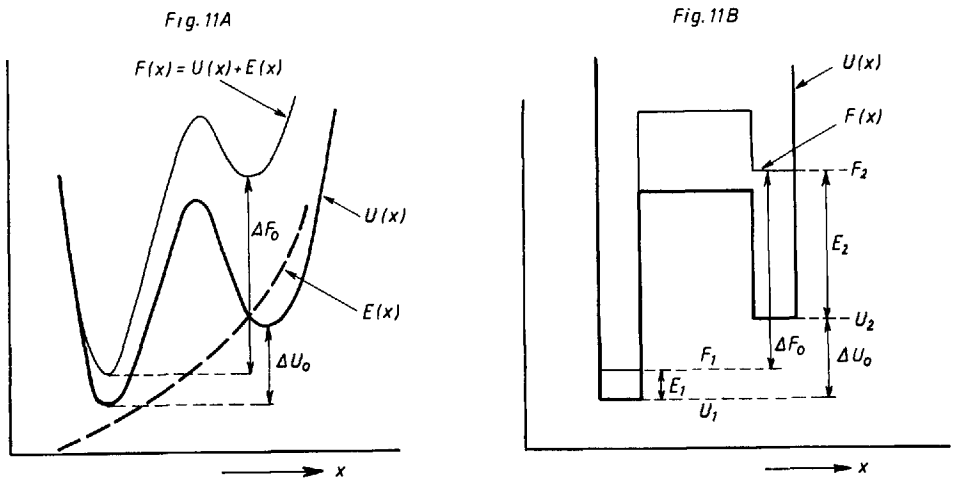

Fig. 11. Illustration of the modified two-potential well model. The curves are given for *zero external stress*. Fig. 11A shows the smooth curves, Fig. 11B the square well approximation

Since ΔE is of the order of the activation energy and greater than ΔU_0 (Eqs (5.5) - (5.6)), the potential energy curve of the molecule is heavily distorted by the coupling with the environment (cf. Fig. 11A). How this harmonizes with the experimental finding that the CH-relaxation is almost insensitive to the environment is discussed in Section 5.3.

We now have to incorporate the external stress into the theory, i.e. we have to find an interpretation for Eq. (2.1) or to derive an alternative. We proceed as follows: Take as example an external tensile stress σ_0 in the x-direction*). This stress is added to the internal stresses σ_{ij1} and σ_{ij2}, so in Eq. (5.2) the internal stresses σ_{x1} and σ_{x2} are increased by an amount σ_0; all other stress components remain unchanged. This leads to:

$$E_1(\sigma_0) - E_1(\sigma_0 = 0) = \frac{1}{2}\frac{\sigma_0^2 V}{E} + \sigma_0 \iiint \varepsilon_{x1}\, dxdydz \qquad (5.11)$$

$$E_2(\sigma_0) - E_2(\sigma_0 = 0) = \frac{1}{2}\frac{\sigma_0^2 V}{E} + \sigma_0 \iiint \varepsilon_{x2}\, dxdydz \qquad (5.12)$$

where: V = volume of sample (5.13)

$$\varepsilon_{x1} = \frac{1}{E}[\sigma_{x1} - \nu(\sigma_{y1} + \sigma_{z1})] \qquad (5.14)$$

$$\varepsilon_{x2} = \frac{1}{E}[\sigma_{x2} - \nu(\sigma_{y2} + \sigma_{z2})]. \qquad (5.15)$$

*) This space coordinate x should not be confused with the reactioncoordinate x of Figs 10 and 11.

Subtracting (5.12) from (5.11) and writing σ instead of σ_0 we find:

$$\Delta F(\sigma) = \Delta U_0 + [E_2(\sigma) - E_1(\sigma)] = \Delta F_0 + b\sigma \tag{5.16}$$

where:

$$\Delta F_0 = \Delta U_0 + [E_2(\sigma = 0) - E_1(\sigma = 0)] \tag{5.17}$$

$$b = \iiint \Delta\varepsilon_x \, dxdydz \tag{5.18}$$

$$\Delta\varepsilon_x = \varepsilon_{x2} - \varepsilon_{x1} \quad . \tag{5.19}$$

Eq. (5.16) replaces the original equation (2.1), and its form is almost identical. As in the conventional theory, the external stress σ changes the energy difference ΔF between states II and I and this change is proportional to σ. In contrast with the situation in Section 2, quantity b has a clear physical meaning (Eq. (5.18)) and can directly be calculated from $\Delta\sigma_{ij}$ ($\Delta\sigma_{ij}$ gives $\Delta\varepsilon_x$ through Eqs (5.14), (5.15) and (5.19)).

It will be clear that a reformulation of the theory of Section 2 on the basis of Eq. (5.16) (instead of Eq. (2.1)) will lead to identical results, provided that U_1 is replaced by F_1, U_2 by F_2, ΔU_0 by ΔF_0, etc. So, all results of Section 2 remain valid. The problem, however, is that we don't know the interaction energies E_1 and E_2; moreover, these energies may vary from molecule to molecule. We come back to this problem in Section 5.4.

5.3 The insensitivity of the cyclohexyl relaxation to the local environment of the ring

Experiments clearly show that the CH-relaxation is very insensitive to the local environment of the ring (points 1-3 of Section 3). This finding formed a strong barrier against the development of the present theory (how can strong coupling (Section 5.1) be harmonized with insensitivity to the environment?). Part of the solution will be given in Section 6, the other part will be given here.

The salient point is that for the cyclohexylring the energy curves of Figs 1A and 11A are unrealistic. The actual intramolecular energy $U(x)$ is as shown in Fig. 12: two relatively sharp minima (the two chair states) are separated by many intermediate (boat) states [8].

Fig. 12 also shows the coupling energy $E(x)$. In view of Eq. (5.6) we took $E_2 - E_1 = E(x_2) - E(x_1)$ comparable in magnitude to activation energy H: the actual course of $E(x)$ shown in Fig. 12 is arbitrary. As shown in Fig. 12, the energy curve of the molecule is heavily distorted by the mechanical coupling. Yet, the change in activation energy from H to H' is only limited. This change is of the order of

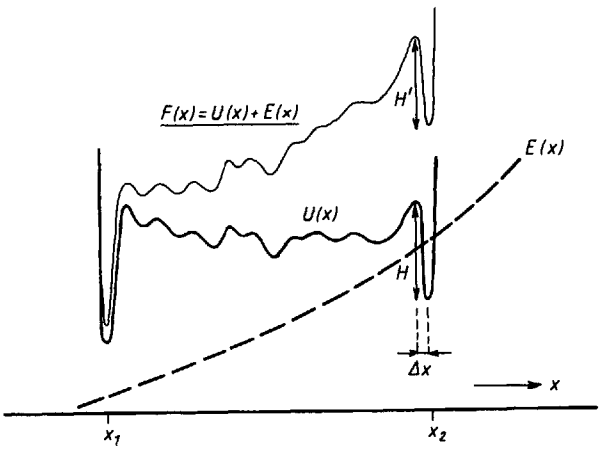

Fig. 12. Potential energy curve for the cyclohexylring; schematic, for details see text

$\Delta x\ dE(x)/dx$ (see Fig. 12); the sharper the wells are, the smaller the change will be. So, for the chair-chair transition of cyclohexyl, it is the relative sharpness of the wells that, at least partially, explains why the activation energy of the process is so insensitive to the environment. That τ_o (cf. Eq. (2.32)) shows a similar insensitivity, is obvious. τ_o is determined by the force constant d^2F/dx^2 for vibrations at the bottom of the well. Also this parameter becomes insensitive to $E(x)$ when the wells are sharp. That the relaxation strength ΔG is insensitive to the environment can not be derived from Fig. 12 (see Section 6).

It should be realized that the above reasoning is limited to molecules with an intramolecular potential as shown in Fig. 12. In other cases (cf. Fig. 11A and Section 6) the coupling energy may (strongly) change the activation energy of the process.

5.4 The fitting of the molecules in their environment; formation of the glass by cooling from above to below T_g

We will now show how the coupling energies E_1 and E_2 can be calculated. As discussed in Section 5.1, the molecule cannot perfectly fit in its environment for both states (I and II). Therefore, one of the two energies must be non-zero; for generality we assume that:

$$E_1 \neq E_2\ ,\ E_1 \neq 0,\ E_2 \neq 0. \tag{5.20}$$

We now start from the obvious fact that the glassy polymer once has been a liquid ($T > T_g$) and once has been prepared by cooling from above to below T_g. In almost all studies on secondary relaxation this fact is ignored and the glass is taken as given. Yet, the cooling from above to below T_g will turn out to be a keyfactor for

obtaining E_1 and E_2, and the final formulae for the relaxation strength will contain T_g as a parameter. So, in studying secondary processes, the glass transition cannot be disregarded.

Let us start with considering the molten state. The cyclohexylgroup will rapidly commute between states I and II, just as in the glass. The transitions occur at such a high frequency that the melt responds as a solid, i.e. the elastic stress fields around the moving molecule are then the same as in the glassy state.*) This is particularly so when the temperature is only slightly above T_g. The typical difference between melt and glass, however, is that the melt cannot withstand prolonged stationary stresses. Consequently, *the time average of the stresses produced by the commuting molecule must be zero for* $T > T_g$. This is achieved by slow adjustments of the (viscous) environment; the environment of the molecule changes until the fit in states I and II becomes such that the average stress produced on the environment is zero.

5.5 Derivation of the differential equation

To make the problem tractable, we assume that the matrix is linear elastic. We thus have (cf. Fig. 10):

$$E(x) = \frac{1}{2} S(x - x_0)^2 \ . \tag{5.21}$$

S is a stiffness parameter which, in principle, is known; it follows from the geometry of the CH-ring and the elastic constants of the matrix. Parameter x_0 is the unknown which we have to find. If x_0 is known, our problem is solved since we then have found the desired quantities $E_1 = E(x_1) = \frac{1}{2} S (x_1 - x_0)^2$ and $E_2 = E(x_2) = \frac{1}{2} S (x_2 - x_0)^2$ (cf. Section 5.2).

The 'force' $K(x)$ acting between CH-group and matrix can be defined as:

$$K(x) = \frac{dE}{dx} = S(x - x_0) \ . \tag{5.22}$$

We further define the quantities p_1 and p_2. These represent the time fractions the molecule is in states I and II, respectively. As in Section 2, we neglect the time fraction the molecule stays in the activated state. Thus:

$$p_1 + p_2 = 1 \qquad p_1 , \ p_2 > 0 \ . \tag{5.23}$$

The condition formulated in Section 5.4 (time average of stress must be zero) leads to:

*) Because of the higher temperature, the (unrelaxed) modulus of the (glassy) matrix may have decreased somewhat due to the thermal expansion; we neglect this here.

$$p_1 K_1 + p_2 K_2 = 0 \tag{5.24}$$

where K_1 and K_2 are the 'forces' in states I and II, respectively.

Eq. (5.24) shows that K_1 and K_2 must have opposite signs. Consequently, the coupling energy $E(x)$ has its minimum at the point $x = x_0$ somewhere between x_1 and x_2. This is depicted in Fig. 13; for the definition of x_1 and x_2, see Fig. 10.

Eqs (5.23) and (5.24) yield:

$$\frac{p_1}{p_2} = \frac{-K_2}{K_1} = \frac{x_2 - x_0}{x_0 - x_1} \quad . \tag{5.25}$$

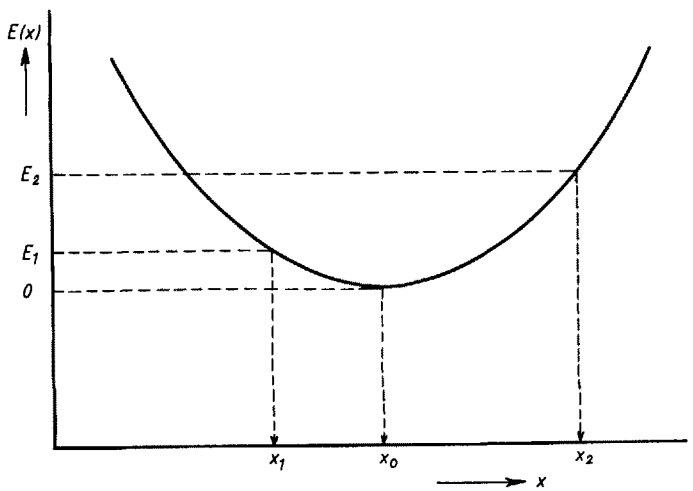

Fig. 13. Curve for the mechanical coupling energy $E(x)$; for details see text

Further, ratio p_1/p_2 follows from Boltzmann's formula:

$$\frac{p_1}{p_2} = e^{(\Delta U_o + E_2 - E_1)/RT} \quad . \tag{5.26}$$

Combining (5.21), (5.25) and (5.26) we find:

$$\frac{p_1}{p_2} = \frac{x_2 - x_0}{x_0 - x_1} = \exp\{(\Delta U_o + \tfrac{1}{2} S\,[(x_2 - x_0)^2 - (x_1 - x_0)^2])/RT\} \quad . \tag{5.27}$$

This is an equation for finding the *only unknown* variable x_0. All other quantities are determined; x_1 and x_2 from the geometry of the molecule, ΔU_o from the in-

tramolecular energy of the molecule and S from the elastic constants of the matrix combined with geometrical data of the molecule. If x_o is known, we know E_1 and E_2 (see above). So, x_o is the parameter that describes how the molecule fits in its environment. If $x_o = x_1$, the molecule fits exactly in position I, if $x_o = x_2$ there is perfect fit in position II, if $x_o = (x_1 + x_2)/2$ the molecule fits exactly just in the middle between x_1 and x_2, etc.

If $x_o = x_1$, we have the situation discussed in Section 5.1 in connection to the definition of parameter ΔE. Consequently:

$$\Delta E = \frac{1}{2} S (x_2 - x_1)^2 . \tag{5.28}$$

So, parameter S is connected to ΔE.

To simplify the mathematics, we now introduce the variable ξ defined by:

$$\xi = \frac{2x_o - (x_1 + x_2)}{x_2 - x_1} = \frac{x_o - (x_1 + x_2)/2}{(x_2 - x_1)/2} \tag{5.29}$$

or:

$$x_o = \frac{1}{2}(x_1 + x_2) + \frac{1}{2}\xi(x_2 - x_1) . \tag{5.30}$$

Quantity ξ tells how far x_o is removed from the symmetric position $\frac{1}{2}(x_1 + x_2)$. In fact, we have

$$-1 \leq \xi \leq +1 \tag{5.31}$$

$$\xi = -1 \quad \text{for} \quad x_o = x_1 \tag{5.32}$$

$$\xi = +1 \quad \text{for} \quad x_o = x_2 \tag{5.33}$$

$$\xi = 0 \quad \text{for} \quad x_o = \frac{1}{2}(x_1 + x_2) . \tag{5.34}$$

After some rearrangements, Eqs (5.27), (5.28) and (5.30) yield:

$$\frac{1 - \xi}{1 + \xi} = \exp\{(\Delta U_o - \xi \Delta E)/RT\} \tag{5.35}$$

which is the same equation as that for ferromagnetism [9].

5.6 Solution for $\Delta U_o = 0$; the splitting from 2 into 6 states

To find the solutions of Eq. (5.35) we first consider the special case of $\Delta U_o = 0$. Eq. (5.35) now reduces to:

$$\frac{1 - \xi}{1 + \xi} = e^{-\xi \Delta E/RT} . \tag{5.36}$$

We consider the functions $f(\xi)$ and $g(\xi)$ defined by:

$$f(\xi) = (1 - \xi)/(1 + \xi) \tag{5.37}$$

$$g(\xi) = \exp\left[-\frac{\Delta E}{RT}\,\xi\right] . \tag{5.38}$$

One obvious root of Eq. (5.36) is $\xi = 0$. To find possible other roots, we consider the functions:

$$F(\xi) = \ln f(\xi) \tag{5.39}$$

$$G(\xi) = \ln g(\xi) . \tag{5.40}$$

It is easily found that:

$$dF/d\xi = -\left(\frac{1}{1-\xi} + \frac{1}{1+\xi}\right) \tag{5.41}$$

$$d^2F/d\xi^2 = -\left[\frac{1}{(1-\xi)^2} - \frac{1}{(1+\xi)^2}\right] \tag{5.42}$$

$$dG/d\xi = -\frac{\Delta E}{RT} . \tag{5.43}$$

So, $dG/d\xi$ is negative and constant over the whole range $(-1 < \xi < +1)$. Further, $dF/d\xi$ is negative whilst $d^2F/d\xi^2$ is positive for $\xi < 0$ and negative for $\xi > 0$. The resulting course for G and F is given in Fig. 14.

Since $dF/d\xi = -2$ for $\xi = 0$, Eq. (5.36) will possess a single root $(\xi = 0)$ if $\Delta E/RT < 2$ and 3 roots when $\Delta E/RT > 2$. According to Eq. (5.4), $\Delta E/RT \gg 1$, so there will be three roots in general: ξ_1 between -1 and 0, $\xi_2 = 0$, and ξ_3 between 0 and $+1$. Moreover, if $\Delta E/RT \gg 1$, roots ξ_1 and ξ_3 will be close to -1 and $+1$ respectively. As can easily be verified (Eq. (5.36)), we then have

$$\xi_1 - (-1) \sim 1 - \xi_3 \sim 2e^{-\Delta E/RT} \ll 1 . \tag{5.44}$$

The occurrence of three roots implies that the group can fit in its environment in 3 different ways, all fulfilling the requirement of Eqs (5.24):

1. $\xi_1 \cong -1$ i.e. $x_0 \sim x_1$. The molecule fits almost perfectly in its environment for state I. For the energy levels we find $E_1 \sim 0$ and $E_2 \sim \Delta E$. This follows from Eqs (5.21), (5.28) and (5.29):

$$E_1 = \frac{1}{2}S\,(x_1 - x_0)^2 = \frac{\Delta E}{4}\,(1 + \xi)^2 \tag{5.45}$$

$$E_2 = \frac{1}{2} S (x_2 - x_0)^2 = \frac{\Delta E}{4} (1 - \xi)^2 \qquad (5.46)$$

2. $\xi_3 \cong +1$ i.e. $x_0 \sim x_2$. The molecule now almost perfectly fits for state II. For the energies we find $E_1 \sim \Delta E$, $E_2 \sim 0$.

3. $\xi_2 = 0$ i.e. $x_0 = \frac{1}{2}(x_1 + x_2)$. In this case, the molecule exactly fits for an x_0-value just in the middle between x_1 and x_2. For the energies we find $E_1 = E_2 = \Delta E/4$.

In the molten polymer, we thus have to distinguish between *three types of molecules:* types 1 and 3 (ξ_1 and ξ_3) are asymmetrically fitted in their environment and have a large energy difference $\Delta E >> RT$ between states I and II; type 2 is symmetric. A summary of these results is given in Table 1: the distribution over the 3 types (last column) was calculated with Boltzmann's formula.

The conclusion of this section is: due to the strong coupling with the environment ($\Delta E >> RT$), the 2 states (I and II) split into $6 = 3 \times 2$ states. So we have the states i_I, i_{II} with $i = 1,2$ or 3. On the short time scale of the secondary motion I$\rightleftharpoons$II transitions are only possible without change in i (type number). On the long time scale (relaxation of the environment) also the type number i (i.e. x_0) may change.

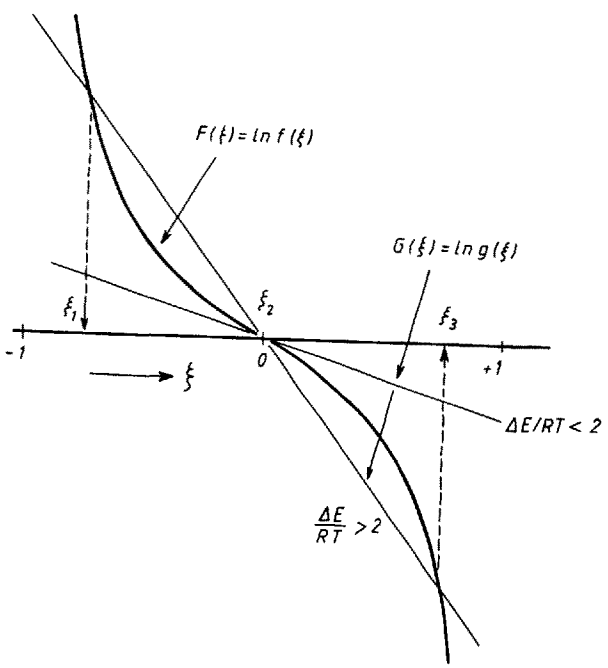

Fig. 14. On the roots of Eq. (5.36); for details see text

Table 1: Data for the 3 types of molecules in the molten polymer; special case of $\Delta U_o = 0$; $\Delta E/RT \gg 1$

Type	ξ	F_1 *)	F_2 *)	fraction of types 1,2, and 3 +)
1	~ -1	~ 0	$\sim \Delta E$	$(1+e^{-k})/Q$
2	0	$\frac{\Delta E}{4}$	$\frac{\Delta E}{4}$	$(2e^{-k/4})/Q$
3	$\sim +1$	$\sim \Delta E$	~ 0	$(1+e^{-k})/Q$

*) $F = U + E$ (see Eq. (5.7)); for simplicity we took $U_1 = 0$; because $\Delta U_o = 0$ we thus have $U_2 = 0$.

+) $k = \Delta E/RT$ and $Q = 2[1 + e^{-k} + e^{-k/4}]$.

5.7 Solution for the Case $\Delta U_o > 0$ and $\Delta E \gg \Delta U_o$

The general case of $\Delta U_o > 0$ can be analysed in the way described in Section 5.6. Depending on the magnitudes of ΔE and ΔU_o, the number of roots may be 1,2 or 3; for $\Delta E \gg \Delta U_o$, there will be 3 roots. The roots can easily be found numerically.

For the case $\Delta E \gg \Delta U_o$ which was suggested in Section 5.1, we can find an approximate analytical solution. As in Section 5.6, the roots ξ_1 and ξ_3 lie close to -1 and +1 respectively, and Eq. (5.44) is replaced by:

$$\xi_1 - (-1) \sim 2 \exp[-(\Delta E + \Delta U_o)/RT] \ll 1 \tag{5.47}$$

$$1 - \xi_3 \sim 2 \exp[-(\Delta E - \Delta U_o)/RT] \ll 1 \ . \tag{5.48}$$

By substituting $\xi = \xi_1 \sim -1$ and $\xi = \xi_3 \sim +1$, these equations follow immediately from Eq. (5.35).

Applying Eqs (5.45) and (5.46), we find the energies E_1 and E_2 for these two values of ξ. The results are given in Table 2; for state II we have added $U_2 = \Delta U_o$ to find the total energy F_2.

Root ξ_2 lies close to zero (for $\Delta E \gg \Delta U_o$; $\Delta E \gg RT$). By (carefully!) developing both sides of Eq. (5.35) into a Taylor series, we find the approximate solution:

$$\xi_2 \cong \frac{\Delta U_o}{\Delta E}\left(1 + 2\,\frac{RT}{\Delta E}\right) \cong \frac{\Delta U_o}{\Delta E} \ll 1 \ . \tag{5.49}$$

Table 2: Data for the three types of molecules in the molten polymer; $\Delta U_o > 0$, $\Delta E >> \Delta U_o$, $\Delta E >> RT$

Type	ξ	F_1 *)	F_2 *)	fraction of types 1,2, and 3 +)
1	~ -1	~ 0	$\sim \Delta U_o + \Delta E$	$[1 + e^{-(k+\lambda)}]/Q'$
2	$\sim \Delta U_o/\Delta E$	$\sim \frac{\Delta E}{4} + \frac{\Delta U_o}{2}$	$\sim \frac{\Delta E}{4} + \frac{\Delta U_o}{2}$	$2[e^{-(\frac{k}{4}+\frac{\lambda}{2})}]/Q'$
3	$\sim +1$	$\sim \Delta E$	$\sim \Delta U_o$	$[e^{-k} + e^{-\lambda}]/Q'$

*) $F = U + E$ (see Eq. (5.7)); $U_1 = 0$ $U_2 = \Delta U_o > 0$.

+) $k = \Delta E/RT$ $\lambda = \Delta U_o/RT$.

+) $Q' = 1 + e^{-(\lambda+k)} + 2e^{-(\frac{\lambda}{2}+\frac{k}{4})} + e^{-k} + e^{-\lambda}$.

For the energy levels Eqs (5.45), (5.46) and (5.49) yield:

$$E_1 \cong \frac{\Delta E}{4}\left(1 + \frac{\Delta U_o}{\Delta E}\right)^2 \cong \frac{\Delta E}{4} + \frac{\Delta U_o}{2} \tag{5.50}$$

$$E_2 \cong \frac{\Delta E}{4}\left(1 - \frac{\Delta U_o}{\Delta E}\right)^2 \cong \frac{\Delta E}{4} - \frac{\Delta U_o}{2} . \tag{5.51}$$

For the total energy $F = U + E$, we thus find:

$$F_1 = U_1 + E_1 = 0 + \frac{\Delta E}{4} + \frac{\Delta U_o}{2} = \frac{\Delta E}{4} + \frac{\Delta U_o}{2} \tag{5.52}$$

$$F_2 = U_2 + E_2 = U_o + \frac{\Delta E}{4} - \frac{\Delta U_o}{2} = \frac{\Delta E}{4} + \frac{\Delta U_o}{2} . \tag{5.52}$$

These values are given in Table 2; remarkably, the type 2 molecules are again symmetric, notwithstanding the fact that we started from $\Delta U_o > 0$.

5.8 Relaxation behaviour in the glassy state; solution of Heijboer's problem

In the preceeding sections we showed that at $T > T_g$ the two states (I and II) of the isolated (free) molecule split into 3×2 states. The distribution over the three types of molecules is given in Tables 1 and 2. For $T > T_g$, it changes with temperature.

If the material is now cooled to below T_g, the environment of each molecule becomes frozen and the molecule can no longer change its type (1,2 or 3). So, below T_g, the

distribution over the three types is given by the last columns of Tables 1 and 2; *provided that* T *is replaced by* T_g. Of course, the distribution over the two states within one type may still change with temperature below T_g (for $I \leftrightarrows II$ transitions within one type, x_o remains the same, i.e. there is no rearrangement of the environment).

To describe the relaxation in the glassy state, we apply the theory of Section 2, i.e. Eq. (2.15). We distinguish between the three types of molecules and for each we calculate the contribution to ΔJ; in formula:

$$\Delta J = \Delta J_1 + \Delta J_2 + \Delta J_3 \tag{5.54}$$

where ΔJ_1, ΔJ_2 and ΔJ_3 are the contributions of the type 1, 2 and 3 molecules respectively. For the N in Eq. (2.15) we substitute the fractions given in the last columns of Tables 1 and 2 multiplied by the total number of molecules per unit volume (N). For the energy difference ΔU_o in Eq. (2.15), we substitute the $F_2 - F_1$ values found from Tables 1 and 2. For the special case $\Delta U_o = 0$ (Table 1) we thus obtain:

$$\Delta J_1 = \Delta J_3 = \frac{BN}{4RT} \frac{1 + e^{-\frac{\Delta E}{RT_g}}}{Q(T_g)} \cosh^{-2}\left(\frac{\Delta E}{2RT}\right) \tag{5.55}$$

$$\Delta J_2 = \frac{BN}{4RT} \frac{2e^{-\Delta E/4RT_g}}{Q(T_g)} \quad . \tag{5.56}$$

Because the type 2 molecules are symmetric, the $\cosh^{-2}$ term is not contained in Eq. (5.56) $(\Delta F = F_2 - F_1 = 0)$.

Dividing ΔJ_1 by ΔJ_2, we obtain:

$$\frac{\Delta J_1}{\Delta J_2} = \frac{\Delta J_3}{\Delta J_2} = \frac{1 + e^{-\Delta E/RT_g}}{2e^{-\Delta E/4RT_g}} \cosh^{-2}\left(\frac{\Delta E}{2RT}\right) . \tag{5.57}$$

For $\Delta E >> RT_g > RT$ this reduces to:

$$\frac{\Delta J_1}{\Delta J_2} \sim 2e^{+\frac{\Delta E}{4RT_g}} e^{-\frac{\Delta E}{RT}} = 2 \exp\left[-\frac{\Delta E}{RT}\left(1 - \frac{T}{4T_g}\right)\right] . \tag{5.58}$$

For $T < T_g$, we have $1 - T/4T_g > 3/4$, so with $\Delta E >> RT$, Eq. (5.58) shows that

$\Delta J_1 = \Delta J_3 << \Delta J_2$. The same argument holds for the case of $\Delta U_o > 0$ and $\Delta E >> \Delta U_o$ (Table 2), so the general result is:

$$\Delta J_1 << \Delta J_2 \tag{5.59}$$

$$\Delta J_3 << \Delta J_2 \tag{5.60}$$

$$\Delta J \sim \Delta J_2 \ . \tag{5.61}$$

Using Table 2 we then finally obtain:

$$\Delta J \sim \Delta J_2 = \frac{BN}{4RT} \frac{2e^{-(\frac{\Delta E}{4} + \frac{\Delta U_o}{2})/RT_g}}{Q'(T_g)} \ . \tag{5.62}$$

According to Eqs (5.59) - (5.61), the type 1 and 3 molecules hardly contribute to the relaxation, in spite of the fact that the fraction of type 1 and 3 molecules will be (much) greater than that of the type 2 molecules (see last columns of Tables 1 and 2). The reason for this lies in the asymmetry of the type 1 and 3 molecules. The energy difference between the states I and II is large (order of ΔE, see Tables 1 and 2) and this difference enters into the $\cosh^{-2}$ term of Eq. (2.15). Therefore, the $\cosh^{-2}$ terms become very small and so the largeness of the fraction of the type 1 and 3 molecules is fully compensated.

Eqs. (5.59) - (5.62) immediately solve Heijboer's problems (point 5 and 6 of Section 3). In the glassy state, the relaxation is determined by the symmetric type 2 molecules. There will be no $\cosh^{-2}$ dependence on $\Delta U_o/RT$ and the relaxation strength will only vary in proportion with $1/T$ (see Eq. (5.62)). This solves point 6 of Section 3. To solve the problem of point 5 of Section 3, we consider how the retardation strength decreases with increasing ΔU_o. From Eq. (5.62) we find:

$$Z = \frac{\Delta J(\Delta U_o \neq 0)}{\Delta J(\Delta U_o = 0)} = \frac{Q(T_g)}{Q'(T_g)} e^{-\Delta U_o/2RT_g} \tag{5.63}$$

where Q and Q' can be found from Tables 1 and 2. With $\Delta E >> RT_g$ and $\Delta E >> \Delta U_o$ we find:

$$Q = 2\left[1 + e^{-\Delta E/4RT_g}\right] \tag{5.64}$$

$$Q' = 1 + 2e^{-(\frac{\Delta E}{4} + \frac{\Delta U_o}{2})/RT_g} + e^{-\Delta U_o/RT_g} \ . \tag{5.65}$$

Assuming further that also $e^{-\Delta E/4RT_g} << 1$, we finally obtain:

$$Q \sim 2 \tag{5.66}$$

$$Q' \sim 1 + e^{-\Delta U_o/RT_g} \tag{5.67}$$

$$Z \sim \frac{2e^{-\Delta U_o/2RT_g}}{1+e^{-\Delta U_o/RT_g}} = \cosh^{-1}\left(\frac{\Delta U_o}{2RT_g}\right) . \tag{5.68}$$

So, in agreement with experiment ΔJ and therefore also ΔG (cf. Eq. (2.23)) decreases with increasing ΔU_o; the origin lies in the decrease in the fraction of type 2 molecules. A quantitative comparison with experiment is given in Fig. 15. The data of Fig. 6 were replotted vs. $\Delta U_o/2RT_g$. For ΔG at $\Delta U_o = 0$ we took the empirical value of 113 kJ/mol. It is obvious that in Fig. 15 theory and experiment agree much better than in Fig. 6

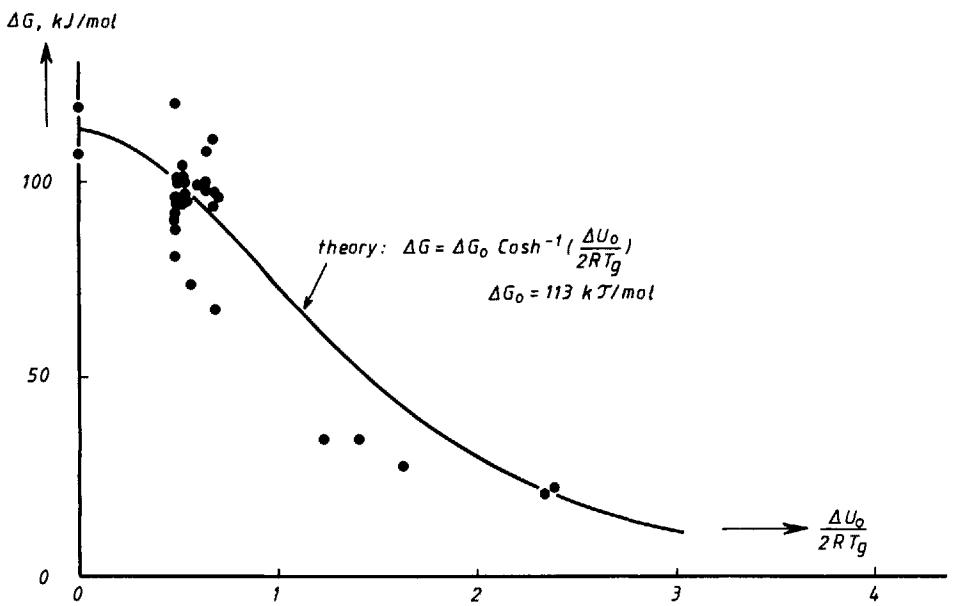

Fig. 15. Comparison of theory (Eqs (5.63) and (5.68)) and experiment; data from Table 7.1 of [3]

6. Discussion

With the present theory Heijboer's problem (Section 3) seems to be solved. Notwithstanding the strong coupling of the CH-group to its environment, the invariance of the activation parameters could be explained (Section 5.3). The predicted effect of

the intra-molecular energy difference ΔU_o is in quantitative agreement with experiment: relaxation strength ΔG decreases with $\cosh^{-1}$ $(\Delta U_o/2RT_g)$ (Fig. 15) and is independent of temperature for $T < T_g$, except for the slowly varying $1/T$ term (cf. Fig. 8).

A more comprehensive check of the theory is presently under way. Using finite element methods, we try to calculate ΔE and b from the geometry of the CH-ring and the elastic constants of the matrix. If ΔE and b (and thus B, Eq. (2.9)) are known, the relaxation strength for $\Delta U_o = 0$ can be calculated (Eqs (5.62) and (2.20)); it would be very satisfying to find the empirical value of 113 kJ/mol given in Fig. 15. Another advantage would be that we then no longer need the approximations ($\Delta E >> \Delta RT$, $\Delta U_o << \Delta E$) made in Sections 5.6 - 5.8; if ΔE is known, Eq. (5.35) can be solved numerically and ΔG can be calculated without further approximations.

A point not discussed so far is the insensitivity of ΔG on the environment of the CH-ring (point 1 of Section 3; in Section 5.3, the discussion was limited to the insensitivity of the activation parameters). According to Eq. (5.62) and Table 1, we find for $\Delta U_o = 0$ and $\Delta E >> RT_g$:

$$\Delta J = \frac{BN}{4RT} \frac{1}{[1 + \exp(\frac{\Delta E}{4RT_g})]} \quad . \tag{6.1}$$

This formula correctly predicts that ΔJ (and thus also ΔG) will be proportional to the number of CH-groups per unit volume (cf. Fig. 4). It further shows that ΔJ depends on the environment via its effect on ΔE. For the dependence of ΔJ on ΔE, Eq. (6.1) yields:

$$\frac{d \ln \Delta J}{d \ln \Delta E} = - \frac{\Delta E/4RT_g}{1 + \exp[-\Delta E/4RT_g]} \quad . \tag{6.2}$$

With the estimate of Eq. (5.3) we have $\Delta E = 38$ kJ/mol = 9 kcal/mol. For a T_g of 400 K, we find: $\Delta E/4RT_g = 2.8$. Consequently:

$$d \ln \Delta J/d \ln \Delta E \sim -2.6 \; . \tag{6.3}$$

So, if the variations in ΔE are small, the same will hold for the relative variations in ΔJ, although to a lesser extent (factor of 2.6 in Eq. (6.3)).

According to Section 5.1, ΔE will be proportional to the modulus of the matrix, i.e. to the modulus of the material in the absence of the CH-relaxation. This modulus was denoted by G_o in Section 2 and experimentally, this is the modulus found at temperatures below the CH-relaxation peak. Proportionality between ΔE and G_o implies that Eq. (6.3) can be rewritten as:

$$\frac{d \ln \Delta J}{d \ln G_o} \sim -2.6 \ . \tag{6.4}$$

Since ΔG is proportional to $G_o^2 \Delta J$ (Eq. (2.23)), Eq. (6.4) yields:

$$\frac{d \ln \Delta G}{d \ln G_o} \sim -0.6 \ . \tag{6.5}$$

Inspection of Heijboer's data [3] reveals that for the materials of Fig. 4 G_o varied only slightly (10-20%); together with Eq. (6.5) this explains why no effect of the environment on ΔG could be detected; the changes in G_o were too small.

The above reasoning implies that the insensitivity of ΔG is only apparent; large changes in matrix modulus would certainly have an effect. Further, the above reasoning started from a very crude estimate for ΔE (Eq. (5.3)); therefore the conclusion can have a qualitative value only.

Another point to be considered is that substituents to the CH-ring have little effect on ΔG. From the viewpoint of the free-volume package theory (Section 4, point b), this is difficult to understand: the package, already unrealistically large, should also grow in proportion to the 'sweeping volume' of the ring. From the present model the difficulty is much less serious. As illustrated in Fig. 16, the essential thing the ring does when it jumps from I to II is to produce a shear step of magnitude ΔZ. This shear step is independent of the substituents, it is a property of the ring itself. In the present model, we further assume that the ring is mechanically coupled to the environment. So, in a first approximation, it does not matter whether we consider the substituent (dashed in Fig. 16) as a part of the ring or as a part of the environment. So, in a first approximation, we would expect no effect of substituents on ΔG, just as found experimentally for substituents which are not large [3].

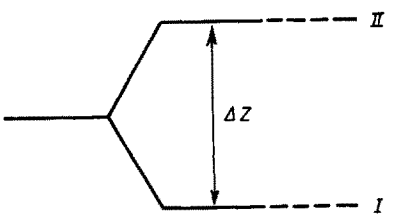

Fig. 16. On the effect of substituents (---) to the CH-ring (——); for explanation, see text

The approximation made above is too crude, however. The substituent is connected to the ring with covalent bonds. The ring is coupled to the environment by (weaker) v.d. Waals bonds and also the elastic constants of the environment (matrix) are due to the v.d. Waals bonds. Consequently, the substituent modifies the stress field in the environment; particularly with long and stiff substituents, ΔE will increase above its value for the simple CH-ring and ΔG will decrease. This effect has indeed been

found for phenyl-ring substituents (Fig. 7.11 of [3]). The critical substituent size can be estimated as follows: the environment is not a continuum; it consists of 'particles' with a 'grain size' comparable to ΔZ. These particles are monomer units, side chains, other CH-groups, etc. The particles consist of covalently bonded atoms and are bonded together by v.d. Waals forces. This suggests that the stress field around the substituted CH-ring will be influenced by the substituent when its size exceeds the 'grain size' of the environment.

Let us finally consider some corollaries.

1. Effect of physical aging on secondary relaxation. In [10], we showed that changes in free volume as produced by changes in thermal history do not affect secondary relaxations. This finding was explained from the free-volume package theory mentioned in Section 4 under point b. The present theory predicts the same result, although from an entirely different basis. We now say: the molecule is completely coupled to its environment; changes in free volume cannot make the coupling better than complete, so these changes will have no effect.

2. Effect of steric hindrance on secondary relaxations. An increase in steric hindrance may have the peculiar effect shown in Fig. 17. The diagram shows loss factor tan δ vs. temperature; β denotes the secondary peak, α the glass-rubber transition. It is known for decades (see e.g. [11]) that an increase in steric hindrance does not change the position of the β-peak on the temperature scale; only its height is decreased and this is accompanied by an increase in height of the α-peak; the α-peak may also shift to higher temperatures (not shown). Experiment thus suggests that the molecule has only two possibilities: it either contributes to the β-peak or to the α-peak, there is nothing in between

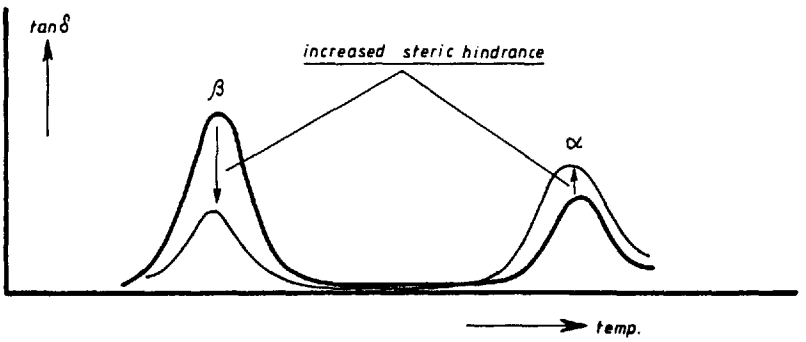

Fig. 17. Effect or steric hindrance; schematic, for explanation see text

The pecularity shown in Fig. 17 is exactly what the present model predicts. The molecule can either be of type 2 or of types 1 and 3. Only the type 2 molecules contribute to the β-relaxation and their activation parameters hardly depend on steric hindrance (= coupling energy ΔE; for the CH-ring see Section 5.3, for the more

general case see point 3 below). So, the position of the β-peak on temperature scale will be (almost) independent of steric hindrance. This factor, however, determines ΔE and with increasing ΔE, the fraction of type 2 molecules will decrease and so will do the height of the β-peak. The type 1 and 3 molecules will not contribute to the β-peak; their fraction increases with ΔE and their contribution to tan δ is found at temperatures above T_g .

3. Effect of mechanical coupling on the activation parameters (general case).
Due to the typical intramolecular energy curve of cyclohexyl (Fig. 12) we could argue (Section 5.3) that the coupling has only a limited effect on the activation energy. The more general case will be discussed now. We consider the $U(x)$ curve shown in Fig. 18; for simplicity we take a symmetric molecule ($\Delta U_0 = 0$). For secondary relaxations we only have to consider the type 2 molecules (see Section 5.8). The coupling energy $E(x)$ will be zero for a $x = x_0$ just in the middle between x_1 and x_2. The barrier height will not be changed and the energy levels in states I and II will be increased to $\Delta E/4$ (Table 1). Consequently, the activation energy will decrease from H to H':

$$H' = H - \Delta E/4. \tag{6.6}$$

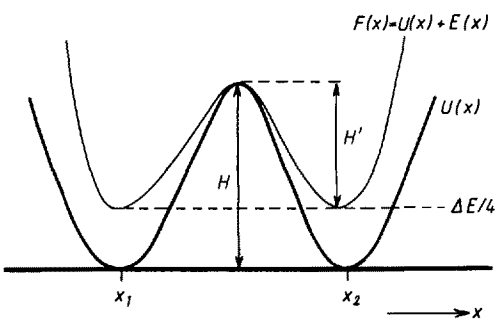

Fig. 18. Effect of mechanical coupling on the activation energy (general case)

According to Heijboer [12], the position on temperature scale of the secondary peak is directly given by the activation energy. For a frequency of 1Hz we have:

$$T_{max} = 16.7\ H\ ;\quad \nu = 1\ Hz \tag{6.7}$$

where T_{max} is in K and H in kcal/mol. Consequently, the change in activation energy given by Eq. (6.6) will give rise to a shift ΔT_{max} in the peak position:

$$\Delta T_{max} = 16.7\ (H' - H) = -4.2\ \Delta E\ . \tag{6.8}$$

Assuming that the peak height $\tan \delta_{max}$ is proportional to ΔG or ΔJ, Eq. (6.2) gives:

$$\frac{d \ln \tan \delta_{max}}{d \Delta E} = - \frac{1/(4RT_g)}{1 + \exp(-\frac{\Delta E}{4RT_g})} \sim - \frac{1}{4RT_g} \qquad (6.9)$$

the last approximation being valid if $\Delta E >> 4RT_g$.

Combining Eqs (6.8) and (6.9) we find:

$$\frac{d \ln \tan \delta_{max}}{d \Delta T_{max}} = + \frac{1}{16.8\ RT_g} \ . \qquad (6.10)$$

So, with increasing ΔE (coupling energy) the peak shifts to *lower* temperatures and decreases in height. The decrease in height is much more pronounced than the shift to lower temperatures. For example, with T_g = 400 K, Eq. (6.10) predicts a decrease in peak height by a factor of 3 for a shift in peak temperature of only 14.5^{o}C. This explains the empirical finding that the activation parameters are rather insensitive to the coupling energy.

7. Conclusions

1. The usual two-potential-well model is inadequate for describing secondary relaxation in glassy polymers; the origin of the discrepancy is that the coupling of the relaxing molecule to its immediate environment is not taken into account properly.
2. A model based in a more realistic coupling could be worked out; the coupling energy could be obtained by considering the fact that the glassy polymer has once been prepared by cooling from above to below T_g .
3. The new model correctly describes how the intra-molecular energy difference between the two states influences secondary relaxation and so Heijboer's problem could be solved.
4. Even with strong coupling, the activation parameters of the relaxation are influenced only slightly.
5. Due to the coupling, the two states split into 3×2 states.

8. Acknowledgements

The author would like to thank Dr. J. Heijboer and Dr. K.E.D. Wapenaar for many stimulating discussions and for critically reading the manuscript.

9. References

[1] McCrum, N.G., Read, B.E. and Williams, G., Anelastic and Dielectric Effects in Polymeric Solids. Wiley, London, 1967.

[2] Rosato, V. and Williams, G., Adv. Molec. Relaxation and Interaction Processes, 1981, 20, 233.

[3] Heijboer, J., Mechanical Properties of Glassy Polymers Containing Saturated Rings. Thesis Leiden, 1972, Waltman, Delft. TNO Central Lab. Communic. 435.

[4] Bendler, J.T., Macromolecules, 1982, 15, 1325.

[5] Staverman, A.J. and Schwarzl, F.R., in: Die Physik der Hochpolymeren. H.A. Stuart, Ed., Berlin, 1956, Vol. IV.

[6] Ferry, J.D., Viscoelastic Properties of Polymers. Wiley, New York, 1961.

[7] Timoshenko, S. and Goodier, J.N., Theory of elasticity. McGraw-Hill, New York, 1951.

[8] Orville-Thomas, W.J., Ed. Internal Rotation of Molecules. Wiley, London, 1974, see also U. Burkert and N. Allinger, Molecular Mechanics, ACS Monographs 177 (1982) 93.

[9] Becker, R., Theory der Wärme. Springer, 1966, Chapter V, § 70.

[10] Struik, L.C.E., Physical Aging of Amorphous Polymers and Other Materials. Elsevier, Amsterdam, 1978.

[11] Heijboer, J. and Schwarzl, F.R., in: Struktur und physikalisches Verhalten der Kunststoffe. Nitsche, R. and Wolff, K.A., Eds., Springer, Berlin, 1962, Vol. VI, 375.

[12] Heijboer, J., Annals New York Acad. of Sci., 1976, 279, 104.

DYNAMIC MECHANICAL AND CREEP STUDIES OF PMMA IN THE α- AND β-RELAXATION REGIONS. PHYSICAL AGEING EFFECTS AND NON-LINEAR BEHAVIOUR

B.E. Read

Division of Materials Applications
National Physical Laboratory,
Teddington, TW11 OLW, England

Summary

Dynamic mechanical results for PMMA illustrate that the secondary (β) relaxation interacts with both shear and hydrostatic stress fields and covers a very broad range of frequency which becomes narrower with increasing temperature. It is suggested that the β-process involves coupled local motions of side groups and main chain which are hindered by a broad distribution of potential barriers (activation energies) corresponding to a wide range of local environments. The variation of the tensile creep compliance over 14 decades of timescale for as-received PMMA demonstrates the dominating influence of the β-relaxation region on the room-temperature creep behaviour and the onset of the overlapping primary (α) region at around 10^2s. A method is proposed for extracting the α-contribution to the net creep compliance and is applied to linear data obtained as a function of ageing time at room temperature and to non-linear results at different stress levels for as-received material. The onset of marked non-linear creep behaviour is ascribed largely to stress-induced deageing which preferentially decreases the α-relaxation times and increases the merging of the α- and β-regions. The increased mobility of the α-process is discussed by means of an adaptation of Robertson's theory of plasticity. This suggests that the shear stress increases the fraction of high-energy conformations, and hence the structural temperature, in local environments having relatively low glass transition temperatures. The magnitude of this effect may be influenced by the hydrostatic stress component in accordance with the yield investigations of Duckett, Rabinowitz and Ward.

Introduction

The mechanical relaxation behaviour of PMMA, and its dependence on thermal history and applied stress, is largely determined by the relative contributions from the primary (α) and secondary (β) regions in given ranges of timescale and temperature [1,2]. Some insight into the molecular mechanism of the β-process has been provided

by results from dynamic mechanical experiments covering a wide frequency and temperature range and different stress states [3-5]. A combination of transformed dynamic data with creep results can yield information on the overlapping α- and β-regions at room temperature [6].

In this report a brief survey will first be presented of dynamic mechanical investigations of the β-relaxation for as-received PMMA. Recent creep results at room temperature will then be discussed in terms of the contributions from the α- and β-processes as influenced by physical ageing of the polymer. Consideration will be given to changes in aged state produced not only by variations in thermal history (elapsed time) but also by changes in the stress level and stress state. Postulated effects of high stress on the deageing of glassy polymers can have an important bearing on the non-linear mechanical response [2].

Dynamic Moduli and Creep Compliance

The dynamic mechanical properties of an isotropic polymer subjected to a time-harmonic tensile force or displacement are specified in terms of the components of a complex modulus [7]

$$E^* = E' + iE'' = E'(1 + i \tan \delta_E) \qquad (1)$$

where $i = (-1)^{1/2}$ amd E', E'' and $\tan \delta_E$ are the frequency dependent storage modulus, loss modulus and damping factor respectively. δ_E is the phase angle by which the stress cycle leads the strain cycle in a low frequency, non-resonance test.

The two basic types of stress field correspond to shear and to hydrostatic tension or compression and the relevant complex moduli obtained from dynamic tests on isotropic materials are the shear modulus $G^* = G'(1 + i \tan \delta_G)$ and bulk modulus $K^* = K'(1 + i \tan \delta_K)$ respectively [7]. Methods for determining the components of G^* and K^* for glassy polymers have been described [5,7].

From measurements of both the longitudinal strain $\varepsilon_x(t)$ and lateral strain $\varepsilon_y(t)$ during uniaxial creep under a constant stress σ we may evaluate, as a function of time t, the tensile (or compressive) compliance $D(t) = \varepsilon_x(t)/\sigma$ and the volumetric strain $\Delta V(t)/V = \varepsilon_x(t) + 2\varepsilon_y(t)$. In the absence of an applied load, values of $\Delta V(t)/V$ relative to the original volume may be similarly determined to monitor the isothermal contraction during physical ageing.

For low applied stresses, corresponding to the range of linear viscoelastic behaviour, $D(t)$ is independent of σ and can be evaluated at very short times after loading from the transformation of dynamic data. For this purpose it is convenient to employ the following approximation due to Schwarzl and Struik [8],

$$D(0.48t) \approx 1/E'(\omega) \quad \text{at} \quad t = 1/\omega \qquad (2)$$

where ω is the angular frequency and it is assumed that $\tan^2\delta_E << 1$.

Experimental

Full details have previously been given [5,7,9] of our range of dynamic test methods for measuring the different storage moduli and damping factors of glassy polymers at frequencies between 10^{-2} and 10^{7} Hz. The tensile creep machine and associated extensometers for determining $D(t)$ and $\Delta V(t)/V$ at times between 10^{2} and 10^{6}s have also been described [6]. Some preliminary measurements of $D(t)$ under uniaxial compression have recently been made using a machine which can also apply loads to samples of rectangular cross-section via lever arms. Full details of this method will be included in a future report.

The PMMA employed in the dynamic and creep investigations was a commercial grade (ICI Perspex) obtained in the form of cast sheets. All dynamic measurements and most creep studies were made on strips machined from the as-received sheets. Some creep measurements were made on samples with prescribed thermal histories as described below.

Results and Discussion

The β-Relaxation

The variation of G' and $\tan\delta_G$ with frequency (Fig. 1) exemplifies the extreme breadth of the β-relaxation at room temperature. The extrapolated loss peak has a width of about 6 decades at a loss level equal to half the peak value.

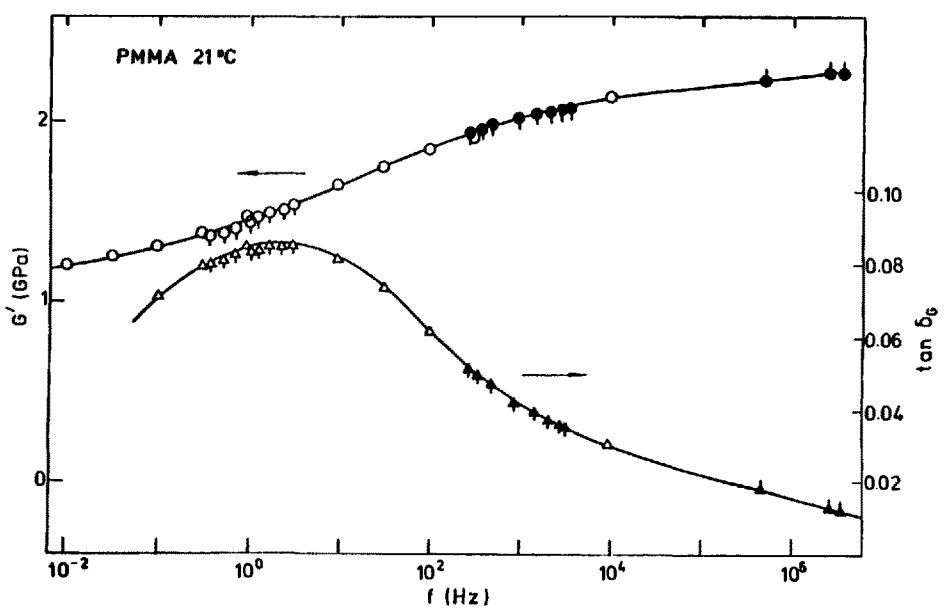

Fig. 1: G' and $\tan\delta_G$ versus frequency for PMMA at 21°C. ○, △, torsion pendulum; ●, ▲, torsional resonance; ●, ▲, ultrasonic shear wave propagation; ○, △, calculated from E^* and ν^* tensile non-resonance data [5]

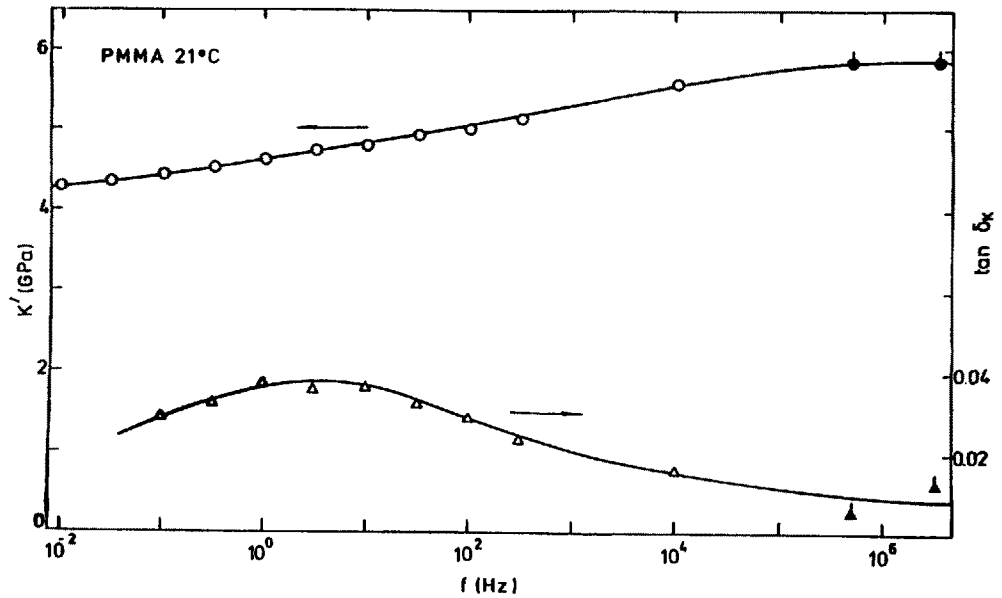

Fig. 2: Variation of K' and tan δ_K with frequency for PMMA at 21°C. ●, ▲, ultrasonic data; O, Δ, evaluated from E* and ν* results [5]

The dispersion in K', shown in Fig. 2, illustrates that the molecular rearrangements involved in the β-process are activated by hydrostatic as well as shear stresses and give rise to local changes in both volume and shape. The magnitude of the bulk modulus relaxation is about one half the magnitude of the shear modulus relaxation based on the relative heights of the peaks in tan δ_G (0.08) and tan δ_K (0.04) or the relative fractional modulus increments $(G_U - G_{R\beta})/G_U = 0.6$ and $(K_U - K_{R\beta})/K_U = 0.3$. Here subscripts U and R refer to the limiting unrelaxed and relaxed moduli for the β-process at high and low frequencies, respectively, and the modulus increments were estimated from areas under the extrapolated loss modulus-log frequency plots. We may note that the magnitude of the shear and bulk modulus β-relaxations in PVC, defined in the above way, are closely similar [5]. Bearing in mind that the β-relaxation in PVC must involve only main-chain motions, it is tempting to speculate that the β-process in PMMA may involve coupled motions of the main-chain and side groups and that the hydrostatic stress interacts preferentially with the main-chain part of the motion.

Figs. 3 and 4 show plots of E' and E" against frequency for the β-relaxation at 21, 60 and 100°C. With the aid of measured areas under the E" peaks, the calculated magnitude $(E_U - E_{R\beta})/E_U$ was about 0.6 and essentially independent of temperature. The frequencies of maximum loss f_m depend on temperature according to the Arrhenius equation

$$\tau = 1/2\pi f_m = \tau_o \exp (E_a^{\#}/RT) \qquad (3)$$

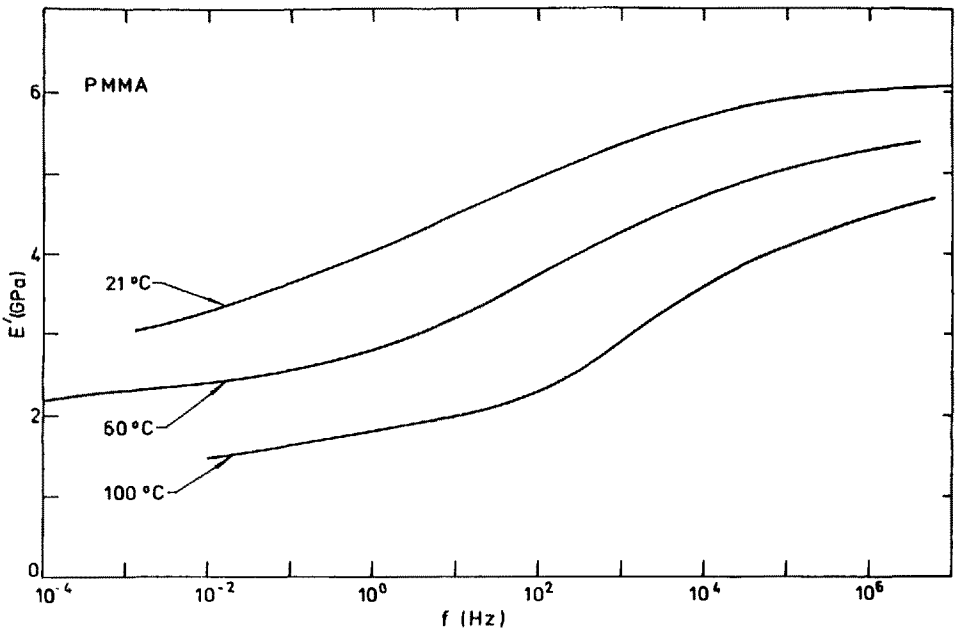

Fig. 3: Variation of E' with frequency for PMMA at 21°, 60° and 100°C

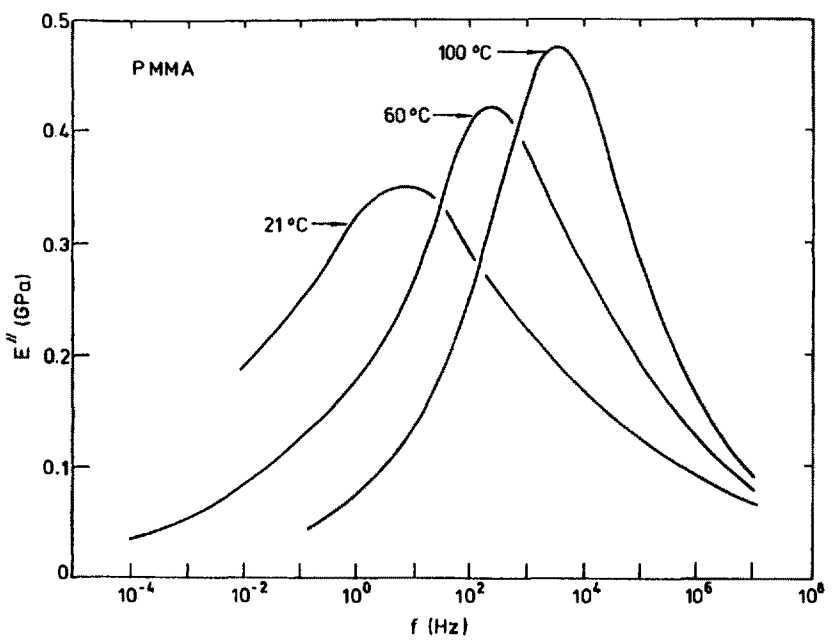

Fig. 4: Variation of E'' with frequency for PMMA at 21°, 60° and 100°C

where τ is the mean relaxation time, $E_a^{\#}$ is the (average) activation energy associated with τ and τ_o is the value of τ in the limit of infinite temperature. Plots of log f_m versus $1/T$ yielded a value of 74 kJ/mole for $E_a^{\#}$. However, the marked narrowing of the loss peak with increasing temperature is indicative of a broad range of activation energies. A distribution of activation energies calculated from the E" plots [5] shows that the activation energies are spread about the average value by about ± 40 kJ/mole. This result suggests that the molecular motions responsible for the β-relaxation occur in a broad range of local environments.

The (α + β)-Region. Creep Studies

In discussing the creep data for PMMA, we first consider the linear viscoelastic behaviour observed at low applied stress and present in Fig. 5 the variation of D(t) over 14 decades of timescale for an as-received sample 1 at 23°C. At times between 10^{-8} and 10s, D(t) was obtained from the dynamic storage moduli E'(ω) using Equation (2). In the time range between 10^2 and 10^6s the D(t) values were determined directly from creep measurements at an applied stress of 9.1 MPa which is close to the critical stress for the onset of non-linearity. The correspondence between the data derived from the dynamic and static methods is good and illustrates the dominating influence of the broad β-relaxation on the creep behaviour at room

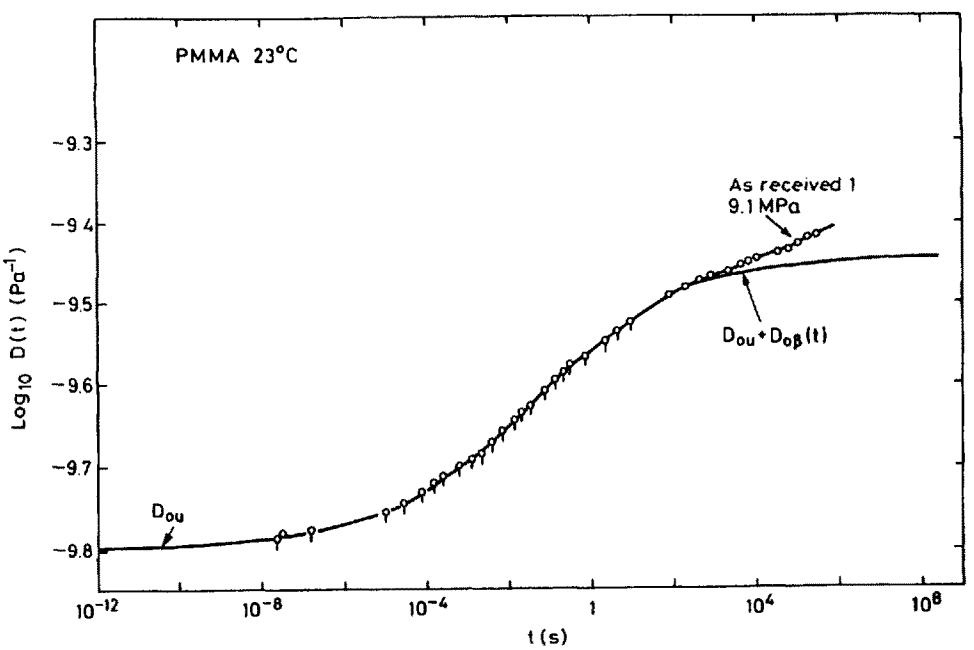

Fig. 5: Dependence of the tensile creep compliance D(t) upon time for PMMA at 23°C. ○, derived from dynamic data at stress amplitudes below 1 MPa; ●, from direct strain measurements with σ = 9.1 MPa. Extrapolated β-relaxation region is indicated at long times

temperature. The onset of the α-relaxation region is also indicated by the upturn in the $D(t)$ curve at times above 10^2s.

The extent of merging of the α- and β-relaxations, and hence the shape of the creep curve, will depend on factors such as temperature, pressure, thermal history and stress level each of which may have a different effect on the respective α- and β-regions. In order to study the influence of these variables on the individual processes it is instructive to consider methods for resolving contributions to $D(t)$ from the α- and β-regions. Denoting these contributions by $D_\alpha(t)$ and $D_\beta(t)$, respectively, we thus write

$$D(t) = D_U + D_\beta(t) + D_\alpha(t) \tag{4}$$

where D_U is the unrelaxed compliance at short times,

$$D_\beta(t) = (D_{R\beta} - D_U)\psi_\beta(t/\tau_\beta, m_\beta) \tag{5}$$

and

$$D_\alpha(t) = (D_{R\alpha} - D_{R\beta})\psi_\alpha(t/\tau_\alpha, m_\alpha) \ . \tag{6}$$

In these equations $D_{R\beta}$ and $D_{R\alpha}$ are the relaxed compliances for the β- and α-regions and $\psi_\beta(t/\tau_\beta, m_\beta)$ and $\psi_\alpha(t/\tau_\alpha. m_\alpha)$ are normalised creep functions which depend on the mean retardation times τ_β and τ_α and distribution parameters m_β and m_α respectively. The creep functions may, for example, be of the Williams-Watts form $\psi = 1 - \exp-(t/\tau)^m$ where $0 < m \leq 1$ and τ and m specify the respective location and width of a given relaxation region.

It follows from Equation (4) that $D_\alpha(t)$ may be obtained from the measured $D(t)$ if estimates can be made of $D_U + D_\beta(t)$. With regard to the room temperature creep curve in Fig. 5, we therefore assume that $D_\alpha(t)$ is negligible at short times and that the β-region is symmetrical about the inflection point at $10^{-1.4}$ s on the double logarithmic plot. Values of $D_U + D_\beta(t)$ at long times are then obtained for the as-received material by extrapolation. This is indicated in Fig. 5 where the reference zero subscript on D_{oU} and $D_{o\beta}(t)$ is now included to denote an as-received sample tested at room temperature in the linear low-stress region.

We now assume that variations in D_U and $D_{R\beta}$ with temperature, pressure, thermal history or stress level arise largely from changes in intermolecular spacing and are thus dominated by volume changes. The dependence of D_U and $D_{R\beta}$ on volume may be estimated from a knowledge of the volume expansion coefficient for PMMA and the fractional changes in E_U and E_R with temperature for the β-relaxation (Fig. 3) assuming that these changes arise principally from volume changes. On this basis we obtain

$$D_U/D_{oU} = D_{R\beta}/D_{oR\beta} \approx 1 + 10\ \Delta V/V \tag{7}$$

where $\Delta V/V$ is the fractional volume change relative to the reference state produced by a change in temperature, pressure, thermal history or stress. The factor 10 in Equation (7) is approximate but compares reasonably with a factor 8 obtained for the dependence of E_U on volume from ultrasonic measurements under hydrostatic pressure [10].

Physical Ageing

Fig. 6 shows plots of $D(t)$ against $\log t$ for PMMA samples which had been heated to a temperature ($130^{o}C$) above the glass transition temperature, cooled rapidly in air to room-temperature and tested after various periods of elapsed time t_e. The duration of each creep test was short compared with the previous elapsed time.

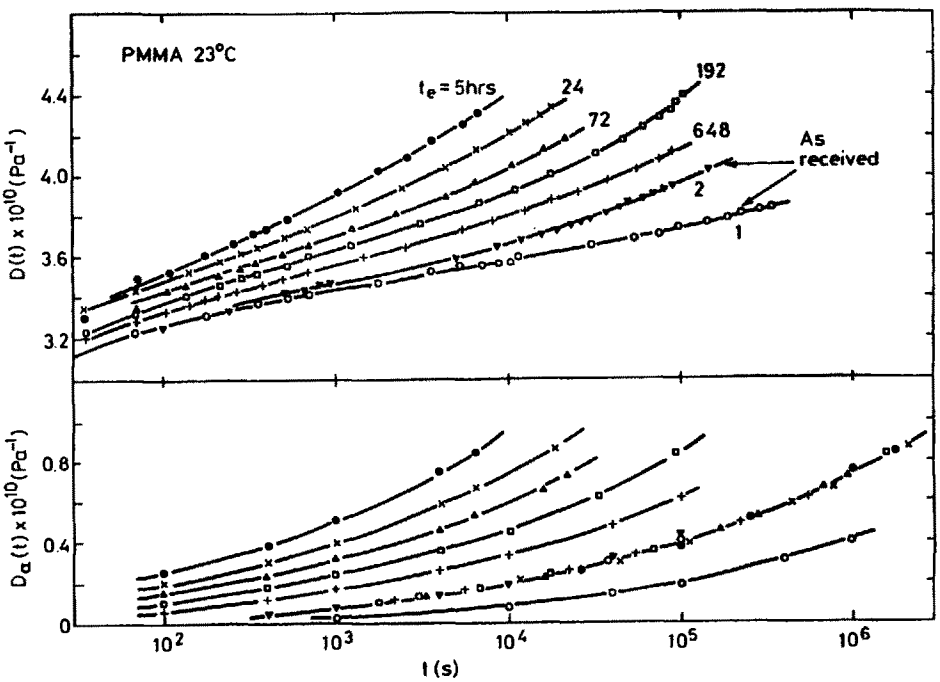

Fig. 6: Tensile compliance $D(t)$ and estimated contribution $D_\alpha(t)$ from the α-relaxation process versus time for PMMA at $23^{o}C$. Corresponding curves are indicated by identical point symbols. Data are shown for two as-received samples 1 and 2 and for a sample at various elapsed times t_e after cooling quickly from $130^{o}C$

The well-established shift of curves to longer times with increasing t_e is evident, although the curves cannot be superimposed by horizontal shifts, whether or not vertical shifts are also applied. The changing shape of the creep curves suggests [6,11] that the α-relaxation region shifts more rapidly to longer times than the β-region during ageing of the polymer at room-temperature, resulting in a decreased merging

of the α- and β-regions. We thus assume that the principal result of ageing is an increase in τ_α corresponding to a decrease in ψ_α. If we further assume that the ageing does not affect ψ_β and that changes in D_U and $D_{R\beta}$ are negligible, owing to the small measured volume changes (Eq. (7)), then Eqs. (5) and (7) yield $D_U + D_\beta(t) = D_{oU} + D_{o\beta}(t)$. We may then employ the values of $D_{oU} + D_{o\beta}(t)$ from Fig. 5 to evaluate $D_\alpha(t)$ from Eq. (4) and the measured $D(t)$.

Plots of $D_\alpha(t)$ computed as above against $\log t$ are included in Fig. 6. Within experimental error the curves now appear to superimpose by simple horizontal shifts, supporting the above interpretation of the ageing effects. From the variation of horizontal shift factor $a(t_e)$ with t_e we obtain $d \log a(t_e)/d \log t_e = 0.80$, a value somewhat higher than previously reported values at room temperature [2]. Based on this value, the data in Fig. 6 for the two as-received samples 1 and 2 correspond to elapsed times of about 15 years and 8 months respectively.

Non-Linear Creep and Stress-Induced Deageing

In Fig. 7 $D(t)$ is plotted as a function of $\log t$ for the as-received sample 1 at stress levels ranging from 4.5 to 26.3 MPa. A substantial departure from linearity

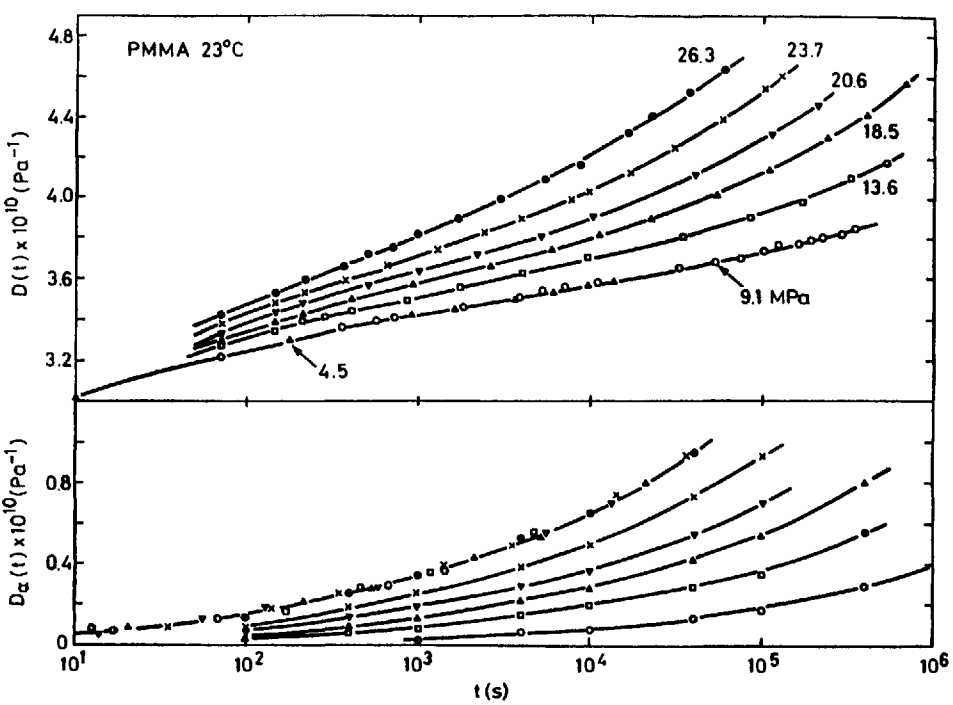

Fig. 7: Tensile compliance $D(t)$ and estimated contribution $D_\alpha(t)$ from the α-relaxation process for as-received PMMA sample 1 at 23°C and different stress levels. Corresponding curves are indicated by identical point symbols

is seen from the dependence of $D(t)$ on stress for stresses above some critical value around 9 MPa. The marked onset of non-linearity may be regarded as arising principally from a shift of the creep curves to shorter times with increasing stress which, by comparison with Fig. 6, represents a stress-induced deageing of the polymer. Again, however, the curves cannot be superimposed by horizontal shifts and their shape changes indicate a preferential shift of the α-region and an increased merging of the α- and β-relaxations. We therefore assume that the deageing involves mainly a decrease in τ_α (increase in ψ_α) and that τ_β is not significantly affected.

The measured volume changes $\Delta V(t)/V$ with extension attained a level of 0.25% at 26.3 MPa and would produce significant vertical (elastic) shifts of the compliance curves, corresponding to changes in D_U and $D_{R\beta}$ according to Eq. (7). Neglecting changes in ψ_β it follows from Eqs. (5) and (7) that $D_U + D_\beta(t) = (D_{oU} + D_{o\beta}(t))$ $(1+10\Delta V/V)$. Consequently values of $D_U + D_\beta(t)$ were calculated from the $D_{oU} + D_{o\beta}(t)$ values (Fig. 5) together with the measured $\Delta V/V$, and Eq. (4) was subsequently employed to determine $D_\alpha(t)$ from $D(t)$.

The resolved curves of $D_\alpha(t)$ versus $\log t$ in Fig. 7 appear to be superposable by horizontal shifts, the similarity in shape of the curves suggesting that no significant reactivation of ageing [2] has occurred during the creep periods investigated. In the following Section consideration will be given to the dependence of the horizontal shift factors on applied stress. Prior to this analysis it should be emphasized that similar shifts of compliance curves to shorter times with increasing stress were observed under uniaxial compression. Although the magnitude of this shift was somewhat less than that produced by tension, this result indicates that the shift is primarily related to the shear component rather than the hydrostatic component of the applied stress field.

The Resolved α-Process. Molecular Aspects of Ageing or Deageing

Most discussions of ageing in glassy polymers attribute the phenomena to changes of free volume within the material. In the present work attempts are being made to interpret the dependence of horizontal shift factors (or τ_α) on t_e or σ in terms of changes in fractional free volume estimated from the measured volume changes. Although this investigation is incomplete, it indicates that the free volume approach is not quantitatively valid if the experimental $\Delta V/V$ are identified with the overall changes in fractional free volume. The measured $\Delta V/V$ during thermal ageing and a part of the total $\Delta V/V$ observed during the non-linear creep tests may, however, reflect fluctuations in fractional free volume in local regions of the polymer.

The stress-induced decrease in τ_α, thought to be largely responsible for the creep non-linearity, has also been analysed by an adaptation of Robertson's theory [12] of plasticity in glassy polymers as modified by Duckett, Rabinowitz and Ward [13].

In this theory it is considered for simplicity that each bond in the polymer chain

can exist in either of two equilibrium rotational states, a low-energy trans state and a high-energy cis state the latter being referred to as a "flexed" conformation. The energy difference between the two states is specified by ΔE. Prior to the application of stress the (initial) fraction of bonds frozen in the high energy state will be that fraction χ_i existing in equilibrium at the glass transition temperature denoted by Θ_g. Bearing in mind that Θ_g will depend on the thermal history of the polymer we have

$$\chi_i = \frac{\exp(-\Delta E/k\Theta_g)}{1+\exp(-\Delta E/k\Theta_g)} \tag{8}$$

where k is Boltzmann's constant.

An applied tensile stress σ may be resolved into a shear stress component $s = \sigma/2$ and hydrostatic stress $p = -\sigma/3$. The shear stress is considered to change the energy difference between the two states to $\Delta E - sv\cos\Theta$ by virtue of the work done $sv\cos\Theta$ in the transition from the low energy to the high energy state. If the transition produces some dilatation due to a reduction in molecular packing efficiency, then the hydrostatic stress will also do work and slightly modify the energy difference further to $\Delta E - sv\cos\Theta + p\Omega$. Here v and Ω are constants with the dimensions of volume and Θ is the angle defining the orientation of a particular structural element with respect to the shear stress direction.

After application of the stress at temperature T the final (equilibrium) fraction of flexed bonds

$$\chi_f = \frac{\exp[-(\Delta E - sv\cos\Theta + p\Omega)/kT]}{1+\exp[-(\Delta E - sv\cos\Theta + p\Omega)/kT]} . \tag{9}$$

It follows from (8) and (9) that the flexed bond fraction will decrease for some orientations and increase for others. In particular χ will <u>increase</u> for orientations Θ between 0 and Θ^* where

$$\frac{\Delta E - \sigma[\frac{v}{2}\cos\Theta^* + \frac{\Omega}{3}]}{T} = \frac{\Delta E}{\Theta_g} . \tag{10}$$

Since an increase in the fraction of high energy bonds represents a change in the structure toward that characteristic of a higher temperature, and thus having an enhanced mobility, bond flexing will occur much more rapidly than bond unflexing in the respective orientation ranges. On this basis the following relation is obtained for the maximum flexed-bond fraction χ_{max}, averaged over all orientations, after the load application [13]

$$\chi_{max} = \frac{kT}{v\sigma}\left\{ \ln\left[\frac{1 + \exp\left[-\left(\Delta E - \sigma(\frac{v}{2} + \frac{\Omega}{3})\right) / kT\right]}{1 + \exp(-\Delta E/k\Theta_g)}\right] + \left\{\frac{\sigma v}{2kT} - \frac{\sigma\Omega}{3kT} + \frac{\Delta E}{kT} - \frac{\Delta E}{k\Theta_g}\right\}\frac{\exp(-\Delta E/k\Theta_g)}{1 + \exp(-\Delta E/k\Theta_g)}\right\} . \quad (11)$$

With this value of χ_{max} the structure is equivalent in the fraction of flexed bonds to the equilibrium structure at temperature Θ_1 above Θ_g given by

$$\chi_{max} = \frac{\exp(-\Delta E/k\Theta_1)}{1 + \exp(-\Delta E/k\Theta_1)} . \quad (12)$$

In attempting to adapt this model to the analysis of the non-linear creep behaviour, we consider that the effective Θ_g may vary throughout the polymer and in some local regions may be substantially lower than the accepted glass transition temperature. We then propose that the marked onset of non-linearity occurs at a critical stress σ_c corresponding to $\Theta^* = 0$ in Eq. (10). For stress levels above σ_c some structural elements in certain regions may then be suitably oriented for the stress to induce an increase in flexed-bond fraction and thus raise the local structural temperature to Θ_1 above Θ_g. A decrease in retardation times associated with the short-time tail of the α-region may then result. Putting $\Theta^* = 0$ in Eq. (10) we obtain

$$\Theta_g = \frac{T\,\Delta E}{\Delta E - \sigma_c(\frac{v}{2} + \frac{\Omega}{3})} \quad (13)$$

which enables the evaluation of a (minimum) Θ_g from the measured σ_c and parameters ΔE, v and Ω of the model. Assuming that the local environments are sufficiently large to contain a randomly oriented distribution of elements, the derived Θ_g may be used to evaluate Θ_1 as a function of applied stress using (11) and (12).

The stress-induced horizontal shift of a creep compliance curve, relative to the curve obtained in the low-stress linear range, may now be written

$$\log a_\sigma = \log \frac{\tau_{\alpha,T}^{\Theta_1}}{\tau_{\alpha,T}^{\Theta_g}} = \frac{1}{2.303}\left[\frac{\Delta G^{\#}(\Theta_1) - \Delta G^{\#}(\Theta_g)}{RT}\right] \quad (14)$$

where $\tau_{\alpha,T}^{\Theta_1}$ and $\tau_{\alpha,T}^{\Theta_g}$ are retardation times at the prevailing (vibrational) temperature T associated with structural temperatures Θ_1 and Θ_g respectively. Eq. (14) assumes [12] that the two retardation times are governed by activation free energies $\Delta G^{\#}(\Theta_1)$ and $\Delta G^{\#}(\Theta_g)$ at the respective structural temperatures and yields, in terms of the universal WLF parameters C_1^g and C_2^g

$$\log a_\sigma = \frac{C_1^g}{T}\left[\frac{C_2^g\,\Theta_1}{\Theta_1 - \Theta_g + C_2^g} - \Theta_g\right]. \qquad (15)$$

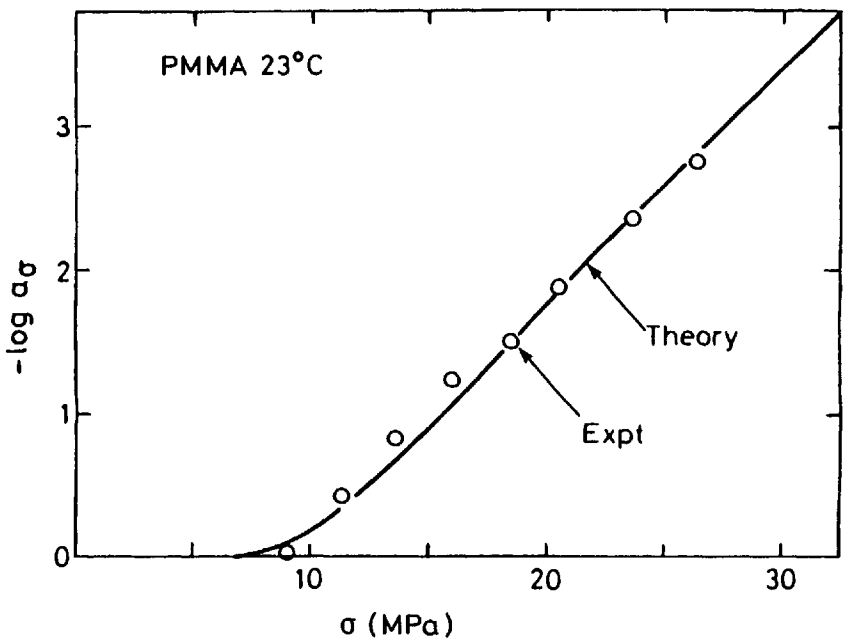

Fig. 8: Plot of the stress-induced horizontal shift $\log a_\sigma$ against σ for the α-relaxation process in PMMA at 23°C. Experimental points from lower curves in Fig. 7. Theoretical line determined from parameters given in the text

In Fig. 8 experimental shift factors determined from Fig. 7 are compared with a theoretical curve calculated by means of Eq. (15). In these calculations we employed the universal constants $C_1^g = 17.44$ and $C_2^g = 51.6^\circ C$ together with values of $\Delta E = 6.03$ kJ/mole and $v = 8.43 \times 10^{-5}$ m^3/mole suggested by Robertson [12] and the ratio $\Omega/v = 0.175$ determined by Duckett, Rabinowitz and Ward [13]. The best fit to the experimental data was obtained using $\sigma_c = 7$ MPa which yielded, from (13), $\Theta_g = 40.1^\circ C$. The agreement between theory and experiment seems good and illustrates the rather abrupt onset of deageing and the apparently low structural temperature Θ_g

characterising the onset of localised conformational rearrangements associated with the α-relaxation process. The above model is currently being considered in relation to the stress-induced deageing of samples with different initial aged state and is also being applied to creep data under uniaxial compression.

Acknowledgments

The author wishes to thank Dr. G.D. Dean and Dr. G.D. Small for their contributions in constructing the creep testing facilities and obtaining data, and Mr. J.C. Duncan for assistance with programming of computations.

References

[1] McCrum, N.G., Read, B.E. and Williams, G., 'Anelastic and Dielectric Effects in Polymeric Solids', Wiley, London and New York, 1967

[2] Struik, L.C.E., 'Physical Ageing in Amorphous Polymers and Other Materials', Elsevier, Amsterdam, 1978

[3] Heijboer, J., Int. J. Polym. Mater. 6 (1977) 11

[4] Koppelmann, J. and Hirnbock, R., Polym. Eng. Sci. 18 (1978) 1087

[5] Read, B.E., Polymer 22 (1981) 1580

[6] Read, B.E. and Dean, G.D., Polymer 25 (1984) 1679

[7] Read, B.E. and Dean, G.D., 'The Determination of Dynamic Properties of Polymers and Composites' , Adam Hilger Ltd., Bristol, 1978

[8] Schwarzl, F.R. and Struik, L.C.E., Adv. Mol. Relaxation Processes 1 (1968) 201

[9] Read, B.E. and Duncan, J.C., Polymer Testing 2 (1981) 135

[10] Koppelmann, J., Hirnbock, R., Leder, H. and Royer, F., Colloid Polym. Sci. 258 (1980) 9

[11] McKenna, G.B. and Kovacs, A.J., Polym. Eng. Sci. 24 (1984) 1138

[12] Robertson, R.E., J. Chem. Phys. 44 (1966) 3950

[13] Duckett, R.A., Rabinowitz, S. and Ward, I.M., J. Mat. Sci. 5 (1970) 909

RELAXATION PROCESSES IN GLASSY IONIC SOLIDS

C.A. Angell, H.G.K. Sundar, A.R. Kulkarni, H. Senapati and S.W. Martin
Department of Chemistry
Purdue University
West Lafayette, IN 47906 / U.S.A.

Abstract

We examine features of primary and secondary relaxations in ionic glasses of the "fragile" (non-network) type, using time domain and frequency domain relaxation methods. Using the Rheovibron in a static mode we obtain new data on the well-studied $Ca(NO_3)_2$-KNO_3 system, and extend the measurements to a fast-ion conducting glass $40AgI \cdot 60AgPO_3$. We then study the latter glass, which is a fast cation conductor, and a PbF_2-MnF_2-$Al(PO_3)_3$ glass which is a fast anion conductor, in the deep sub-T_g regime where the mobile ions are being frozen out. Comparisons of electrical and mechanical relaxation in the same frequency range show the mechanical relaxation to be more exponential than the electrical relaxation and to have more symmetrical relaxation spectra which are not well-described by Kohlrausch-Williams-Watts function.

Introduction

In this paper we report new measurements on both primary and secondary relaxations on ionic systems in which the viscous modes which determine the primary relaxation are highly decoupled from the mobile ion diffusive modes which determine the electrical conductivity. These are the so-called "fast-ion conducting glasses" [1]. In these, stress relaxation and conductivity relaxation phenomena due to the mobile ion motions may be observed at temperatures very far below the normal glass transition temperature and tend to give large, easily measured losses, and large dispersions in the relevant moduli. The relaxations are due to relatively well-defined motions compared with other secondary relaxations and, furthermore, can be studied free from interferences from the tail end of the main structural relaxation. Hence they provide an interesting case for study amongst secondary or subsidiary relaxation phenomena.

All glasses studied have viscosity versus temperature characteristics which place them at the "fragile" edge of the overall liquid behavior pattern [2]. Since most relaxation studies in the α-region have been performed on liquids towards the "strong" edge, the present results are of interest for comparison. We also introduce a new instrumental technique for performing these measurements in the time domain. We use Rheovibron,

the usual application of which is in the frequency domain, to follow stress relaxation at constant strain. For comparison, we will introduce data obtained in the time domain for one of these systems using optical probe site relaxation studies [3].

The mobile ion secondary relaxations we report will be distinguished from earlier work by the focus on fast anion conducting glasses which have recently been developed in this laboratory [4]. Emphasis is placed on comparison of the relaxation kinetics for mechanical and electrical stresses, and on what is implied about the generality of the Kohlrausch-Williams-Watts relaxation function.

Experimental

Stress Relaxation in the α-Relaxation Regime

To study long time relaxation processes in two "fragile" liquids, $2Ca(NO_3)_2 \cdot 3KNO_3$, and $40AgI \cdot 60AgPO_3$ we have adapted the Rheovibron mechanical analyzer, which is usually employed for oscillating stress relaxation studies, to measure stress relaxation in the time domain over long relaxation times. The measurement is simple, and, for β relaxations, the results obtained may be compared with those obtained in the frequency domain at slightly higher temperatures using the instrument in its normal mode.

To perform the stress relaxation measurement, moisture-protected rod-shaped samples mounted in the flexure conformation (see Fig. 1 insert) are subjected to a bending stress which is applied instantaneously on the time scale of the relaxation process being monitored. Maintaining the strain constant, the diminution of the stress as a function of time is monitored. At higher temperatures the entire stress relaxation process can be recorded. At low temperatures only the initial stages are followed, but the remainder can be inferred using the assumption of rheological simplicity (or some known deviation from it) and the results of higher temperature studies. Calibration of the instrument is performed using quartz rods.

At each temperature, a series of relaxations was observed, the first in many cases being made immediately after the temperature had stabilized on cooling from a previous higher temperature. Results of such runs are designated (e.g. in Fig. 5) as "unannealed". Further relaxations were studied at successively later times to observe the dependence of the stress relaxation behavior on the (slowly equilibrating) structural state of the glass.

Optical Probe Relaxation Studies in the β-Relaxation Regime

The basic idea behind the optical probe relaxation technique is that the equilibration of the probe between sites of different enthalpy or volume can be monitored as a func-

tion of time following a step change in either temperature or pressure. Consequently, it is possible to obtain information on the kinetics of reorganization of specific elements of the structure which are not necessarily fully coupled to the total structural reorganization [5]. These measurements may serve as probes of the α-relaxation itself or in principle (but so far not in practice), of processes which are largely decoupled from the α-process. Since, in the slow relaxation regime, temperature and pressure equilibrate in the glass much more rapidly than does structure, the structural relaxation can be monitored under isothermal or isobaric conditions. Unfortunately, the sensitivity of suitable, spectroscopically-characterizable, equilibria to temperature and pressure changes is not great enough that the perturbation in temperature or pressure necessary to probe it is within the small-perturbation (linear) regime. Since this complicates the analysis, steps are being taken to develop a.c. techniques in which the sensitivity will be much greater. For the moment we review earlier studies in which the equilibration of Co^{2+} ions between tetrahedral and dodecahedral sites in the same $2Ca(NO_3)_2 \cdot 3KNO_3$ glass studied by stress relaxation (but doped with Cl^- ions to give a tetrahedral site, which is preferred by the Co^{2+} at low temperatures in this system) so that comparison of local and global processes in the same system can be made.

Mechanical Relaxation Studies in the β-Relaxation Regime

The dissipation of mechanical energy far below T_g by the stress-induced jumping of mobile cations or anions (Ag^+ or F^-) has been monitored using a Rheovibron mechanical analyzer in its normal mode, operating in the frequency range 3.5 - 110Hz. We have not applied the full frequency range of the Rheovibron to this problem. To make comparisons with the electrical relaxation in the same glasses, we will use a constant frequency, reciprocal temperature plot believing it to be a more reliable basis for comparison.

Conductivity Relaxation in the β-Relaxation Regime

A detailed study of conductivity relaxation in the $2Ca(NO_3)_2 \cdot 3KNO_3$ system has been reported previously by Howell et al. [6]. To contrast with the results of that study we present here two studies of the relaxation of an imposed electric field by mobile ions. We compare electrical relaxation due to cations (silver using the same glasses whose mechanical relaxation is being reported), with relaxation due to mobile fluoride anions. Measurements were made in the frequency range $12 - 10^5$ Hz using a Genrad digibridge and automatic data-taking techniques described elsewhere [7]. The systems on which we report are the Ag^+ conductors $40AgI \cdot 60AgPO_3$ and $50AgI \cdot 25Ag_2SO_4 \cdot 25Ag_2WO_4$ (an interesting mixed anion system) [8], and a new F^--conductor $70PbF_2$-$20MnF_2$-$10Al(PO_3)_3$ with $\sigma(25) = 1 \times 10^{-9}\ \Omega^{-1}\ cm^{-1}$ [4]. To obtain the same conductivity in the $2Ca(NO_3)_2 \cdot 3KNO_3$ system the temperature must be raised well above the glass transition

temperature of $68^{o}C$ [6].

The conductivity of these glasses are reported elsewhere [4]. Here we concentrate on the frequency dependence of the electrical moduli M' and M'' defined by [9]

$$M^* = 1/\varepsilon^* = [\varepsilon'/(\varepsilon'^2+\varepsilon''^2)] + [i\varepsilon''/(\varepsilon'^2+\varepsilon''^2)] = M' + iM'' \qquad (1)$$

where $\varepsilon'' = \sigma/\omega e_o$, e_o being the permittivity of free space.

Results

In Fig. 1 we show the relaxation of stress $S(t)$ reduced by its initial value $S(o)$ for the annealed samples of $2Ca(NO_3)_2$-$3KNO_3$ glass at a fixed temperature, at different times after the isotherm was initially reached by cooling from a higher temperature. The effect of slow structural equilibration on the stress relaxation time is very pronounced. The asterisks added to the lowest and highest curves are points calculated from a KWW (Kohlrausch-Williams-Watt) expression

$$S(t)/S(0) = \qquad (2)$$

with τ_o and β best fitting the data. The agreement is excellent.

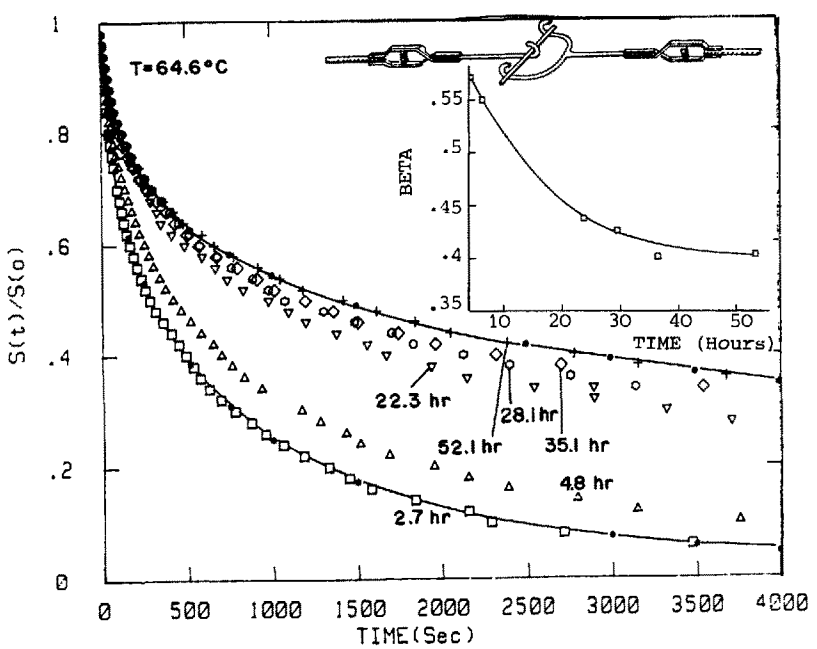

Fig. 1. Normalised stress on rod of $2Ca(NO_3)_2 \cdot 3KNO_3$ glass as a function of time after application, at various times after T ($<T_g$) was imposed on sample. Inserts: sample-stress configuration, and plot of KWW parameter β for different annealing times

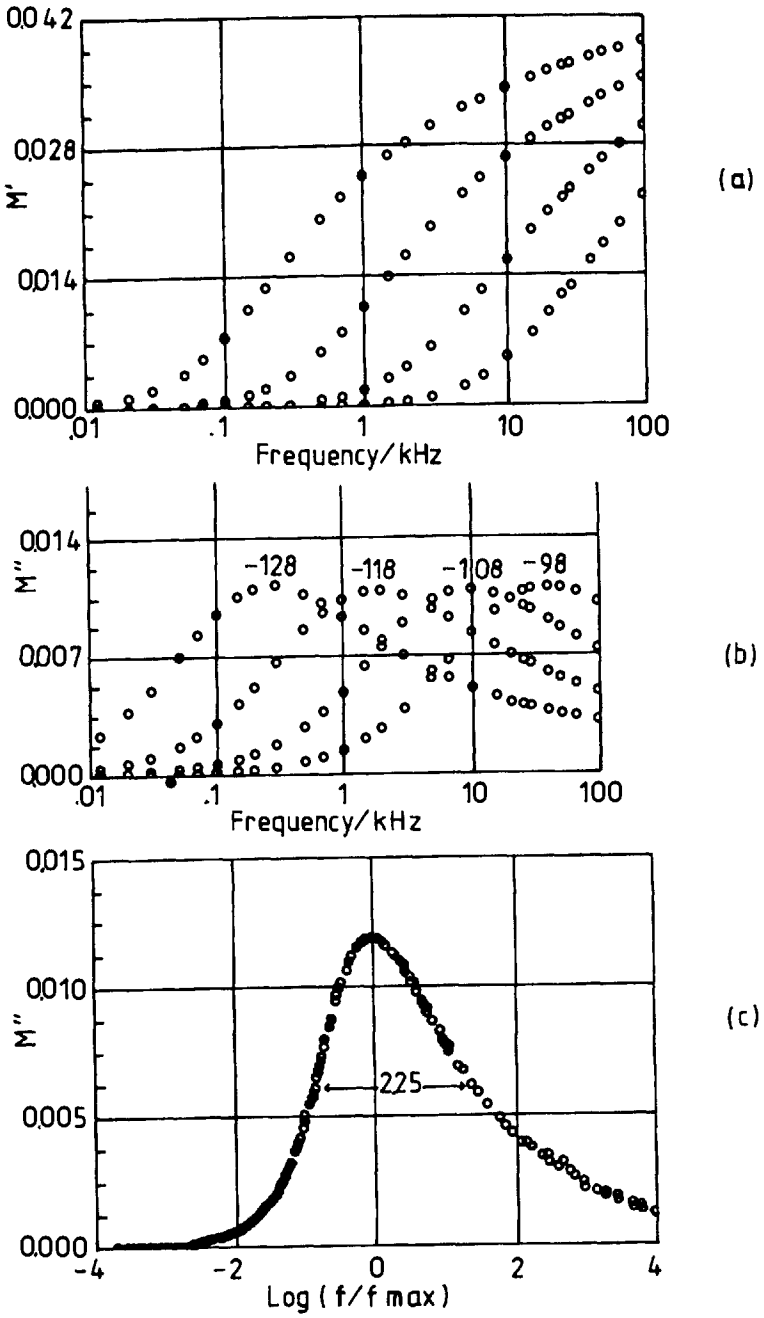

Fig. 4. (a) and (b) Real, M', and imaginary, M", parts of the complex electrical modulus for the mixed anion glass $50AgI \cdot 25Ag_2SO_4 \cdot 25Ag_2WO_4$, at various temperatures. The dielectric constant implied by the high frequency value of M' is subject to correction. (c) Master plot of M" for $50AgI \cdot 50AgPO_3$ in the temperature range -140 to -70°C

Figures 4(a) and (b) demonstrate the frequency dependence of the real and imaginary parts of the electrical modulus M^* for the Ag^+-conducting glass $50AgI\text{-}25Ag_2SO_4\text{-}25Ag_2WO_4$ at various temperatures. Figure 4(c) shows how these M"

versus f plots are essentially independent of temperature by showing how they can be superposed to give a master plot just by shifting along the frequency axis so that their maxima coincide at the origin.

Corresponding plots for the PbF_2-MnF_2-$Al(PO_3)_3$ glasses are shown in Fig. 5. Note that the half-width of the loss curves in the latter case is considerably smaller than that for the Ag^+-conducting glasses of Fig. 4. However, glasses of the sodium silicate type in which the conductivity is comparable to those of the fluoride conductors show half-widths of essentially the same value. The large values of M' for the fluoride glass are unexpected though appear to be reproducible.

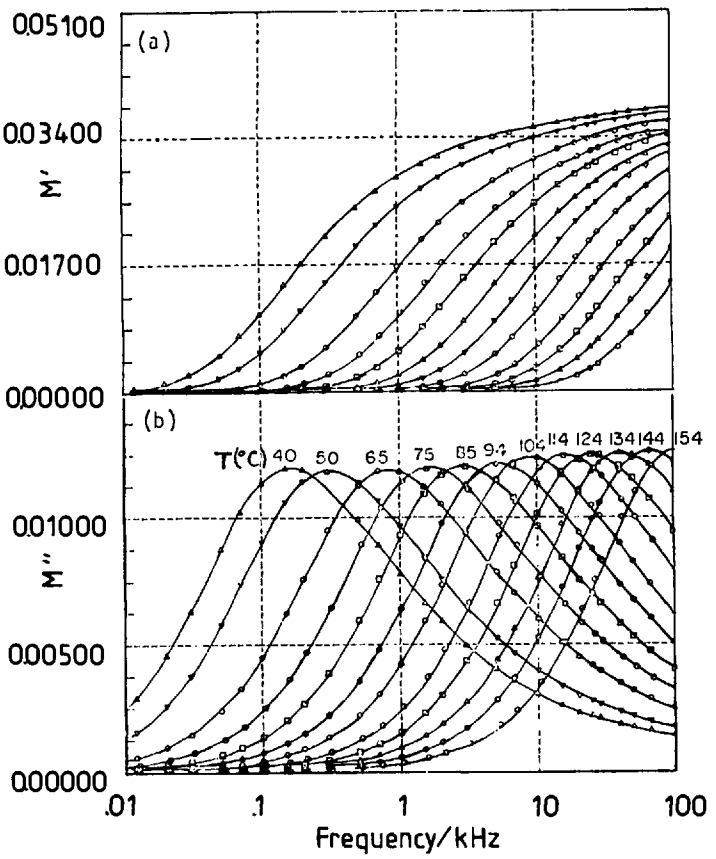

Fig. 5. Real, M', and imaginary, M'' , parts of the electrical modulus for the F^--conducting glass $80PbF_2 \cdot 20MnF_2$ $10Al(PO_3)_3$

In Fig. 6 we display as tan δ(= E'' /E') the results of mechanical loss measurements on the AgI-$AgPO_3$ Ag^+-conducting glass for temperature scans at a fixed frequency of 110Hz. We use a 1/T scale in order to give a shape to the "spectrum" which is equivalent to that obtained in a constant temperature variable frequency plot of the Fig. 4,5 type.

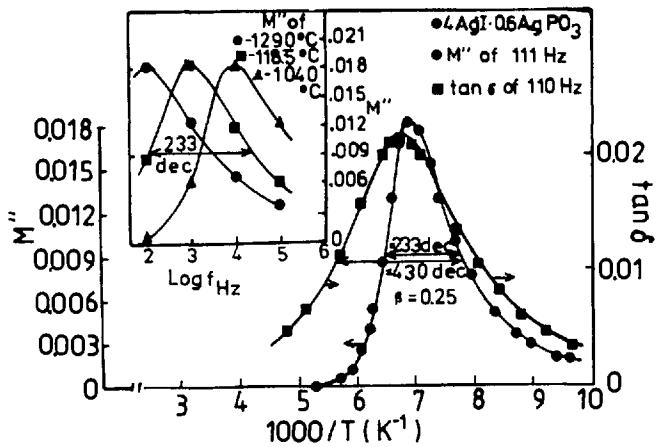

Fig. 6. Constant frequency (110 Hz) scans in temperature of the mechanical loss tan δ (= E" /E') for $40AgI \cdot 60AgPO_3$ glass. The electrical loss M" at the same frequency is included for comparison. Insert shows isothermal modulus spectra

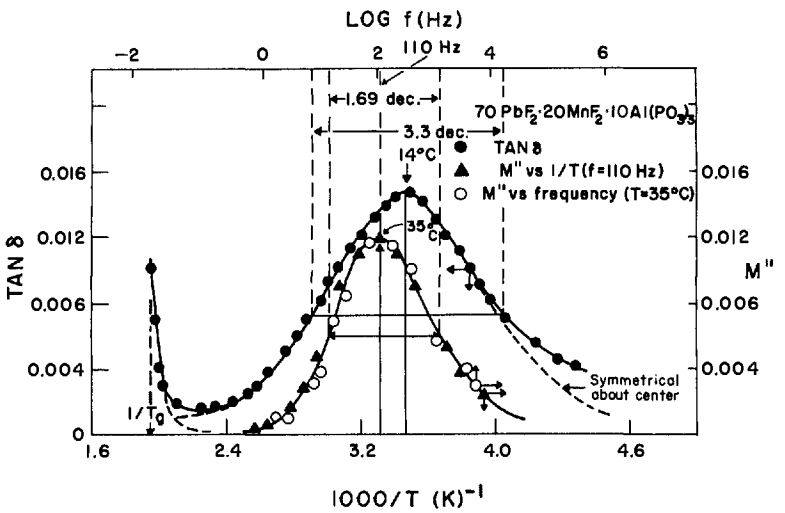

Fig. 7. Comparisons of mechanical and electrical loss "spectra" (using 1/T plots) for F^- conducting glass. Note the reversal, from Fig. 3 of relative and maximum loss temperature for electrical and mechanical stresses

Figure 6 contains in the insert the individual isothermal spectra which are combined in Fig. 4(c) to give a master plot. However, the composition is $40AgI \cdot 60AgPO_3$ - the same as that for which the α-relaxation study is reported in the Fig. 2. The constant frequency 110 Hz variable temperature scan of the electrical modulus for this glass is included in Fig. 7 to permit direct comparison of the electrical and mechanical responses. The mechanical data for the fluoride ion conductor are likewise compared with electrical data in Fig. 7. We take advantage of the simplicity of this plot to demonstrate how accurately the shape of the frequency domain plot is reproduced by the 1/T plot of constant frequency data. For this we use the wide frequency range of the M"

data to superimpose a plot of the isothermal M'' data on the isofrequency data. This is done by choosing a linear log frequency scale determined by the peak (at 35°C) in the 1/T plot (to fix the position of log (110 Hz)) and by the half width in 1/T which is assumed to be the known halfwidth in the frequency, 1.89 decades. Using this scale, the rest of the isothermal data at 35°C are plotted, and the resulting curve is seen to superimpose faithfully on the isofrequency 1/T plot. While the frequency scale should also apply to the mechanical relaxation it cannot accurately represent the whole mechanical loss curve because the α-relaxation has a different (and much larger) activation energy. Consistent with this, the upswing in $\tan\delta$ at 1/T appears to occur at higher frequency than the $1/2\pi\tau$ characteristic of the glass transition (τ_{struc} at $T_g \approx 200$ sec. [5,10]). Thus the frequency scale should be regarded as pertinent only to the fast-ion processes.

Figure 8 shows how the loss peak frequencies of the sort seen in Figs. 4 and 5, vary with temperature, and how the loss peak temperatures of Fig. 5 vary with frequency, using an Arrhenius representation. The silver ion conductor values show an interesting departure from Arrhenius behavior which was first noted and analyzed by Ingram et al. [12]. The fluoride conductors, however, are strictly Arrhenius in behavior.

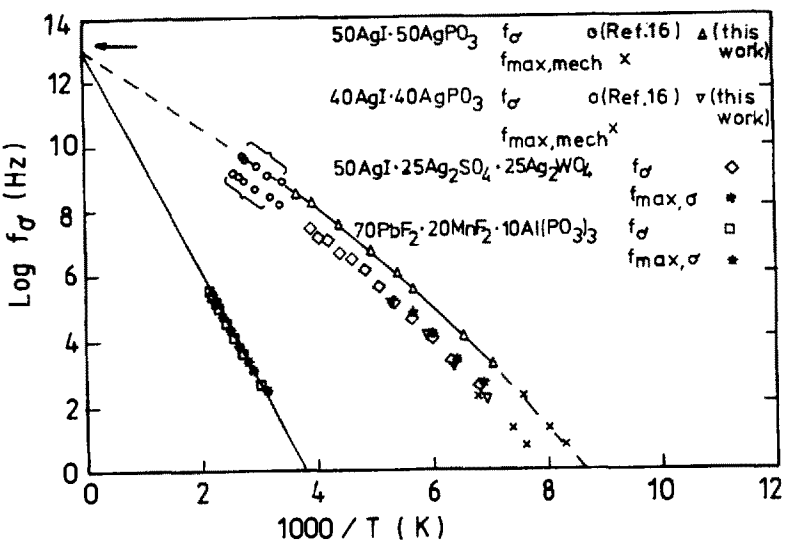

Fig. 8. Temperature dependence of the frequencies of maximum loss for the glasses of this study. Note non-Arrhenius behavior of the Ag^+-conducting glasses. The arrow indicates the frequency of the far IR absorption band due to mobile cation vibrations [1]

DISCUSSION

1. α-Relaxations

There are three features of the α-relaxation study which require discussion. They are, (i) the annealing time or 'structural state' dependence of the stress relaxation time, and the relation of structural relaxation to stress relaxation times, (ii) the temperature dependence of the equilibrium stress relaxation times in relation to that for structural relaxation process (which is presumably the same process observed by enthalpy relaxation at the glass transition temperature as seen by DTA or DSC), (iii) the non-exponentiality of each type of process.

In the first place it is clear from Figs. 1 and 2 that the stress relaxation process is not the slowest process occurring in the glass. Indeed, the dependence of the stress relaxation time on the temperature of measurement has been studied many times before both for inorganic glasses [13] and for polymers [14]. Here we characterize it for the first time in the sub-T_g regime of a "fragile" liquid. If we obtain the average relaxation time $\langle\tau\rangle$ from the expression

$$\langle\tau\rangle = \frac{\tau_o}{\beta}\,\Gamma(\beta) \tag{3}$$

where Γ is the Γ-function, and plot it against the holding (annealing) time (see Fig. 2, insert) we can observe the relaxation towards an equilibrium state in which the average stress relaxation time is independent of time. From the form of Fig. 2, insert, we can estimate the approximate relaxation time of this slower process, and find it is about an order of magnitude longer than the stress relaxation time in the equilibrium state. The latter is itself an order of magnitude longer than the relaxation time in the unannealed state. The latter presumably depends on the temperature from which the sample was quenched to the isotherm in question (either T_g or the temperature of the previous run). We have not studied this latter question in detail.

The final value of the stress relaxation time is plotted versus 1/T in Fig. 9 for several temperatures below the 10^{o}/min OSC T_g, using data on two different glasses of OSC T_g values 71.2 and 73^{o}C respectively. Some runs were carried out at a lower temperature, 54.5^{o}, but an equilibrium state could not be reached in an acceptable time (90 hr.). According to Fig. 9, relaxation time would be ≈300 hr. Included in Fig. 9 is a value of the relaxation time for the slower structural equilibration process (see Fig. 2, insert) type obtained from the data in Fig. 1, and also the value of τ_H = 200 sec. characteristic of the glass transition for this glass determined at a heating rate of 10K min^{-1}. The data available (which were only intended as initial tests of the technique) are insufficient to warrant analysis for the activation energy. Instead we draw lines through each set of points based on a common value of the activation energy for viscosity [15] enthalpy relaxation [16] and probe ion relaxation [3] of

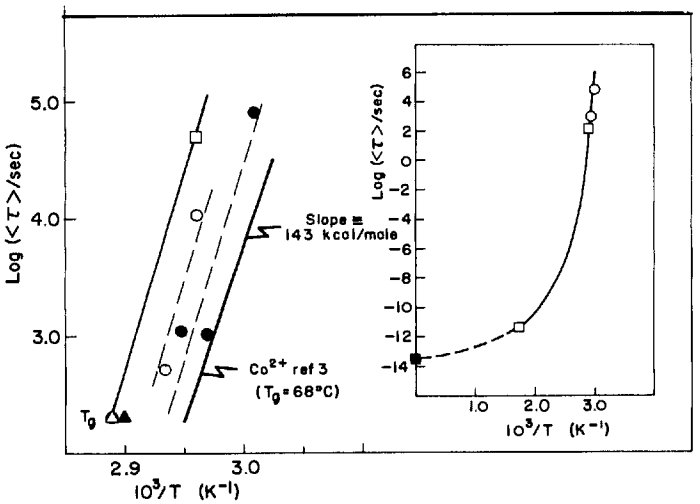

Fig. 9. Arrhenius plot of average stress relaxation times, ○,○ for two $2Ca(NO_3)_2 \cdot 3KNO_3$ glasses of slightly different T_g (73 and 71.2°C). □ is the structural equilibration time based on Fig. 1 data (see also Fig. 2, insert); Δ and ▲ are enthalpy relaxation times, 200 sec. at T_g - assumed equivalent to structural equilibration times. Insert shows the relation of these $\langle\tau\rangle$ values to the single τ value characteristic of the short time structural relaxation process in this system observed by Brillouin scattering [17] and the vibrational limit to τ,■

143 kcal mole^{-1}. The heavy line represents the values of the Co^{2+} probe ion relaxation times obtained from data like those in Fig. 2, in ref. 3. It seems, not surprisingly, that the two processes monitored in this work are consistent with the same activation energy.

The insert to Fig. 9 puts the present data in context with short time relaxation processes in the same system monitored by techniques discussed elsewhere [15,16]. Because of the compressed scale the differences between the various long time process times at a given temperature is almost lost. Suffice it to say that the present data are consistent with the plot previously generated on the basis of viscosity and elastic (G_∞ from light scattering measurements [17,18]) data using the Maxwell relation

$$\tau_S = \eta/G_\infty \ . \qquad (4)$$

Figure 10 shows data for the "slow" structural relaxation and stress relaxation processes for the fast ion conducting system $40AgI \cdot 60AgPO_3$ for which no previous data were available. These data are of improved quality (aided by the immunity of the sample to atmospheric moisture) and indicate an activation energy for both slow and fast processes of approximately 150 kcal mole^{-1}, close to that of the $2Ca(NO_3)_2 \cdot 3KNO_3$ glass. Since the T_g values are comparable this indicates that the fast ion glass is also "fragile" in character which had already been suggested by an earlier Brillouin scattering study

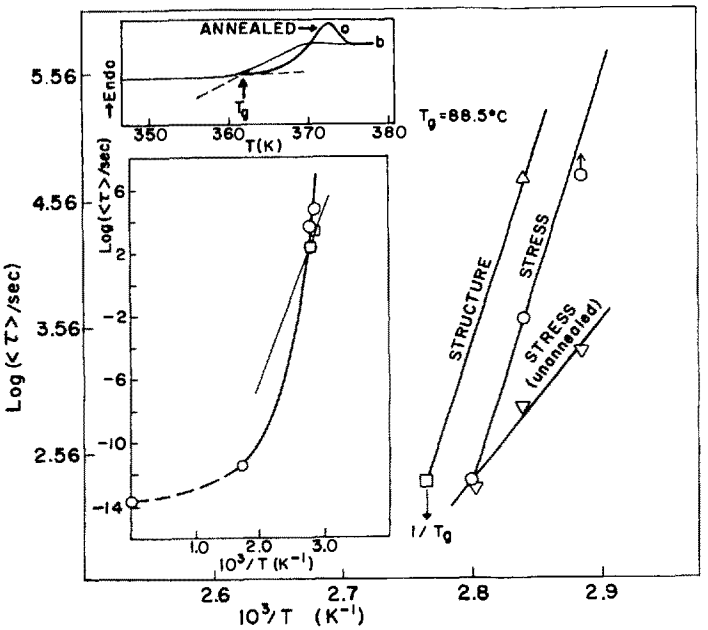

Fig. 10. Stress and structural relaxation times for $40AgI \cdot 60AgPO_3$ glass, described in Fig. 5 caption. Included are results for the pre-annealing stress relaxation time which has a characteristically smaller activation energy. Insert relates long time data to short time relaxation data for this system [23].
in a separate article

of this system [23]. As in the case of $2Ca(NO_3)_2 \cdot 3KNO_3$, the structural equilibration (judged by the relaxation time extracted from Fig. 2, insert, combined with the value of 200 sec. for T_g), occurs about an order of magnitude more slowly than does stress relaxation. Included in Fig. 10 is a set of data marked "unannealed" which represents $\langle\tau\rangle$ obtained from the first run of each series before an annealing has been allowed. This plot shows a much smaller activation energy and is reminiscent of viscosity data measures at "constant structure" [19]. In fact, some annealing has always occurred during sample preparation, temperature stabilization, etc., so the plot is only of qualitative interest. This phenomenon warrants more detailed study. As in the nitrate glass case all the data are put in a broader context in the extended time range plot shown as an insert to Fig. 10. The insert emphasizes the highly non-Arrhenius character of the relaxation time in this system, and shows the similarity to the better-characterized $2Ca(NO_3)_2 \cdot 3KNO_3$ case.

The question of non-exponential relaxation and its dependence on temperature and structural state is taken up briefly in the insert to Fig. 1. First, note that the upper and lower curves in Fig. 1 have a second set of points and a solid line through them. These are calculated plots of Eq. (2) to indicate the conformity of the data to the KWW or

"fractional exponential" relaxation function. The function is evidently very satisfactory. There is evidently a systematic variation of the best fit β value with annealing time as shown in the insert to Fig. 1. This is not just a consequence of the diminished range of $S(t)/S(0)$ values followed since the value of β obtained by analyzing different fractions (1/4, 1/2, 3/4) of the complete relaxation time shows a constant value of β over the whole relaxation range. The value of β decreases as equilibrium is approached and tends to a value of 0.42. This is close to the value 0.35 found from analysis of the enthalpy relaxation process by DeBolt et al. [11]. This may reflect the increased coupling of the two processes as the equilibrium state is approached. We note that analysis of the Co^{2+} probe site relaxation time [3], which (like stress relaxation) is also a faster process (see Fig. 9), yielded β values larger than for enthalpy relaxation. Both processes may occur by taking advantage of a subset of the broad distribution of processes which constitute the total structural relaxation. This tendency is however to be contrasted with that towards much greater departures from exponential relaxation found in the truly decoupled β mechanical relaxation process to be discussed next.

Sub-T_g-Relaxations

We have not yet attempted a time-domain study of the relaxation by the fast ions in the Ag^+ or F^--glasses, though the strength of the relaxation (decrease in modulus associated with the relaxation) is sufficient that such a study should be possible. Instead we will make comparisons in the frequency domain, using the isothermal and isofrequency T^{-1} plot of Figs. 7 and 8.

The Fourier transform of the primary (α) stress relaxation function for $40AgI \cdot 60AgPO_3$ at 91^oC would have the same asymmetric shape seen for the conductivity (M" versus frequency) in Figs. 4 and 5 with a halfwidth almost the same as for the F^--conducting glass. Comparing this with the secondary mechanical relaxation peaks in Figs. 6 and 7, it is immediately clear that the fast ion relaxation, which is a secondary relaxation, is much broader. This is appropriate since secondary relaxations are always found to be broader than the corresponding primary relaxation. In this case, if Eq. (2) were to be obeyed, however, we would expect the peak to be more asymmetrical, but it is not. In fact, both the Ag^+ cation relaxations, and the F^- ion mechanical relaxation are almost symmetrical. This raises serious doubts about the appropriateness of the KWW form for secondary mechanical relaxations. The "distribution of τ" based on the idea of a distribution of activation energies which is Gaussian in form seems more successful, both in the ultrasonic regime [20] and in the present case.

It is interesting and provocative, therefore, that the electrical relaxation which occurs in the same frequency range and has a closely similar activation energy, should recover the KWW form. The asymmetry seen in the spectra of Figs. 4-6 can be well-

Figure 2 shows similar data for a fast-ion conducting glass, $2AgI \cdot 3AgPO_3$.

Figure 3 is a comparable plot for the change in intensity at the absorption frequency characteristic of tetrahedrally coordinated Co^{2+} (660 nm) in Cl^--doped $2Ca(NO_3)_2 \cdot 3KNO_3$ as these ions relax into the more favorable tetrahedral sites on decrease of temperature. Data are shown for temperatures as close as possible to those in the stress relaxation study.

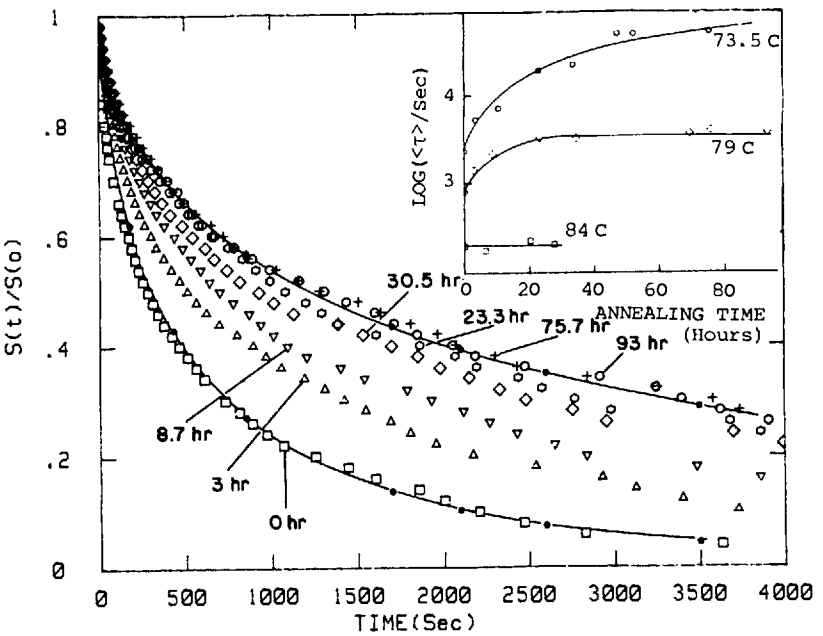

Fig. 2. Normalised stress versus time for AgI-$AgPO_3$ rod sample for different annealing times, as in Fig. 1. Insert: average stress relaxation time as function of annealing time, at different temperatures. The curves imply relaxation times for equilibration of $\approx 10\langle\tau_{stress}\rangle$ at equilibrium

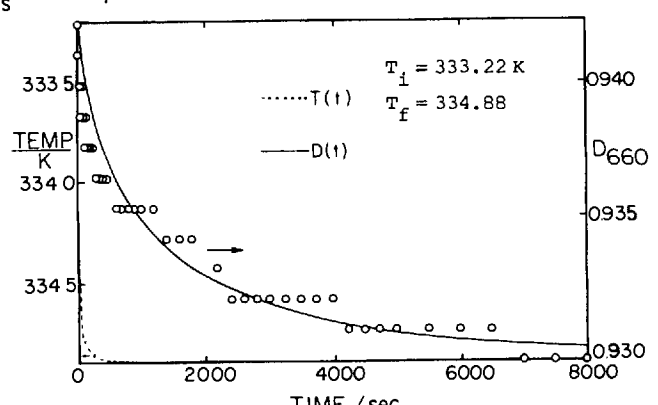

Fig. 3. Intensity of the spectrum for the $[CoCl_4]^{2-}$ site at 660 nm as a function of time after upward T-jump of 1.7 K to 61.8° C (T_g = 68°C). Dashed line (lower left) shows rapid temperature equilibration

described by the KWW function with β values of 0.4 , 0.41 and 0.56 respectively. The question raised is, why should certain elements of the set of processes having a Gaussian distribution of barriers which oppose jumping under a mechanical stress, become inactive when the stress is electrical? Carini et al. [20] and Sladek and Bogue [21] have found that the response to shear or longitudinal (compressional plus shear) stresses is the same within the experimental error, so it is not the tensorial rank of the stress which is important. We cannot answer the question at this time but we note particularly the circumstance that in the case of cationic conductors the most probable relaxation time for conductivity is shorter than for mechanical relaxation while, for the anionic conductors, this situation is reversed. We have under study at this time a system in which the conductivity switches from anion-dominated to cation-dominated as a function of a composition variable [22] and we hope the findings on this system will provide guidance, if not answers, to the problem to which we have drawn attention in this paper. Details of the present measurements which are not presented here for reasons of space, will be discussed in subsequent publications.

Conclusions

Primary relaxations studied at long times appear to follow the KWW form, with a β value which is dependent on the structural state of the system, if the primary relaxation is a response to mechanical stress. If it is a response to electrical stress in a configurationally arrested state, then β is independent of T. Secondary mechanical relaxations, at least those due to mobile ions, show broad spectra which are better described by symmetrical relaxation functions e.g. log Gaussian distributions of τ, which are not strongly dependent on temperature in the range of this study.

Acknowledgments

This work has been supported by the Department of Energy under Grant No. DE 84.ER45102.

References

[1] C.A. Angell, Solid State Ionics, January 1986 (in press)

[2] C.A. Angell, in "Relaxation in Complex Systems", Ed. K. Ngai and G.B. Wright, National Technical Information Service, U.S. Department of Commerce, Springfield, VA 22161, 1984 (in press)

[3] A. Barkatt and C.A. Angell, J. Phys. Chem. 82 (1978) 1972

[4] A. Kulkarni and C.A. Angell, Materials Res. Bull. (in press)

[5] R. Barkatt and C.A. Angell, J. Chem. Phys. 70, 901 (1979)

[6] F.S. Howell, R. bose, C.T. Moyniham, P.B. Macedo, J. Phys. Chem. 78, 639 (1974)

[7] S.W. Martin and C.A. Angell, J. Non-Crys. Sol. (in press)

[8] H. Senapati, Mat. Res. Bull. (in press)

[9] P.B. Macedo, C.T. Moyniham and R. Bose, Phys. Chem. Glasses 13, 171 (1972)

[10] M.A. DeBolt, A.J. Easteal, J. Wilder and J. Tucker, J. Phys. Chem. 78, 2673 (1974)

[11] M.A. DeBolt, A.J. Easteal, P.B. Macedo, C.T. Moyniham, J. Am. Ceram. Soc. 59 (1976) 16

[12] M.D. Ingram, C.A. Vincent, A.R. Wandless, J. Non-Cryst. Solids, 53 (1982) 73

[13] (a) A.L. Zijlstra, Phys. Chem. Glasses 4, 143 (1963)
(b) C.R. Kurkjian, Phys. Chem. Glasses 4, 128 (1963)
(c) See review by R.W. Douglas in Amorphous Materials, Wiley Interscience, eds. R.W. Douglas and B. Ellis, New York (1972), 3-23

[14] See reviews by A.J. Kovacs, Ann, N.Y. Acad. Science 371, 38 (1981)

[15] H. Tsea, N. Laberge and P.B. Macedo, J. Am. Ceram. Soc. 54, 121 (1971)

[16] C.T. Moyniham, A.J. Easteal, J. Wilder and J. Tucker, J. Phys. Chem. 78, 2673 (1974)

[17] C.A. Angell and L.M. Torell, J. Chem. Phys. 78, 937 (1983)

[18] R. Aronssen and L.M. Torell, J. Chem. Phys. 78, 1121 (1983)

[19] O.V. Mazurin, Yu.K. Startsen and S.V. Stoljan, J. Non-Cryst. Solids 52, 105 (1982)

[20] G. Carini, M. Cutroni, M. Federico, G. Galli and G. Fripado, Phys. Rev. B29, 7219 (1984)

[21] R.J. Sladek and R. Borgue, J. de Phys. (1984) in press

[22] A, Kulkarni and C.A. Angell, to be published

[23] L.M. Torell, Phys. Rev. B 31, 4103 (1985)

SECONDARY RELAXATIONS AND THE PROPERTIES OF GLASSES AND LIQUIDS

G.P. Johari
Department of Materials Science and Engineering
McMaster University
Hamilton, Ontario, Canada L8S 4L7

Abstract

Thermally activated translational and/or rotational motions of groups of atoms or molecules occur in localized regions of the rigid matrix of glasses, glassy liquid crystals and glassy crystals. Known as secondary relaxations, these are observed by dielectric and mechanical relaxation spectroscopy at temperatures near and below T_g and show features which are remarkably similar amongst the various types of disordered solids. An analysis of the heat capacity and entropy of the three types of disordered solids also shows a substantial non-vibrational contribution from the availability of configurational states in localized regions in an internal thermodynamic equilibrium embedded in a rigid matrix. In this article, the relevance of the kinetic and thermodynamic aspects of such relaxations, their temperature, density and time dependence and their link with the low-temperature tunneling states in a glass are considered.

That the tunneling centres responsible for the low temperature thermodynamic behaviour of a glass are linked with, or identified as, those local regions where thermally excited orientational and/or translational diffusion over short distances in an otherwise rigid glassy matrix occurs, is tested by three sets of different experiments, namely, (i) physical ageing, (ii) regions created in crystals by neutron irradiation and (iii) regions created by addition of a second component to a glass. All of these seem to suggest that the concept of a disordered solid as an elastic continuum is unsatisfactory and that a description of its heat capacity should also include the energy associated with the configurational states involved in secondary relaxations.

1. Introduction

It now seems generally accepted that the occurrence of secondary or β-relaxation is an intrinsic property of the disordered structures. They occur in liquids and solids whose molecules have no conformational degrees of freedom. These relaxations are

observed on application of an external stress, e.g. mechanical or electrical, which, by biasing the molecular motions, reveals their existence, usually as a peak or a shoulder in the relaxation spectrum of the imaginary component of the shear modulus, or permittivity, of liquids and disordered solids. These motions can, of course, also be observed in the absence of a stress but so far, less attention has been paid to this. There is also a thermodynamic consequence of the occurrence of secondary relaxations in terms of heat capacity and expansivity of a disordered solid, namely, that a fraction of the heat capacity of the solid is configurational in origin and involves thermally excited transitions between the configurational states in localized loose-packed regions or "islands of mobility", embedded in the rigid matrix of a disordered solid. This suggests that the high temperature thermodynamic properties of a disordered solid are not entirely determined by vibrations of a rigid lattice in which every atom is bound to a fixed site and a description of the high temperature heat capacity of a disordered solid in terms of the Debye theory alone is insufficient. The situation becomes particularly interesting when one realizes that the configurational states of higher energy also have lower frequency of vibrations and vice versa, so that the vibrational frequencies themselves have an intrinsic dependence on the energy of configurational states.

This article provides a brief account of our current understanding of secondary relaxations in a variety of glasses and glassy crystals, their relevance to the properties of both liquids and glasses, the changes in the accessible configurational states in the localized regions within the structure of a glass that occur on their cooling and ageing, and a connection between the secondary relaxation and the two level systems, or low energy excitations which cause amorphous solids to exhibit anomalous heat capacity and thermal conductivity at low temperatures. While most of the observations on which this article is based are taken from our published work, several results from our unpublished work are included.

2. Nature of Disorder in Solids

Glasses - a special case amongst the amorphous states of materials - are solids in a thermodynamically non-equilibrium metastable state, obtained by supercooling a liquid below its freezing point, which lack a long-range order of both molecular orientations and positions in their arrangements. This description now seems restrictive because similarly metastable solids with a long-range order for either only molecular positions or only orientations have recently been obtained by supercooling. The first among such solids is the glassy state of molecular liquids wherein the strong anisotropy of the optical transition moments and the steric effects of the rod-, or lath-like molecules cause a mutual alignment of their long axes. Thus the molecular arrangements in their glassy states have a long-range order for the average molecular orientations but not for molecular positions. The second is a glass-like state of orientationally disordered, or plastic, crystals wherein the molecular arrangements

have a long-range order for their average molecular positions but not for their molecular orientations. In the former case, the situation is akin to magnetic ordering, in the latter to spin disorder, and one may consider such glasses as molecular analogs of these two states. Nematic o-hydroxy paramethoxy-benzylidine-p-butylaniline [1], cholesteric cholesteryl hydrogen phtalate [2] and smectic p-benzoxy benzylidine-p-butylaniline [3] are a few examples of the second type.

The variety of disorder in the glassy state of liquids and glass-like state of crystals now allows us to selectively study the effects of a particular disorder on the hindering potentials that determine the configurational changes associated with relaxations in condensed matter. Glass transition in liquid crystals is particularly interesting because packing in them involves mainly the positions (centre of mass) of molecules and not the orientations of the local director. In this respect glass transition in them is similar to that observed in metallic alloys and in computer simulation experiments on aggregates of hard spheres. In both cases, the choice of spheres precludes the possibility of an orientational disorder.

The translational invariance of molecular positions in glassy crystals seems to allow one an enormous mathematical simplification for a theoretical treatment. But, a detailed consideration of such a disorder reveals that this mathematical simplicity is not strictly true, for in glassy crystals too, one can envisage the lack of translational invariance in molecular and atomic positions similar to that of an ordinary glass. In such crystals, the centre of mass of a molecule does not exactly lie on a lattice site and a molecule can be considered as an assemblage of spheres asymmetrically distributed about the lattice site. This assemblage may be represented by several unequal-sized spheres, each of which is capable of acquiring any of the several positions relative to the other similar spheres, which in turn represent other molecules on other lattice sites. But all spheres representing a given molecule are constrained within the assemblage near the lattice site. The mutual positions of the molecularly separate but same size spheres near the different lattice sites are equivalent to a positional disorder of the spheres. In its pictorial representation, for example, a cyclohexanol molecule can be envisaged as an assembly of two spheres, the first representing the O-H group and the second obtained by rotating the C_6H_{11} group about an axis along its plane. All possible arrangements of the two spheres within the constraint of the covalent bond near a lattice site can now be pictured. This process when repeated simultaneously at all lattice sites generates a structure in which the arrangement of neither of the two spheres has a long-range order. The orientational disorder of molecules would thus appear as a positional disorder of their constituent atoms or group of atoms. Such consideration can be useful in developing a unified mathematical description of diffusion in disordered solids.

There is yet another approach to the study of disordered solids, which involves scaling up the size of a unit cell of a crystal. Formally speaking, the unit cell in a crystal is relatively small. In a glass, it is infinitely large. Thus the long

wave length phonon properties of crystals when investigated in order of increasing size of their unit cells, would show that, at a certain large size of the unit cell, the properties of a crystal approach a magnitude that is characteristic of a glass or glassy crystal. The significance of this approach is yet to be theoretically and experimentally determined.

The three types of disorder, namely, (i) orientational and positional, as in ordinary glasses, (ii) positional, as in glassy liquid crystals, and (iii) orientational, as in glassy crystals, are observed in an ice clathrate [5]. Its lattice is formed by water molecules hydrogen-bonded in a framework of closest packing of polyhedral cage-like structures, which are occupied by molecules of a suitable size, known as guests. The centre of mass of the guest molecules does not lie at the centre of symmetry of the cage they occupy and they are randomly oriented. Thus there is no long-range order for either the positions or the orientation of the guest molecules. Certain guest molecules inside the clathrate cages become ferroelectrically ordered at low temperatures [5]. Below such temperatures, there is a long-range order for the orientations of the guest molecules but no long-range order for their positions - a situation analogous to nematic liquid crystals. Water molecules that form the framework of cage-like structures have no long-range order for their orientations, but their centre of mass is almost translationally invariant - as in a glassy crystal. The structure and properties of an ice clathrate also have a certain resemblance to that of a glass in that it has a relatively large unit cell and its thermal conductivity [6] is about 1/5th of that of the disordered crystal of hexagonal ice. The large size of the unit cell in the ice clathrate may affect the mean free path of phonons enough to reduce its thermal conductivity to values which are characteristic of disordered solids. A similar situation has been observed in feldspars, namely sodium and calcium aluminosilicates, whose thermal conductivity is lower than that of α-quartz but higher than that of feldspar glass.

3. Relaxation Processes in Liquids and Glasses

The polarization or viscous flow of a liquid subjected to an electrical or mechanical stress, is a consequence of a bias in the directions of translational and rotational diffusions of atoms or molecules in it. The dielectric and viscoelastic responses of the liquid correspond to a relaxation, generally known as main, primary, or α-, relaxation. (The term 'main" presumably refers to the relatively large amplitude of this relaxation and to its appearance at the lowest frequency or at the highest temperature in our usual measurements made with increasing order of frequency or decreasing order of temperature.) The rapid decrease in the rate of molecular diffusion with temperature causes the liquid to become essentially rigid, or a glass, over a period of say 10^4s, at a temperature known as glass transition temperature, T_g. Thus the main relaxation is said to have a rate of $10^{-4}s^{-1}$ at T_g.

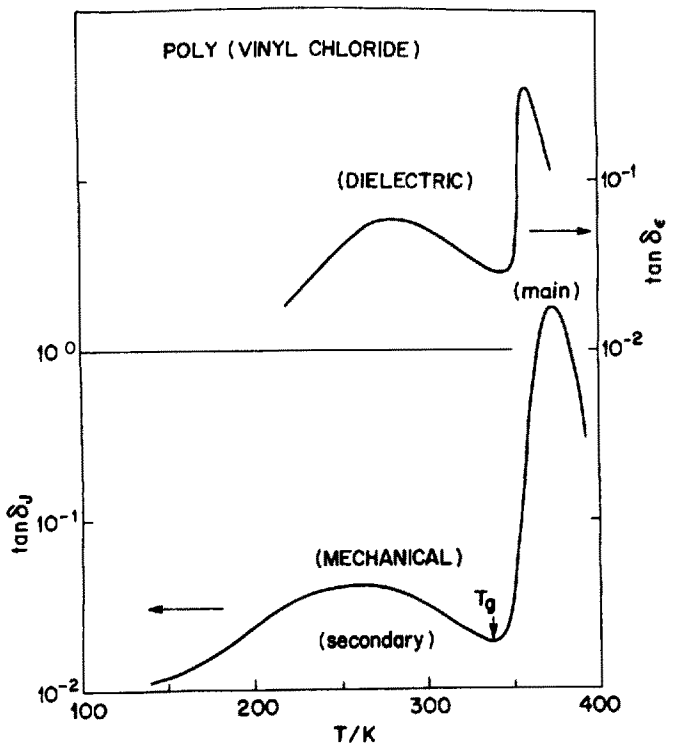

Fig. 1: The dielectric and mechanical loss factor of poly(vinyl chloride) at 0.1 kHz plotted against temperature, showing the two relaxations (ref. 8)

Below T_g the response of an electrical or mechanical stress is relatively small, but nevertheless significant and appears as a polarization [7,8,9,10] or an internal friction of glass [11]. The dielectric and internal friction measurements show a relaxation known as secondary or β-relaxation [7,8,9,10], whose rate is several orders of magnitude higher than the extrapolated rate of main relaxation. The secondary relaxation appears as a peak at low temperatures (usually below T_g) in the isochronal measurements of dielectric or mechanical loss plotted as a function of temperature, and as a peak at a frequency higher than that of the main relaxation in the isothermal measurements of the dielectric or mechanical loss spectra. Examples of these measurements showing a dielectrically and mechanically observed secondary relaxation in different glasses are given in Figs. 1-3. Remarkably similar relaxations also occur in amorphous polymers [13,14], which, owing to this similarity, are now being interpreted in a way that transcends the details of molecular structure and does not require models for specific motions within a molecule.

4. Features of Secondary Relaxations

It is now generally recognized that irrespective of identifiable sub-groups, e.g. side groups, ions, etc., the secondary relaxations occurring in molecular, ionic or atomic glasses exhibit several features [7,8,11,14]. Each of these is briefly described

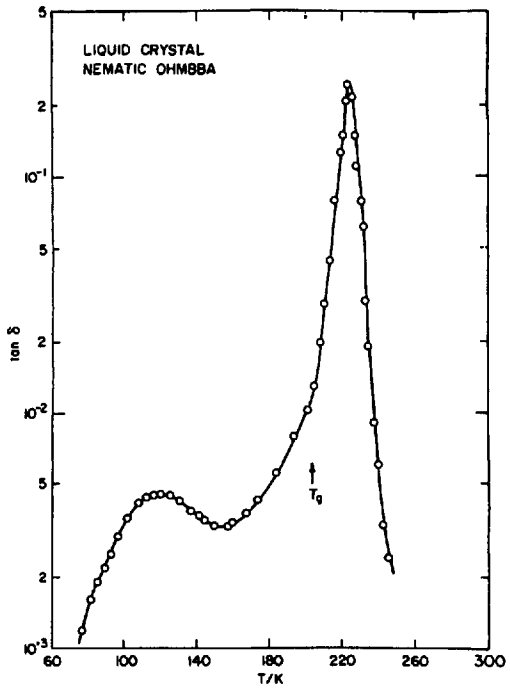

Fig. 2: The dielectric loss factor of the nematic phase of o-hydroxy-p-methoxy benzylidine-p-butylaniline at 1 kHz plotted against temperature, showing two relaxations (Ref. 1)

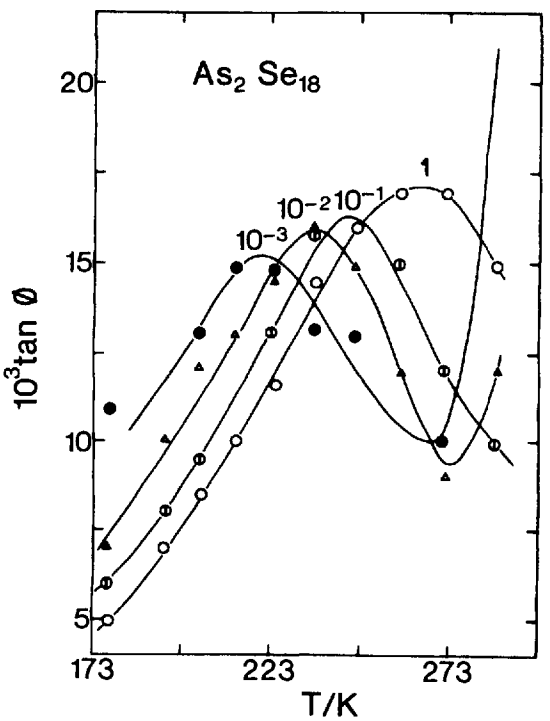

Fig. 3: The mechanical loss factor of As_2Se_{18} glass at four frequencies plotted against temperature (T_g = 384 K) (Ref. 20)

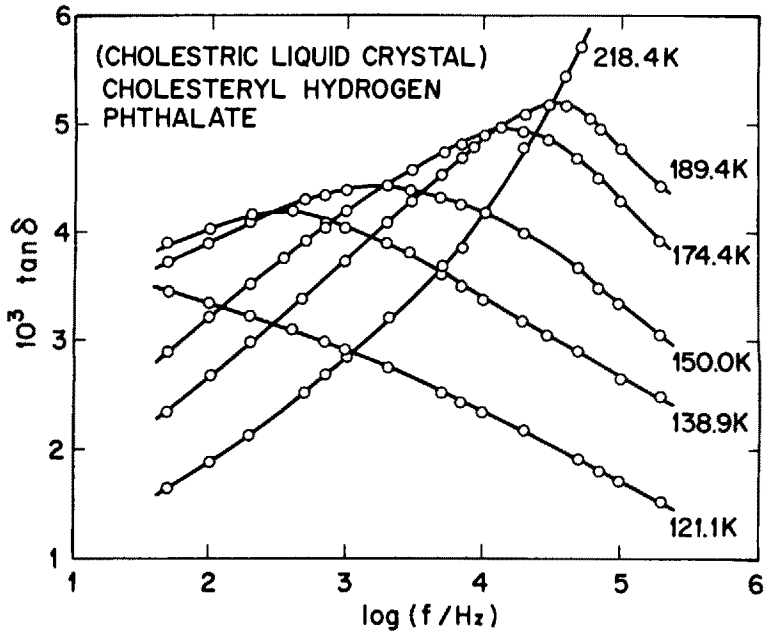

Fig. 4: The dielectric loss factor of a cholesteric glass plotted against frequency (Ref. 2)

in the following:

(i) A secondary relaxation has a very broad loss curve, which is arbitrarily suggested to indicate a wide distribution of relaxation times as shown in Fig. 4. The half-width (frequency width at half height) of the relaxation spectrum is four to six decades of frequency, in contrast to 1.14 decades characteristic of the Debye-type single relaxation process. This half-width increases with decreasing temperature.

(ii) The total polarization or modulus associated with a secondary relaxation rapidly decreases with temperature. This obviously indicates a rapid decrease on cooling in the number of molecular groups that contribute to the kinetic properties of a glass. Thus the amplitude of secondary relaxation does not follow the Curie Law of inverse proportionality of the polarization to temperature.

(iii) The height of the dielectric or mechanical loss peak for a secondary relaxation decreases with temperature, as evident in Fig. 4

(iv) The average rate of a secondary relaxation, or the frequency of its maximum dielectric or mechanical loss, varies with temperature according to the Arrhenius equation, $\omega = \omega_0 \exp(-E/RT)$, with an activation energy E between 18 and 100 kJ $mole^{-1}$ for different materials. E is generally higher for inorganic and network glasses than for organic glasses and its value obtained from dielectric studies differs from that obtained from mechanical measurements [15].

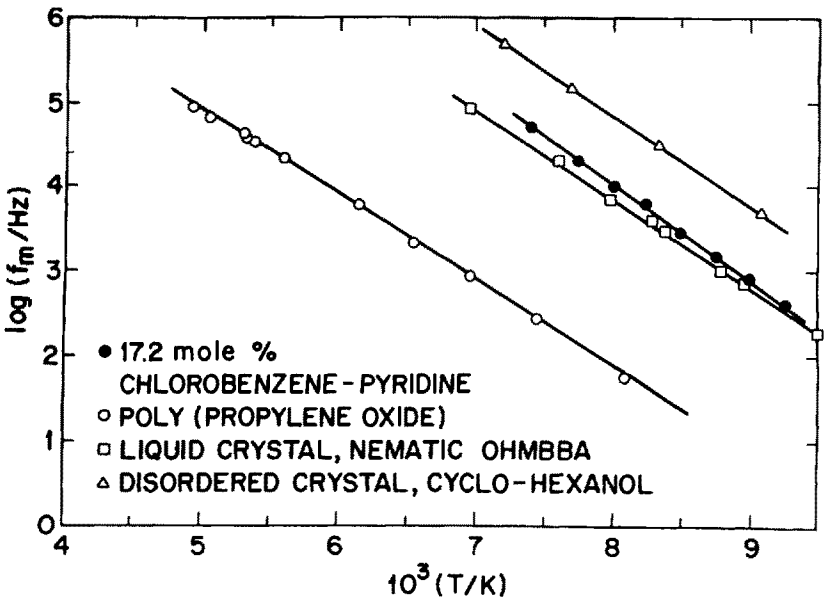

Fig. 5: The Arrhenius plots of the dielectric relaxation rates of secondary relaxation in several types of glasses (Ref. 8)

Examples of the Arrhenius behaviour and low values of E for three types of glasses are shown in Fig. 5.

(v) The occurrence of a secondary relaxation is demonstrably a property of the liquid state [7,10] above T_g, and is not associated with the thermodynamic state of a glass. Several molecular and polymeric glasses show the existence of a secondary relaxation in the equilibrium liquid state. The measured magnitude of polarization associated with a secondary relaxation suggests that 20-30% of the total polarization of the liquid above T_g is due to the types of molecular motions that persist in a glass [10,16].

(vi) The height of the secondary relaxation peak relative to that of the main relaxation peak in a dielectric experiment is generally found to be highest for polymers and molecular glasses, lower for the glassy liquid crystals and lowest for the glassy crystals. Thus the number of molecules contributing to secondary relaxation varies with the nature of packing in a glass as well as the nature of disorder in its rigid matrix.

In addition to dielectric and mechanical relaxation studies, the d.c. conductivity measurements of highly conducting ionic glasses also exhibits the presence of some ionic motions whose activation energy is an order of magnitude less than that of the main structural relaxation [17]. Detailed electrical measurements of a different type, such as hole and electron drift mobilities, and space charge limited currents on

α-Se [18] also show a certain degree of atomic mobility, and quite separate experiments involving decay rates of excited triplet states [19] of aromatic guests in glasses also reflect these relaxations.

In a variety of glasses, several modes of molecular or ionic motions are either dielectrically inactive, or the dielectric loss arising from them is masked by a relatively large dc conductivity, as for example in $Ca(NO_3)_2 \cdot KNO_3$ mixture [15], metallic glasses [11] and As_2Se_{18} glass [20]. These motions couple to a mechanical stress, and internal friction measurements have now shown the presence of secondary relaxations in them [15,20]. In yet other cases, the secondary relaxation peak is not clearly separated from the main relaxation peak, and the former relaxation appears as a shoulder to the main peak. Here, they have been resolved by lower frequency measurements, as for example in polystyrene [21], or by an analysis which relies on the difference in the values of dielectric loss measured at two different frequencies.

5. Secondary Relaxations and Thermodynamics

Molecular degrees of freedom which remain active in the glassy state at temperatures well below T_g, and which are observed as a secondary relaxation, are also evident in the thermodynamics of a glass as contributions from the configurational states available to certain localized regions in the glass. The theromdynamic consequences of the relaxation is that the expansivity, heat capacity and entropy of a glass must have contributions from two sources: first, the lattice vibrations and, second, the

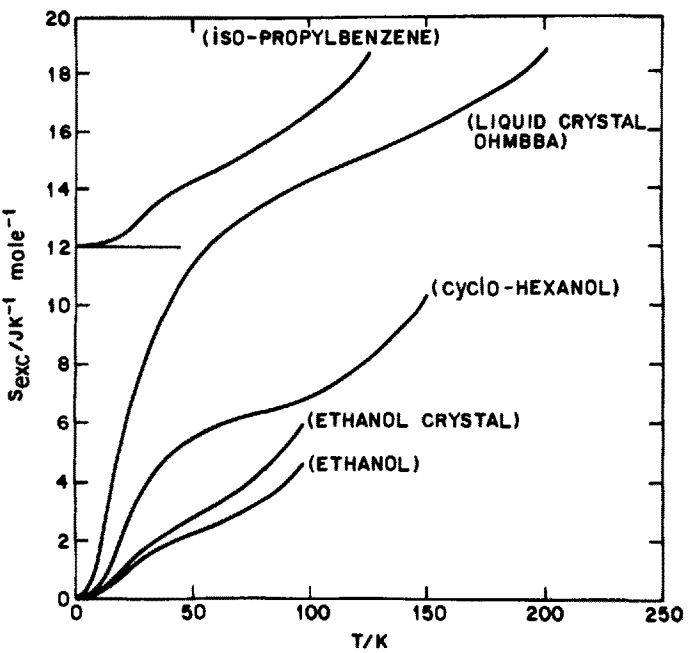

Fig. 6: The excess entropy of several types of glasses plotted against temperature. The curves are terminated at T_g. $S_{exc} = 0$ at 0K for all glasses (Ref. 8)

Table I: Thermodynamic parameters of several types of glasses and disordered solids

Substance	T_g	T_2	$\Delta C_p(T_g)$	$\Delta S(T_g)$	$\Delta S(0K)$	$S_{exc}(T_g)$	x
				Glasses			
Isopropylbenzene	126	106	72	21	12	9.0	0.57
Isopentane	65	50	68	19	14	5.0	0.74
Ethanol	97	75	35	13.6	8.9	4.7	0.65
				'Glassy' liquid crystal			
N-(o-hydroxy-p-methoxy) - benzylidine-p-butylaniline (OHMBBA)	204	180	107	32	12.7	19.3	0.40
				Glassy crystals			
Cyclohexene	81	68	19	19.6	11.7	7.9	0.60
2,3-dimethylbutane	76	65	51	19	7.4	11.6	0.39
Molecular compound of 2,3 and 2,2-dimethylbutane	69	52	56	18	10	8.0	0.55
cis, 1,2-dimethyl cyclohexane	94	82	63	17	8.6	8.4	0.50
Ethanol	97	81	23	10.2	4.2	6.0	0.41
Cyclohexanol	148	128	24	14.9	4.7	10.2	0.32
Cycloheptanol	140	100	32	3.9	0.7	3.2	0.18
				Vapour-deposited solid			
Vitreous ice	135	-	-	<15.5	<13.4	2.1	<0.86

T_2 is the hypothetical temperature at which the configurational entropy would be zero if the liquid or the orientationally disordered crystal could be cooled below T_g while maintaining it in an internal equilibrium: $\Delta S(T_g)$ is the difference between the entropy of the disordered and the crystalline phase at T_g, and $\Delta S(0K)$ at 0 K; $S_{exc}(T_g) = \Delta S(T_g) - \Delta S(0K)$, and $x = \Delta S(0K)/\Delta S(T_g)$, is a measure of the configurational entropy at T_g. All quantities are in K or in $JK^{-1}mol^{-1}$.

configurational states. Simha et al. [22] have shown that secondary relaxations make a significant contribution to the expansivity of an amorphous polymer, and Goldstein [23] and Johari [24] have concluded that a substantial fraction of the heat capacity and entropy of a glass and glassy crystals is attributable to the secondary relaxations.

One may define excess entropy of the disordered solid over the corresponding crystalline phase as S_{exc} ($= S_{glass} - S_{crystal}$). This quantity is evaluated from the difference between the area of their respective (C_p/T) against temperature plots, similar to those given in Ref. [25]. The evaluated excess entropy of three types of disordered solids is plotted against temperature in Fig. 6, and the other relevant quantities are given in Table I.

In Fig. 6, the variation of S_{exc} with temperature for the three types of disordered solids is seen to be qualitatively remarkably similar. In general, on heating from 0 K, there is a slow increase in S_{exc} followed by a tendency towards a constant value and then a progressively higher increase beginning at a temperature of $0.8 \times T_g$ or lower. For two phases of a material having the same anharmonic vibrational contributions and configurational entropy, a plot of S_{exc} against temperature would resemble the Debye heat capacity curve. This would be the case also if the contribution to S_{exc} in both phases were entirely vibrational in origin and the vibrations were harmonic.

The progressively higher increase in S_{exc} with temperature, in Fig. 6, is largely a reflection of the configurational changes involving small scale molecular rearrangement. A small contribution to S_{exc} from the difference between the anharmonic effects in the disordered and the ordered forms is also anticipated, but whether this contribution would raise or lower S_{exc} is not known. Such a contribution depends upon the changes in the force constant, and in the density of the low-frequency lattice modes with temperature and volume, and neither of these changes is known. The contribution to S_{exc} from anharmonic effects should be much less in glassy crystals than in glasses, and yet the S_{exc} of the two classes of solids shows a remarkably similar increase beginning at about 20 to 80^{o} below their respective T_g's. This seems to be an argument against the predominant role of anharmonicity in the variation of excess entropy with temperature. But,convincing evidence for a greater importance of configurational S_{exc} comes from our interpretation of Suga and Seki's [26] measurements on isopropylbenzene glass. Our analysis of their data [8] shows that a decrease in the excess heat capacity occurs near the temperature where the extrapolated rate of secondary relaxation is $\approx 10^{-4} s^{-1}$. The decrease is much less than that observed at T_g, as anticipated in view of the very broad range of relaxation times and low activation energy of secondary relaxations. The freezing out of the localized configurational states in a glass occur over a wide temperature range.

The decrease in the contribution to the entropy from secondary relaxations on cooling a glass has an interesting consequence for the residual entropy of a glass. It is generally assumed that a glass is in a configurational state that is one of the configurational states associated with a certain potential minimum of the liquid at a temperature T_g. Thus the residual entropy of the glass corresponds to the configurational entropy of the liquid at equilibrium at T_g and the greater the cooling rate through T_g, the greater the residual entropy of the glass. It is evident in

Table I that there is a considerable difference between $\Delta S(T_g)$ and $\Delta S(0K)$. The fraction of the entropy difference at T_g and 0K, ranges from 0.2 to 0.7 for a variety of glasses and glassy crystals. Thus, 20 to 70% of the total decrease in the entropy of these materials that occurs on cooling from T_g corresponds to small scale configurational changes in a glass. The assumption that the residual entropy of a glass is associated with the configurational states that are kinetically frozen in at T_g seems, therefore, unjustifiable. Evidently, the thermodynamic properties of a disordered solid are partly determined by the vibrations of a rigid lattice in which every atom is bound to a fixed site, and partly by the number of configurations explored by groups of molecules in an internal thermodynamic equilibrium in localized regions of its otherwise rigid matrix.

6. Secondary Relaxation and Physical Ageing

The change in the structure during physical ageing of a glass is concommitant with a decrease in its volume, enthalpy and entropy, an increase in its modulus and permittivity and with corresponding changes in the magnitude of its optical (refractive index, attenuations), electronic (semiconducting, band gaps, electron transport, etc.), magnetic (Curie point, etc.), and spectroscopic (infrared, Raman, etc.) properties. This change in the structure may be envisaged in two ways: first, as a compaction of homogeneous, coherent, essentially irregular assemblages of molecules capable of passing over quite remote (energy) saddle points in the structure, as for the dense random packing of hard spheres, but in a manner by which the essential elements of local topology of the structure remain unchanged, and, second, as a collapse of lower-density, higher-energy and entropy (or loosely packed) regions, which join together high-density (and lower-energy) regions in the structure of the glass.

The changes in the kinetic properties, e.g. static permittivity and modulus, of a glass on physical ageing, or structural relaxation, are caused by at least four processes [27], namely:

(i) The contribution to the property from the main relaxation at the temperature and frequency of the secondary relaxation peak decreases. This is because a decrease in volume during ageing of a glass shifts the main relaxation process to a higher temperature and/or a lower frequency.

(ii) A decrease in the height and amplitude of the secondary relaxation peak occurs as a consequence of a decrease in the number of molecules contributing to the relaxation. This is the case when a decrease in volume is due partially to the collapse of localized high-volume, high-entropy regions which remain in an internal thermodynamic equilibrium in an otherwise macroscopically metastable, rigid state of a glass.

iii) The magnitude of the property associated with the main relaxation increases with increasing number density of molecules.

iv) The frequency-independent background loss, both electrical and mechanical, over which the secondary and main relaxations are superposed, decreases with decrease in the volume.

During isothermal ageing, all the four processes occur and cause a change in the property of a glass, but the relative importance of each depends upon the temperature of ageing. This can be determined from measurements of either the isothermal spectrum, or the isochronal temperature variation of a property during or after the ageing period. The criteria used for determining their relative importance in both types of measurements have been given earlier [27]. The plots in Figs. 7 and 8 show the change in the dielectric and mechanical loss on ageing of two types of glasses. Both the isothermal spectra and isochrones given exhibit a decrease in the height of the secondary relaxation peak. Our analysis of the dielectric loss data of the quenched and the annealed states of 0.2 NaKO-0.8 B_2O_3 glass obtained by Stevels [28] also showed a decrease in the height of secondary relaxation peaks by ~35% on annealing the glass.

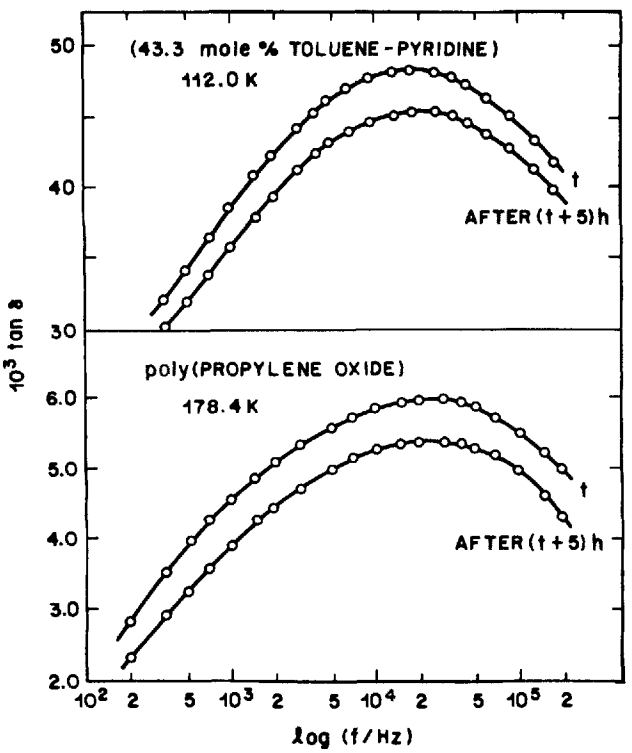

Fig. 7: Isothermal spectra showing a decrease in the dielectric loss factor on ageing of two types of glasses at the indicated temperature (Ref. 8)

Both dielectric [10,27,29] and mechanical [20] measurements on glasses have shown that while the height of the secondary relaxation peak decreases on physical ageing (It seems noteworthy that Struik's data on physical ageing of polymers given in Figure 8 of Ref. [32] can be explained only if the height of the secondary relaxation peak in polymers itself decreased during physical ageing. This is contrary to Struik's own conclusion that physical ageing does not affect the height of the secondary relaxation peak.), its position in a temperature or frequency plane remains unaltered. It is a significant observation, for it shows that physical ageing affects only the number of molecules and not the rate of secondary relaxation. Internal friction measurements on a chalcogenide glass [20] clearly show that densification on physical ageing does not have the same effect on the mechanical

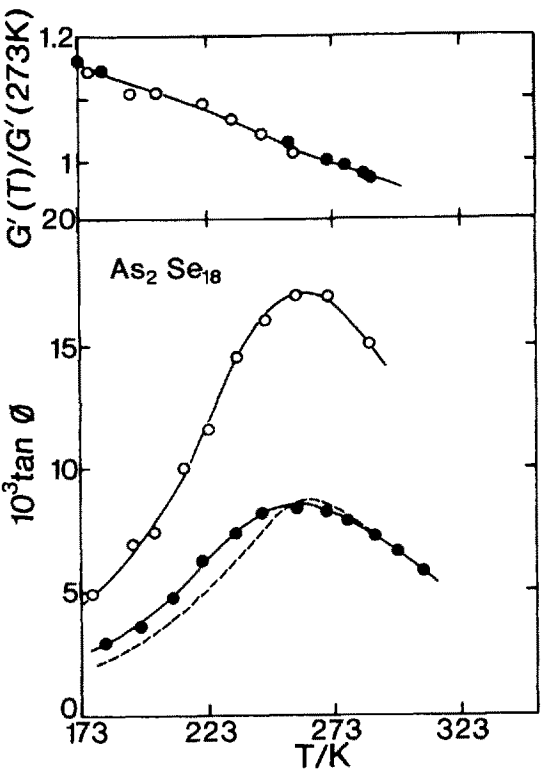

Fig. 8: The internal friction, tanϕ, of As_2Se_{18} glass at 1.19 Hz is plotted against temperature. O represents a sample quenched from 359 K to 295 K (T_g = 384 K) and ⊕ the same sample but annealed at 293±2K for 28 days. The dotted line is Δtanϕ, the difference between the tanϕ of quenched and annealed sample. As shown in the top portion of the figure, the modulus G' (≈G) of the quenched and annealed sample has the same temperature dependence (Ref. 20)

relaxation time as densification on cooling. Thus a glass annealed for a very long time would show a very small amplitude of secondary relaxation. This raises an interesting question, namely, would the amplitude of secondary relaxation decrease to an equilibrium value as the glass approaches its metastable thermodynamic equilibrium state below T_g? The answer is that it would, for it has been shown that there is an equilibrium magnitude of the secondary relaxation above T_g [30]. But, if so, would there be a secondary relaxation at a hypothetical temperature T_0 or T_2 where the configurational entropy [31] of the liquid or disordered crystal is anticipated to become zero? It seems a definite possibility that the magnitude of the secondary relaxation would be very small, if any, at this temperature. There is no experiment to test this suggestion directly, but on the other hand no existing result contradicts it. An indirect test of this suggestion can be made by measuring the effect of volume on the magnitude of secondary relaxation and extrapolating the volume to a value corresponding to temperature T_0 or T_2.

There are two further effects that are relevant to the secondary relaxations:

(1) The occurrence of molecular motions, as a reflection of the configurationally high entropy and volume states in the microstructure of a glass, seems relevant to our understanding of the thermodynamic [33] and kinetic [34] effects observed on increasing the temperature of a previously annealed glass. Referred to as "memory effect", the effect appears as a spontaneous expansion followed by contraction under isothermal conditions when the temperature of an annealed glass is raised. The decrease in the number of configurational states on physical ageing, discussed above, and their partial recovery on heating are also partly responsible for the "memory effect" in glasses,

observed both in its thermodynamic and kinetic behaviours [34].

(2) In polymer blends, e.g. polystyrene with polyphenylene oxide, and polystyrene with polyvinyl ether, an appreciable motion of the molecularly stiffer e.g. PPO chain, occurs at a temperature where the localized motions or secondary relaxation occur in pure polystyrene [35]. Such co-operativeness of localized motions may also exist in pure glass forming polymers and other substances. Indications of such behaviour were also observed from dielectric studies of rigid molecules in a polystyrene matrix, which show that as the size of the molecule is increased, the temperature of its relaxation peak first increases and then remains unchanged with a further increase in the size of the molecule. The saturation temperature is in the range where the secondary relaxation of pure polystyrene occurs.

7. Densification on Compression and on Ageing

Macroscopically, compression has qualitatively the same effect on the volume of a glass as physical ageing. But, in the kinetic properties, which are sensitive to changes at a molecular level, the distinction between the effects of densification on compression and densification on ageing is remarkable. The former causes a shift of the secondary relaxation peak to a lower frequency (or high temperature) by an amount represented as volume of activation, a decrease in its height and an increase in its half-width (whether or not the area under the peak changes is not certain). Thus the rate of secondary relaxation is volume-dependent through the compressibility of a glass. The latter causes no detectable shift of the peak and merely decreases its height and the area under it, as seen in Figures 7 and 8.

The vibrational frequencies are also affected in remarkably different manners during the two types of densification. Compression, for example, increases the frequency of the fundamental band at 250 cm^{-1} in selenium glass by $\sim 4\ cm^{-1}\ kbar^{-1}$. Densification on ageing causes no shifts in the frequency of its fundamental [36], first and second harmonics [37].

It is noteworthy that the Curie point of a metallic glass is decreased by densification on compression [38] but increased by densification on ageing [39,40].

We conclude that densification on compression decreases the rate of molecular relaxation in qualitatively the same manner as densification on cooling of a glass, but densification on ageing decreases only the number of molecules contributing to the relaxation and not significantly their average rates. Compression undoubtedly decreases uniformly all interatomic or intermolecular distances and the average overall decrease, which can be estimated from the compressibility, is significant. Therefore, the rate of relaxation and the vibrational frequencies change in qualitatively the same manner as on cooling a glass. Ageing, we contend, does not decrease the intermolecular distances in the same manner, but rather by the likely collapse of the low-density, high-entropy regions where restricted diffusion of molecules is observed as a secondary

relaxation. Since such regions may constitute a substantial volume fraction of a glass, the change in vibrational frequencies is undetectably small. The former type of densification causes an overall decrease in the intermolecular distance much greater than the latter, for the same decrease in volume. The foregoing discussion indirectly supports the hypothesis that a glass has a microscopically heterogeneous structure, for, if the structure was random close-packed or continuous random network, densification by the two procedures would seem to affect qualitatively similar changes in its kinetic, vibrational and electronic properties.

8. Secondary Relaxations and Structure of Glass

In a view expressed before [8], we proposed that at $T >> T_g$, the total dipolar reorientation involves potential energy barriers that are different from those involved in the cooperative rearrangements. At these temperatures, therefore, the secondary relaxation should be similar to that seen in low-viscosity liquids and in disordered crystals at microwave frequencies. This is shown in Fig. 9, where the dashed line

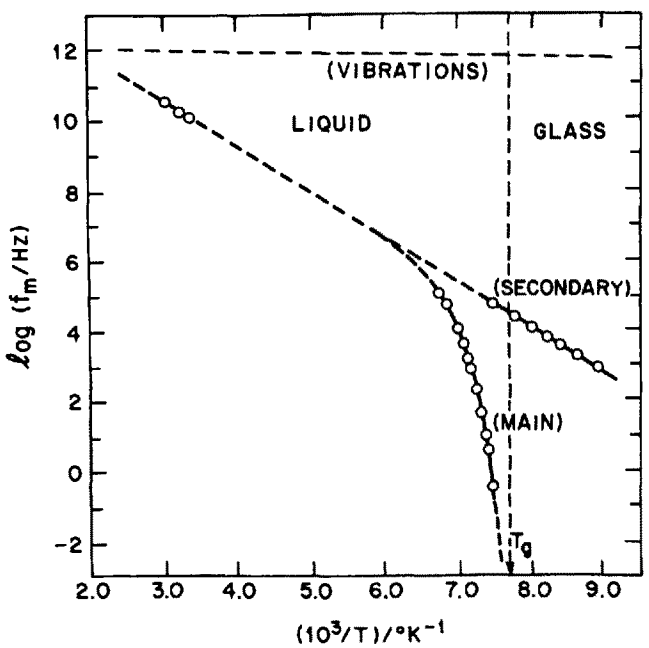

Fig. 9: The dielectric relaxation rates in a liquid and glass of 17.2 mole% chlorobenzene-cis-decaline solution (Ref. 8)

indicates a possible extension of the rates of the main relaxation process. It is evident that the rate of the secondary relaxation in the glassy state extrapolates linearly to the values of the relaxation rates at room temperature and above with an Arrhenius energy at 24.4 kJ $mole^{-1}$. Although the extrapolation is not unambiguous,

it is significant that the secondary relaxation has about the same Arrhenius energy as the relaxation process seen in liquids at a viscosity of several centipoises. We conclude, therefore, that both the cooperative and hindered types of molecular rearrangements occur at $T \geq T_g$. The relative contribution of the main and secondary relaxation processes to the transport property varies with the temperature. As the liquid or crystal is cooled towards T_g, there is an increasing proportion of cooperative molecular processes in the rate-temperature plane. This is considered as the main relaxation. The glass transition occurs at the cessation of this relaxation on the time scale of one's measurement. The secondary relaxation, which in this view is due to the hindered rearrangement of the molecules confined to local regions, continues to exist through the complete temperature range of the liquid and glass, or the disordered crystal and glassy crystal. It is necessary, therefore, that the existence of molecular motions associated with secondary relaxations should be treated as a part of the dynamic theory of liquids and of disordered crystals and should be considered essential to our models of the structure of a glass. The concepts of loosely packed local regions has appeared in the literature as defects or vacant sites arising from local steric or spatial effects in the structure of glass. These are equivalent to the short-lived effects of local density fluctuations in liquids.

The fact that secondary relaxation is also observed in the equilibrium liquid above T_g, along with the main relaxation, in a spectrum measured over a wide frequency range [30,41], suggests the accessibility to a liquid of a bimodal spectral distribution of configurational states in the time domain, and this bimodal distribution of orientational diffusion probabilities is unique to a glass or a liquid (in contrast, a crystal has a unimodal distribution). Now if the structure of a glass were truly represented by random close-packed spheres, or a continuous random network model, one would expect that the unimodal spectral distribution of a crystal would simply be broadened and shifted in a glass.

We suggest that the occurrence of thermally-activated transitions between configurational states, which contributes also to the volume, entropy and enthalpy of a glass, indicates the persistence of stable, local regions in thermodynamic equilibrium in a macroscopically metastable thermodynamically non-equilibrium state of a glass. Local regions such as these, in a metastable matrix, are known to constitute the structure of certain 'crystalline' solids, namely ice clathrates, which also show a glass-like behaviour [6]. Thus a glass is structurally non-uniform in that a number of presumably statistically distributed regions of low-density and high-entropy, where molecules undergo limited diffusion, exist in its structure.

8. Low Temperature Tunneling and Secondary Relaxations

It is now well-known that amorphous solids [42], notably glasses, exhibit an anomalous behaviour of heat capacity and thermal conductivity at temperatures below 1K. This

suggests a limitation of the Debye theory of heat capacity to amorphous solids whose structure, following Bernal's description [43], was assumed as a "homogeneous ... irregular assemblage of molecules containing no crystalline regions", or as an isotropic elastic continuum. The universality of the linear dependence of heat capacity on temperature, low thermal conductivity, and the corresponding behaviours observed in other properties of amorphous solids at temperatures below 1K have been explained by Anderson et al. [44] and by Phillips [45] in terms of a phonon-assisted quantum mechanical tunneling model, also known as the two-level system. According to this model, a number of localized groups of atoms in an amorphous solid have internal degrees of freedom with two stable states which in turn do not significantly increase the internal energy of the system. At low temperatures, atoms lack sufficient energy to surmount the barriers between configurations and they tunnel from one configuration to the other. The small energy difference is made up by lattice vibrations. Thus it seems that the Debye theory of heat capacity based on Planck's theory of black body radiation, and applied to elastic waves in homogeneous isotropic solids, or elastic continuum, is a less satisfactory description of the low-temperature behaviour of disordered solids.

Tunneling is treated via a model Hamiltonian for two level systems representing the ground states in the two local energy wells and the tunneling states are commonly associated with a small group of atoms undergoing a local rearrangement. The larger the number of atoms involved, the easier it is to find two ground states of equal energies and therefore, the number of atoms involved is presumed to be small so that the distance between the states in configurational space could be minimized. The zero point entropy of a glass is a measure of the other energetically equivalent regions into which the glass could have been trapped. These states are mutually inaccessible, because they are distant in configurational space. But, mutually accessible, nearly degenerate states which can tunnel, do exist.

If the molecules in local regions of loosely packed structure, whose restricted diffusion is observed as a secondary relaxation, were to be connected with or identified as tunneling centres, one would expect three distinct regions of the variation of C_p with T in the range from $0K$ to T_g, namely, (i) the linear increase of C_p with T, (ii) its T^3 dependence approximately according to the Debye equation and (iii) its rapid increase with temperature beyond the T^3 variation as T_g is approached. This means a change first from the $C_p \propto T$ to an approximate Debye behaviour and then a progressive deviation of C_p towards values higher than expected from the Debye behaviour, when the degrees of freedom giving rise to potential energy associated with the configurational states become kinetically unfrozen. The observations of the first behaviour are well-documented in the literature [46] and the excess entropy of glasses and other disordered solids has shown the second and third regions [23,24].

An important consequence of the postulated connection between the high-temperature and the low-temperature non-Debye behaviours is that any procedure that affects the

magnitude of a property in the high temperature regime would affect qualitatively similarly the property in the tunneling regime. This means that an increase (decrease) in the number of molecules in local high-volume, high entropy, regions, or in the strength of the secondary relaxation, would increase (decrease) the C_p of a glass both at $T > T_g$ and at $T < 1K$. Therefore, a decrease in configurational C_p at $T \leq T_g$ would also cause a decrease in the linear term of C_p at $T < 1K$. This consequence can be tested by three types of experiments as follows:

(i) It has been shown that spontaneous densification on physical ageing of a glass lowers the strength of its secondary relaxation [7,20,27,47,48] and the number of molecules contributing to its C_p and entropy at $T \leq T_g$ [23,24] and that similar effects occur when the fictive temperature, T_f, of a glass is decreased by slowly cooling the melt or when two glasses, one obtained by quenching and the other by slow cooling, are measured [27]. One would expect that densification of a glass would also reduce the number of tunneling centres, or the density of localized excitations, thereby decreasing its C_p and dielectric loss, increasing its thermal conductivity and affecting changes in the related properties at $T < 1K$. This means that a glass would approach the Debye behaviour or the magnitude of its C_p anomaly would decrease on densification during physical ageing, or on lowering of its T_f.

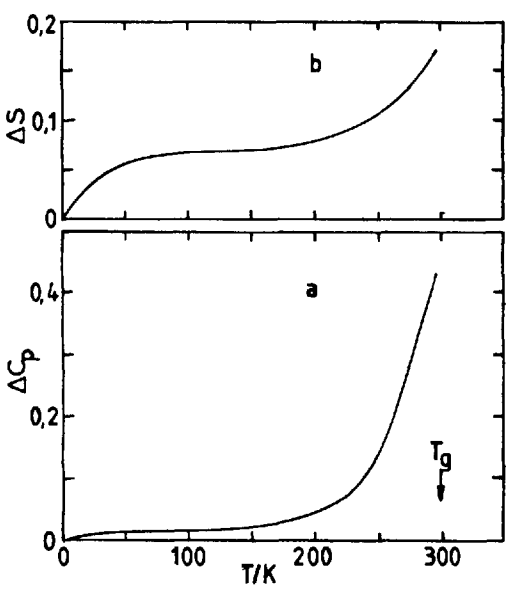

Fig. 10: (a) The excess heat capacity of a melt-quenched over a slowly cooled selenium glass plotted against temperature showing the effect of slow cooling the melt on the C_p of its glass (J mole^{-1} K^{-1}).

(b) The excess entropy of melt-quenched over the slow-cooling-melt Se glass (J mole^{-1} K^{-1})

The above given deduction neither agrees with nor opposes the conclusion of other tunneling models [49,50] which suggest that a high T_g indicates a small concentration of two-site atoms, or tunneling centres, and therefore the amplitude of the C_p anomaly is less in glasses of high T_g. It is also in contrast to the observed approximate inverse relationship between the coefficient of the linear term of C_p and the fictive temperature of vitreous silica [51,52] though these findings also have been questioned recently on grounds of experimental interpretation [53].

Only selenium glass has been studied accurately enough over a wide temperature range to provide a test of this consequence. Figures 10 and 11 show

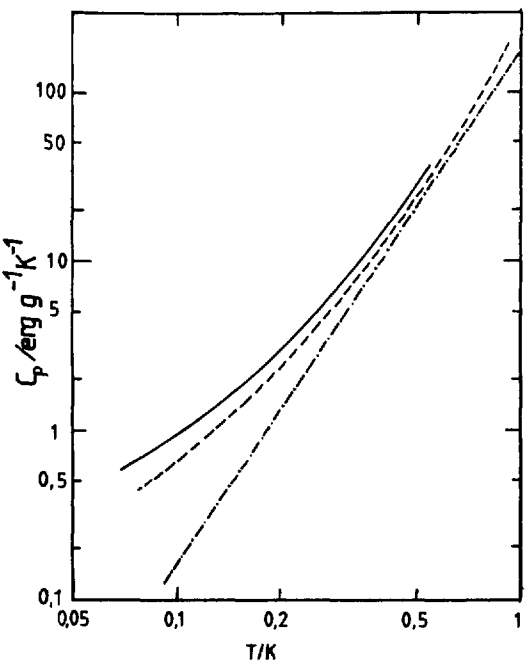

Fig. 11: The heat capacity of Se glass in the tunneling regime. Full line for a glass before ageing or annealing and dashed line for a glass physically aged for 15 months at 278 K. The straight line represents the acoustic contribution to C_p, equal to $T^3 \times 171$ ergs/gK^4

the changes in C_p and S at $T \leq T_g$ and in C_p at $T < 2K$, respectively, observed on ageing selenium glass. The high temperature data in Fig. 10 are taken from Chang and Bestul's work [54], the low-temperature data in Fig. 11 for C_p from Lasjaunias and others [55]. The data in Fig. 11 show that ageing for 15 months at 278 K decreased by 50% the C_p associated with the tunneling, i.e. after the acoustic T^3 contribution was deducted from C_p [55 and private communication]. At T near T_g, glassy Se obtained by slow cooling the melt had 0.36% lower entropy and 1.5% lower C_p than that obtained by quenching the melt, as seen in Fig. 10. In addition, Etienne [56] has observed a decrease in the mechanical loss tangent at $T < T_g$ on annealing the selenium glass. Calemeczuk [57] has observed that thermal conductivity of Se glass at $T < 2K$ increased by ~25% when its fictive temperature was decreased by ~10%, or ~30°K.

Several other glasses also show this effect. For example, Lasjaunias et al. [58] found that densification of silica glass by ~0.1% on ageing at 1573K appreciably decreased its C_p at $0.5 < T < 1K$ and by ~10% at $0.1 < T < 0,5K$, the temperature range for the tunneling centre excitations. The same group [59] also showed that, conversely, expansion of B_2O_3 glass on thermal treatment above its fictive temperature increased its C_p by ~10% at $T \leq 1K$. Ageing or annealing of sputtered amorphous films of metallic alloys seems to cause the largest known decrease in their C_p and increase in their thermal conductivity [60]. Since the authors [61] have independently confirmed that ageing densified the sputtered amorphous films, in particular of Zr_{76} Cu_{24}, we suggest that densification reduced the number of local regions identified here as tunneling centres.

(ii) Neutron and electron irradiation of certain crystals causes them to acquire an anomalous behaviour of their C_p and k at $T < 2K$. As a consequence of our view, such crystals should also acquire a secondary relaxation at $T > 0K$. For example, neutron irradiation of synthetic quartz has been found to introduce local excitations in the crystal and the consequent anomalies in the temperature dependence of both

its thermal conductivity [62,63] and low-temperature heat capacity [63]. Concommitant with the appearance of these anomalies, as Stevels [28] has found, is an increase in the number of atoms involved in localized motions in its crystal at $T \approx 50K$, which appears as a pronounced increase in the height of its dielectric relaxation peak at 50K measured at 32 kHz. Thus neturon irradiated synthetic quartz behaves like an amorphous solid in both its low and high temperature regimes.

(iii) Addition of a second component to a glass occasionally increases the density of localized excitations or the magnitude of its C_p anomaly. As a consequence of our view it should also increase the strength of its secondary relaxation. In a careful study of the effect of addition of K_2O to SiO_2 glass, McDonald et al. [53] observed that the addition of K_2O increased the low-temperature anomalous C_p or the density of the localized excitations of the SiO_2 glass. Stevels [28] has found that the height of the secondary relaxation peak at $\sim$60K measured at 1 MHz is increased by $\sim$50% on addition of K_2O to SiO_2 glass and that further addition of K_2O increased the height of the peak further. Our own measurements on $K_2O{\cdot}SiO_2$ confirm Stevels' observations.

Thus the above mentioned three experiments seem to confirm the postulated connection between the localized states involved in tunneling and those involved in configurational relaxations of a glass. We have observed [10,16] that nearly 10-30% of the total dielectric polarization is associated with the secondary relaxations of a glass. Since only one in $\sim 10^6$ molecules is effectively involved in dielectric relaxations at the low electric fields generally used, it means that the total number of molecules in localized regions is $\sim 10^{16}$ per mole and that the number of localized regions containing this number of molecules is appreciably less than $\sim 10^{16}$ per mole.

Thus the tunneling centres at $T \approx 1K$ may be connected in origin with those local regions where thermally activated molecular motions at $T \leq T_g$, which are observed as secondary relaxations, occur and contributes to the C_p of a glass. Therefore, the low-temperature C_p anomaly is concomitant with the high temperature ($T \leq T_g$) non-Debye behaviour. Ageing of a glass decreases both these anomalies, and this has been observed in both the heat capacity and dielectric measurements. The thermal conductivity at $T < 2K$ is found to be increased on lowering the fictive temperature of a glass. Ageing causes a glass to spontaneously approach a structure with the properties of an isotropic elastic continuum. Its C_p would tend towards the Debye behaviour in the entire range of $0 < T \leq T_g$, when contributions from the tunneling effects at low temperatures, together with the thermally activated transitions at $T \leq T_g$, gradually cease to dominate.

References

[1] Johari, G.P., Phil. Mag. 46 (1982) 549

[2] Johari, G.P., J.W. Goodby and G.E. Johnson, Nature (London) 297 (1982) 315

[3] Johari, G.P., and J.W. Goodby, J. Chem. Phys. 77 (1982) 5165

[4] Suga, H. and S. Seki, J. Noncryst. Solids 16 (1974) 171

[5] Gough, S.R., S.K. Garg and D.W. Davidson, Chem. Phys. 3, 239 (1974). See also Johari, G.P., J. Chem. Phys. 74 (1981) 1326

[6] Ross, R.G. and P. Andersson, Can. J. Chem. 60 (1982) 881

[7] Johari G.P., and M. Goldstein, J. Chem. Phys. 53 (1970) 2372

[8] Johari, G.P., in "Plastic Deformation of Amorphous and Semicrystalline Materials", Les Houches Lectures 1982, ed. B. Escaig and C.G'Sell (Les Editions du Physique, 1982), p. 109

[9] Williams, G. in NATO Advanced Study Institute, Proceedings ed. Orville, Thomas and Yarwood (1983)

[10] Johari, G.P., Ann. N.Y. Acad. Sci. 279 (1976) 117

[11] Perez, J., J.Y. Cavaille, S. Etienne, F. Fouquet and F. Guyot, Ann. Phys. (Fr.) 8 (1983) 417

[12] Pathmanathan, K. and G.P. Johari, J. Phys. C.18 (1985) 6535

[13] McCrum, N.G., R.E. Read and G. Williams, Anelastic and Dielectric Effects in Polymeric Solids (Wiley, London 1967)

[14] Williams, G., "Static and Dynamic Properties of Solid Polymers", NATO Advanced Study Institute Proceedings, ed. R. Pethrick and R.W. Richards (D. Reidl Publ. Holland 1982)

[15] Mai, C., S. Etienne, J. Perez and G.P. Johari, Phil. Mag. 50 (1984) 657

[16] Johari, G.P. and C.P. Smyth, J. Chem. Phys. 56 (1972) 4411

[17] Boehm, L. and C.A. Angell, J. Noncryst. Solids 40 (1980) 83

[18] Abkowitz, M. and D.M. Pai, Phys. Rev. B18 (1978) 1741

[19] Leduc, J. and A.H. Kalantar, J. Chem. Phys. 73, (1980) 5330

[20] Etienne, S., J.Y. Cavaille, J. Perez and G.P. Johari, Phil. Mag. 51A (1985) L35

[21] Petrie, S.E.B., J. Macromol. Sci. Phys. 12 (1976) 225

[22] Simha, R., J.M. Roe and V.S. Nanda, J. Appl. Phys. 43 (1972) 4312

[23] Goldstein, M., Ann. N.Y. Acad. Sci. 279, 68 (1976); J. Chem. Phys. 64 (1976) 4767

[24] Johari, G.P., Ann. N.Y. Acad. Sci. 279, 102 (1976); Phil. Mag. 41 (1980) 41

[25] Johari, G.P., Phil. Mag. 35 (1977) 1077

[26] Suga, H. and S. SEki, Bull. Chem. Soc. Japan 46 (1973) 3020

[27] Johari, G.P., J. Chem. Phys. 77 (1982) 4619

[28] Stevels, J.M., J. Non Cryst. Solids 40 (1980) 69

[29] Haddad, J. and M. Goldstein, J. Noncryst. Solids 30 (1978) 1

[30] Johari, G.P., J. Chem. Phys. 58 (1973) 1766

[31] Adams, G. and J.H. Gibbs, J. Chem. Phys. 43 (1965) 139

[32] Struik, L.C.E., Ann. N.Y. Acad. Sci. 279 (1976) 78

[33] Kovacs, A.J., Fortschr. Hochpolym. Forsch. 3 (1963) 394

[34] Cavaille, J.Y., S. Etienne, J. Perez, L. Monnerie and G.P. Johari, Polymer 27 (1985) 686

[35] Pathmanathan, K., G.P. Johari, J.P. Faivre and L. Monnerie, J. Polymer Sci. (Polymer Phys.) 24 (1986) 1587

[36] Stephens, R.B., J. Appl. Phys. 49 (1978) 5855

[37] Etienne, S., Thesis, University of Lyon, France, 1986

[38] Bouzabata, B., R. Ingalls and K.V. Rao, J. Appl. Phys. 53 (1982) 2324

[39] Chen, H.S., R.C. Sherwood, H.J. Leamy and E.M. Georgy, IEEE Trans. Magn. 12 (1976) 933

[40] Libermann, H.H., C.D. Grahm and P.J. Flanders, ibid. 13 (1977) 1541

[41] Johari, G.P., Polymer 27 (1986) 866

[42] Zeller, R.C. and R.O. Pohl, Phys. Rev. B4 (1971) 2029

[43] Bernal, J.D., Nature (London) 185, 68 (1960: Proc. Roy. Soc. Lond. A280 (1964) 229. "The Geometry of the Structure of Liquids" in Liquids: Structure, Properties and Solid Interactions. T.J. Hughel, Ed. (Elsevier, 1965) pp. 25

[44] Anderson, P.W., B.I. Halperin and C.M. Varma, Phil. Mag. 25 (1972) 1

[45] Phillips, W.A., J. Low Temp. Phys. 7 (1972) 351

[46] Pohl, R.O., Phase Transitions 5 (1985) 239

[47] Frank, M. and H.A. Stuart, Kolloid. Ziet. 225 (1968) 1

[48] Guerdoux, L. and E. Marchal, Polymer 22 (1981) 1199

[49] Cohen, M.H. and G.S. Grest, Phys. Rev. Lett. 45 (1980) 1271

[50] Phillips, J.C., Phys. Rev. B24 (1981) 1744

[51] Raychaudhury, A.K. and R.O. Pohl, Solid State Commun. 37 (1980) 105

[52] Raychaudhury, A.K. and R.O. Pohl, Phys. Rev. B25 (1982) 1310

[53] McDonald, W.C., A.C. Anderson and J. Schroeder, Phys. Rev. B31 (1985) 1090

[54] Chang, S.S. and A.B. Bestul, J. Chem. Thermodyn. 6 (1974) 325

[55] Lasjaunias, J.C., B. Picot, A. Ravex and M. Vandorpe, The Second Conference of the Condensed Matter Division of the European Physical Society on Dielectrics and Phonons, Budapest, extended abstracts p. 199, 1974

[56] Etienne, S., thesis 1986, Université de Lyon, France

[57] Calemczuk, R., Thêsê, Docteur des Sciences, L'Universitê Scientifique et Medicale et L'Institut Nationale Polytechnique de Grenoble, p. 133 (1983)

[58] Lasjaunias, J.C., G. Penn, A. Ravex and M. Vandorpe, J. Physique L41 (1980) L131. J. Noncryst. Solids 57 (1983) 157

[59] Lasjaunias, J.C., G. Penn and M. Vandorpe in "Phonon Scattering in Condensed Matter", H.J. Maris, ed. (Plenum, 1980) p. 25

[60] Lasjaunias, J.C., A. Ravex, D. Laborde and O. Bethoux, Physica 126B (1984) 126

[61] Ravex, A., J.C. Lasjaunias and O. Bethoux, J. Phys. F. Met. Phys. 14 (1984) 329

[62] Berman, R., Proc. Roy. Soc. (Lond.) A208 (1951) 90

[63] Gardner, J.W. and A.C. Anderson, Phys. Rev. B23 (1981) 474

DEVELOPMENTS IN THE NON-NEWTONIAN RHEOLOGY OF GLASS FORMING SYSTEMS

Leslie V. Woodcock

Schools of Chemical Engineering
University of Bradford
Bradford, BD7 1DP
England

Summary

An extensive simulation study using homogeneous shear NEMD of a soft-sphere model covering a wide scaling range of density/thermal energy/shear rate is reported. The model results relate to molecular fluids in the glassy region and to dense colloidal suspensions.

All the common non-Newtonian flow phenomena, dilatancy and shear thickening, shear thinning, structural ordering effects, shear flocculation, normal pressure effects, normal diffusivity differences, and associated time-dependent phenomena viscoelasticity, thixotropy, rheopexy and Bingham plasticity (yield stress effects), can be seen to occur in certain density-shear rate-time domains and relate to a characteristic phase diagram. Many of these non-Newtonian effects involve phase transitions and two-phase behaviour and are described by shear perturbations of the static system at thermodynamic equlibrium or metastable equilibrium.

In the glass transition region both the particle pressures and diffusivities are highly anisotropic; under shear flow the fluid may become vitreous in either of the two directions normal to flow. This gives rise to shear-induced kinetic glass-transition-like effects which dominate the rheology at high packing density and high shear rates.

1. Introduction

When a liquid is supercooled below its equilibrium freezing point the thermodynamic and transport properties behave continuously in the metastable region. The shear viscosity increases with further supercooling until the configurational relaxation times become of the same order as the experimental time-scales. At this operational glass transition the metastable equilibrium Newtonian shear viscosity, as we ordinarily define it, ceases to be measurable and only a non-Newtonian stress-strain rate flow curve may be observed.

The flow curve, or constitutive rheological relation, is defined as the ratio of

shear stress to strain rate (the apparent viscosity) as a function of the strain rate frequency at steady state. Although there has been a great deal of literature discussion about the Newtonian shear viscosity up to glass formation, very little is known about the nature of shear rate-dependent apparent viscosities in the amorphous high density regions. In the absence of any understanding or formalism, the traditional approach for regular non-Newtonian materials, such as polymer melts, plastisols or dense colloidal suspensions, is to parametrise the flow curve in a simple power law, to substitute into the hydrodynamic equations-of-motion, and then to solve for particular boundary conditions [1].

Methods of non-equilibrium molecular dynamics (NEMD) were originally introduced as an alternative means to calculating equilibrium shear viscosities of simple liquids [2]. The techniques were subsequently shown to yield valuable information on the behaviour of simple liquids under severe shearing conditions such as elastohydrodynamic lubrication [3]. Theoretical aspects of the onset of non-Newtonian (non-linear) behaviour have also been studied [4]. An important outcome of these early excursions into the non-Newtonian region was that even simple fluids could be both shear thinning and shear dilatant, implying a shear-rate dependent equation-of-state p-V-T ($\dot{\gamma}$) [5].

More recently, by studying the behaviour of dense suspensions, and introducing variable time-step algorithms, we are now beginning to elucidate the originating physics that determines entire non-Newtonian constitutive relations [6,7] and related time-dependent effects such as viscoelasticity, yield stresses (Bingham plasticity), thixotropy and rheopexy. One outcome of this recent work is that non-Newtonian rheology is coincidental with shear-induced changes in the equilibrium thermodynamics of materials. Moreover, many common non-Newtonian flow phenomena can be related to perturbative effects by the flow field on equilibrium thermodynamic phase transitions [8].

In this report it will be explained how crystallisation and glass formation in simple hard- and soft-sphere models can be perturbed by the shear flow field to give normal pressure and diffusivity differences, and phase transition behaviour, which accounts for many non-Newtonian flow phenomena commonly observed in dense colloidal suspensions.

Many dense suspensions and plastisols have a characteristic relaxation time τ of the order seconds or minutes, so that at ordinary laboratory shear rates the Weissenberg number $\tau\dot{\gamma}$ is around unity. This characteristic dimensionless number is the marking point for the onset of both shear-dependent thermodynamics and non-Newtonian behaviour. Simple liquids have values around 10^{-10}. Supercooled liquids approaching the glass transition may have Weissenberg numbers exceeding unity as the relaxation times lengthen by orders-of-magnitude but the study of these simple glasses is compounded by state changes due to heating effects. In colloidal suspensions the viscous heat of dissipation is negligible compared to the heat capacity of the liquid medium and these materials as observed under relative high shear-rate conditions are

effectively thermostatted internally.

In Figure 1 the shear viscosity of the hard-sphere fluid at equilibrium is compared with a range of experimental dense suspension viscosity data [9]. The hard-sphere model is seen to have very similar phenomenological behaviour when the shear viscosity is expressed relative to the low density limit. In the case of suspensions this limit is the viscosity of the medium η_m. The low density theoretical predictions of Einstein (for suspensions) and Enskog (for the hard-sphere gas) are also shown.

Neglecting particle-particle correlations Einstein obtained the simple result [10]:

$$\frac{\eta}{\eta_m} = 1 + \frac{5}{2} y \qquad (1)$$

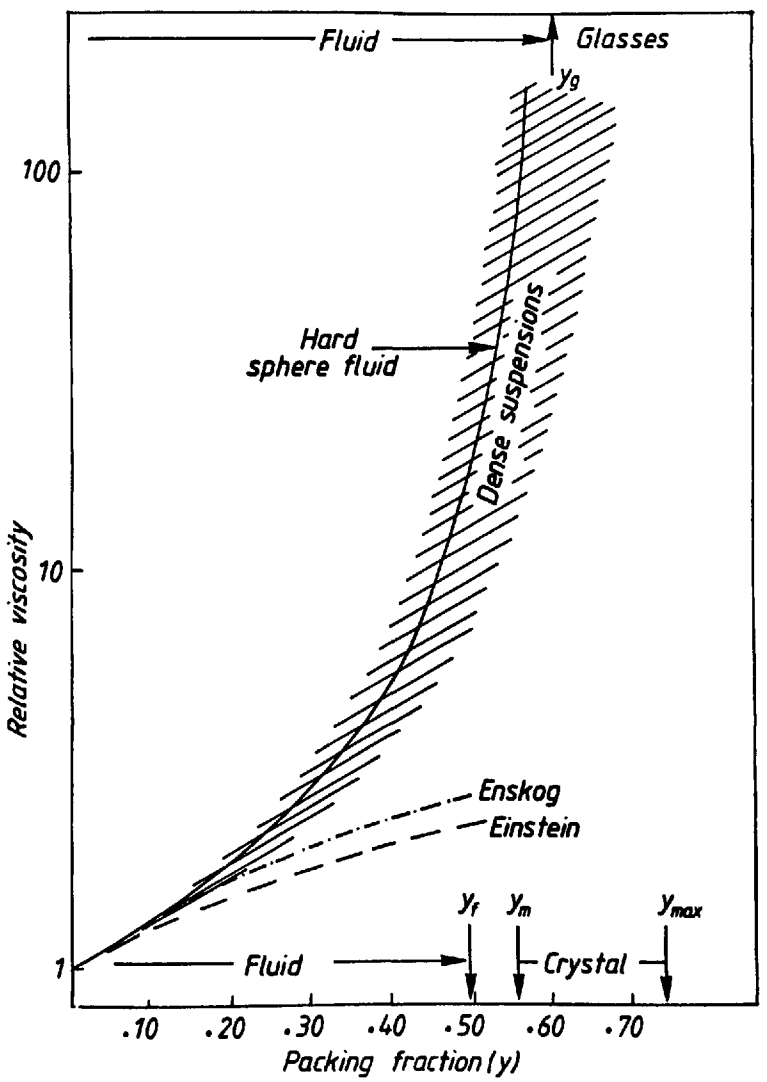

Fig. 1:
A comparison of the viscosity of the classical hard-sphere fluid with experimental dense suspension data; the hard-sphere data up to the freezing point (y_f) is taken from Alder et al., J. Chem. Phys. 53, 3813 (1970); for densities above y_f the H-S viscosity data are calculated using the Stokes-Einstein expression from the diffusion-coefficients given in Ann. N.Y. Acad. Sci. 371, 274 (1981); the experimental data is given and discussed in Ref. [9]

where y is the packing fraction. As η_m approaches zero the suspension is said to be "hydrodynamically weak". In this limit at low density, from the kinetic theory of gases due to Enskog [11] the viscosity is:

$$\eta = \frac{5}{16\sigma^2}\left(\frac{mkT}{\pi}\right)^{1/2}\left|\frac{1}{g(\sigma)} + \frac{16y}{5} + 12g(\sigma)y^2\right| \qquad (2)$$

where $g(\sigma)$ is the normalised pair contact probability.

Strenuous mathematical efforts have been made to improve upon Einstein's theory over the last half-century by calculating two- and many-body terms in the higher coefficients [13], but with little success at higher densities. Figure 1 suggests that when full collisional or geometric correlations are taken into account, in the spirit of Enskog but by exact many-particle dynamical simulations, the hard-sphere viscosity models the dense suspension results, to within the general uncertainty, and over the whole range up to the glass transition, quite well. The complex many-body hydrodynamic interactions may only be of small secondary importance relative to the hard-sphere geometric effects in determining the general physics of dense suspension rheology.

2. Equations of Motion

The NEMD method involves the imposition of a flow field upon a periodic system of particles contained in a basic cubic or rectangular cubic cell. By permitting the periodic boundaries to move obliquely with the shear flow the system remains homogeneous and surface effects are eliminated [3,4].

The equations of motion to be integrated numerically may take the form of straightforward Newtonian dynamics:

$$m\frac{d^2\underline{r}_i}{dt^2} = \underline{F}_i \qquad (3)$$

where $\underline{F}_i$ is the total force acting on particle i.

For colloidal supsensions the interparticle inertial forces are to some extent hydrodynamically damped; the heat capacity of the medium is large compared to the viscous heat. Isothermal Newtonian dynamics using velocity scaling techniques can be regarded as a first approximation to the equations of motion of dense suspensions.

In the purely viscous form the N-particle configuration and velocity dependent frictional forces in the hydrodynamic equations are deemed to be dominant. This method is referred to as Stokesian dynamics [13] and the equations-of-motion take the form of N-coupled first-order differential equations of the form:

$$\frac{d\underline{r}_i}{dt} = v_o(y) + \frac{\underline{F}_i}{6\pi\eta_m\sigma} + \sum_{j\neq i} \underline{\underline{S}}_{ij}\underline{f}_j \; . \qquad (4)$$

The last term on the RHS represents the pairwise approximation to many-body hydrodynamic interactions and $\underline{\underline{S}}_{ij}$ is the two-body friction tensor.

At zero shear the Stokesian dynamics cannot bring the system to thermodynamic equilibrium and it is necessary to involve Brownian motion.

The general equations of motion in the Brownian form are approximated by the Langevin equation:

$$m \frac{d^2 r_i}{dt^2} = - \underline{F}_i + \sum_{i,j} \underline{\underline{S}}_{ij} f_j + \underline{A}(t) \qquad (5)$$

where $\underline{A}(t)$ is a stochastic random force. A Brownian dynamics algorithm has been devised by Ermak and McCammon [14] and applied to flocculation rates in colloidal suspensions [15].

Very little is presently known about the consequences of the approximations of the Stokesian and Brownian dynamics algorithms on the dynamical properties of dense suspensions. For equilibrium properties the Stokesian technique is inapplicable and the Brownian method [14] always overestimates the pressure for particles with steep repulsive forces such as hard- and soft-spheres.

Initially we have neglected the explicit incorporation of hydrodynamics and Brownian motion in favour of a simple isothermal Newtonian dynamics algorithm to explore the basic physics of non-Newtonian flow. The soft-sphere potential defined by:

$$\phi(r) = \varepsilon(\sigma/r)^{12} \qquad (6)$$

can be regarded as a potential of average force between the particles, and should be a good representation where the dynamics are predominantly geometrically determined by the repulsive potential.

Some justification for relating damped Newtonian dynamics to dense suspension mechanics can be obtained from a rough calculation of the average distance to the first neighbour in the hard-sphere fluid/glass as follows.

The osmotic equation of state is given by:

$$pV/NkT = 1 + \frac{2}{3} \pi \rho \, g(\sigma). \qquad (7)$$

To obtain $g(\sigma)$ we can use a reasonably accurate self-consistent free volume equation of state for hard spheres up to amorphous close packing [16] ($v_o = \pi^2\sigma^3/12$):

$$\frac{pV}{NkT} = \left| 1 - \left[\frac{V_o}{V}\right]^{1/3} \right|^{-1} \qquad (8)$$

where V_o is the amorphous close-packed volume. The number of neighbours up to a short distance x from a sphere is:

$$n(x) = \int_{\sigma}^{\sigma + x} 4\pi r^2 \rho g(\sigma)\, dr$$

putting $n = 1$ and solving for x we obtain an average nearest neighbour distance:

$$x = \left| \frac{1}{3\pi y} + \frac{5}{6} \right|^{1/2} - 1 . \qquad (9)$$

The simple result shows that even when y is 0.5 the average distance between first neighbours is $\sigma/100$. For 1 micron particles in molecular media this is as little as 10's of molecular diameters. Since there are surface ordering effects and surface roughness of the same order, we do not expect the long-range hydrodynamic effects or Brownian motion to be of importance in the intermediate to high packing range. The predominant force on a particle derives from near neighbour geometric effects and a slightly soft potential of average force such as Eq. (6) should capture the basic physics of non-Newtonian flow in the concentrated particle regions.

All the results referred to in the following section refer to NEMD studies of $N = 512$ soft-spheres at the constant total particle energy $N\varepsilon$.

3. Soft-Sphere Rheology

Figure 2 summarises the results to date for the effect of a shear field on the average pressure for the soft-sphere model. The results show a number of phase boundaries which derive from equilibrium behaviour of the soft-sphere model.

In the higher density range at lower shear rates there is an ordering phase transition which stems from a shear perturbation of the equilibrium field freezing point. Over a finite shear rate range at constant volume two-phase regions are observed. The ordered phases take the form of smectic-like layers sliding over each other. This ordering effect accounts for the well-known time-dependent shear thinning effect known as thixotropy and has been discussed previously [7]. This depression of the "freezing" transition to lower densities with shear rate can be understood since the layered crystal-like phase is more amenable to shear flow than the disordered phase.

At higher shear rates the smectic phase-amorphous fluid phase coexistence line appears to terminate at a triple point at around $\dot{\gamma} = 10^2$ in reduced units.

To understand this behaviour we must consider the evidence for a percolation transition that may exist in all rigid models in the intermediate density range. This transition may be associated with a discontinuity in viscosity and other transport properties, even without a hydrodynamic flow field, a requirement postulated by

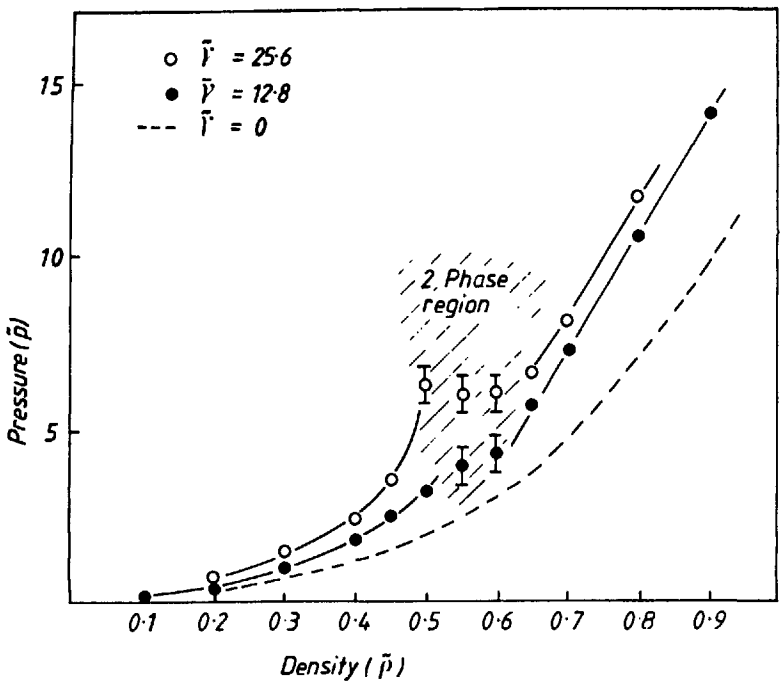

Fig. 2:
Density dependence of the sheared soft-sphere fjluid pressure along two "iso-shears" compared with the equilibrium equation-of-state (dashed line) from Cape and Woodcock, J. Chem. Phys. 72, 976 (1980); excepting the two-phase region the statistical uncertainties are of the order of the circle radii

de Gennes [17].

Hoover at al. [18] reported an exact relation for the equation of state of hard core systems of diameter σ:

$$\frac{pV}{NkT} = 1 + \frac{\sigma}{2D} \langle s_f/V_f \rangle \tag{10}$$

where S_f and V_f are, respectively, the surface areas and volume asseccible to a single particle in a fixed configuration of the remaining (N-1) particles. D is the dimensionality. At low densities, where a single particle can, on average, percolate the whole configuration, S_f and V_f are extensive, being proportional to N. At higher densities S_f and V_f are intensive and independent of N. In the thermodynamic limit of large N there is a critical density point at which S_f and V_f change from extensive to intensive. This is the percolation transition.

Speedy [19] has derived a very similar relation using the "spare" volume concept. This is the volume accessible to the (N+1)st. particle ensemble, i.e.

$$\frac{pV}{NkT} = 1 + \frac{\sigma}{2D} \langle S_s \rangle / \langle V_s \rangle \ . \tag{11}$$

$\langle V_s \rangle$ is related to the chemical potential by:

$$\mu_{N,V,T} = - kT \ \ell n \ \langle V_s/V \rangle \ . \tag{12}$$

At very low densities $S_s \equiv S_f$, $V_s \equiv V_f$ and Eqs. (10) and (11) become identical. Eq. (3) shows that any discontinuity in $\langle V_s \rangle$ of order n would lead to a thermodynamic phase change of order (n+1).

The relationship between V_f and V_s at densities above the percolation transition, where V_s takes the form of many discrete cavities, has also been examined by Speedy [20]. The ratios are related to fluctuations about the mean value of V_f:

$$\langle V_f \rangle = \langle V_s \rangle \ (1 + \langle \Delta V_f^2 \rangle / \langle V_f \rangle^2). \tag{13}$$

Thus, at the percolation transition, $\langle V_f \rangle / \langle V_s \rangle$ increases abruptly from unity. This suggests that the transition could be associated with a higher-order thermodynamic discontinuity depending on the variations of $\langle S_f \rangle$ and $\langle V_f \rangle$ through the transition.

So far, there is no evidence to suggest any such thermodynamic transition for hard-spheres. Intuitively, however, one might expect the virial expansion based on the Mayer cluster integrals to fail to converge when a single cluster (defined as particles separated by unit diameter or less). The percolation transition has, however, been located for a system of two-dimensional discs by direct numerical calculations of $\langle V_f \rangle$ [21]. It occurs at the density $\rho/\rho_0 = 0.245$, i.e. 22% packing.

Diffusion and viscosity data for hard-sphere fluids exhibit two distinct regions as do many experimental supercritical dense fluids. Only above a density around 25% packing do fluids adhere to the exponential Arrhenius form, and obey the Stokes-Einstein relationship.

Hiwatari and co-workers [22] have reported a distinct change in the forms of the velocity autocorrelation function and the pair distribution function, "from gas-like to liquid-like", for the $n = 12$ soft-sphere model at the reduced density 0.5. For $kT = \varepsilon$ this corresponds to a packing fraction of 0.262.

The imposition of a perturbing shear strain on such a percolation transition disturbs the statistical geometry, and hence $\langle V_s \rangle$ and should therefore affect the chemical potential differently on either side of the transition. This implies the possibility of a first-order thermodynamic phase transition between high- and low-density phases, or, at constant volume, the existence of two fluid phase regions stemming from the percolation transition. The effect of a shear perturbation can be compared with the gradual imposition of an attractive potential to a purely repulsive fluid system yielding a critical point and two fluid phases. The stronger the perturbing potential the greater the entropy/density gap. The shear strain has an effect similar to the imposition of a non-symmetric attractive potential in the directions normal to the velocity gradient.

Calculations carried out for the soft-sphere model in the intermediate density range have verified the existence of a two-phase, gas-like and liquid-like regions. Figure 3 shows the pressure along two "isohears" as a function of density. The origin of the

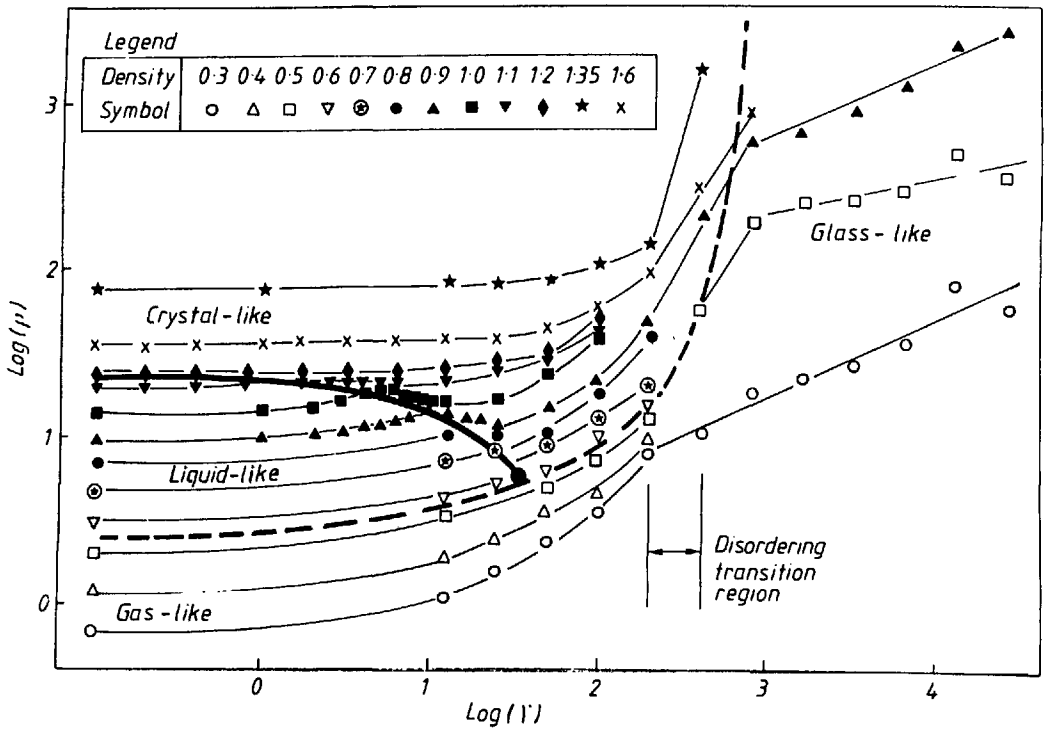

Fig. 3: NEMD mean pressure data for the soft-sphere model showing the phase behaviour on logarithmic scales; the pressure and shear rate are in reduced soft-sphere units of σ^3/ε and $(m\sigma^2/\varepsilon)$ respectively. The points sit on isochores at the reduced densities shown in the legend and the thermal energy is ε. The larger solid sphere at the junction of the two-phase co-existence denotes a triple point

transition is close to the value 0.5 predicted by Hiwatari and co-workers [22]. This can account for shear flocculation [23].

Clearly these phase transitions will have a strong number dependence and much more extensive simulation data is required for precise characterisation. The important point at this stage is that the soft-sphere model is exhibiting all the non-Newtonian effects commonly encountered in dense supsensions. We now have an understanding and explanation for the complex constitutive rheological relations found for colloidal materials.

4. Glass Transition Effects

One effect of the shear field anisotropy is that the state functions such as the pressure, thermal energy and diffusivity become highly anisotropic. Large normal pressure differences are observed and these can explain well-known phenomena such as wall slip in open systems and Weissenberg effects [1].

Of particular interest in relation to the glass transition is the behaviour of the three diffusion coefficients, D_{xx}, D_{yy} and D_{zz}, which can be computed from the mean square displacement.

In the amorphous fluid region of the phase diagram, and the metastable amorphous region (which can be observed if the observation time is short compared to the thixotropic structural relaxation time), D_{yy} and D_{zz}, the normal diffusivities, decrease with increasing shear rate. This gives rise to the phenomenon of a shear-induced glass transition point decreasing with increasing shear rate associated with very long relaxation times and pronounced time-dependent viscoelastic effects.

At very high shear rates the smectic phases (crystal-like) shown in Figure 2 become unstable, probably with respects to a solid-like and gas-like two-phase behaviour. At these very high shear rates $10^2 - 10^3$, however, the metastable sheared fluid is effectively vitreous and a reversion to the, now glass-like, amorphous phase is observed, accompanied by very long relaxation times and viscoelasticity. This is the commonly observed shear thickening effect found in dense suspensions [6]. The transition shows two-phase behaviour and appears first-order.

In order to demonstrate the effects of packing restrictions in the high density regions, and the general patterns of non-Newtonian behaviour a schematic picture of the approximately predicted behaviour of the hard-sphere model is shown in Figure 4. The ordering transition has already been observed by Erpenbeck [24].

The general steady-state non-Newtonian rheology is seen to be a shear perturbation of the equilibrium phase behaviour, observed explicitly for soft-spheres. Superimposed on the steady-state equilibrium phase diagram are the glass transition and amorphous packing singularities. The amorphous two-dimensional glass-like region which is metastable becomes dominant both in computer experiments and in real experiments at high shear rates [6]. The reason is that the relaxation times in the directions perpendicular to the flow eventually exceed the structural re-equilibration times. It seems likely that the sheared-crystal phase in the packing range 64-74% is non-existent at high shear rates, above $\sim 10^2$, which is the characteristic crystal frequency. In this case the fluid may either have a diverging pressure with strong solid-like viscoelastic effects or dilate and disorder into the metastable amorphous region.

Conclusions

From the results obtained to date a number of general conclusions about the nature of non-Newtonian flow may be stated.

Non-Newtonian behaviour is associated with a shear perturbation of a system in thermodynamic equilibrium which is sufficient to change the thermodynamic properties. The characteristic time for the onset of non-Newtonian behaviour is the Weissenberg number $\dot{\gamma}\tau$. All materials become, therefore, non-Newtonian fluids in this shear domain.

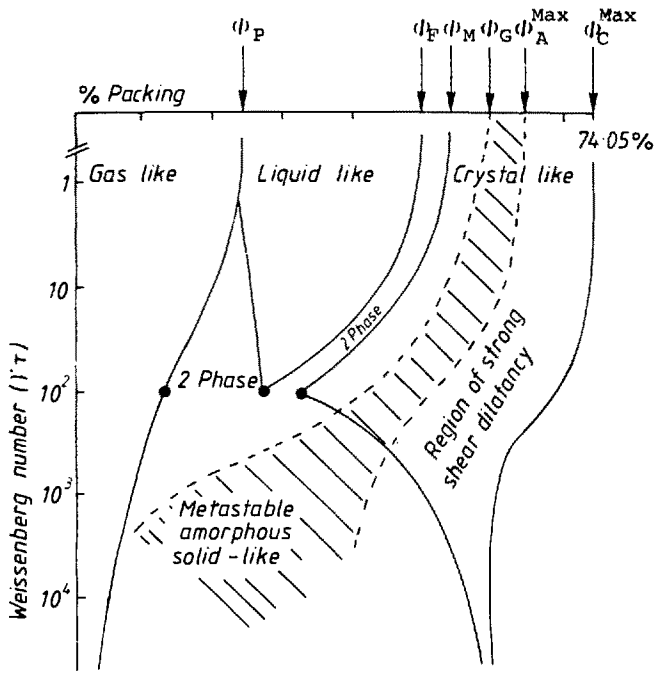

Symbols

- $\dot{\gamma}$ *Shear rate*
- τ *Characteristic time*
- ϕ_P *Percolation transition density*
- ϕ_F *Fluid freezing density*
- ϕ_M *Crystal (HCP or FCC) melting density*
- ϕ_G *Glass transition*
- ϕ^{Max} *Maximum amorphous and crystal packing*

Fig. 4: Schematic picture of the predicted phase behaviour in a hard-sphere model showing how the two-phase regions stem from the known equlibrium phase transition; the phase diagram shows remarkable similarity to the effect of an attractive potential on the hard-sphere model as the temperature is reduced

All the common non-Newtonian effects which occur in dense colloidal suspensions have been seen to occur in the simple soft-sphere model. These effects such as shear flocculation and shear induced ordering can be traced to shear perturbations of equilibrium phase transition phenomena.

The effect of a shear field on the glass-transition is to decrease the density (or increase the temperature) at which it occurs. The diffusivity, besides the pressure, exhibits large normal differences over the whole non-Newtonian range and the diffusivities D_{xx} and D_{yy} decrease markedly leading to long relaxation times, eventually infinite, and shear induced glass transition effects.

The overall effect of a shear perturbation on the phase diagram of a simple repulsive sphere model, hard or soft, is remarkably similar to the effect of an attractive

potential in giving rise to two "fluid" phases and a reduction in the "solid-fluid" freezing and melting densities, and a triple point.

This similarity can be loosely understood; to move past each other more comfortably in the direction of the velocity gradient (dv_y/d_x) the particles must be effectively more cohesive in the other two directions (the x-z plane). Thus, the effect of the shear field is rather like an anisotropic attractive potential, acting in the plane perpendicular to the gradient, which is strong relative to kT .

References

[1] See e.g. J. Harris, "Rheology and non-Newtonian Flow", Longman Inc. (New York: 1977)

[2] W.T. Ashurst and W.G. Hoover, Phys. REv. A11, 658 (1975)

[3] D.M. Heyes, J.J. Kim, C.J. Montrose and T.A. Litovitz, J. Chem. Phys. 73, 3981 (1980)

[4] D.J. Evans, Physica 118A, 51 (1983)

[5] See e.g. Physics Today Special Issue "Fluids Out of Equlibrium", January (1984), Edited by H.J.M. Hanley

[6] L.V. Woodcock, Chem. Phys. Lett. 111, 455 (1984)

[7] L.V. Woodcock, Phys. Rev. Lett. 54, 1513 (1985)

[8] L.V. Woodcock, J. Non-Newtonian Fl. Mech. 19, 349 (1986)

[9] Taken from D.C.-H. Chen, Powder Tech. 37, 255 (1984); see also L.V. Woodcock and M.F. Edwards, I. Chem. E. Symposium Series 91, 107 (1985)

[10] "Brownian Motion", A. Einstein (Dover Publications Inc., 1956)

[11] See e.g. S. Chapman and T.G. Gowling, "The Mathematical Theory of Non-Uniform Gases", Chapter 16 (Cambridge University Press: 1939)

[12] W.R. Schowalter, "Mechanics of Non-Newtonian Fluids", Chapter 13 Pergamon, New York (1978)

[13] G. Bossis and J.F. Brady, J. Chem. Phys. 80, 5141 (1984)

[14] D.L. Ermak and J.A. McCammon, J. Chem. Phys. 69 1352 (1978)

[15] J. Bacon, E. Dickinson and R. Parker, Farad. Disc. Chem. Soc. 76, 165 (1983)

[16] L.V. Woodcock, Ann. N.Y. Acad. Sci. 371, 274 (1981)

[17] P.G. De Gennes, J. Phys. 40, 783 (1979)

[18] W.G. Hoover, W.T. Ashurst and R. Grover, J. Chem. Phys. 57, 1259 (1972)

[19] R.J. Speedy, J. Chem. Soc. Farad. Trans. II, 76, 693 (1980)

[20] R.J. Speedy, J. Chem. Soc. Farad. Trans. II, 77, 329 (1981)

[21] W.G. Hoover, N.W. Hoover and K. Hanson, J. Chem. Phys. 70, 1837 (1979)

[22] Y. Hiwatari, H. Matsuda, T. Ogawa, N. Ogita and A. Ueda, Prog. Theor. Phys. 52, 1105 (1974)

[23] See e.g. "Polymer Colloids", Eds. R. Buscall, T. Corner and J.F. Stageman, Chapters 5 and 6 (R. Buscall and I. Krieger), Elsevier (New York: 1985)

[24] J.J. Erpenbeck, Phys. Rev. Lett. 52, 1333 (1984)

^{13}C NMR INVESTIGATION OF LOCAL MOTIONS INVOLVED IN SECONDARY RELAXATION OF POLYMERS

Lucien Monnerie

Laboratoire de Physicochimie Structurale et Macromolèculaire,
associé au CNRS, Ecole Supérieure de Physique et de Chimie
Industrielles de la Ville de Paris,
10, rue Vauquelin
75231 Paris Cedex 05
France

Summary

The ^{13}C NMR methods which can be used to study the local dynamics of solid samples through the cross-polarization and magic angle spinning technique are briefly reviewed. We present results obtained on solid polycycloalkyl methacrylates, polybutylene terephtalate, polystyrene and substituted polystyrenes and compare them with mechanical relaxation measurements.

Introduction

For many years classical high resolution ^{13}C NMR technique has been used to investigate the local dynamics of polymers in solution. Unfortunately, the study of solid polymers with classical NMR experiments is hindered by the breath of the observed resonance lines, resulting from the chemical shift anisotropy and the dipolar coupling.

The recent development of the cross-polarization and magic angle spinning technique allows the observation of high resolution ^{13}C NMR spectra of solid samples. Thus, it is possible to apply these methods to solid polymers and to examine the local motions which occur.

In this paper, we briefly review the ^{13}C NMR methods which can be used to study dynamics in solid samples. Then, we present several examples of investigations of local motions in solid polycycloalkyl methacrylates, polybutylene terephtalate, polystyrene and its derivatives.

^{13}C NMR Methods for Studying Dynamics in Solid Samples

A recent review on high-resolution ^{13}C NMR in solid polymers, including studies on dynamics can be found in Ref. [1]. Ref. [2-5] contain more detailed information.

^{13}C is naturally present in the skeleton of molecules but because of low isotropic abondance (~1%) there is no dipolar coupling between ^{13}C spins. However, there is a remaining dipolar coupling with proton spins.

The magnetic relaxation times of a ^{13}C will depend upon the orientational motions of the vectors between the ^{13}C and its bounded protons exclusively. More distant protons cannot efficiently contribute. In particular, there are no intermolecular contributions.

The main interest of ^{13}C NMR studies is that the resonance lines of the different C atoms of a molecule are usually sufficiently well separated to study the orientational motion of a specific C-H bond.

Information on mobility can be obtained from the high chemical shift anisotropy observed for ^{13}C lines. In a static sample, the chemical shift of a given ^{13}C depends on the orientation of the molecule relative to the applied magnetic field. In a powder sample, the spectrum obtained without magic angle spinning corresponds to the superposition of chemical shifts arising from various orientations (Fig.1a). If sufficiently fast molecular motions occur (with correlation times, τ, in the range 10^{-2}s to 10^{-5}s), the chemical shift anisotropy tensor will be averaged by the motions and the shape of the line will be changed. Fig. 1b and 1c show the case of a phenyl ring undergoing a fast rotation around an axis either perpendicular or parallel to the plane of the phenyl ring. It is worth noting that this effect is large for C = C, C = O but small for aliphatic C .

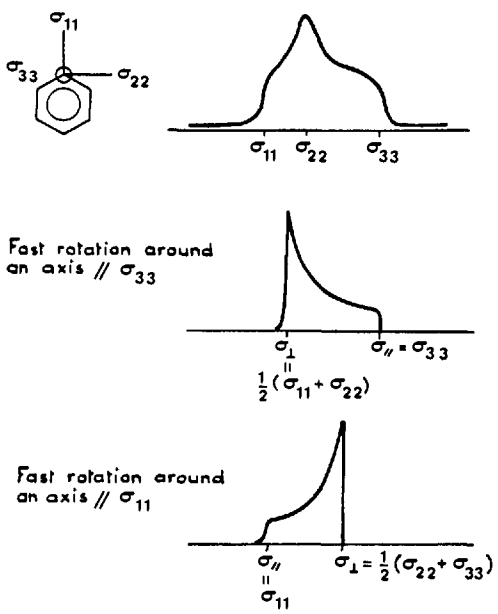

Fig. 1. Effect of molecular motions on the shape of the ^{13}C spectrum of benzene due to the chemical shift anisotropy

In some cases, the aspect of the ^{13}C spectrum can be modified by local motions. This deals with chemical exchange and corresponds to the fact that ^{13}C sites of a molecule which would be inequivalent in a rigid molecule (and would result in different lines) can become equivalent if molecular motions occur (leading to a single line). In these cases, the aspects of the spectrum is strongly dependent on the correlation time, τ, of the motion in the range 10^{-1} s to 10^{-4} s. Such an effect is illustrated

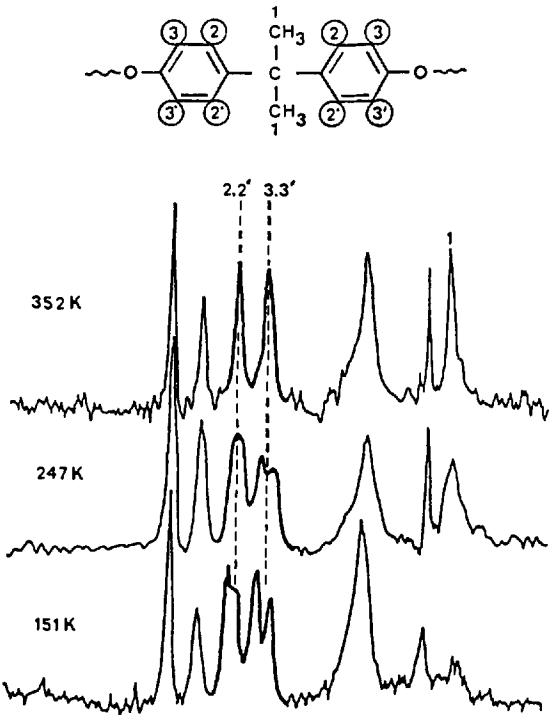

Fig. 2. Example of the chemical exchange effect on ^{13}C spectra obtained with cross-polarization and magic angle spinning. From Ref. [22]

in Fig. 2 for an epoxy resin in which the occurrence of phenyl ring flipping in the bis-phenol A unit renders some carbons equivalent.

Another way of obtaining information on molecular motions is from line-width measurements. Both static and dynamic mechanisms can broaden resonance lines. Among the static contributions, the most significant are the variation of the local magnetic susceptibility in the sample, the chemical shift dispersions due to packing effects, bond distortions, conformational inequivalences, however these have a small effect relative to the dynamic contributions. The dynamic mechanisms include the motional modulation of the chemical shift anisotropy (as above) and the motional modulation of the dipolar ^{13}C-H coupling. This latter produces a large effect when the rate of molecular motion is equal to the Larmor frequency of the protons (10^{-4} s > τ > 10^{-7} s). As a typical example, Fig. 3 shows the dependence of the line-width of a CH_2 group undergoing a libration of amplitude 7^o within a characteristic correlation time, τ.

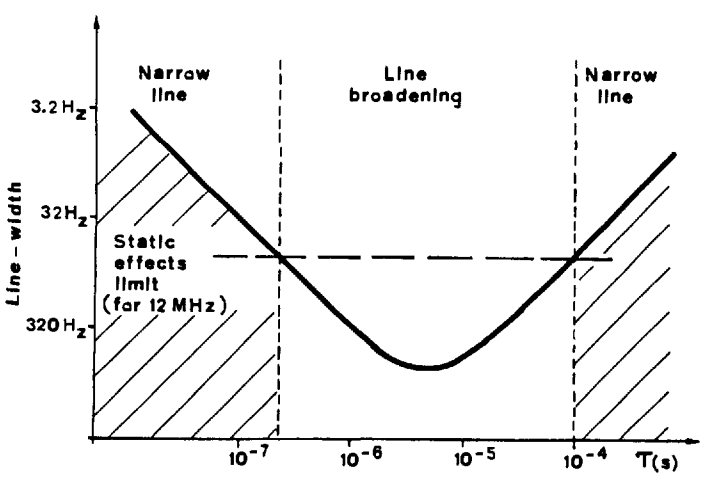

Fig. 3. Variation of the line-width of a CH_2 group with the correlation time of the 7^o libration performed by the group. $\omega_{1H} = 2.32$ KHz

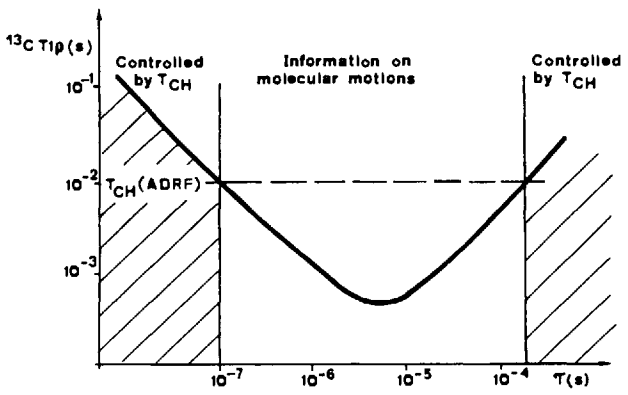

Fig. 4. Variation of the ^{13}C T_1 of a CH_2 group with the correlation time of the 7^0 libration performed by the group. ω_{1H} = 2.32 KHz

These methods give qualitative information about the molecular motions in the appropriate frequency range. More quantitative results can be obtained through the longitudinal relaxation of the total magnetization (also called spin-lattice relaxation), measured either in the static magnetic field (the characteristic relaxation time is T_1) or in the rotating magnetic field (the characteristic relaxation time is $T_{1\rho}$). As regards the T_1 relaxation time, there is no contribution from the ^{13}C-^{13}C spin diffusion and in order to be efficient the molecular motions have to get very short correlation times (5.10^{-7} s > τ > 5.10^{-10} s). The situation is more complex in the case of $T_{1\rho}$ because two different mechanisms are involved. The first one is related to the molecular motions with correlation times in the range 10^{-6} s to 10^{-4} s and this contribution to $T_{1\rho}$ is called $(^{13}C\ T_{1\rho})_{spin\text{-}lattice}$, and it is the quantity of interest for the investigation of dynamics. The second contribution deals with the polarization transfer from ^{13}C to ^{1}H and corresponds to an adiabatic demagnetization the rotating frame and it is called T_{CH}(ADRF). This transfer increases when strong static dipolar interactions ^{1}H - ^{1}H exist, which lead to spin diffusion. The ^{13}C T_1 relaxation time can be written as:

$$[^{13}C\ T_{1\rho}]^{-1} = [^{13}C\ T_{1\rho}]^{-1}_{spin\text{-}lattice} + [T_{CH}(ADRF)]^{-1}\ .$$

In crystalline polymers where the spin diffusion process is dominant, one obtains:

$$^{13}C\ T_{1\rho} \cong T_{CH}(ADRF)$$

and no information on molecular motions can be derived from ^{13}C $T_{1\rho}$ measurements. On the contrary, for amorphous polymers both processes contribute to ^{13}C $T_{1\rho}$ in such a way that it is possible, after estimating the contribution of the ADRF, to obtain information on molecular motions. The range of motional correlation times which can be studied through ^{13}C $T_{1\rho}$ measurements is pictured in Fig. 4 for the

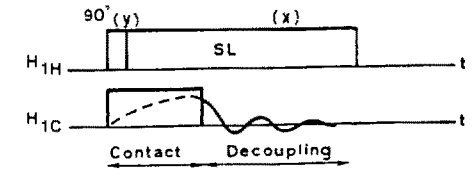

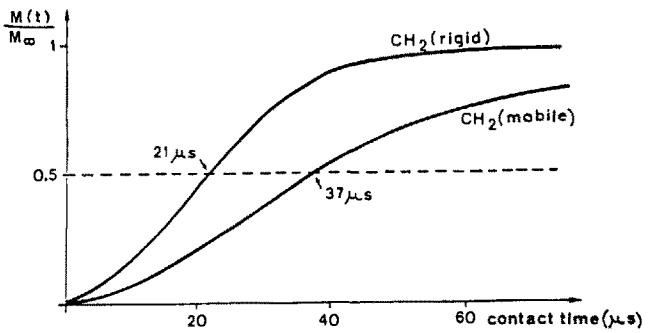

Fig. 5. Rise of ^{13}C polarization of a CH_2 group vs. the contact time in a spin-lock cross-polarization experiment

case of a CH_2 group undergoing libration with an amplitude of 7^o.

Finally, molecular motions can be detected by measuring the cross-polarization relaxation time in a spin-lock experiment. The increase of ^{13}C polarization during the contact time with the spin-lock polarized ^1H depends on the residual static dipolar interactions. Thus, when fast motions occur, the rise of ^{13}C polarization as a function of contact duration becomes slower. This is illustrated in Fig. 5 for CH_2 groups. The time to reach half of the total polarization, $t_{1/2}$, depends on the strength of the dipolar interaction of the C atom under consideration and its bound protons. For example, values of $t_{1/2}$ as short as 20 μs for a CH_2 group or 28 μs for a CH group are indicative of rigid-lattice type behaviour at the involved frequency ($\sim 10^5$Hz). Longer $t_{1/2}$ values are evidence for motions.

Local Motion in Solid Poly(Cycloalkylmethacrylates)

The series of poly(cycloalkylmethacrylates) provide a very interesting illustration of the use of high-resolution solid state ^{13}C NMR to investigate molecular motions in solid amorphous polymers. This series of polymers has been extensively studied by Heijboer [6] with mechanical relaxation techniques. The strong mechanical loss peak observed in these compounds has been assigned to molecular motions of the rings. However, this assignment was a painful task and required determinations of mechanical relaxations for a large series of poly(cyclohexylmethacrylates) modified by various substitutions of the cyclohexyl ring. Recently this series of polymers has been investigated by ^{13}C NMR by Lauprêtre et al. [7,8].

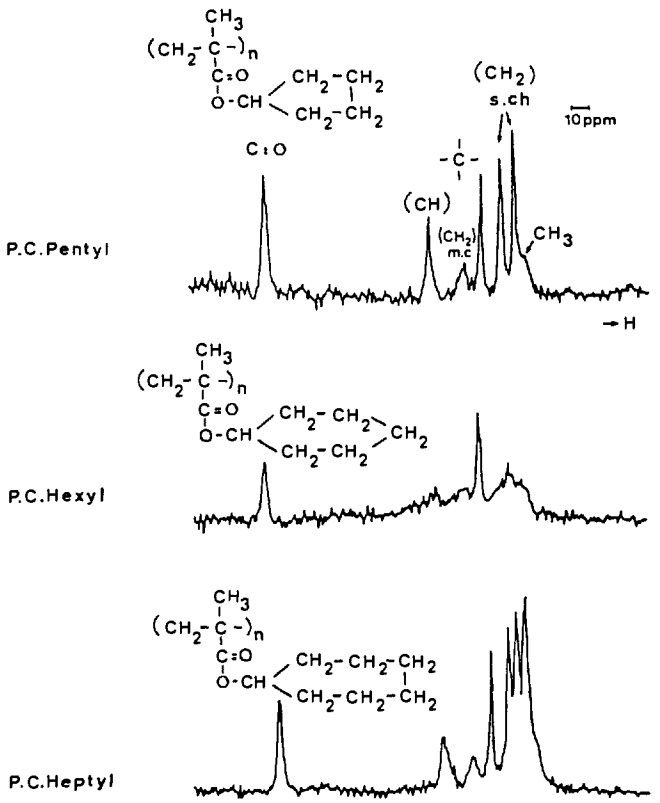

Fig. 6. 12 MHz-MAS-CP ^{13}C NMR spectra of solid poly(cyclopentyl methacrylate) (a), Poly(cyclohexyl methacrylate)(b), poly(cycloheptyl methacrylate) (c). From Ref. [7]

The first study [7] dealt with the mobility of cyclopentyl, cycolhexyl, cycloheptyl, polymethacrylates at 25°C. The corresponding spectra are shown in Fig. 6 and it is clear that the cyclohexyl derivative exhibits broad aliphatic lines indicating the occurrence of motions of the side-chain ring with correlation times around 10^{-5} s-10^{-6}s. On the contrary, for cyclopentyl and cyclohexyl derivatives, the aliphatic lines are narrow and at this stage it is not possible to distinguish between very fast ($\tau << 10^{-6}$s) or very slow ($\tau << 10^{-5}$ s) motions of the side-chain rings. This ambiguity is overcome by measuring the rise in ^{13}C polarization. From the results reported in Fig. 7, it can be concluded that the side-chains CH and CH_2 are substantially mobile, but that the motional averaging is not complete indicating that the rings undergo fast anisotropic movements at frequencies higher than 10^5 Hz. On the contrary, the motions of the main-chain CH_2 are much slower than 10^5 Hz. Mechanical relaxation measurements for poly(cyclopentylmethacrylate) (6) indicate that the maximum loss due to ring motions observed at 180 KHz occurs at -185°C and the associated activation energy is 13.3 KJ.mole^{-1}, leading to a correlation time of 3.10^{-12}s at 25°C. Similarly, for poly(cycloheptylmethacrylate), the maximum loss observed at 1 Hz occurs at

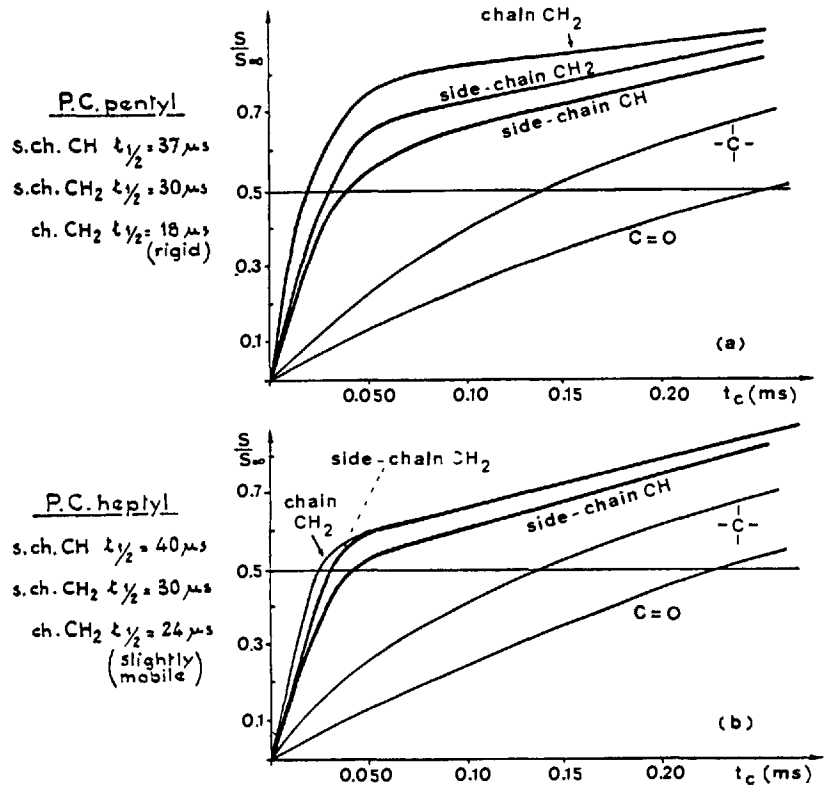

Fig. 7. Variation of ^{13}C magnetization in a spin-lock experiment as a function of contact duration t_c : (a) poly(cyclopentyl methacrylate), (b) poly(cycloheptyl methacrylate). From Ref. [7]

-180°C and the activation energy is 26.6 KJ.mole^{-1}, yielding a correlation time of 5.10^{-10} s at 25°C. These values of the correlation times of the side-chain ring motions are in agreement with the ^{13}C NMR observations.

As regards poly(cyclohexylmethacrylate), $^{13}C_{1\rho}$ measurements show that the values for the side-chains CH_2 and CH are 10 times shorter for cyclohexyl than for the two other derivatives, indicating that the side-chain motions in this polymer have correlation times around 10^{-6} s at 25°C. This observation is in agreement with the value $.3.10^{-6}$ s derived from the mechanical relaxation data, i.e. a maximum loss at -80°C for 1 Hz and an activation energy of 48.6 KJ.mole^{-1}.

Moreover, the chemical shift anisotropy measurements of the C = O group performed on the three poly(cycloalkylmethacrylates) and on solid methyl acetate (at low T) show that the side-chain motions induce very limited reorientation of the ester group (less than 10° to 20°) in a time range shorter than 10^{-2} s .

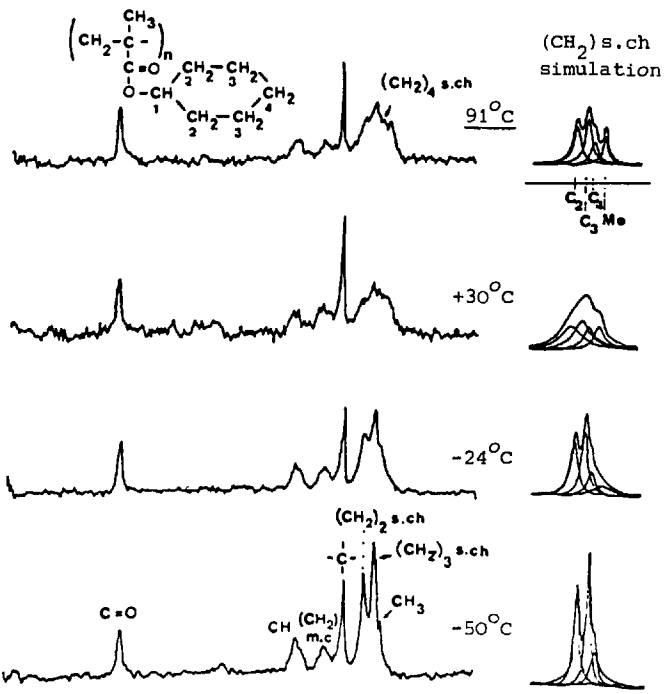

Fig. 8. Experimental 12 MHz MAS CP ^{13}C NMR spectra of solid poly(cyclohexylmethacrylate) at various temperatures. From Ref. [8]

Complementary information on the type of motion undergone by the cyclohexyl side-chain has been obtained from measurements at various temperatures between -50°C and +91°C [8]. It is clear from Fig. 8 that the resonance line of carbon C_4 is broadened to a smaller extent than those of C_2 and C_3, and CH_2 is independent of temperature. Thus, the ring motion mainly affects C_2-H and C_3-H vectors but leaves C_1-H and C_4-H vectors nearly unchanged. Such a behaviour is in complete agreement with the chain-chain conformational change, proposed for the cyclohexyl side-chain motion [6], and represented on Fig. 9. Indeed, this conformation change translates but does not affect the orientation of the C_1-H and C_4-H vectors, whereas it modifies the orientations of C_2-H and C_3-H vectors.

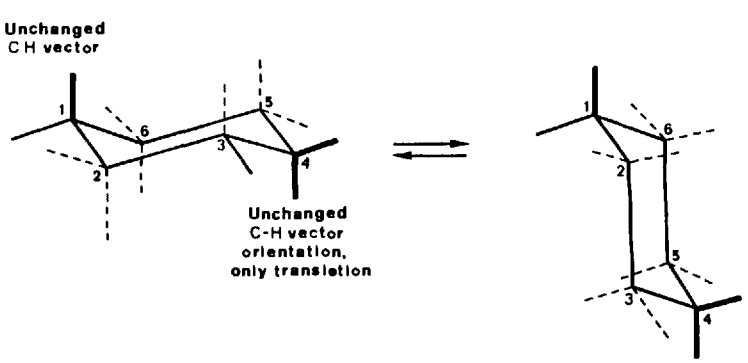

Fig. 9. Chain-chain inversion of a cyclohexyl ring with carbon 1 in a fixed position. From Ref. [8]

Finally, the activation energy for the cyclohexyl motion deduced from NMR data is identical to that obtained by mechanical relaxation.

Local Motions in Polybutyleneterephtalate

Another interesting example of investigation of motions in solid polymers deals with the series of NMR (^{13}C and D) studies performed by Jelinski et al. on poly(butyleneterephtalate) and various copoly ester-ethers [9-14].

The poly(butyleneterephtalate) (PBT) is a semicrystalline polymer, with the following chemical structure:

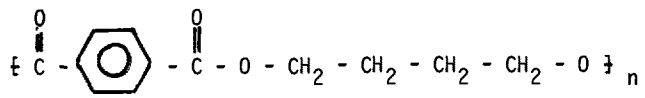

and it exhibits a glass-transition temperature at around 80°C, as observed by DSC.

Chemical shift anisotropy measurements performed by changing the spinning angle and comparing the experimental and calculated spectra (Fig. 10) leads to the results reported in Table I for both P.B.T. and solid dimethylterephtalate. It is clear that the chemical shift anisotropy of the central CH_2-groups is partially averaged by motions which do not involve the OCH_2-groups to a great extent.

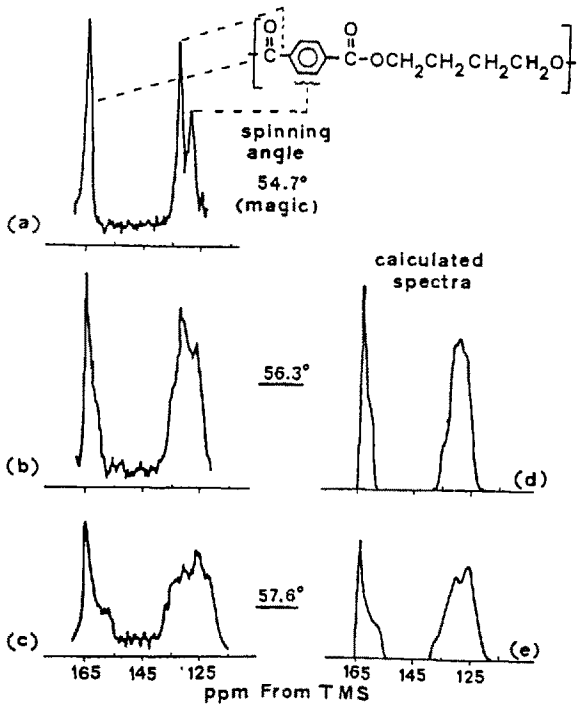

Fig. 10. 50.3 CP ^{13}C NMR spectra of solid poly(butyleneterephtalate) for various spinning angles with respect to the magnetic field. From Ref. [11]

Table I: Chemical shift parameters for P.B.T. and di Methyl Terephtalate

	$(\sigma_{33} - \sigma_{11})$ in p.p.m.	
	P.B.T.	di Methyl Terephtalate
OCH_2	60 (rigid)	
CH_2	14 (mobile)	
C = O	127	137
Protonated Arom. C	198	215
Non-proton Arom. C	202	201

^{13}C relaxation times (T_1 and $T_{1\rho}$) have been measured for PBT in solid state and in solution; the results are gathered in Table II. The short values of ^{13}C T_1 for OCH_2 and central CH_2-groups in solid PBT indicate a substantial spectral density in the MHz range, i.e. the occurrence of motions with correlation times in the range 10^{-5} s - 10^{-6} s. Furthermore, the different T_1-values observed for OCH_2 and CH_2 prove that the central CH_2-groups undergo motions of larger amplitude or greater frequency than the OCH_2-groups. This last conclusion is also drawn from measurements performed on PBT in solution.

Table II: Relaxation times T_1, $T_{1\rho}$ and Overhauser effect for P.B.T. in solid state and solution

I - Solid State	^{13}C T_1	^{13}C $T_{1\rho}$	
		37 KHz	20 KHz
Protonated Arom. C	2s	8.3 ms	3.8 ms
O - CH_2	0.47 s	4.8 ms	1.5 ms
Central CH_2	0.3 s	5.0 ms	1.8 ms

II - Solution in m-cresol at 100°C

	$^{13}C\ T_1$	NOE
$O-CH_2$	0.33 s	2.73
central CH_2	0.50 s	3.03

In order to learn more details about the type of motion undergone by the flexible aliphatic sequence of PBT, D-NMR spectra have been recorded at various T for selectively deuterated PBT:

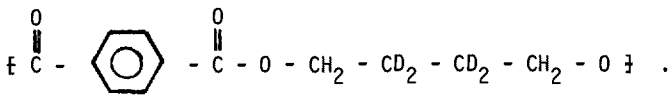

They are compared in Fig. 11 with the spectra calculated by assuming a model of jumping between two sites separated by 103° with the rate constants indicated in the figure. These data yield a correlation time of 7.10^{-6} s at 20°C and an activation energy of 25 KJ.mole^{-1}.

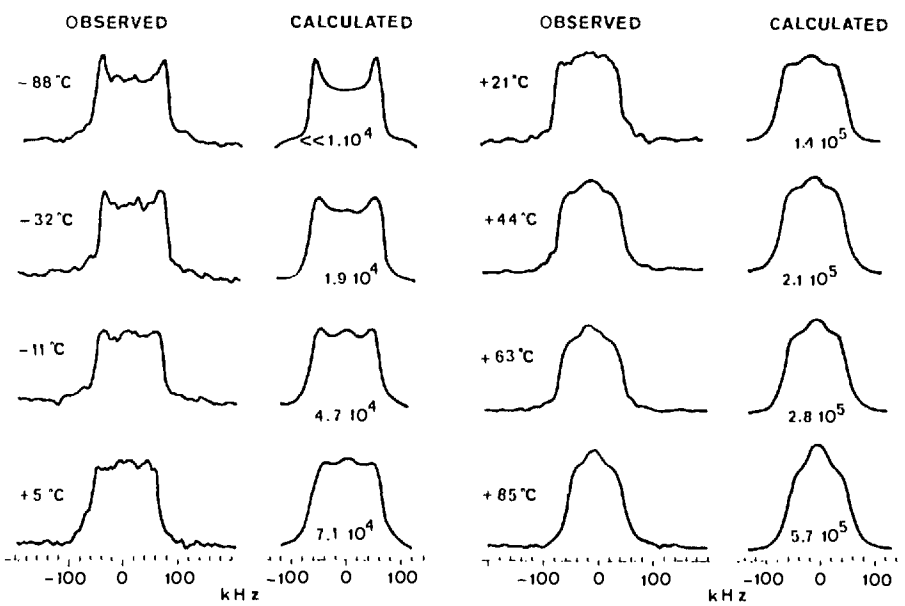

Fig. 11. Observed and calculated solid state D-NMR. Spectra of poly(butylene terephtalate) selectively deuterated on the central butanediol carbins, spectra at different temperatures. From Ref. [13]

Different types of motions can be considered for the aliphatic sequence of PBT, and they are pictured in Fig. 12. We will successively discuss each of them and compare their effect on the relative mobility of OCH_2 and central CH_2-groups with the experimental evidence that the central CH_2 undergo motions of either larger amplitude or greater frequency than the OCH_2-groups. The simplest motion (Fig. 12a) corresponds to a discrete isomerization about the central bond. As it was pointed out

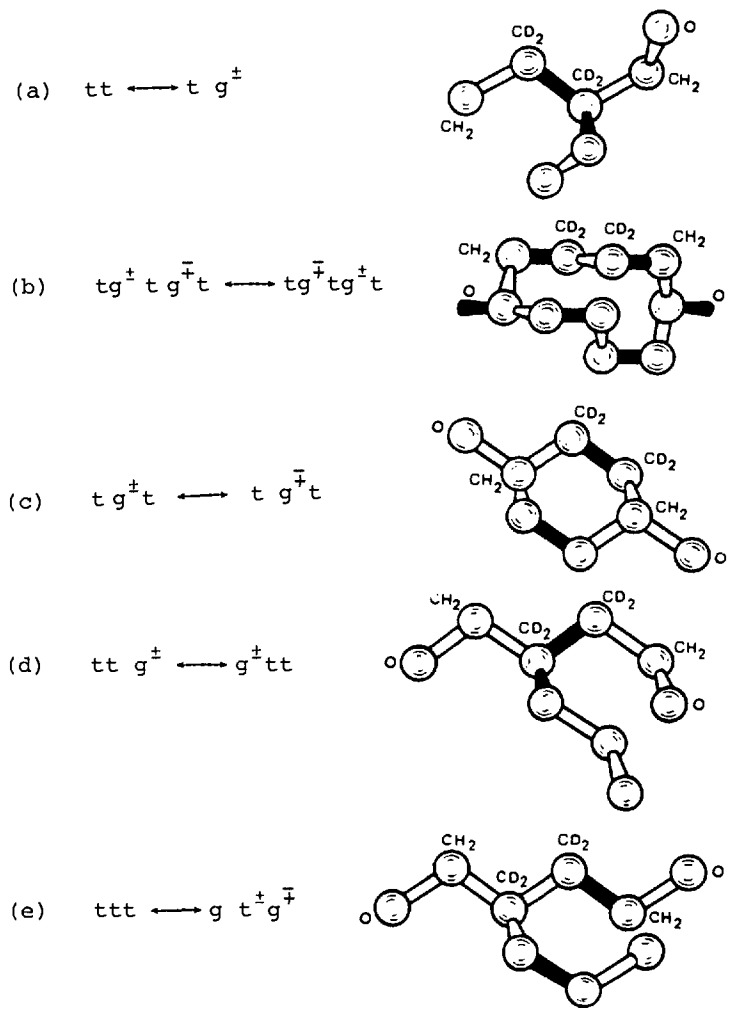

Fig. 12. Different types of motions of the aliphatic sequence of poly(butylene terephtalate).

(a) Discrete isomerization
(b) crankshaft rotation
(c) 3-bond motion
(d) gauche-migration
(e) pair-gauche production

earlier by Helfand [15], this type of motion is quite unlikely because it would imply a large scale reorientation of the tails of the polymer. In addition, it would lead to the same mobility for OCH_2 and CH_2-groups. The second type of motion, illustrated in Fig. 12b, called the crankshaft rotation, was proposed by Schatzki to account for mechanical relation in polyethylene. This motion requires tgt conformations which have not been observed in PBT by infrared or X-ray scattering. Furthermore, the crankshaft rotation should produce, in the rapid motion limit (high T spectra), a narrowed Pake spectrum which is not observed in D-NMR. Finally, it yields the same mobility for OCH_2 and central CH_2-groups. The third type of motion, the 3-bond motion with fixed ends, pictured in Fig. 12c, was used by Monnerie [12] to perform Monte-Carlo simulations of the dynamics of a polymer chain in a tetrahedral lattice. This motion results in the same mobility for OCH_2 and central CH_2-groups and furthermore it would require the simultaneous crossing of two energy barriers. This should result in an activation energy of about 2×16 KJ.mole^{-1} instead of the observed value 25 KJ.mole^{-1}. The two last types of motions (Fig. 12d and e) were proposed by Helfand [15]. They are represented in Fig. 12d and called 'gauche migration', less than 2 barrier heights are required due to the distortions in the nearest neighbour bond angles, bond lengths and internal rotation angles [18]. The polymer tails undergo only a translation instead of a rotation in the motion pictured on Fig. 12a. Such a motion leads to a difference in the mobility of OCH_2 and central CH_2, as observed by NMR, since two O-CH_2-groups are unaffected or translated. In the last type of motion (Fig. 12e), called pair-gauche migration, the $g^{\pm}t\,g^{\mp}$ conformations which are required have been predicted in PBT by conformational energy calculations and observed by infrared and X-ray spectroscopies. The activation energy would correspond to slightly more than one barrier height and there is large scale reorientation for central CH_2-groups but not for OCH_2-groups. For these reasons, this type of motion appears to be the most likely for the flexible aliphatic sequence of PBT. The two sites of the motional model could likely be $g^+\,t\,g^-$ and $g^-\,t\,g^+$.

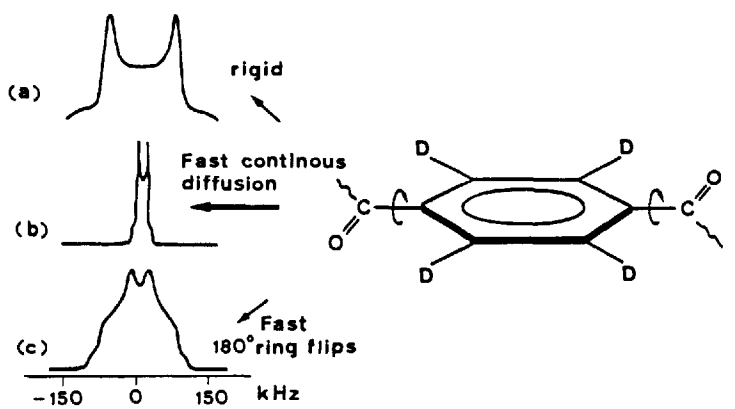

Fig. 13. Typical D-NMR spectra for different possible phenyl motions

In a complementary investigation of the local motions of PBT, Jelinsky et al. examined the motions of the phenyl ring of PBT with D-NMR by selectively deuterating phenyl rings [14]. Fig. 13 illustrates different D-NMR spectra arising from the different frequencies and types of the phenyl ring movements. By using suitable pulse sequences, it is possible to discriminate the crystalline regions, the interphase regions (amorphous phases nearby the crystals) and the amorphous regions. Fig. 14 compares experimental spectra obtained at 70°C with spectra calculated by assuming a 180° ring flip

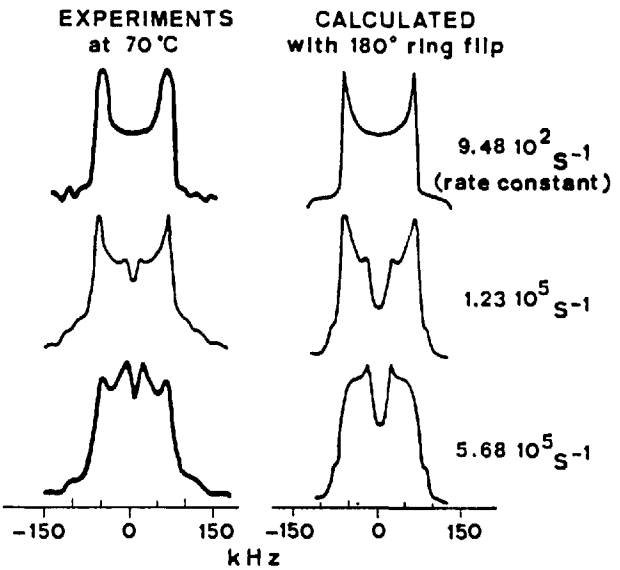

Fig. 14. Typical D-NMR spectra for crystalline, interphase and amorphous regions of poly(butylene terephtalate) with deuterated phenyl rings. Calculated spectra for 180° ring flip. From Ref. [14]

motion. More details can be obtained on the movement of phenyl rings in the amorphous phase from the T-dependence of the spectra. These are represented in Fig. 15 along with the calculated spectra for 180° ring flips and the rate constants indicated in the figure. The good agreement clearly indicates the occurrence of such ring flips in the amorphous regions with an activation energy equal to 25.4 KJ.mole^{-1}. However, the centers of the experimental lines are more filled in than predicted and there is also a poor definition at the edges of the band. These two observations indicate additional high-frequency libration of the phenyl rings, with $(\overline{\Delta\theta^2})^{1/2} = 15^\circ$ corresponding to an angular displacement of 40°. In the interphase regions ring flips occur but at a lower frequency than in the amorphous regions. For example, at 70°C the correlation times are $8.1.10^{-6}$ s and $1.7.10^{-6}$ s for ring flips in the interphase and amorphous regions respectively.

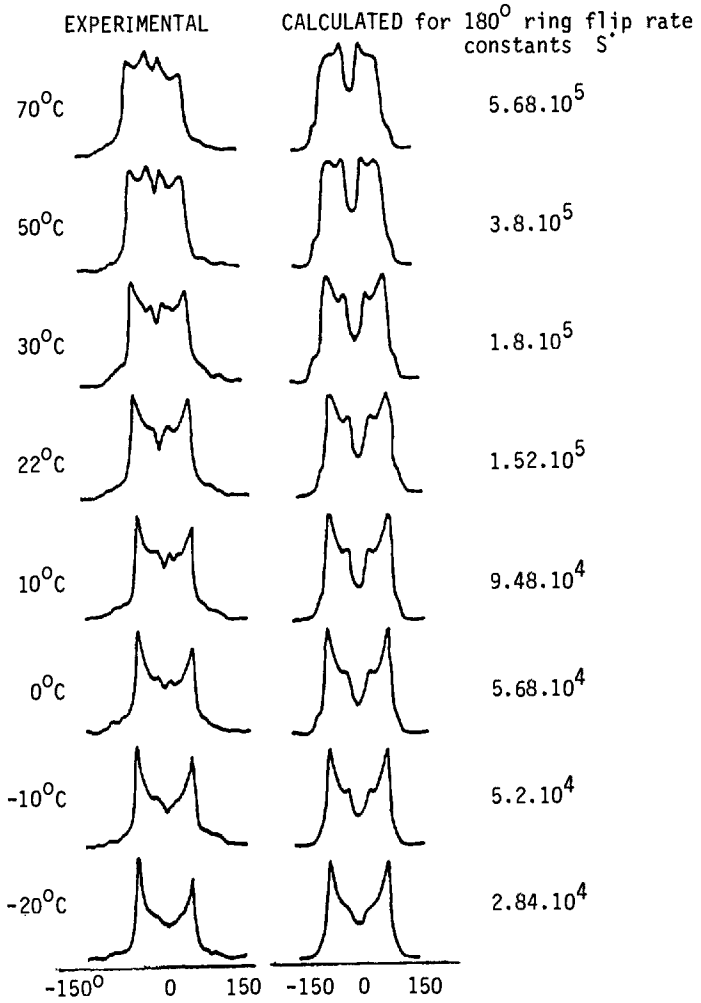

Fig. 15. Experimental and calculated D-NMR spectra of amorphous regions of poly(butylene terephtalate) with deuterated phenyl rings. Calculated spectra for 180° ring flip with rate constants indicated. From Ref. [14]

Local Motions in Polystyrene and Substituted Polystyrenes

Local motions of polystyrene (PSt) have been studied by several relaxation techniques including mechanical and dielectric relaxation, electron spin resonance of nitroxide probes ... Recently Schaefer et al. [19] have performed an extensive series of ^{13}C NMR measurements, using most of the methods available for the investigation of dynamics in solid polymers. Their study examines the movements of phenyl rings and their coupling with main chain motions in polystyrene and various derivatives. Hereafter we summarize the main results which have been obtained.

At once, it is found that large amplitude and high frequency motions of the phenyl rings occur at 25°C in polystyrene. About 7% of the phenyl rings of atactic PSt undergo a 180° ring flip in the 10 MHz range. Furthermore, the fraction of rings that flips is unaffected by annealing at T lower than Tg, quenching or slow cooling from temperatures higher than Tg, solution casting, precipitation or tacticity (provided the amorphous state is maintained). These ring flips are part of a cooperative motion involving the polymer main chain, as inferred from the ^{13}C NMR behaviour of the CH sites. These high frequency motions would occur at sites in the glass where lower packing has resulted in some main-chain flexibility. The mole fractions of phenyl rings undergoing large amplitude high frequency motion in a series of substituted polystyrenes are reported in Table III. It appears that the para-substituents do not

Table III: Mole fraction, F, of phenyl rings undergoing large amplitude high frequency motions in substituted polystyrenes at 25°C

Polymer	F
P. p Bromostyrene	6%
P. p Methylstyrene	7%
P. p Isopropylstyrene	10%
P. P-tert-Butylstyrene	11%
P. σ-Chlorostyrene	0%
P. α-Methylstyrene	0%

suppress these fast ring flips. Schaefer et al. proposed that the para-substituents make room for their attached main chain in the melt and that this freedom translates into sufficient main chain flexibility in the glass to allow ring flipping. On the other hand, ortho- and α-substituents are known to increase the main chain rigidity and lead to the steric hindrance of ring rotation [20,21]. The α-methyl could reduce the main chain flexibility in the glassy state due to steric hindrance with the surrounding. These ring flips could be mechanically active for they are strongly coupled with main chain motions and with the surrounding. The γ-relaxation observed at 1 Hz in dynamic mechanical measurements at -120°C with an activation energy equal to 43 KJ.mole^{-1} would correspond to a motion of frequency 8 MHz at 25°C. The agreement with the frequency range of the ring flip observed by ^{13}C NMR enables one to assign the γ-relaxation to coupled motions of the phenyl ring and the main chain occurring in sites in the glass with less-dense packing.

^{13}C $T_{1\rho}$ measurements at 25°C show the presence of small amplitude, low frequency motions of the phenyl rings. There is a distribution of frequencies with an average

value of the order of 100 KHz for PSt and its derivatives. The angular fluctuations and the total angular displacement of these phenyl ring motions are reported in Table IV. It is worth noting that all the considered polymers exhibit dynamical heterogeneities and the reported angular data are averages over the whole sample. Measurements performed on the main chain carbons show that these ring jumps are connected to main chain motions and that it is likely that the ring jumps occur when the main chain motions relieve local steric constraints in the glass.

Table IV: Amplitude of the root-mean square angular fluctuations and total angular displacement of phenyl rings in polystyrene and substituted polystyrenes at 25°C

	$\left(\text{Angular fluctuations}\right)^{1/2}$	Total angular displacement
P. p.tert.butylstyrene	23^{o}	70^{o}
P. p.isopropylstyrene	21^{o}	
P. styrene	18^{o}	
P. p.methylstyrene	18^{o}	
P. α.methylstyrene	16^{o}	
P. σ.chlorostyrene	14^{o}	40^{o}

As regards the main chain motions, in addition to the 10 MHz and 100 KHz range motions which are coupled to 180^{o} ring flip and small amplitude ring rotations respectively, motions in the KHz range are observed. These movements are insensitive to ring substitution and they are not coupled with phenyl ring rotations. Schaefer et al. have proposed a possible mechanism to account for this type of main chain motion; it is pictured in Fig. 16. The small rotation around the $CH\text{-}CH_2$ bond would imply only limited translations of the phenyl ring. Thus, this type of main chain motion could occur in sites where the phenyl rings are rotationally constrained.

Although the lack of measurements at various temperatures prevents a precise comparison with the mechanical relaxation data, it is likely that the low frequency motions (100 KHz and KHz) are involved in the β-relaxation.

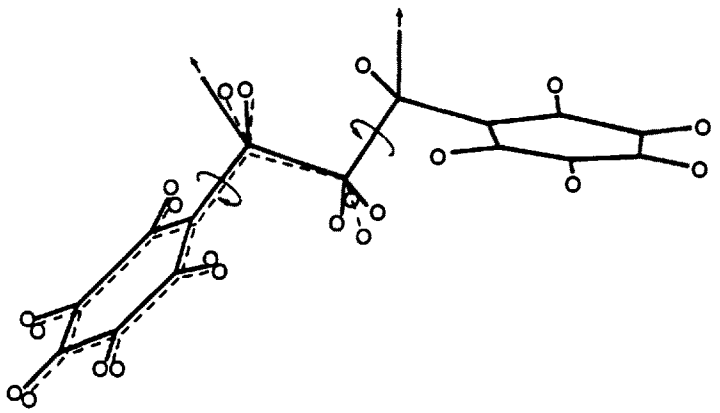

Fig. 16. Schematic representation of a main-chain rotation in polystyrene without rotation of phenyl rings. From Ref. [19]

Conclusion

The studies of local motions in solid polymers presented in this paper, as well as the experiments on polymer melts under progress in our laboratory, clearly demonstrate that high resolution solid state ^{13}C-NMR and D-NMR provide very powerful tools to investigate the molecular motions of side-chains and main-chain. They allow the unambiguous assignment of the mechanical relaxations observed in polymers to specific molecular motions.

^{13}C-NMR can be used to investigate any type of polymers, whereas the D-NMR requires selective D-labelling. On the other hand, D-NMR yields information on the dynamic behaviour of well-defined groups in the polymer chain.

References

[1] Havens, J.R., Koenig, J.L., Appl. Spectroscopy 1983, 37, 226

[2] Abragam, A., "The Principles of Nuclear Magnetism", Oxford University, 1961

[3] Wehrli, F.W., Wirthlin, T., "Interpretation of Carbon-13 N.M.R. spectra", Heyden, London, 1976

[4] Farrar, T.C., Becker, E.D., "Pulse and Fourier Transform N.M.R.", Academic Press, New York, 1971

[5] Mehring, M., "High Resolution N.M.R. Spectroscopy in Solids", N.M.R., Vol. 11, Springer Verlag,Berlin, 1976

[6] Heijboer, J., Ph.D. Theses, University of Leyden, 1972

[7] Lauprêtre, F., Monnerie, L., Virlet, J., Macromolecules, 1984, 17, 1397

[8] Lauprêtre, F., Virlet, J., Bayle, J.P., Macromolecules, 1985, 18, 1846

[9] Jelinski, L.W., Schilling, F.C., Bovey, F.A., Macromolecules, 1981, 14, 1341

[10] Jelinski, L.W., Macromolecules, 1981, 14, 1341

[11] Jelinski, L.W., Dumais, J.J., Engel, A.K., Macromolecules, 1983, 16, 403

[12] Jelinski, L.W., Dumais, J.J., Watnick, P.I., Engel, A.K., Sefcik, M.D., Macromolecules, 1983, 16, 409

[13] Jelinski, L.W., Dumais, J.J., Engel, A.K., Macromolecules, 1983, 16, 492

[14] Cholli, A.L., Dumais, J.J., Engel, A.K., Jelinski, L.W., Macromolecules, 1984, 17, 2399

[15] Helfand, E., J. Chem. Phys., 1971, 54, 4651

[16] Schatzki, T.F., Polym. Prepr. Am. Chem. Soc., Div. Polym. Chem., 1965, 6, 646

[17] Gêny, F., Monnerie, L., J. Polym. Sci., Polym. Phys. Ed., 1979, 17, 131, 147

[18] Skolnick, J., Helfand, E., J. Chem. Phys., 1980, 72, 5489

[19] Schaefer, J., Sefcik, M.D., Stejskal, E.O., Mc.Kay, R.A., Dixon, W.T., Cais, R.E., Macromolecules, 1984, 17, 1107

[20] Gorin, S., J. Chim. Phys. (Fr.), 1970, 67, 878

[21] Lauprêtre, F., Noël, C., Monnerie, L., J. Polym. Sci., Polym. Phys. Ed., 1977, 15, 2127

[22] Garroway, A.N., Ritchey, W.M., Moniz, W.B., Macromolecules, 1985, 15, 1051

^{2}H NMR INVESTIGATIONS ON GLASS FORMING SYSTEMS

Ernst Rössler
Institut für Atom- und Festkörperphysik
Freie Universität Berlin, Arnimallee 14
1000 Berlin 33, FRG

Introduction

In the last years ^{2}H NMR has become a powerful tool for the investigation of molecular motion in solids [1].

Deuterons represent a well-defined nuclear spin label. The spectra are almost exlusively governed by the quadrupole interaction with the electric field gradient of one covalent bond. In organic compounds the field gradient originates from the electron distribution of the C-H bond, in most cases being axially symmetric around this bond. Thus in ^{2}H NMR motion is monitored by the reorientation of the C-H vector being an intramolecular probe.

By combining measurements of spin lattice (T_1) and spin spin (T_2) relaxation times with line shape studies of spectra obtained by the solid echo two pulse and the spin alignment three pulse sequences the dynamic range of the different ^{2}H NMR methods can extend over more than 14 decades from 0.01 Hz to 10^{12} Hz. This allows the study of ultraslow motions associated with the glass transition.

^{2}H NMR is highly selective. By selective deuteration of different groups in a molecule the mobility of these groups can be studied exclusively. In mixed systems, e.g. a polymer with a low molecular weight additive, the two components can be measured separately.

It is the goal of this article to summarize first results of the ^{2}H NMR study of three glass forming systems, i.e. toluene, o-terphenyl and polystyrene in mixtures with toluene.

Theory

In the absence of motion and for one orientation of the electrical field gradient the NMR spectra are given by a doublet:

$$\omega = \omega_0 \pm \Delta\,(3\cos^2\theta - 1)$$

$$\omega = \omega_0 \pm \omega_Q$$

where Δ is the quadrupole coupling constant, θ the angle between the C-H bond and the direction of the magnetic field and ω_o is the Larmor frequency.

In an isotropic sample the C-H bonds are uniformly distributed in space resulting in a powder spectrum, the so-called Pake spectrum.

In the case of motion of the C-H bonds the time scale of this motion has to be considered. For glass forming systems being well above the glass transition temperature the motion is fast enough to average out the quadrupole interaction. The spectra collapse to a very sharp line. T_1 and T_2 measurements give rise to dynamical information, only. When the correlation time of the motional process is of the order of the reciprocal coupling constant at lower temperatures, distortions of the Pake spectrum are found. This can be studied for the absorption spectra or the solid echo spectra. Ultraslow motion can be analysed by the spin alignment three pulse sequence. Table 1 reviews the dynamic ranges of the different ^2H NMR methods.

$\tau \ll \Delta^{-1}$	$\simeq 10\mu s$	T_1 , T_2
$\tau \simeq T^*_{2SE}$	$\simeq 200\mu s$	Solid Echo
$\tau \simeq T_1$	$\simeq 1$ s	Spin Alignment

Tab. 1: Dynamic ranges of the different methods in ^2H NMR spectroscopy

The combination of all these methods should make it possible to study the entire dynamic range of the glass process.

In the theory of Bloembergen, Purcell and Pound T_1 is connected with a correlation time of motion τ by the following equation:

$$T_1^{-1} = f\Delta^2 \left\{ \frac{\tau}{1+(\omega_o\tau)^2} + \frac{4\tau}{1+(2\omega_o\tau)^2} \right\}.$$

f stands for a numerical factor. A similar equation holds for T_2. The BPP formula predicts the absolute maximum of the relaxation curve, because Δ, i.e. the coupling constant, can be measured independently. For all supercooled liquids studied so far, the predicted maximum is not reached. To overcome this difficulty a distribution of correlation times for the motional process can be introduced [2,3]. This description is equivalent with an introduction of a nonexponential correlation function for the motion. The combination of T_1 and T_2 measurements is very powerful because for low temperatures T_2^{-1} is proportional to τ for all of the usual distribution functions used. With the assumption that not only T_1 but also T_2 leads to the same correlation time for the motion a proper choice for a specific distribution function can be made. Thus the analysis of the T_1 and T_2 data reveals correlation times

with the same characteristic temperature dependence:

$$\left.\begin{matrix} T_1 \\ T_2 \end{matrix}\right\} \rightarrow \ln\tau = f(T).$$

These correlation times can be compared with solid echo and spin alignment experiments and, hopefully, will lead to a consistent picture of the glass process. In addition to the time scale of the motion solid echo and spin alignment studies give information upon the type of reorientation [1].

Results

1. Toluene [4]

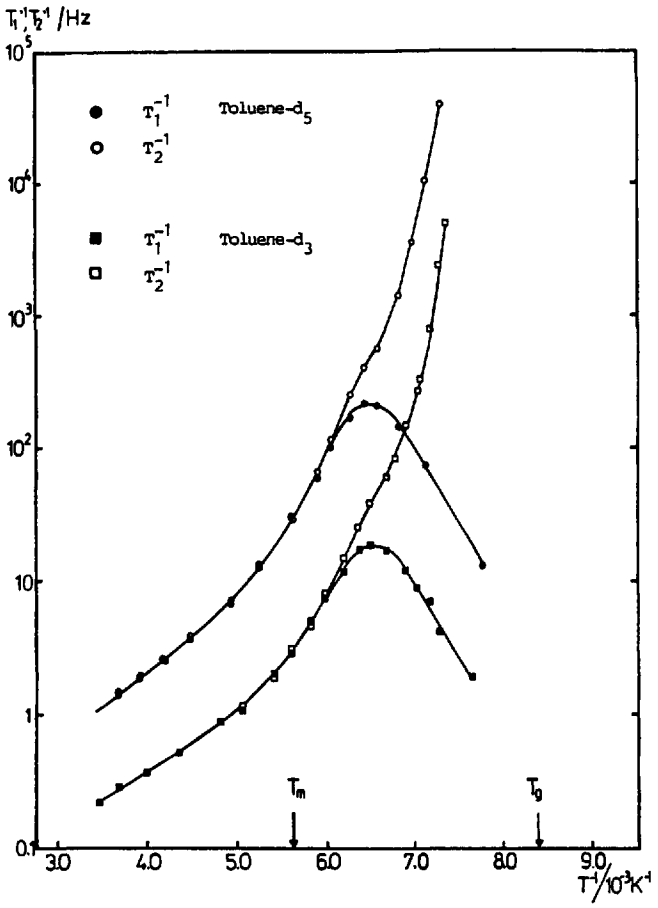

Fig. 1: Relaxation rates of toluene as a function of the reciprocal temperature

Toluene can be deuterated selectively in two ways:

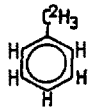

toluene-d_3

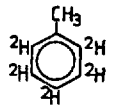

toluene-d_5

The liquid could easily be supercooled, however, the sample always crystallized at -142°C on heating from low temperatures.

The relaxation rates $1/T_1$ and $1/T_2$ measured in toluene-d_3 and toluene-d_5 are drawn in Fig. 1 as a function of the reciprocal temperature. Obviously, the relaxation curves are not symmetric. The asymmetric Cole-Davidson distribution function with a width parameter of 0.33 can reproduce all the T_1 and T_2 data of both toluenes. This is demonstrated in Fig. 2. All correlation times are on the same line, only for temperatures above the melting point the correlation times of toluene-d_3 are too long. This is not surprising because the fast methyl group rotation cannot

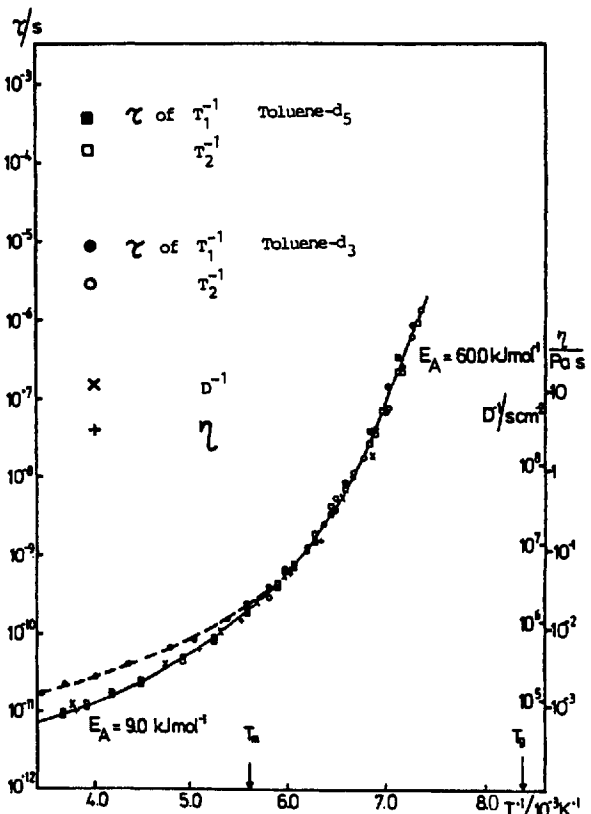

Fig. 2: Correlation times of toluenes as a function of the reciprocal temperature

be ignored at highest temperatures. Symmetric correlation time distributions yield no agreement between the average correlation time obtained by NMR, self-diffusion and viscosity data. Equally good fits may be expected from other unsymmetrical correlation time distributions. Up to correlation times of about 1 μs all methods reproduce the same characteristic temperature dependence for the time constant.

2. o-Terphenyl [5]

o-Terphenyl is one of the best characterized glass forming systems. It can easily be supercooled, the glass transition temperature being $T_g = -30^oC$. For the ^2H NMR studies the molecule was completely deuterated. In Fig. 3 the relaxation rates are given as a function of the reciprocal temperature. The curve looks very similar to the one found for toluene. Again the Cole-Davidson distribution function gives a very good fit for the T_1 and T_2 data. This is demonstrated in Fig. 4. A width parameter of 0.5 is found. The onset of the glass transition is indicated by a dramatic increase of the correlation times below the melting point. Up to correlation times of about

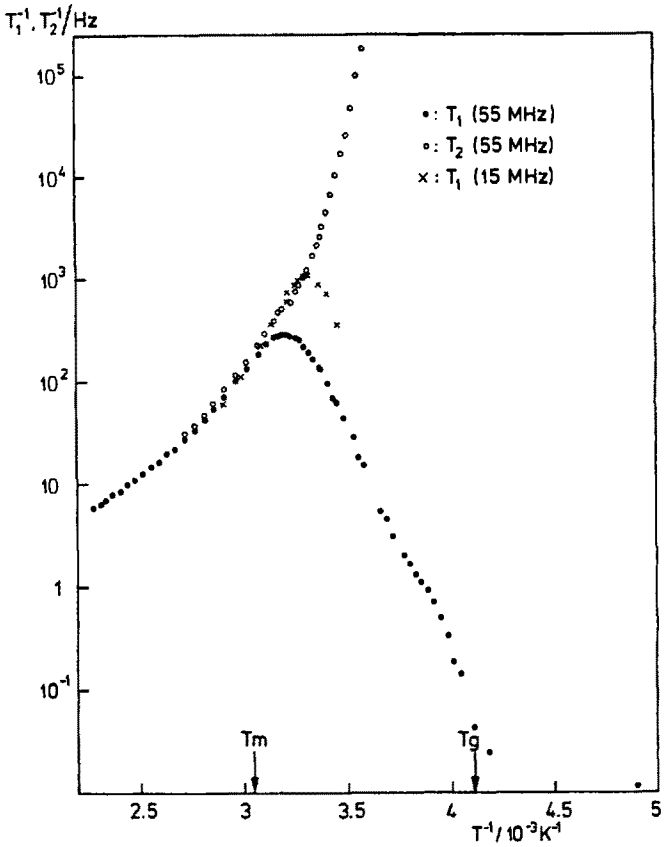

Fig. 3: Relaxation rates of o-terphenyl as a function of the reciprocal temperature

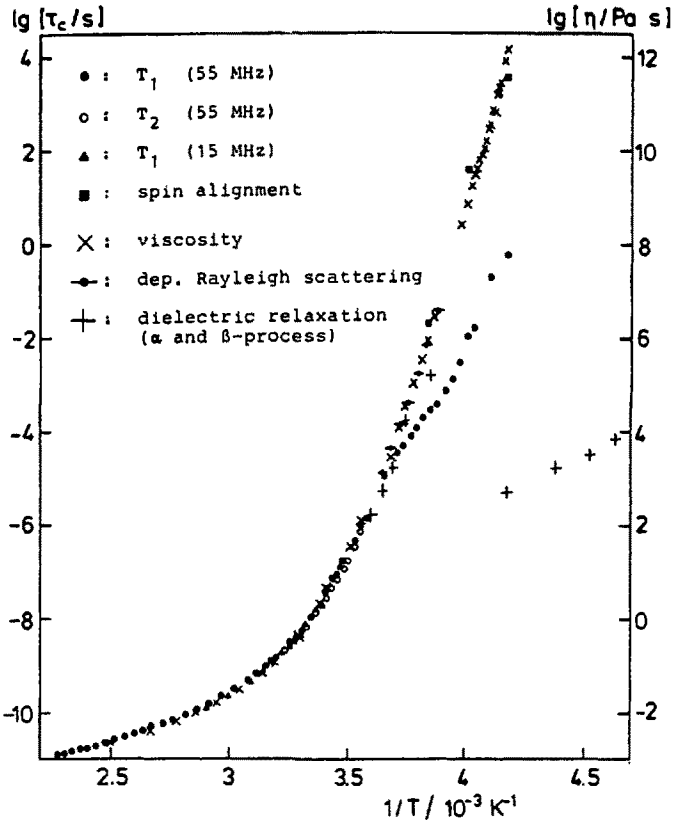

Fig. 4: Correlation times of o-terphenyl as a function of the reciprocal temperature

10 μs the different relaxation methods, e.g. NMR, dielectric relaxation, viscosity and Rayleigh scattering agree very well. However, at lower temperatures the correlation times found by the measurement of T_1 are much shorter than those obtained by Rayleigh scattering or viscosity data. Two reasons for this discrepancy may be considered.

i) The Bloembergen, Purcell and Pound theory may not hold for low temperatures, because the correlation times are of the order of the reciprocal coupling constant. This usually is given as à limitation of the theory. But we consider this condition more a limitation for T_2 than T_1. In solids with reorientational motion the BPP theory for T_1 in principal has been proved even for very long correlation times.

ii) T_1 is shortened by an additional process. This process can be the ß-process or an internal motion of o-terphenyl. Spin alignment experiments below the glass transition temperature support the hypothesis of an internal degree of freedom. However, further experiments are necessary in order to clarify the interpretation of T_1 and T_2 around T_g. First spin alignment experiments above T_g confirm the longer corre-

lation times found by the other relaxation methods (Fig. 4).

In summary, the following picture seems to emerge from the ^{2}H-NMR studies for the reorientation of the C-H bonds. Above T_g, the C-H vectors show full reorientations, and rotational diffusion may be a proper model of motion. Below T_g, only reorientation by small angles survives on the NMR time scale.

3. Polystyrene-Toluene Mixtures [6,7,8]

In mixtures of polystyrene and toluene we have two possibilities of deuterating the components. We start with labeling of the polymer; again two different ways have to be distinguished:

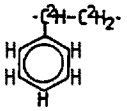

PS-d_3

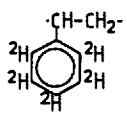

PS-d_5

Above the glass transition temperature the motion of the phenyl ring reflects the motion of the chain. Thus by studying PS-d_s as well as PS-d_5 the motion of the chain

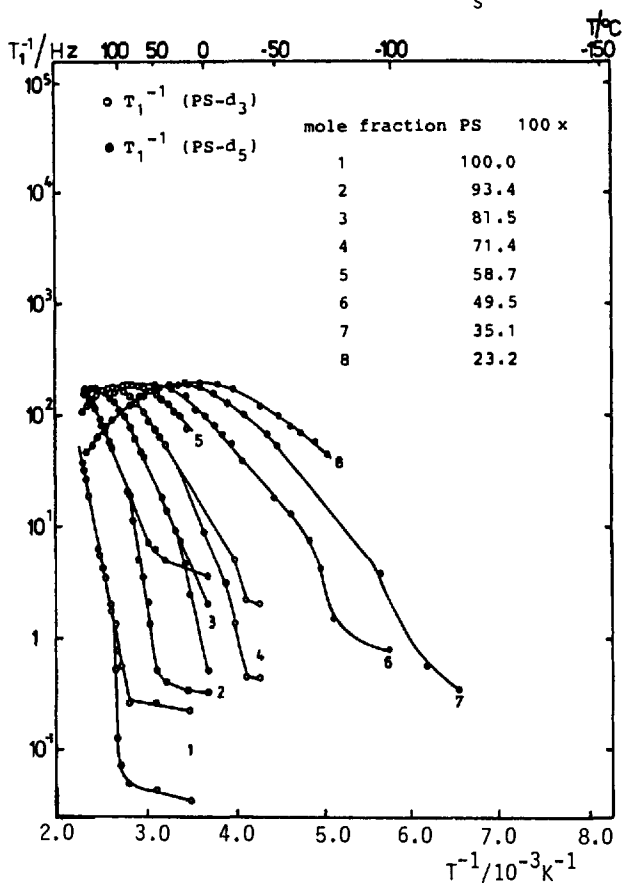

Fig. 5: Relaxation rates of PS-d_3 and PS-d_5 in mixtures of polystyrene and toluene

can be monitored. In this system T_1 is measured, only. Fig. 5 shows the relaxation time as a function of the reciprocal temperature for different concentrations of the mixtures. On adding more toluene the relaxation curve becomes broader, and the T_1^{-1} maximum shifts to lower temperatures. Now the choice of a proper correlation time distribution is not as unambigous as in the case of toluene or o-terphenyl alone. Frequency dependent T_1 measurements and comparison with self-diffusion coefficient and viscosity data lead us to assuming the symmetric Fuoss-Kirkwood distribution function as a fit for the T_1 data [8,9]. Additionally, the relaxation curves (Fig. 5) give no indication of asymmetry, this favours a symmetric distribution function. Fig. 6 summarizes the correlation times as a function of the reciprocal temperature. For all concentrations Arrhenius straight lines are found, the apparent activation energy decreasing with rising fraction of toluene in the mixture. Addition of toluene accelerates the motion of the chain. This is the well-known plasticizer ef-

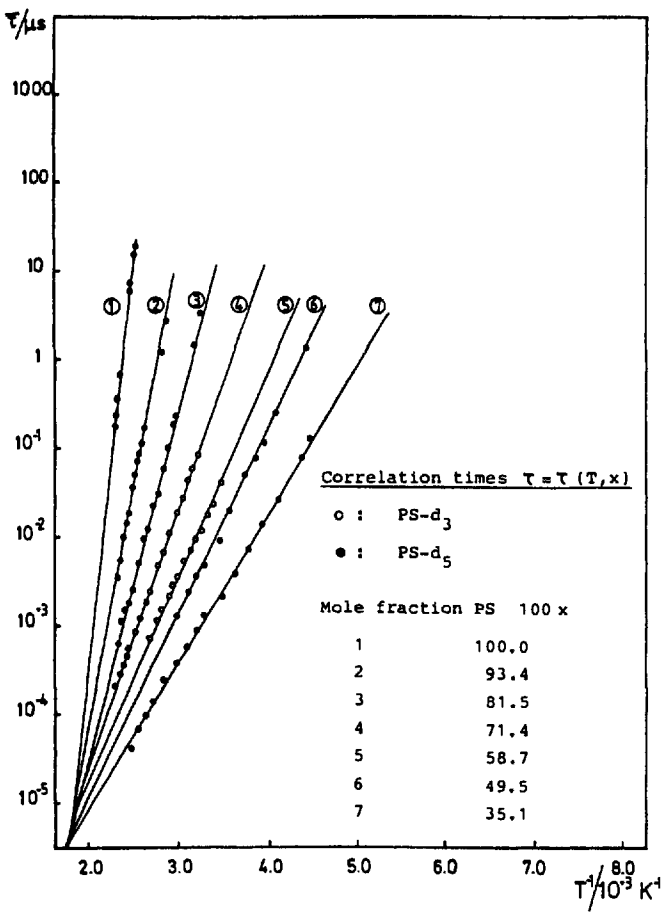

Fig. 6: Correlation times of PS-d_3 and PS-d_5 in mixtures of polystyrene and toluene

fect. No indication for the onset of a fluid regime is found in the systems. Apparently, the straight lines have a common intersection at very high temperatures.

The dynamics of the polymer chain can be described by a modified Arrhenius equation:

$$\ln(\tau/\tau_0) = E(x_2)/R(1/T - 1/T_0).$$

T_0 is the temperature of the common intersection of the straight lines in Fig. 6, x_2 stands for the mole fraction of toluene. The concentration dependence of the activation energy E is given by:

$$E(x_0) = E_0/(1 + B\ x_2).$$

This is easily shown by plotting $1/E$ as a function of x_2, a straight line is found as demonstrated in Fig. 7.

Finally, the modified Arrhenius equation can be derived within the framework of the Eyring transition state theory where Gibbs free energy of activation is given by:

$$\Delta G^{\#} = \Delta G_0^{\#} / (1 + B\ x_2).$$

Thus a rather consistent picture is revealed by the ^2H NMR results. However, as for toluene and o-terphenyl the correlation times at low temperatures are much shorter than expected from free volume theory. It is a common feature of all systems studied that in the viscous regime T_1 reproduces no WLF-behaviour but an Arrhenius straight line with an apparent activation energy much smaller than expected. A possible explanation of this behaviour could be the limited time window of the NMR experiment. Eventually, one detects at low and high temperatures, respectively, the short and long time behaviour of the same correlation function. Then, the temperature dependence of the NMR "mean" correlation time should not be related with an activation energy [2]. This also may explain the deviation of the NMR results from those of other relaxation methods.

In the case of labeling only the toluene molecules in the mixture, a picture of motional heterogeneity emerges where the motion of part of the toluene molecules is about six decades faster than the motion of the chain. Apparently, a fraction of toluene molecules follows the slow motion of the chain; they are "absorbed" along the chain, We can demonstrate unambiguously fast and slow moving toluene molecules below the glass transition temperature of the system, compare Fig. 8. The sharp peak in the middle of the spectrum shows the "liquid like" toluene molecules and the much broader Pake spectrum of the "rigid" molecules. Fig. 8 should, however, not be understood as proving a pure bimodal distribution of correlation times. A very broad distribution should give rise to the similar spectrum with "liquid" and "rigid" denoting the fractions with correlation times smaller and larger than $\simeq$10 s, respectively.

Note added in proof:

Now experiments on o-terphenyl [5] confirm the hypothesis that the low temperature T_1 can be explained by internal motion of the molecule, i.e. a collective flip-process of the two phenyl groups attached to the third benzene ring.

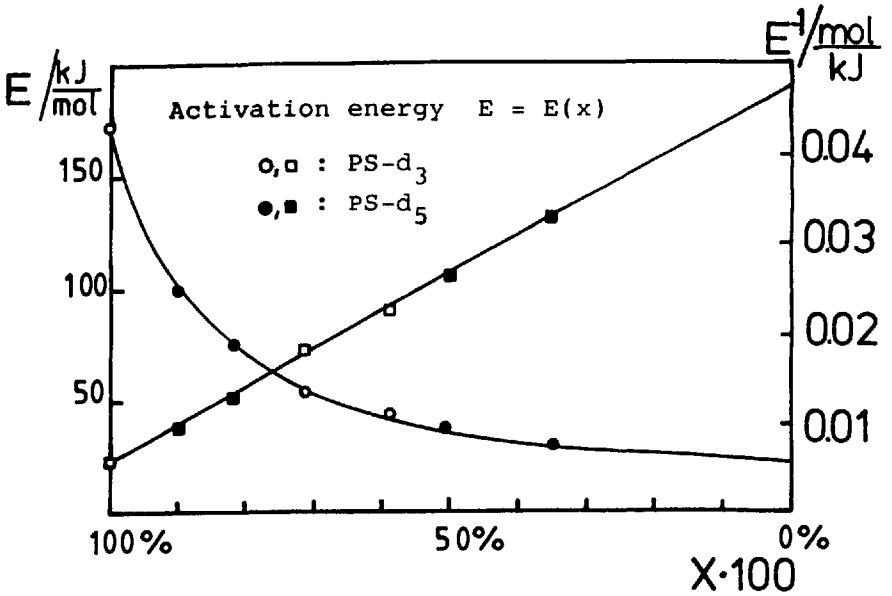

Fig. 7: The activation energy and the reciprocal activation energy as a function of the mole fraction of toluene

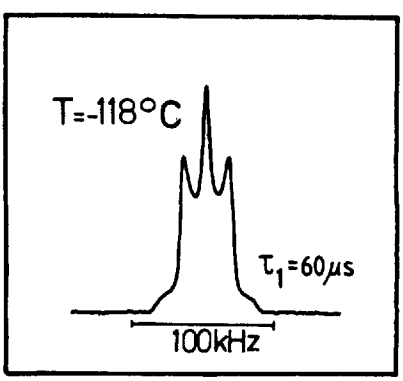

Fig. 8: "liquid like" and "rigid" toluene molecules as seen by the ^2H NMR spectrum below the glass transition temperature

References

[1] H.W. Spiess, Colloid & Polymer Sci. 261, 193 (1983)
[2] F. Noack, in NMR - Basic Principles and Progress, Vol. 3, Berlin 1971
[3] T.M. Connor, Trans. Faraday Soc. 60, 1574 (1964)
[4] E. Rössler, H. Sillescu, Chem. Phys. Lett. 112, 94 (1984)
[5] T. Dries, F. Fujara, E. Rössler, H. Sillescu, to be published
[6] E. Rössler, H. Sillescu, H.W. Spiess, Polymer 26, 203 (1985)
[7] E. Rössler, H. Sillescu, to published
[8] E. Rössler, PhD thesis, Mainz 1984
[9] P. Lindner, E. Rössler, H. Sillescu, Makromol. Chem. 182, 3653 (1981)

PHENYL-RING MOBILITY IN BULK POLYSTYRENE

Th. Dorfmüller and D. Samios
Fakultät für Chemie, Universität Bielefeld
D-4800 Bielefeld 1, FRG

1. Introduction

The dynamics of a polymer like polystyrene extends over a timescale of fractions of a picosecond to hours. A detailed knowledge of the processes over such a timescale is far beyond our present theoretical and experimental possibilities and we generally must restrict our ambition to a piecewise study on different timescales by different techniques. In this sense it appears useful to study a well-defined process over a timescale as large as possible by using different experimental techniques. This should prove especially fruitful if the temperature range includes the glass-transition temperature thus allowing us to follow the dynamics of the process under study above and below the glass transition. Since non-localized processes are known to dramatically slow down in the vicinity of the glass-transition we thus may improve our knowledge on their coupling with much faster localized processes. We chose polystyrene (PS) because the phenyl-ring motion can be well-localized and the measurements of its reorientational correlation times by NMR, light scattering and Raman scattering techniques are quite reliable. Also a large number of mechanical and dielectric studies on the dynamics of polystyrene is known. Furthermore, it is possible to carry out computations giving us a qualitative picture of the local dynamic constraints to which the phenyl groups in PS are subjected.

A numerical calculation [1] of the potential energy surfaces in PS has shown that the phenyl-groups in isotactic and syndiotactic PS are strongly constrained to an angular range of $\pm 20^{\circ}$ about the equilibrium orientation which is normal to the main-chain. This calculation has been carried out for low-MW PS in the all-trans tttttt configuration as well as in tgtgtg and gggggg configurations. It was found that a cooperative motion is energetically favoured, i.e. one where the rotation of the phenyl-group around the C-C bond connecting it to the main-chain is correlated with C-C rotations of the main-chain carbons. In this correlated motion the activation energy is significantly lowered over the non-cooperative, i.e. the single-phenyl group rotation. The activation energy corresponding to the cooperative crossing of the barrier, i.e. rotation by large angles, is of the order of 80-200 kJ/mol. Actually, the values of the activation energy strongly depend on the used potentials and can therefore be calculated only with low accuracy, whereas the shape of the energy surface is quite well-established. Thus, at low temperatures, probably even in

the glass region, the motion will be predominantly oscillatory and weakly temperature dependent whereas at high temperature the barrier-crossing process will dominate. In this region we may observe an Arrhenius temperature-dependence of the reorientational relaxation times and a large value of the activation energy.

On the experimental side a large number of mechanical relaxation and dielectric data indicate the presence of phenyl-ring motions [2,3,4,5,6]. However, due to the unability of this kind of data to unambiguously assign an observed relaxation process to the motion of a specific molecular moiety the exact extent and nature of phenyl-ring motion in liquid and glassy PS is still controversial. A more detailed study of this problem was made possible with NMR and depolarized light scattering techniques.

NMR spin-lattice relaxation times display relaxation minima at different temperatures. Thus Connor [7] found a possible contribution of a phenyl-ring relaxation process on the low-temperature side of the well-known α-relaxation process. Odajima et al. [8] have shown that phenyl-ring motion could be detected by the molecular-weight dependent NMR linewidths in PS. This process, which was labeled as the γ-process, was also observed in dynamic mechanical but not in dielectric relaxation experiments. Recently, Schaefer [9] and Monnerie [10] have reported NMR data of relaxation processes in the glassy state at $25^{o}C$ involving 180^{o} ring flips. This motion is found by ^{13}C NMR measurements to be cooperative, i.e. involving the polymer main-chain and thus is expected to be mechanically active. The observed relaxation times have been assigned to the γ-process which is assumed to occur in sites in the glass with less dense packing than the average [9]. Additionally, at $27^{o}C$ ^{13}C NMR measurements have indicated a small-amplitude, low frequency motion of the phenyl-rings. Using deuterium NMR techniques phenyl-ring motions in solutions of PS in toluene have been obtained over a time-scale from 10^{-5} to 10^{-10} s [11]. But substituting either the main-chain or the phenyl-ring protons by deuterons it was possible to discriminate between main-chain and phenyl motions. The data presently available have been interpreted assuming that both motions are sufficiently coupled to be practically indistinguishable as far as relaxation times and activation energies are concerned.

Depolarized dynamic light scattering is well-suited to study the reorientational motion of phenyl groups in the time range between 1 ps and minutes. However, presently only measurements in solution are available [12,13]. The measurements by means of photon correlation in bulk polystyrene [14] monitor long-range motions and are not directly related to phenyl group-rotation.

2. The Study of Molecular Reorientation by Raman Linewidth Analysis

Molecular reorientation is one of the bandshaping mechanisms of Raman spectra so that this technique can be usefully applied to the study of reorientational dynamics of molecules. The method basically relies on the time-dependence of the rotational matrix $\underset{\approx}{R}(t)$ which transforms the vibration-induced polarizability tensor of the molecule to the laboratory frame of reference and thus determines the shape of the aniso-

tropic Raman line corresponding to a given vibration symmetry. In order to separate the reorientational from the intrinsic bandshapes we use the two spectra in the VV- and the VH-configurations of polarization. The anisotropic spectrum then is:

$$I_a(\omega) = I_{VV}(\omega) - \frac{4}{3} I_{VH}(\omega). \qquad (1)$$

The half-width at half-height (HWHH) Γ_a can then be obtained from the anisotropic spectrum and the corresponding correlation time τ calculated by means of the equation:

$$\tau = \frac{1}{2\pi\Gamma} . \qquad (2)$$

Using conventional Raman techniques the time-window accessible to this method extends from 1 to 10 ps approximately, the lower limit being set by signal to noise ratio and possible interference from neighbouring spectral bands and the higher limit by the limitations of resolving power due to the finite instrumental bandwidth. This latter limitation to correlation times faster than approximately 10 ps has prohibited in the past the application of Raman bandwidth analysis to the dynamics of complex liquid systems. The introduction of high resolution Raman spectroscopy has improved this situation considerably and has enabled us to study phenyl-group reorientation in the time-range between 1 and 200 ps [15]. This can be achieved if we couple a grating monochromator to a Fabry-Perot interferometer allowing us to choose any Raman line with the monochromator and to study it with the high resolution of the interferometer.

The apparent correlation time τ obtained by the described procedure is a measure of the speed at which the orientation of the C_6-axis of the phenyl-groups is changing as a consequence of its random interaction with the environment. Actually, in liquids, especially at high viscosities, τ has little direct connection to a molecular rotation considered as a free motion determined by the moment of inertia of the rotor. What determines τ is the hydrodynamic coupling of molecular motion to the environment by viscosity. In the strong coupling limit the molecular orientation is strongly coupled to the anisotropic density fluctuations of the environment and hence the value of τ reflects the dynamics of the environment rather than that of the probe. With decreasing coupling the motion of the probe being less perturbed by the environment becomes increasingly correlated and τ approaches the correlation time of a free rotor.

3. Materials and Experimental Equipment

The following four atactic polystyrene samples were used:

MW: 2.200	MW/MN = 1.06
MW: 4.000	MW/MN = 1.06
MW: 35.000	MW/MN = 1.06
MW: 50.000	MW/MN = 1.06.

The polystyrene was purchased from "Pressure Chemical Company": special polystyrene standards. The glass points were determined with a Mettler TG-DSC apparatus in both directions with several heating and cooling rates. The Raman spectra were obtained with a high-resolution tandem Raman spectrometer described elsewhere [15].

4. Correlation Times of the Phenyl-Group Reorientation

The table on the next page shows in columns 3 to 5 the obtained values for the HWHH Γ_{VV}, Γ_{HV} and Γ_a at different temperatures for the four samples with different molecular weights. The values of the molecular weight and of T_g for each sample are shown in column 1. In the cases where Γ_{VV} and Γ_{VH} only differ by an amount comparable to the experimental error (approximately 0.03 cm^{-1}) the anisotropic linewidth could not be calculated indicating that the corresponding correlation time must be larger than 200 ps.

Fig. 1 visualizes the values of Γ_{VV} and Γ_{VH} for two extreme samples of the table: the sample with the lowest (2200) and the sample with the highest (50 000) molecular weight. The experimental points have been obtained for each sample at several temperatures below and above T_g. The excess linewidth of Γ_{VH} over Γ_{VV} indicates the effect of reorientation. Below T_g the low molecular-weight sample displays reorientation with a correlation time τ = 30 ps while a reorientation can no more be detected in the high molecular-weight sample where Γ_{VV} and Γ_{HV} coincide within experimental

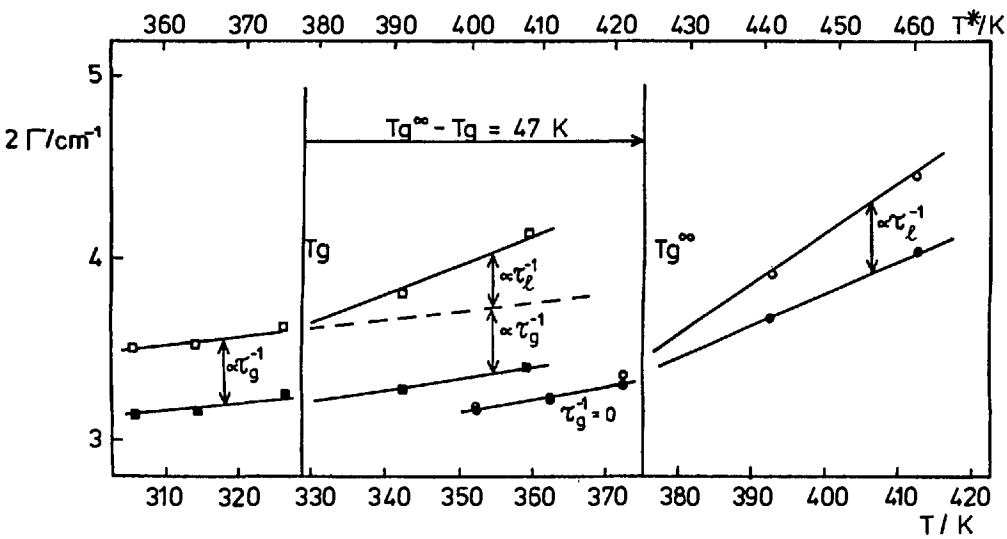

Fig. 1: VV- and VH-linewidths of two polystyrene samples. □ and ■ : 2200 molecular weight samples; ○ and ○ : 50.000 molecular weight samples; full symbols ■ and ● : Γ_{VV}; empty symbols □ and ○ : Γ_{VH}. The double arrows between Γ_{VV} and Γ_{VH} indicate the inverse correlation times of the respective processes. The upper temperature scale which has been shifted on the basis of the difference $T_g - T_g^\infty$ is the scale of the reduced temperature T*

Table: Linewidths of the Spectra and Correlation Times at Temperatures above and below T_g

	$T/^oC$	$2\Gamma_{VV}/cm^{-1}$	$2\Gamma_{HV}/cm^{-1}$	$2\Gamma_a/cm^{-1}$	τ_g	τ_ℓ
MW 2000	33	3.15	3.50	0.18	30	--
	42	3.16	3.52	0.18	30	--
	54	3.25	3.61	0.18	30	--
T_g = 56						
	70	3.15	3.80	0.28	--	51
	87	3.40	4.13	0.37	--	26
MW 4000	54	3.12	3.20	0.04	130	--
	74	3.15	3.25	110	--	--
T_g = 79						
	87	3.15	3.38	0.12	--	79
	103	3.57	3.98	0.21	--	34
MW 3500	90	3.30	3.30	--	τ_g>200	--
T_g = 103						
	113	3.50	3.74	0.12	--	79
	135	3.52	4.02	0.25	--	21
	160	3.54	4.77	0.62	--	9
	233	3.75	6.40	1.33	--	4
MW 50.000	50	3.15	3.15	--	--	--
	70	3.20	3.20	--	--	--
	80	3.13	3.15	--	τ_g>200	--
	90	3.22	3.25	--	--	--
	100	3.31	3.55	--	--	--
T_g = 103						
	120	3.67	3.90	0.12	--	46
	140	4.04	4.45	--	--	26

error. In the high molecular-weight sample the difference between the Γ_{VV} and Γ_{VH} is constant over the whole temperature range indicating a reorientational correlation time with very low activation energy. Above T_g on the other hand, both samples display a measurable difference between Γ_{VH} and Γ_{VV} which furthermore is clearly temperature-dependent. Comparing the linewidths of the two samples one sees that Γ_{VV} is not or only slightly molecular-weight dependent in contrast to Γ_{VH} indicating

that the lineshaping mechanisms which determine the former are very similar for the two molecular weights. From the whole picture it seems plausible to admit that two distinguishable processes with different temperature dependences contribute to the observed correlation times

a) One process characterized by a temperature-independent, but strongly molecular-weight dependent correlation time τ_g. This process is the only one being observed in the Raman line-broadening below T_g.
b) A second process whose correlation time τ_ℓ is also molecular-weight-dependent and additionally temperature-dependent the correlation time shifting out of the Raman time-window near T_g. Above T_g the observed line-broadening is attributed to both processes.

Assuming that the temperature-independent process observed below T_g in the low molecular-weight samples also persists above T_g and that its correlation time is not or only little affected by the change from the glassy to the liquid environment, we may calculate on the basis of a simple kinetic argument involving two parallel decay channels for the reorientational CF the correlation times τ_ℓ and τ_g for the two postulated processes from the measured overall correlation time τ. The following equation can then be used:

$$\frac{1}{\tau} = \frac{1}{\tau_g} + \frac{1}{\tau_\ell} \quad . \tag{3}$$

These assumptions leading to τ_g and τ_ℓ actually amount to a model whereby the observed phenyl-group reorientation takes place by two parallel distinct mechanisms the one being blocked on cooling below T_g while the other remains unaffected in the process of vitrification.

The values of τ_g and τ_ℓ obtained from Eq. (3) and the above mentioned assumptions are given in columns 6 and 7 of the Table. As can be seen in Fig. 1 and in column 6 of the Table, τ_g decreases with molecular-weight and at molecular-weights above 4000 (samples with MW 35.000 and 50.000) it has become so long as to be undetectable by Raman spectroscopy ($\tau_g > 200$ ps). The broken line in Fig. 1 indicates Γ_{VH} for the first process extrapolated graphically from below T_g into the melt. This illustrates the two correlation times τ_g and τ_ℓ which result from the application of Eqs. (2) and (3) to the data of the sample with molecular weight 2200. Figure 1 also illustrates the relation between the inverse correlation times at different temperatures in both polymers.

All the calculated data of τ_ℓ from the measured values of τ at different temperatures and molecular weights listed in the Table have been plotted in Fig. 2 as a function of 1000/T. The molecular weight dependence of the correlation times is clearly visible. It would be useful to scale the plot in such a way as to compensate for the differences in the molecular weights. Such a scaling can be based on the observation that most of the dynamics of the kind observed here slows down with the molecular

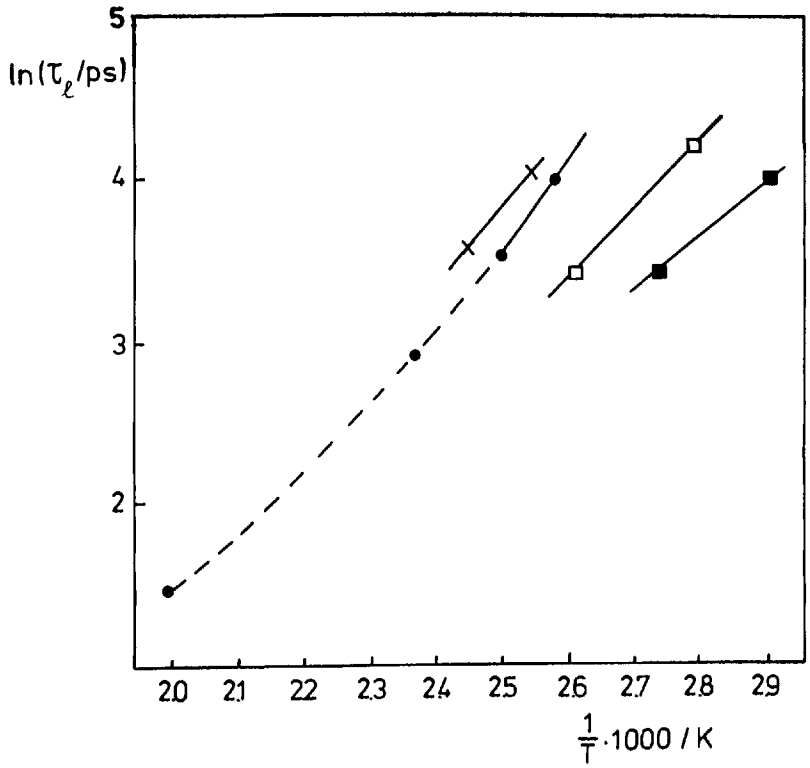

Fig. 2: Arrhenius plot of the Raman lidewidth correlation times τ_ℓ as calculated from Eq. (3). ■ : 2200 MW sample; □ : 4000 MW sample; ● : 35.000 MW sample; x : 50.000 MW sample

weight roughly paralleling the concomitant increase of T_g. This trend levels out at higher values of the molecular weight (approximately for MW > 30.000). Thus, the polymer can be characterized by its molecular weight or, alternatively, by the difference between its glass temperature T_g and the limiting glass temperature of the same species at infinite molecular weight T_g^∞. Instead of referring to the actual temperature of the sample one can describe the thermal state of the polymer by its reduced temperature:

$$T^* = [T - (T_g - T_g^\infty)] \quad . \tag{4}$$

Fig. 3 illustrates the result of this scaling. It is clearly visible that the values of τ_ℓ for all four samples fall on a common curve within experimental error. The differences in the reorientational dynamics observed by the Raman linewidths which are due to the different molecular weight of the samples have been taken into account by only one molecular parameter $(T_g - T_g^\infty)$. The reduced temperature T^* plays the role of a dynamical state-variable in that it uniquely specifies the correlation time τ_ℓ. This result also justifies the separation of the correlation time τ_ℓ from the measured correlation time τ since the former appears to correspond to a defined physical pro-

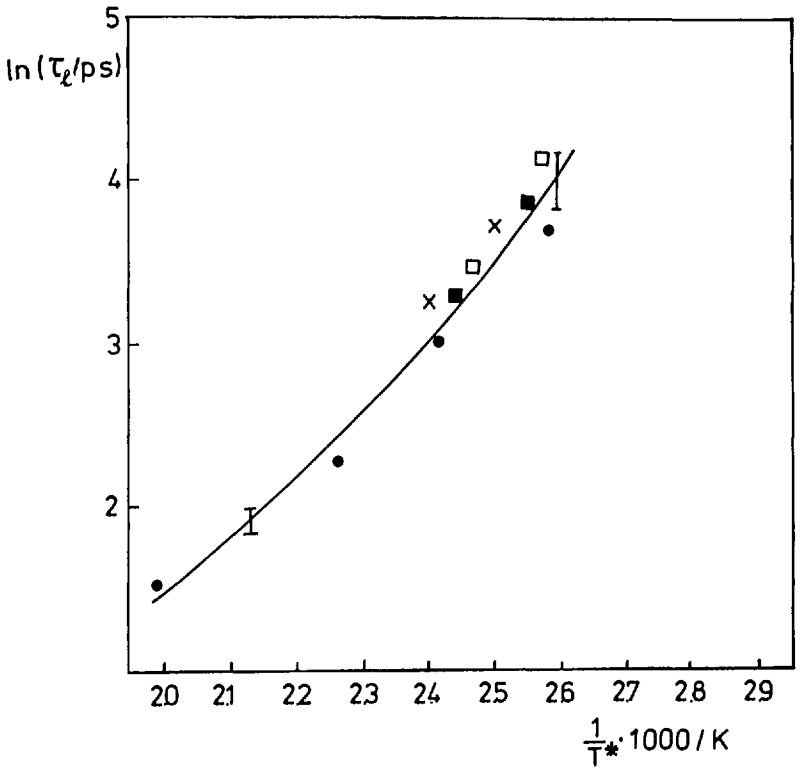

Fig. 3: Arrhenius plot of the Raman linewidth correlation times on a reduced temperature scale. T^* is defined in Eq. (4). The symbols are the same as those in Fig. 2. Note the shift of the experimental points represented in Fig. 2 on a common curve

cess whereas the latter results from an addition of two distinct processes and thus cannot be simply reduced to a master-curve by a change of variables.

As already mentioned in the Introduction, phenyl-group reorientation in bulk polystyrene has been monitored by several experimental techniques either directly as in the case of NMR spectroscopy and to some extent dielectric relaxation or indirectly as in the case of mechanical relaxation. In the latter case a relaxation process is observed as a maximum in mechanical loss curves. Its assignment to a well-defined phenyl-group reorientation has been either based upon changes in the frequency or the temperature dependence of the mechanical loss factor produced by substitution in the o-, m- and p-positions of the phenyl-group or by comparison to dielectric and NMR data. Such mechanical studies have unambiguously established the existence of the so-called γ-relaxation process which has been characterized phenomenologically and was attributed to phenyl-group reorientation. On the other hand, direct evidence for the reorientation of the phenyl-group has been based upon monitoring by dynamic spectroscopic techniques of vectorial (e.g. electric or magnetic dipole moments) or tensorial quantities (e.g. permanent or vibration-induced polarizability anisotropy) located in this group. These techniques have proven in the last decade [16-19] to be very powerful tools for

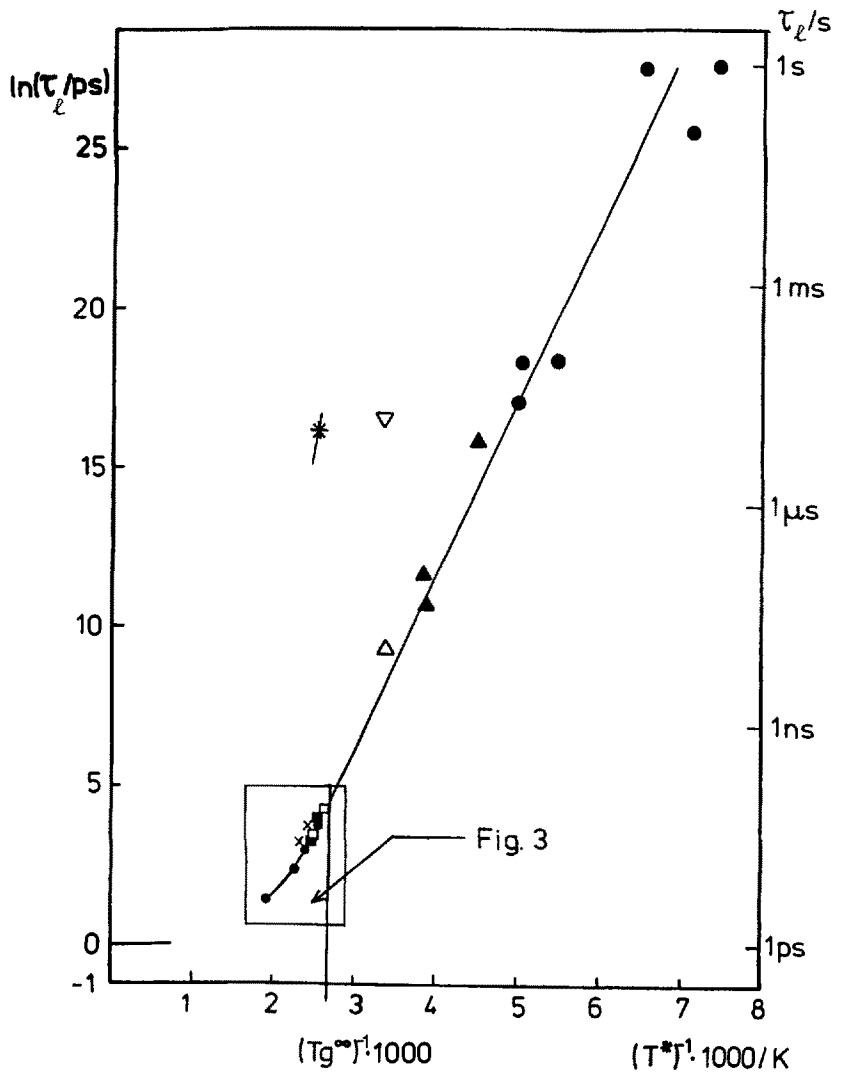

Fig. 4: Arrhenius plot on the reduced T^* scale of the correlation times of the phenyl-group obtained from polystyrene of molecular weight between 2200 and 5.10^6 by different experimental techniques: ●: mechanical relaxation data [2-5]; ▲: NMR data [7,20,21]; Δ∇: NMR data [L. Monnerie, this volume, 10]; *: NMR data [E. Rössler, this volume, 11]. (The line indicates the slope obtained in the figure of the mentioned paper.) The data in the frame indicated by "Fig. 3" are the reduced data represented in Fig. 3 with the same symbols

the study of the detailed dynamics in liquids and polymers. However, the interpretation of such data very often depends on the model used and thus the comparison of data from different sources is extremely valuable.

Such a comparison is illustrated in Fig. 4 where all the available pertinent data of reorientational correlation times of bulk PS have been collected. These are:

1) Mechanical relaxation data

2) NMR data

3) Raman linewidth data.

Fig. 4 shows a plot of $\ln\tau_\ell$ vs. $1/T^*$ for the data above the glass point listed in the Table. This quasi-Arrhenius plot shows that the quantities τ_ℓ and T^* allow us indeed to reduce the dynamical information from very different sources obtained with polystyrene of quite different molecular weights on a common curve.

In a next step the observed process(es) is (are) discussed within the frame of the known data for phenyl-group reorientation obtained by other techniques. As already mentioned, most of the reported data on the γ-process are mechanical relaxation obtained below T_g at samples with much higher MW than ours. However, as illustrated in Fig. 4, the used reduced temperature T^* is adequate also to represent the dynamical data of samples with high molecular weights, i.e. such that $T_g \rightarrow T_g^\infty$. All the data can be described by a smooth curve which is linear from very low temperatures up to several degrees above T_g. In terms of the timescale the linear regime extends over approximately twelve orders of magnitude. The apparent activation energy is thus constant, equal to $E^\# = 45$ kJ/mol, independent on molecular weight and temperature except for the highest temperature above T_g where a decrease to a value typical for liquids is suggested by the data. Actually, this transition, which is connected to a change of the underlying process, takes place in a rather narrow temperature region between T_g and the melting point the passage over T_g leaving the correlation time unaffected.

Some recent NMR data [9] which have also been reviewed by L. Monnerie in this volume have been interpreted in terms of two different reorientational processes: a large amplitude ring-flip motion of 180^0 indicated by Δ and a small-amplitude ring-oscillation represented by ∇ in Fig. 4. The former obviously fits quite well on the plot for the γ-relaxation while the latter is slower by three orders of magnitude. Another correlation time described by E. Rössler in this volume is also indicated in Fig. 4 by *. This point was obtained above T_g by deuteron NMR on a polystyrene sample in which the main-chain methyl protons were substituted by deuterium. The interpretation given for this process is based on the assumption that the observed main-chain motion is strongly coupled to the phenyl-group motion and thus reflects phenyl-group reorientation. The line through this point indicates the trend of the activation energy which seems to be much larger than the value for the γ-process. Apparently the described process is not a γ-process.

The second process which is directly observed below T_g in our measurements slows down with increasing molecular weight from 2200 to 4000 and then becomes undetectable at the higher molecular weights of 35.000 and 50.000. In contrast to the motion observed at higher temperatures this motion although being molecular weight-dependent does not scale with T_g or for that matter with T_g^∞. It seems that temperature is not a convenient quantity to parametrize τ_g but perhaps structural quantities. On the other hand, despite its strong molecular weight dependence, this motion obviously is not simply an

overall reorientation of the whole chain since such a motion is expected to be much slower and should be completely frozen in the glass even in the low molecular weight samples. In fact, overall reorientation correlation times as obtained from light scattering measurements in solutions [12,13] can be scaled to the bulk viscosity and are indeed slower by orders of magnitude. Neither can this motion be simply described as a completely localized, i.e. isolated rotation of phenyl-groups because in this case the correlation time τ_g would depend very little on molecular weight. On the evidence of the present data also the alternative explanation that the observed process is due to the reorientation of terminal phenyl-groups only must be also rejected. The motion of terminal groups which form more mobile regions within the bulk polymer has indeed been invoked in several instances to justify some kind of secondary relaxation processes [9]. In the present case, however, it is evident that the molecular weight of the sample would predominantly affect the number of the mobile groups rather than the correlation time itself. One could argue that the packing of low-molecular weight polystyrene with a high proportion of end-groups creates the possibility of a rather fast reorientation of the phenyl groups even in the glass. By increasing the molecular weight of the sample from 2200 to 4000 the packing becomes more space-filling leaving less free volume resulting in a decrease of local mobility. In other words, a long-range effect affects the structure of the glass which then affects the short-range motion of the phenyl-groups. Such an interpretation would imply the possibility of different packings of the polymer in the glassy region depending on the molecular weight. More precisely, low molecular weight polystyrene glass would be less densely packed than high molecular weight polystyrene. This interpretation is also consistent with our hypothesis that the low-temperature process is surviving the passage from below to above T_g .

5. Summary and Conclusions

The Raman bandshape analysis of bulk polystyrene with different molecular weight above and below the glass point has shown that the phenyl-groups display reorientation with a correlation time in the range of 10 to 100 ps. Below T_g the motion is stronlgy molecular weight dependent and only little temperature dependent. Above T_g the motion is composite. Both the process observed in the glassy region and a second process observable only above T_g contribute to the observed correlation time. The latter is identical with the γ-process observed by mechanical [2-6] and NMR methods [7,20,21]. The data presented here lie at the high-temperature side of the mechanical, dielectric and NMR data which thus are extended into the region immediately above T_g, showing that the γ-process is not significantly altered when the system crosses the glass point. The second process which is only observed in samples with very small molecular weight can be interpreted as resulting from a reorientation of phenyl-groups which is made possible by the nature of the packing in the glass. In samples of relatively low molecular weight freezing below T_g results in a structure which leaves enough free volume

for phenyl-group reorientation to occur by this second process.

References

[1] Y. Tanabe, J. Polym. Sci. Polym. Phys. Ed. 23, 601 (1985)
[2] K.H. Illers and E. Jenckel, J. Polym. Sci. 41, 528 (1958)
[3] K.H. Illers, E. Jenckel and G. Adam, Real. Acta 1, 322 (19587
[4] O. Yano and Y. Wada, J. Polym. Sci. A2 9, 669 (1971)
[5] M. Baccaredda, E. Butta and V. Frosini, J. Polym. Sci. B 3, 189 (1965)
[6] K. Schmieder and K. Wolf, Kolloid. Z. 134, 149 (1953)
[7] T.M. Connor, J. Polym. Sci. A2 8, 191 (1970)
[8] A. Odajima, J.A. Sauer and A.E. Woodward, J. Polym. Sci. 57, 107 (1962)
[9] J. Schaefer, M.D. Seficik, E.O. Stejskal, R.A. McKay, W.T. Dixon and R.E. Cais, Macromolecules 17, No. 6, 1107 (1984)
[10] L. Monnerie, this volume
[11] E. Rössler, this volume
[12] D.R. Bauer, J.I. Brauman and R. Pecora, Macromolecules 8, No. 3, 443 (1975)
[13] F. Strehle, D. Samios and Th. Dorfmüller, to be published
[14] U. Mittag, Diplomarbeit, Universität Bielefeld
[15] D. Samios, Th. Dorfmüller, Chem. Phys. Lett. 117, 165 (1985)
[16] R. Pecora, ed. in: Dynamic Light Scattering. Plenum Press, N.Y. 1985
[17] Ch. Wang, in: Spectroscopy of Condensed Media. Academic Press 1985
[18] W.G. Rothschild, in: Dynamics of Molecular Liquids. John Wiley & Sons 1984
[19] Th. Dorfmüller, Light scattering spectroscopy in liquids, in: Molecular Liquids, A.J. Barnes, W.J. Orville-Thomas and J. Yarwood eds. NATO ASI Series, D. Reidel, Dordrecht 1984
[20] Hirose and Y., Wada, Rep. Progr. Polym. Phys. Japan 9 287 (1966)
[21] B.I. Hunt, J.G. Powles and A.E. Woodward, Polymer 5, 323 (1964)

CORRELATION BETWEEN CHANGES IN MOLECULAR MOBILITY AND VOLUME IN GLASS-FORMING MATERIALS

A.J. Kovacs
Institut Charles Sadron (CRM-EAHP)
67083 Strasbourg, France

It has been well-established [1-6] that on further cooling under constant pressure below a critical temperature (T) range, undercooled liquids, in particular rubberlike polymers, progressively depart from their (metastable) thermodynamic equilibrium. The departure from equilibrium occurs when the rate of the slowest structural rearrangement becomes of the same order of magnitude as the rate of cooling, q_1. This event if often related to the onset of the glass transition, and characterized by a critical temperature $T_g(q_1)$, which depends on the cooling rate alone.

Does this widely accepted kinetic origin of the glass transition correspond to the physical reality, or only to a part of it? If so, to which part? These are two important questions which can be presently raised, and on which this short paper will attempt to provide, among others, some possible answers.

Actually, the above definition of the glass transition appears to be supported by numerous examples reported on both inorganic and organic (polymeric) glass-forming materials. Among those isobaric volume recovery data of polymeric glasses [6] complemented by the relevant changes in the storage and loss moduli, as determined by dynamic mechanical investigations [7], clearly show a gradual departure from the high temperature values of these parameters when extrapolated below $T_g(q_1)$. In addition, this transition temperature appears virtually independent of the particular parameter considered [7].

The same situation holds for the zero shear viscosity, η_o, of these materials including silicate glasses [8]. This parameter characterizing the ability of the material to flow, thus the possible frontier between liquid- and solid-like behaviour directly related to the molecular mobility of the system, does not undergo any discontinuity at T_g. Rather, the negative temperature coefficient of log η_o, obeying a Vogel-Fulcher type temperature dependence [9,10] at high temperatures, displays an important (about 10 fold) decrease when the transition range is passed on cooling. Therefore, not only η_o does not tend to infinity in the glass, but its temperature coefficient becomes much smaller than it was for the undercooled liquid!

Consequently, glasses are generally far from thermodynamic equlibrium and their approach towards equilibrium is reflected by the time-dependence of all the structure

sensitive properties of the system.

Structural recovery, recently referred to as *physical aging* [11], thus occurs when the system is removed from its equilibrium by changes in the intensive variables which can be conveniently monitored experimentally.

When the glass-forming liquid is cooled below $T_g(q_1)$, the kinetics of this approach towards thermodynamic equilibrium is a *self-retarded* process. On the other hand, when the annealed glass is *heated* from an initial equilibrium state reached at low temperature, it approaches its final equilibrium at high temperature in a *self-accelerated* manner, which often has an autocatalytic character [2,5,6]. Thys asymmetric approach towards the same equilibrium state is illustrated in Fig. 1 on a poly(vinyl-acetate) sample [12], the investigated parameter being here the departure: $\delta = (v-v_\infty)v^{-1}$ of the specific volume, v, from its equilibrium value, v_∞.

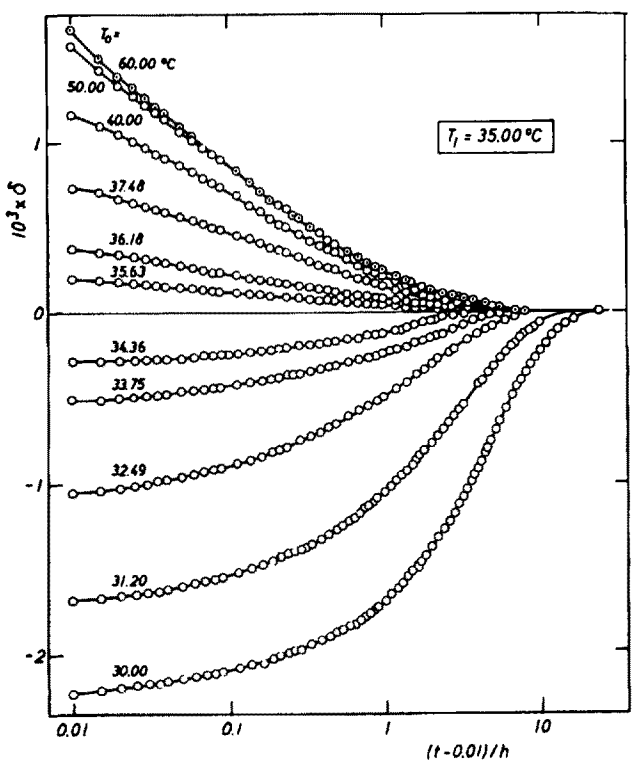

Fig. 1: Isothermal volume recovery at $T_1 = 35^oC$ of a quenched and rapidly reheated poly(vinyl-acetate) sample from various initial equilibrium states reached at different temperatures T_0, as indicated. The ordinate is scaled here by the departure $\delta = (v-v_\infty)v_\infty^{-1}$, from the equilibrium volume v_∞ at 35^oC (A.J. Kovacs, unpublished)

When the initial state at T_0 is not an equilibrium state, the self-accelerated approach may result in an overshoot of the final equilibrium, the approach is then naturally followed by a self-retarded period before reaching the final equilibrium state. Such so-called "memory" or crossover effects have often been observed [2,4,6, 12] and result in a concomitant increase of the molecular mobility of the system followed by its decrease [11]. More complicated effects can easily be conceived by appropriate modifications of the thermal history of the glass [12].

A straightforward interpretation of these phenomena has been proposed by Kovacs [12] on the basis of the empirical *free volume* concept as defined by Doolittle [13] for accounting for the temperature dependence of the viscosity of n-alkanes. Accordingly, the self-retarded volume contraction of quenched glasses (see Fig. 1) should result from the simultaneous decrease of their free volume, whereas the self-accelerated volume expansion reflects the increase of the free volume. This interpretation is well-supported by the quantitative applicability of the WLF equation [14] on the temperature dependence of the longest retardation times [6], controlling the establishment of voluminal equilibrium of polymeric glasses in the transition range, consistently with the above definition of $T_g(q_1)$.

The same free volume concept has been adopted by Struik for interpreting his numerous creep compliance data [11]. Interestingly, he could even apply this empirical relationship semi-quantitatively to complicated "memory" effects he reports for a series of glassy polystyrene specimens submitted to various thermal cycles involving cooling and subsequent heating (see Figs. 82 and 85 in Ref. 11). Although Struik makes some critical comments about the free volume concept in limiting conditions (see Chapter 13 in Ref. 11), the close relationship between molecular mobility and free volume sustains most of the reported data, including those obtained at large deformations.

Kovacs, Stratton and Ferry claim also a quantitative agreement between the variation of the frequency dependence of the storage shear modulus, G', and the *measured* changes of volume during aging of a poly(vinyl-acetate) sample [7]. This agreement fails, however, for the loss modulus, G" , showing that "thermorheological simplicity" does no more apply for the glass. These authors attribute tentatively this discrepancy to the possible changes in the short-time tail of the relaxation spectrum. Such "structural" effect would be clearly inconsistent with the former purely kinetic interpretation of the glass transition, according to which the latter merely reflects rate effects.

During recent years other discrepancies appeared with respect to the early formulation of the free volume concept. Among those we report here the data obtained in two series of experiments, both involving large deformations.

1) Quenched poly(methyl methacrylate) glassy specimens were tested in torque (T_R) and normal-force (N_R) relaxation responses [15] recorded simultaneously at increasing aging times (t_e) and deformations, ranging from $\gamma = 2.7 \cdot 10^{-3}$ to $\gamma = 7.4 \cdot 10^{-2}$.

Contrary to expectations below 80°C the small-deformation relaxation isotherms of T_R could not be superposed by any combination of vertical and horizontal shifts. This failure presumably originates from the inference of a secondary (β) transition superseding the effect of the main glass transition (cf. the paper of B.E. Read in this volume). On the other hand, in the non-linear deformation range, the relaxation isotherms become superimposable simply by horizontal shifts (Δlog a). Nevertheless, as γ increases the curves involve decreasing values of the double-logarithmic shift rates: $\mu = d \log a / d \log t_e$, as defined by Struik [11]. At the same deformation level, however, the shift rate for N_R is significantly higher than for T_R over most of the investigated range of γ. In other words, the same variation of the free volume of the specimen gives rise to uneven changes in the relaxation rates of two simultaneously measured moduli.

2) The final example is displayed by the paradoxical behaviour of a freshly quenched and a cold drawn polycarbonate (PC) specimen, investigated by Pixa, Goett and Froelich [16] at room temperature. While the specific volume of the quenched material exhibits the usual behaviour similar to other polymeric glasses, involving a double logarithmic volume rate [6]: $\beta = -d \log v / d \log t_e$ of the order of 10^{-3}, the cold drawn specimen exhibits a β-value which is more than twice *greater* than the former one, i.e. the cold drawn sample ages about twice faster, in spite of the fact that its density is more than 2% higher than that of the undrawn specimen. Obviously this example shows a reciprocal relationship between molecular mobility and (free) volume rather than a direct one.

Concomitantly, the double logarithmic shift rate, μ, which characterizes the rate of the mobility changes during aging, is more than twice larger for the cold drawn specimen than for the undeformed material. In other words, the molecular mobility is larger in the densified glassy sample than in the normal specimen; another clear contradiction with respect to the simple-minded free volume model [13] based on average values of the volume.

In order to solve this paradox, and many others reported in recent literature, two possible solutions have been proposed. The first considers that the configurational entropy approach of Gibbs and DiMarzio [17], and that of Adam and Gibbs [18] are appropriate to overcome the failures of the free volume concept. An example of this approach is given in this volume by the paper of Dr. Shiro Matsuoka [19]. Other authors maintain the free volume concept but they account for its fluctuations and possibly for its anisotropy. The joint work of Robertson, Simha and Curro is probably the most representative of this trend [20].

Whatever the case, the above examples clearly show that the relationship between molecular mobility and molecular structure still remains a challenging topic for describing more accurately the behaviour of glass-forming materials.

References

[1] F. Simon, Ergebn. Exakt. Naturwiss. 9, 222 (1930) and Z. Anorg. All. Chem. 203, 220 (1931)

[2] A.Q. Tool, J. Am. Ceram. Soc. 29, 240 (1946)

[3] W. Kauzmann, Chem. Rev. 43, 219 (1948)

[4] R.Q. Davies and G.O. Jones, Adv. Phys. (Phil. Mag. Suppl.) 2, 370 (1953)

[5] H.N. Ritland, J. Am. Ceram. Soc. 37, 370 (1954); id. 39, 403 (1956)

[6] A.J. Kovacs, Thèse Far. Sci. Paris, 1954, and J. Polym. Sci. 30, 131 (1958)

[7] A.J. Kovacs, A. Stratton and J.D. Ferry, J. Phys. Chem. 67, 153 (1963)

[8] A.L. Zijlstra, Phys. Chem. Glasses 4, 148 (1963)

[9] A. Vogel, Physik. Z. 22, 645 (1921)

[10] G.S. Fulcher, J. Am. Chem. Soc. 8, 339 and 789 (1925)

[11] L.C.E. Struik, Physical Aging in Amorphous Polymers and Other Materials, Elsevier, Amsterdam 1978

[12] A.J. Kovacs, Fortschr. Hochpolym. Forsch. (Adv. in Polym. Sci.) 3, 394 (1963)

[13] A.K. Doolittle, J. Appl. Phys. 22, 1471 (1951)

[14] M.L. Williams, R.F. Landel and J.D. Ferry, J. Am. Chem. Soc, 77, 3701 (1955)

[15] G.B. McKenna and A.J. Kovacs, Polym. Eng. and Sci. 24, 1138 (1984)

[16] R- Pixa, C. Goett and D. Froelich, Polymer Bull. 14, 53 (1985); id. 16, 381 (1986)

[17] J.H. Gibbs and E.A. DiMarzio, J. Chem. Phys. 28, 373 and 807 (1958)

[18] G. Adam and J.H. Gibbs, J. Chem. Phys. 43, 139 (1965)

[19] Shiro Matsuoak, this volume, p. 188

[20] R.E. Robertson, R. Simha and J.G. Curro, Macromolecules 17, 911 (1984)

THERMAL CYCLING OF GLASSES: A THEORETICAL AND EXPERIMENTAL APPROACH

J.M. Hutchinson

Department of Engineering, University of Aberdeen
King's College, Aberdeen AB9 2UE
Scotland

Summary

A theoretical model for the response of glass-forming systems to three-step thermal cycles is reviewed, and is shown to predict two important features. First, under limiting conditions of rapid heating of well-stabilized glasses, a single (main) peak in the heat capacity occurs at a temperature which depends strongly on the experimental variables. This dependence is a unique function of the parameter x, controlling the relative contributions of temperature and structure to the retardation times, and provides a rational means of evaluating x which is shown to be experimentally feasible. Second, when these thermal cycles involve the opposite conditions of slow heating of poorly stabilized glasses, then either two peaks (a main peak and an upper peak) or a single upper peak may be observed. The main peak and the upper peak are quite different in nature, particularly in respect of the manner in which they depend on the experimental variables, and data in the literature are used to show that all reported observations of double peaks can be explained qualitatively on the basis of this theoretical model.

Introduction

A theory for the structural recovery of glasses in the glass transition region has been developed by Kovacs and co-workers over the past ten years. In its earliest and simplest form the theory described the response of a single retardation time model to thermal cycles involving uniform cooling, isothermal annealing and subsequent heating through the transition region [1]. This response was shown to exhibit a single peak in the specific heat capacity or thermal expansion coefficient on heating at constant rate, and the temperature $\hat{T}$ at which this peak occurred depended upon the values of the experimental variables (cooling rate q_1, isothermal recovery, heating rate q_2). More importantly, though, the variation of $\hat{T}$ with each of these experimental variables (e.g. $\partial\hat{T}/\partial\ln|q_1|$ or $\partial\hat{T}/\partial\ln q_2$) was shown to depend critically upon an important parameter, x $(0 < x < 1)$, which controls the relative contributions of temperature and structure to the retardation time. It was concluded from

this result that, for the single retardation time model, a rational experimental evaluation of x for a glass could be achieved by determining the variation of the peak temperature with the experimental variables defining the thermal cycles (peak-shift method).

Subsequently, this theory was extended to consider the more realistic case in which a spectrum of retardation times is involved [2-4]. The response of this multiparameter model to the same thermal cycles as for the single retardation time model was found to be considerably more complex, in particular involving double peaks. Nevertheless, experimental conditions were clearly identified for which only one peak ($\hat{T}$) is observed, and it was shown that under limiting conditions this peak behaves identically to that found for the single retardation time model. It was thus concluded that the same peak-shift method could be used to evaluate the parameter x when the recovery process involves a distribution of retardation times. Further conclusions were also made with regard to the existence of double peaks, involving a "main" peak at temperature $\hat{T}$ and an "upper" peak at temperature T_u. In particular, clear indications were given about the experimental conditions which favour the existence of an upper peak.

In spite of these conclusions, however, there are still results presented in the literature where the existence of double peaks is overlooked (e.g. Ref. [5]). This paper seeks, therefore, to restate the predictions of the multiparameter model with respect to double peaks, and to clarify the situation by reference to numerous examples from the literature. In addition to this, the peak-shift procedure will also be restated and the results of previous papers [3,4] will be extended to include the effect of a continuous spectrum of retardation times.

Theory

A detailed description of the model can be found in earlier work [2-4]; it will suffice here simply to introduce the basic equations and definitions.

In terms of volume recovery, structural changes are monitored by the relative departure of the system from equilibrium through the dimensionless variable δ defined as:

$$\delta = \frac{v-v_\infty}{v_\infty} \tag{1}$$

in which v is the instantaneous volume and v_∞ its equilibrium value at the same temperature T. In the KAHR multiparameter model [2] δ is considered to consist of N elements:

$$\delta = \sum^{N} \delta_i \quad (1 \leq i \leq N) \tag{2}$$

and the recovery of each element is determined by the differential equation

$$-\frac{d\delta_i}{dt} = \Delta\alpha_i \; q + \frac{\delta_i}{\tau_i} \tag{3}$$

in which q is the cooling (-ve) or heating (+ve) rate and $\Delta\alpha_i = g_i\Delta\alpha$ is the weighted contribution ($\sum_N g_i = 1$) of the ith retardation mechanism to $\Delta\alpha$, the excess thermal expansion coefficient of the equilibrium liquid with respect to that of the glass at any fixed structure.

The retardation times τ_i depend on both T and δ according to the equation:

$$\tau_i = \tau_{i,r} \exp[-\theta(T-T_r)]\exp[-(1-x)\theta\delta/\Delta\alpha] \tag{4}$$

where $\tau_{i,r}$ is the value of τ_i in equilibrium at a reference temperature T_r. The material constants θ and $\Delta\alpha$ can be determined independently by suitable experiments, while the non-linearity parameter x is determined by the T-shift method to be shown below. In the analysis of the response of this model, it is convenient to use reduced variables defined as follows:

$$\begin{aligned} T &= \theta T \\ Q &= \theta q \\ D &= \theta\delta/\Delta\alpha \; . \end{aligned} \tag{5}$$

Finally, the retardation spectrum is defined by the paired values (g_i, τ_i).

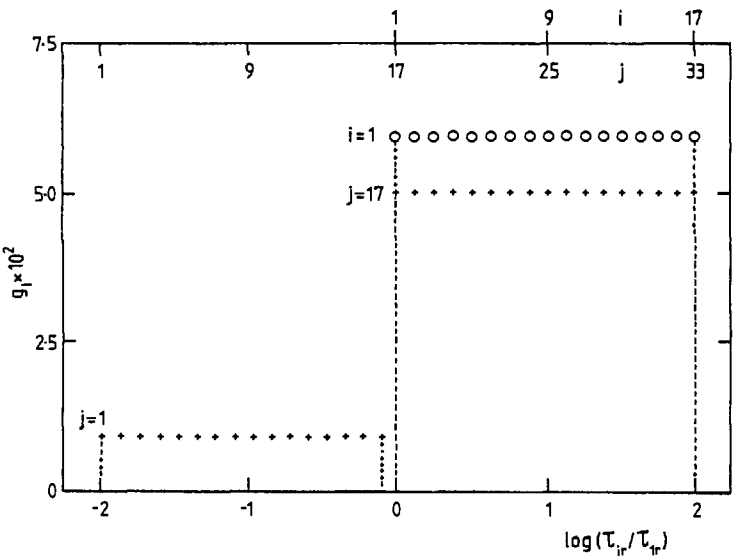

Fig. 1: Structural retardation spectra at T_r. Circles (and i): 17 element, single-box distribution. Crosses (and j): 33 element, double-box distribution

Two discrete spectra have been used to obtain the results described below: a single-box and a double-box distribution, shown in Figure 1. Results will also be presented for an approach which is an alternative to the KAHR multiparameter model. This approach involves a continuous spectrum, in which the recovery function [2] is described by an empirical expression used by Williams and Watts [6]:

$$\bar{R}(z) = \exp\,[-(z/\tau_r)^{\beta}] \tag{6}$$

in which τ_r is the correlation time in equilibrium at T_r, z is a reduced time variable, and the exponent β is inversely related to the width of the spectrum.

Thermal Cycles

The model above defines the response of the glass-forming system to any thermal history. The particular thermal cycles involved here are precisely defined, and involve three steps, which may be described in terms of reduced variables as: cooling from equilibrium at temperature T_0 at a constant rate Q_1, until temperature T_1 is reached; isothermal recovery at T_1, during which D is reduced by an amount $\bar{D}$, from an initial value of D_1 to a final value D_2; reheating at a rate Q_2 until equilibrium is again established. Such a cycle is shown in Figure 2, and the response of the system to these thermal cycles is described below.

It is useful to consider, initially, the response of the single retardation time model. For this unrealistic but simplified system it has been shown [1] that, on heating, a single peak in the thermal expansion coefficient occurs under all circumstances, at a reduced temperature $\hat{T}$ which is a function of T_1, D_2 and Q_2. The dependence of $\hat{T}$ on each of these experimental variables defines a set of shifts:

$$\hat{s}(T_1) = \left(\frac{\partial \hat{T}}{\partial T_1}\right)_{D_2,Q_2} \;;\quad \hat{s}(D_2) = \left(\frac{\partial \hat{T}}{\partial D_2}\right)_{T_1,Q_2} \;;\quad \hat{s}(Q_2) = \left(\frac{\partial \hat{T}}{\partial \ln Q_2}\right)_{T_1,D_2} \tag{7}$$

in which the partial derivatives indicate that the evaluation of the shift $\hat{s}$ for each experimental variable requires the other variables to remain fixed. Each of these shifts was found [1] to depend critically on the value of x, introduced in Eq. (4), from which it was concluded that the value of x for a glass could be determined in a rational manner by evaluating experimentally the shift $\hat{s}$ defined in Eq. (7) above when that glass is subjected to a series of well-defined thermal histories. This is referred to here as the peak-shift method.

While this approach appears straightforward for the single retardation time model, the situation becomes rather complex when a distribution of retardation times is considered [2-4]. First, the response of the multiparameter system will depend upon the cooling rate Q_1 in addition to the other variables T_1, D_2 (or $\bar{D}$) and Q_2. Second, it transpires that the multiparameter response can give rise to multiple peaks in the

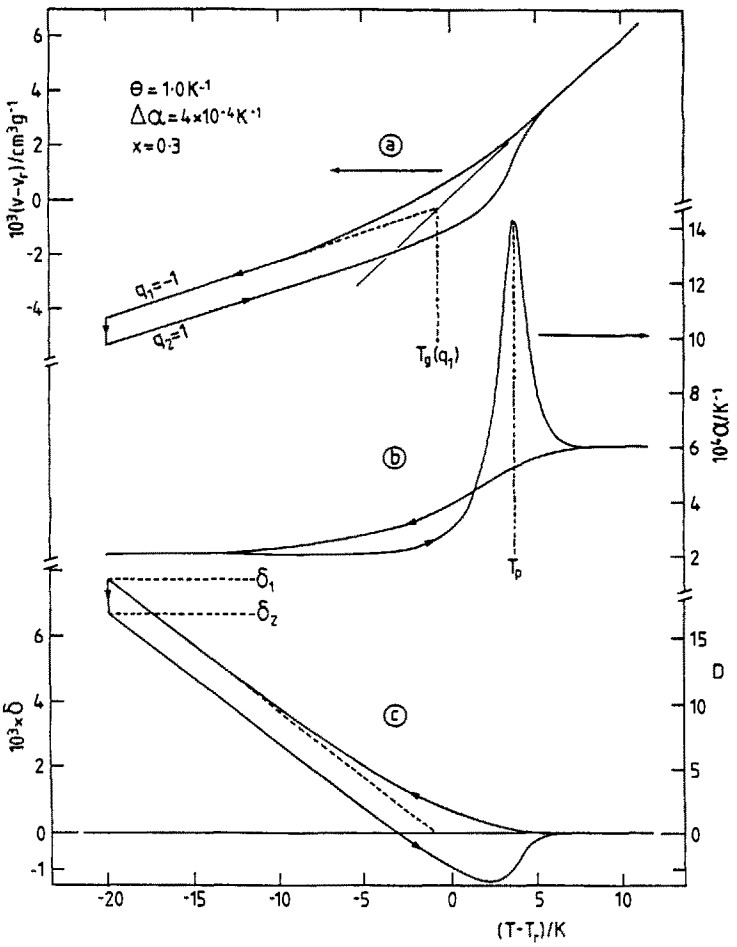

Fig. 2: Typical three-step thermal cycle, shown in terms of volume, thermal expansion coefficient and δ (or D). The system is cooled at rate $q_1 = -1\ tu^{-1}$ to $T_1 = T_r - 20$, followed by isothermal recovery by an amount $\bar{D} = 2.5$ and is then reheated at rate $q_2 = 1\ tu^{-1}$. The time unit (tu) is defined as $\tau_{1,r}$ for the single-box distribution

expansion coefficient or specific heat capacity on heating. For example, some typical theoretical results are shown in Figure 3 for the heating stage of these three-step thermal cycles. It can clearly be seen that the prediction of the multiparameter model is that the response to these thermal cycles can involve multiple peaks. The characteristic features of these peaks are discussed below.

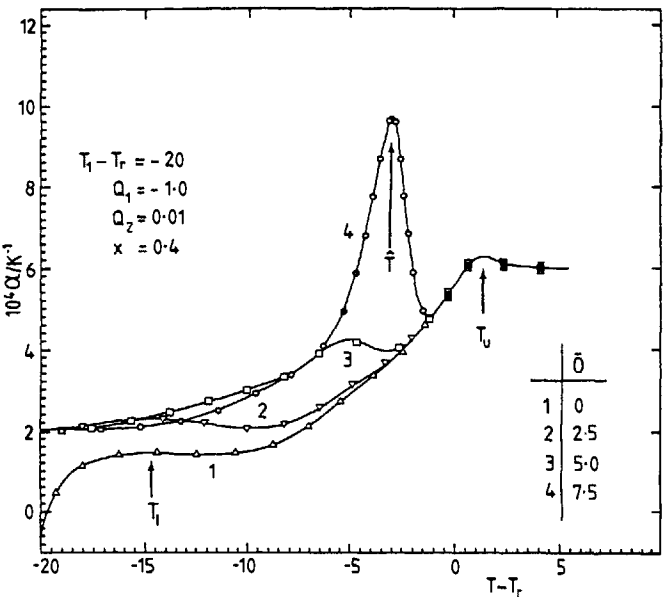

Fig. 3: Family of α isobars predicted by the multiparameter model for thermal cycles involving the set of reduced experimental variables given in the inset. The four curves are obtained for the increasing values of $\bar{D}$ indicated

Multiple Peaks

The curves shown in Figure 3 provide some insight into the conditions under which the different peaks occur. It should be noted that three different kinds of peak can occur: these are labelled T_ℓ (the "lower" peak), $\hat{T}$ (the "main" peak) and T_u (the "upper" peak). The lower peak can be seen to be very broad and shallow, and occurs only under limited experimental conditions: furthermore, since it has never been observed experimentally, it will not be considered further here. On the other hand, the main and upper peaks are well-defined and form the subject of this paper.

From Figure 3 it can be seen that increasing the annealing period at T_1 causes the main peak at $\hat{T}$ to shift to higher temperature and to become stronger, while the upper peak at T_u remains invariant. In the limit, although this is not shown in Figure 3, the main peak will eventually obscure the upper peak, and only a single peak at $\hat{T}$ will be observed. Thus, for well-stabilized glasses, only a single peak at $\hat{T}$ will appear. Conversely, reheating a poorly stabilized glass will favour the appearance of the upper peak.

Some further conclusions can be drawn from the dependence of these peaks on the other experimental variables. For example, the effect of the cooling rate Q_1 is shown in Figure 4. Here it can be seen that as the cooling rate is reduced, the main peak

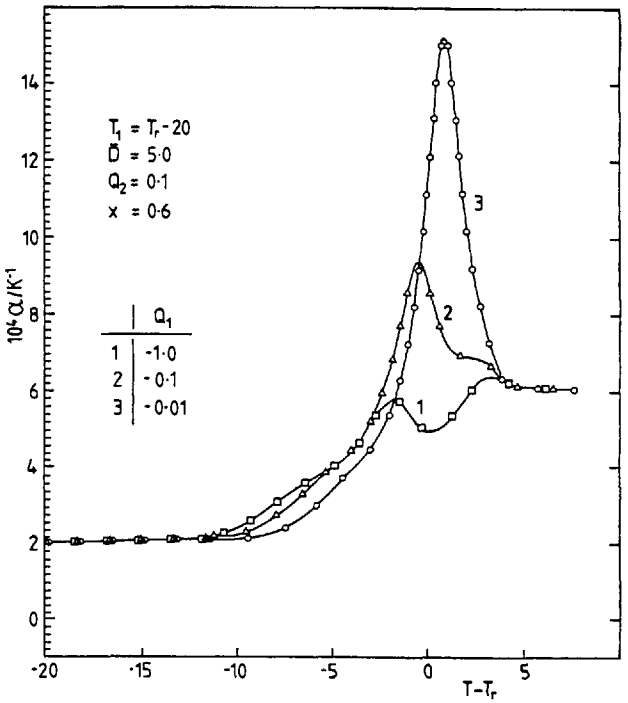

Fig. 4: The effect of cooling rate Q_1 on the α isobars obtained on heating, for thermal cycles defined by the set of reduced variables in the inset

becomes more pronounced and shifts to higher temperatures, eventually overshadowing the upper peak completely. The slower cooling rate in fact implies a better stabilized glass at the lower temperature T_1, if the other experimental variables remain constant. This result therefore supports the previous observation that increasing the amount of stabilization of the glass prior to reheating will promote a single peak at $\hat{T}$.

Finally, the effect of the heating rate Q_2 is shown in Figure 5. As the heating rate is increased, both the main peak and the upper peak shift to higher temperatures. The former peak is, however, much the more sensitive, in respect of both peak size and shift rate, so that with increasing heating rate the main peak eventually overshadows the upper peak. Under these circumstances, once again, only a single peak will appear at $\hat{T}$.

From these observations of the response of the system to a variety of experimental conditions, the following conclusions can therefore be made.

1. The conditions which favour the appearance of a main peak are, in general, rapid heating of a well-stabilized glass.
2. In the limit, increasingly rapid heating of a well-stabilized glass will result in only a single peak at temperature $\hat{T}$.

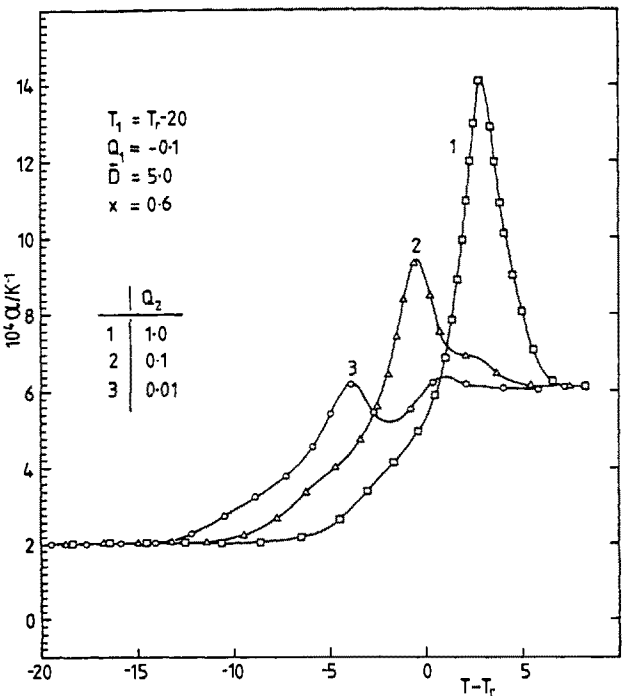

Fig. 5: The effect of heating rate Q_2 on the α isobars obtained on heating, for thermal cycles defined by the set of reduced variables in the inset

3. Conversely, the opposite conditions involving slow heating of a poorly stabilized glass will favour the appearance of an upper peak.

4. Again, in the limiting condition of very slow heating of an unstabilized glass the response will involve only a single peak, but in this case at the temperature T_u. Note that the terminology of referring to T_u as the upper peak does not necessarily imply that there be more than one peak actually present. Thus, in this limiting case, the single peak at T_u implies only that it is a peak with the characteristics of an upper peak (see below).

5. Between the limiting conditions in which either a single main peak or a single upper peak occurs, there exists a range of conditions for which both peaks may occur simultaneously, or for which there is clear evidence of a second peak as a shoulder (e.g. curves 2 in Figures 4 and 5).

The two kinds of peak (main and upper) clearly depend on the experimental conditions in very different ways, implying that they are quite different in nature. Each peak is therefore discussed in detail separately in the following sections.

The Main Peak, $\hat{T}$

In the response of the multiparameter model to the thermal cycles described above,

it is possible to identify the main peak by considering the ranges of experimental variables which favour its appearance, as has been shown in the previous section. It is therefore possible to determine how the main peak shifts as a function of the experimental variables, defining for the multiparameter model a set of shifts denoted by $\hat{s}(\varrho_1)$, $\hat{s}(\varrho_2)$ and $\hat{s}(D_2)$ or $\hat{s}(\bar{D})$. When these shifts are calculated theoretically, it is found that, in the limiting conditions, they depend critically on the value of the parameter x in exactly the same way as did the single peak in the response of the single retardation time model. Furthermore, it is found, and can be shown theoretically, that these shifts are all inter-related and can each be written as a function of x in the form:

$$-\hat{s}(\varrho_1) = \hat{s}(\varrho_2) - 1 = \hat{s}(\bar{D}) = H(x). \tag{8}$$

The function $H(x)$ is illustrated in Figure 6 both for the single retardation time model and also for the multiparameter model involving each of the distributions shown

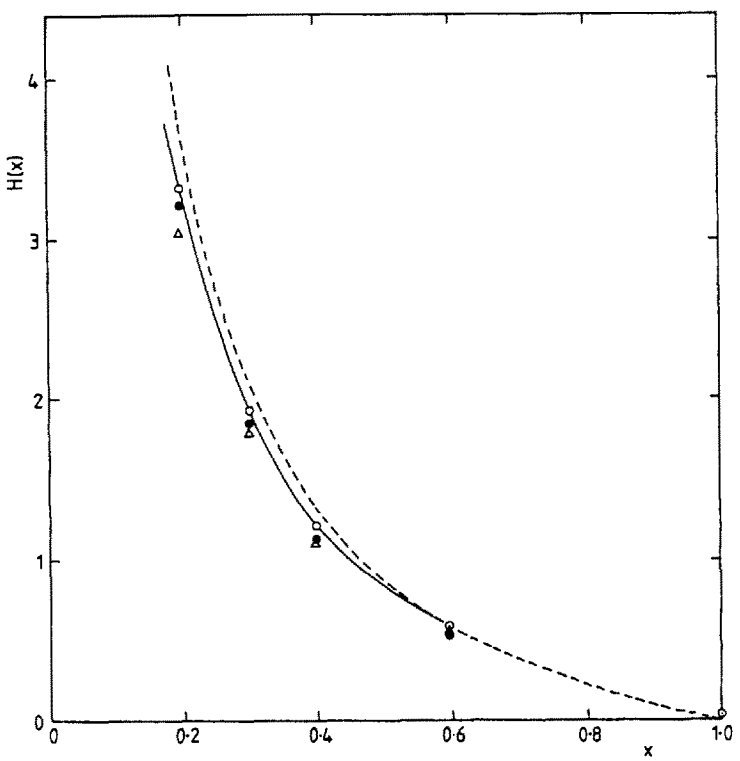

Fig. 6: Theoretically calculated variations of $H(x)$ as a function of x. The results for the single retardation time model are indicated by the dashed line, and those for three different spectra of retardation times are shown as follows: single-box discrete spectrum, filled circles; double-box discrete spectrum, open circles; continuous spectrum WW response function with $\beta = 0.456$, triangles

in Figure 1. It is clear that the function $H(x)$ is essentially independent of the distribution used in the model: indeed, the small discrepancies between the curves shown in Figure 6 are only relative, and indicate the different degrees to which the limiting experimental conditions (rapid heating, large amount of annealing at τ_1) have been reached. Furthermore, the value of $H(x)$ is seen to be very sensitive to the parameter x, particularly within the range of values of x anticipated for glass-forming systems ($0.2 < x < 0.6$). The peak-shift method therefore provides a simple and direct procedure for the evaluation of the parameter x, without the need to make any assumptions about the form of the distribution of retardation times: it suffices to evaluate experimentally any (or all) of the $\hat{s}$ shifts, and then to read off the value of x from the corresponding value of the function $H(x)$ in Figure 6.

The fact that the main peak in the multiparameter model and the single peak in the single retardation time model behave identically in respect of their shifts with the experimental variables is interesting. It implies that these peaks are of the same nature, and is the basis on which, for the multiparameter model, the peak in question is referred to as the main peak. As has been shown in an earlier section, and as will be further detailed below, there are experimental conditions under which an upper peak alone may occur. Despite the fact that this upper peak will be the only peak present under these circumstances, it should not be confused with a main peak: it cannot be a main peak since, as will be shown below, it behaves quite differently in respect of its shifts with the experimental variables, and is therefore quite different in nature from a main peak.

The results presented thus far in Figure 6 have related to the discrete distributions in Figure 1. In concluding the discussion of the main peak, though, it should be pointed out that exactly the same results for the peak shifts are obtained when the recovery is described by a continuous spectrum involving the WW function given in Equation (6). These results are shown in Figure 6 as triangles, for the particular case in which the exponent β takes the value 0.456. This value of β is chosen such that the response function [2,4] corresponds very closely to that of the double-box spectrum in Figure 1. These results further support the conclusion that the peak-shift method is independent of the distribution.

The Upper Peak, τ_u

In the previous section we have examined the main peak, the presence of which can be promoted by rapid heating of a well-stabilized glass. In contrast to this, it is possible to promote an upper peak by considering the opposite experimental conditions: slow heating of a poorly-stabilized glass. Under such circumstances, it is possible to evaluate the shifts of the upper peak τ_u with the experimental variables, in exactly the same way as the main peak shifts were evaluated. Thus for the upper peak one can define s_u shifts as follows:

$$s_u(\varrho_1) = \frac{\partial T_u}{\partial \ln|\varrho_1|}; \quad s_u(\varrho_2) = \frac{\partial T_u}{\partial \ln \varrho_2} ; \quad s_u(\bar{D}) = \frac{\partial T_u}{\partial \bar{D}} . \tag{9}$$

When these shifts are evaluated theoretically, some interesting features emerge, which can be seen from a consideration of the results presented in Table I. This table shows the values of the three s_u derivatives defined in Eq. (9), as a function of the parameter x, for the particular case of the single-box distribution (Figure 1).

Table I: Variations of the upper peak T_u.
Single-box distribution: $\rho_1 = 10$, $\rho_2 = 100$ where $\rho = |\varrho_1|/\varrho_2$

x =	0.2	0.3	0.4	0.6	1.0
$s_u(\varrho_1)$	0.16	0.15	0.14	0.13	0.14
$s_u(\varrho_2)$	0.84	0.85	0.86	0.87	0.86
$s_u(\bar{D})$	0.0	0.0	0.0	0.0	0.0

First, the upper peak shifts present a special case of the interrelationships defined in Eq. (8) for the main peak. In particular, we have

$$s_u(\bar{D}) = 0 \; ; \quad s_u(\varrho_1) + s_u(\varrho_2) = 1 . \tag{10}$$

The result that $s_u(\bar{D}) = 0$ implies that the upper peak remains invariant as the amount of annealing at T_1 is increased. This can clearly be seen in the theoretical curves shown in Figure 3, which are for increasing values of $(\bar{D})$: the main peak grows in magnitude and shifts to higher temperature while the upper peak remains invariant. It will be shown later that exactly the same observations have been made experimentally.

Second, in striking contrast to the main peak shifts, the values of s_u are essentially independent of x. The dependence of the upper peak on the experimental variables cannot therefore provide any information about the parameter x. This contrasting behaviour of the main and upper peaks serves to emphasize the fact that these two peaks are quite different in nature.

Third, the s_u values, particularly the value of $s_u(\varrho_1)$ but also that of $s_u(\varrho_2)$, are significantly smaller than the $\hat{s}$ values over the majority of the range of x. Thus the upper peak will appear much less sensitive to the experimental variables than is the main peak. This is clearly evident in Figures 4 and 5 where the effects

of cooling rate and heating rate, respectively, are illustrated: in each case the main peak shifts much more dramatically than the upper peak, with the former eventually completely overshadowing the latter.

A further interesting feature of these upper peaks emerges when one considers distributions other than the single-box, for which the results are shown in Table II. Other distributions which have been used here include the two-box distribution (Figure 1)

Table II: $s_u(Q_1)$ values for various distributions

$\rho=\lvert Q_1\rvert/Q_2$	x	SINGLE BOX	DOUBLE BOX	WW β=0.456	WW β=0.3	WW β=0.2
ρ_1=10 ρ_2=100	0.2	0.16	0.13	0.30	0.37	
	0.3	0.15	0.15	0.27	0.36	
	0.4	0.14	0.14	0.25	0.36	
	0.6	0.13	0.13	0.23	0.34	
	1.0	0.14	0.14	0.22	0.31	
ρ_1=1 ρ_2=10	0.2		(0.42)*	0.41	0.76	0.96
	0.3		0.31	0.41	0.71	0.96
	0.4		0.29	0.40	0.68	0.94
	0.6		0.27	0.38	0.63	0.90
	1.0		0.28	0.38	0.58	0.87

*In this case, the upper and main peaks have combined to form a composite peak.

and the WW function with values of the exponent β = 0.2, 0.3 and 0.456. In comparing the results for various distributions, it is important to remember three points: i) the ratio ρ of cooling rate to heating rate ($\rho = |Q_1|/Q_2$) needs to be large to promote the upper peak, ii) the value of s_u depends on the range of the variable considered, and hence comparisons should be made for equivalent values of ρ, and iii) since $s_u(Q_1) + s_u(Q_2) = 1$, it suffices to compare only one of these shifts, which we choose to be $s_u(Q_1)$. The $s_u(Q_1)$ values calculated in this way are given in Table II for two different ranges of ρ and for the five distributions discussed above.

Examination of the results presented in Table II shows, as anticipated, that the $s_u(Q_1)$ values are not sensitive to the value of x for any of the distributions considered. On the other hand, for each combination of values of ρ, it is clear that the $s_u(Q_1)$ values are dependent on the choice of distribution (cf. Figure 6), and once again emphasizes the very different characteristics of the upper and main peaks.

It appears from Table II that the $s_u(\varrho_1)$ values increase as the breadth of the distribution increases, which suggests that an experimental determination of the s_u values could provide some information about the width of the distribution of retardation times.

Experimental Observations

The results presented above have been derived theoretically, and predict the response of a glass-forming system to three-step thermal cycles. This response has been shown to involve a main peak and an upper peak, each of these peaks responding quite differently to changes in the experimental variables, and the variation of the main peak providing a means of evaluating the parameter x. It is pertinent at this stage to examine to what extent these theoretical predictions are borne out by experimental results.

Evaluation of x

The evaluation of x from experimental data in the manner outlined above requires close control of the thermal cycles. To evaluate the $\hat{s}$ shifts: i) only one of the experimental variables (q_1, $\bar{\delta}$ or q_2) must be varied while the others are held constant, and ii) a limiting condition must have been reached where the value of $\hat{s}$ has become independent of the experimental variable. These restrictions place severe limitations on the availability of data in the literature. Furthermore, by far the most common experimental variable used in such cycles is the logarithm of the annealing time, which is not one of the variables considered in the above analysis. The majority of literature data is therefore unavailable for analysis by the peak-shift method. Finally, this method uses reduced variables in the analysis (Eq. 5), and consequently requires a knowledge of the values of θ and $\Delta\alpha$ in order to evaluate x.

The result of the above restrictions is that there is not a complete set of data available in the literature for the evaluation of x. It is possible, however, to use the data of Hutchinson and Kovacs [8] to evaluate $\hat{s}(\bar{D})$ for atactic polystyrene. The data in Reference [8] show the variation of $\hat{T}$ with annealing time, while supplementary unpublished data provide the relationship between annealing time and $\bar{D}$, from which one obtains $s(\bar{D}) = 1.23$. It should be noted, though, that these data do not represent a limiting condition, as is required by the peak-shift method, and this value for $\hat{s}(\bar{D})$ can only be regarded as illustrative of the procedure that is involved. Interestingly, however, it can be seen from Figure 6 that, corresponding to the above value of $\hat{s}(\bar{D})$, one obtains $x \doteq 0.38$, which lies within the range of values ($0.2 < x < 0.6$) anticipated for glass-forming sytems.

Multiple Peaks

The analysis above makes precise predictions about the existence of multiple peaks. For the same reasons as discussed above with respect to the main peak, no quantitative experimental analysis of the upper peak shifts can be attempted here. However, it is interesting to observe the qualitative agreement between the theoretical predictions and the experimental observations reported in the literature. Recalling the important features of the upper peak (it is promoted by slow heating of a poorly stabilized glass, and it shifts very little in comparison with the main peak), it is possible to rationalise qualitatively every reported observation of multiple or "spurious" peaks in the heat capacity or thermal expansion coefficient.

The early results of Volkenstein and Sharonov [9] show a small "misplaced" peak when polyvinylacetate is slowly reheated immediately after a quench. The peak is "misplaced" in that, for all peaks apart from this one, an increase in the heating rate shifts the peak to higher temperature as one would expect for a main peak, whereas increasing the heating rate from that pertaining to the "misplaced" peak shifts the peak to lower temperature. The clear implication is that this "misplaced" peak is in fact an upper peak and not a main peak (note that it is not necessary to have two peaks in order to observe a peak of the upper kind), and clearly occurs under conditions favouring the appearance of an upper peak.

The existence of the upper peak has often been overlooked (because it is always small) and viewed instead as a step in the heat capacity or thermal expansion coefficient, with the main peak then appearing as what has been referred to as a "premaximum" [10] or "sub-T_g peak" [11]. Illers observed this "premaximum" on heating a rapidly quenched sample of polyvinylchloride, and found it to move to higher temperatures and increase in magnitude as the amount of annealing prior to heating increased; eventually this "premaximum" completely overshadowed the "upper peak" or step. It is clear from this that the "premaximum" is simply the main peak: for unannealed rapidly quenched samples, the upper peak is promoted and the main peak appears only as a shoulder or small peak. As the amount of annealing increases and the sample becomes more stabilized prior to reheating, the main peak becomes enhanced and shifts to higher temperatures as expected, while the upper peak remains essentially unchanged, leading eventually to a single (main) peak. Similar observations were made by Hodge and Berens [11] who found that their "sub-T_g" endothermal peaks were enhanced by pretreatments which produce a state of increased enthalpy at the start of the annealing process, including thermal quenching as predicted by the theoretical analysis above.

Although peaks of different natures (i.e. main and upper peaks) are implied in the references cited above, they include no report of double peaks, i.e. of the two peaks appearing simultaneously. Double peaks have, however, been observed by Neki and Geil [12] in polycarbonate quenched and then reheated after only a short annealing time. Note that these are exactly the conditions which our analysis predicts as being

favourable for the appearance of an upper peak. Furthermore, these authors observe that with increased annealing time the lower (main) peak shifts to higher temperature, while the upper peak remains essentially unchanged, again qualitatively exactly as predicted by the theoretical shifts. Double peaks were also observed by Hutchinson and Kovacs [8] dilatometrically in polystyrene reheated immediately after a quench.

The above observations all relate to organic polymers as the glass-forming systems. The phenomenon of double peaks, however, should be a feature of all glass-formers, and one should enquire whether it has been observed in other systems, for example in inorganic glasses. Although both main and upper peaks have not been observed to occur simultaneously in inorganic systems, there is clear evidence that both types of peaks occur, inasmuch as the shifts of the peaks as a function of the experimental variables can appear anomalous unless the different natures of the peaks are recognized. For example, the effect of increased cooling rate on the heat capacity of heavy metal fluoride glasses [5] promotes an upper peak, as evidenced by its occurrence at a temperature higher than the peak obtained on heating the glass formed at a slower cooling rate. There is also evidence [5] that annealing the glass results in the growth of a main peak, which is superposed as a shoulder on the upper peak; further annealing would be required in order to transform this shoulder into a peak, similar to the "premaximum" of Illers or the "sub-T_g peaks" of Hodge and Berens, but the experimental time-scale involved precluded this.

Conclusions

The response of glass-forming systems to three-step thermal cycles has been described theoretically on the basis of the KAHR model. Several features of the response have been predicted theoretically, and are compared with available experimental data as follows:

1. The main peak in heat capacity or thermal expansion coefficient is very sensitive to the experimental variables, and an analysis of its variation provides a means of determining the parameter x, controlling the relative contributions of temperature and structure to the retardation times.

2. For certain well-defined experimental conditions, an upper peak rather than a main peak, is observed. This upper peak is relatively insensitive to the experimental variables and is independent of the parameter x. It does appear, however, to be influenced by the width of the distribution of retardation times.

3. Under some circumstances, both upper and main peaks may occur simultaneously in the response on heating. Examples of such situations from the literature have been shown to occur under exactly those conditions predicted by the theoretical model.

The theoretical model therefore predicts qualitatively all experimental observations of the response to three-step thermal cycles. Furthermore, it provides a method for

the quantitative determination of the parameter x, and also possibly of the width of the distribution. Data in the literature are shown to be inadequate for such an analysis, but a precisely controlled set of experiments is currently being performed, and the results will be presented in a later paper.

References

[1] Kovacs, A.J. and Hutchinson, J.M., J. Polymer Sci. - Polym. Phys. Edn., 1979, 17, 2031-2058

[2] Kovacs, A.J., Aklonis, J.J., Hutchinson, J.M. and Ramos, A.R., J. Polymer Sci. - Polym. Phys. Edn., 1979, 17, 1097-1162

[3] Ramos, A.R., Hutchinson, J.M. and Kovacs, A.J., J. Polymer Sci. - Polym. Phys. Edn., 1984, 22, 1655-1695

[4] Hutchinson, J.M. and Kovacs, A.J., Polymer Eng. Sci., 1984, 24, 1087-1103

[5] Moynihan, C.T., Bruce, A.J., Gavin, D.L., Loehr, S.R. and Opalka, S.M., Polymer Eng. Sci., 1984, 24, 1117-1122

[6] Williams, G. and Watts, D.C., Trans. Faraday Soc., 1970, 66, 80

[7] Moynihan, C.T., Macedo, P.B., Montrose, C.J., Gupta, P.K., DeBolt, M.A., Dill, J.F., Dom, B.E., Drake, P.W., Easteal, A.J., Elterman, P.B., Moeller, R.P., Sasabe, H. and Wilder, J.A., Workshop on the Glass Transition and the Nature of the Glassy State, New York Academy of Sciences, New York, 1975.

[8] Hutchinson, J.M. and Kovacs, A.J., J. Polymer Sci. - Polym. Phys. Ed., 1976, 14, 1575

[9] Volkenstein, M.V. and Sharonov, Y.A., Vysokomol, Soed., 1961, 3, 1739

[10] Illers, K.H., Makromol, Chem., 1969, 127, 1

[11] Hodge, I.M. and Berens, A.R., Macromolecules, 1982, 15, 756 and 762

[12] Neki, K. and Geil, P.H., J. Macromol. Sci. - Phys., 1973, B8, 295

APPLICATION OF ADAM-GIBBS' THEORY TO THERMODYNAMIC RECOVERY AND STRUCTURAL RELAXATION

Shiro Matsuoka
G.H. Fredrickson
G.E. Johnson

AT & T Bell Laboratories
Murray Hill, New Jersey 07974
USA

Abstract

The Vogel-Fulcher equation $\ln\tau \propto H/R(T-T_2)$, and the WLF equation, $\ln\tau \propto -C_1(T-T_0)/[C_2+(T-T_0)]$, can be expressed in the same form. They are known to fit well with relaxation data of liquids in equilibrium. Doolittle's free volume equation, $\ln\tau \propto 1/f$, and Adam-Gibbs's entropy equation, $\ln\tau \propto C/RTS$, can be reduced to the Vogel-Fulcher equation with reasonable assumptions on the temperature dependence of the free volume fraction, f, and/or the configurational entropy, S. However, in predicting the relaxation behavior in the nonequilibrium state, the Adam-Gibbs equation can be shown to be a clearly better theory than the Doolittle equation. Moreover, with the Adam-Gibbs equation, it is shown that the kinetic parameters required to describe physical aging are the same as those necessary to describe dielectric relaxation behavior.

1. Introduction

It is generally agreed that the relaxation behavior of dense fluid is not described by a simple exponential function of time, nor its temeprature dependence by an Arrhenius formula. Other aspects are less clear cut and some are even controversial, but we believe that the rate of recovery and the rate of dielectric or mechanical relaxation can be expressed by the same equation when properly analyzed. We also believe that the distribution of relaxation times depends on temperature and the aging, though less dramatically than does the relaxation time itself. A theory must be able to predict all these aspects of the complex phenomena. A spin model for cooperative relaxation in dense fluids, recently proposed by Fredrickson and Andersen, can predict all these features of relaxation phenomena in dense fluids and thereby can aid in elucidating the nature of the nonequilibrium glassy state.

2. The Relaxation Time and the Thermodynamic Recovery Time

By relaxation behavior we mean the time dependent response to an external perturbation such as mechanical stress, or an electrical potential. By thermodynamic recovery, we mean the aging process, or the time dependent process of reaching the equilibrium state in volume, enthalpy and entropy from a perturbed state caused by a shift in temperature or pressure. Intuitively, it seems that there should be no fundamental differences between relaxation and recovery processes at the molecular level, and it may be suspected that the relaxation time and the recovery time may well be equal, or at least proportional to each other. Difficulties are encountered, however, in quantifying such a concept with experimental data. One of the reasons is that, with the broad relaxation spectrum that real materials exhibit in the glassy regime, the "characteristic" relaxation time is frequently arbitrarily defined with respect to its relative position to the spectrum itself, and its value could be different by a wide margin, depending on the method of calculation. Secondly, the relaxation and recovery functions are in general nonlinear, i.e. dependent on the amplitude of the perturbation itself such as mechanical strain or a shift in temperature. For example, the fact that viscoelastic relaxation is observable in most glassy polymers in a relatively short time range of the order of minutes indicates that mechanical strain is sufficient to shorten the relaxation time from the very long time of the order of days or months. Since a shear deformation can cause this nonlinear viscoelastic behavior, a strain-induced increase in free volume is not a necessary condition, although the nonlinear effect under tension can be quantitatively predicted from the increase in free volume resulting from the Poisson effect. We have observed a temperature drop during the deformation of thermally well insulated polymer glass specimens, as shown in Fig. 1. This is an indication that the enthalpy increases with small strain, up to the point where the mechanically dissipated heat begins to raise the temperature beyond the yield strain. As it is shown, the enthalpy increase is accompanied by the tensile as well as the shear deformation. Robertson's model [1] invokes the shear-induced change in density fluctuations that results in the increase in the configurational entropy accompanied by the shortening of the relaxation time.

In the case of thermodynamic recovery, such as is observed in Kovacs' classic experiment [2] of the isothermal volume change following the initial shift in the temperature, the recovery time is indeed shorter when the volume is greater, and vice versa. In a quenching experiment where the sample is suddenly cooled from a high temperature, the recovery time is observed to increase with time in keeping with the volume as it decreases toward the new equilibrium value at the new temperature, resulting in a nonexponential behavior. However, this apparent slowdown in the recovery process can also be mathematically modeled by a linear relaxation function with a distribution of relaxation times. In reality both of the above two factors,

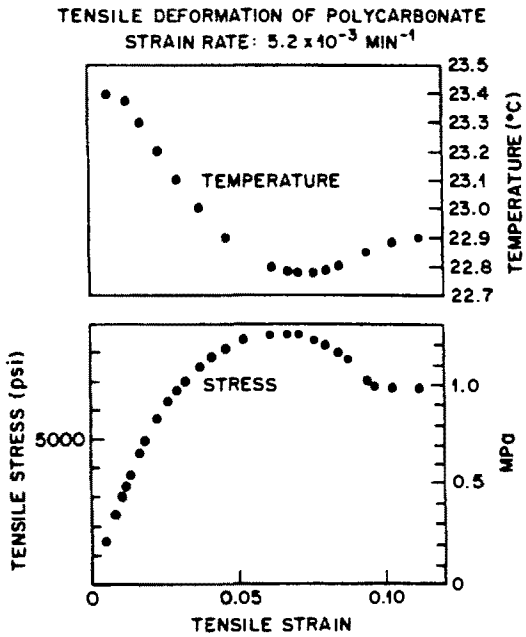

Fig. 1. The temperature drop with tensile strain observed in a thermally well insulated sample specimen indicates that the enthalpy increases with deformation. The same effects are observed in shear as well

i.e. the broad spectrum and the nonlinearity, must be taken into consideration in order to analyze the volume recovery behavior. The two factors can be separated by comparing the data from the quenching experiment as discussed above with data obtained following a sudden heating. In the experiment by Kovacs in which the temperature is suddenly brought up from a lower to a higher temperature, the recovery process accerelates as the volume increases, but analysis reveals that this autocatalytic phenomenon is partially blunted by the smearing effect from the broadly distributed relaxation times. The governing differential equation for all those cases can be written in the form:

$$-d\delta/dt = \Sigma G_i \delta_i / \tau_i \qquad (1)$$

where δ is the deviation of the property of interest from equilibrium, G_i is the weighting factor for the relaxation time τ_i, and the latter is a function of temperature and δ. In our recent article [3] we have illustrated that the recovery curves against time from above

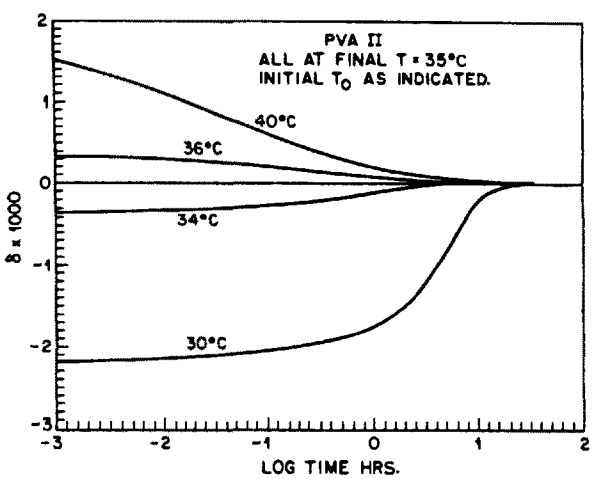

Fig. 2. Two reasons for the recovery process for not conforming to the $\exp(-t/\tau)$ behavior: (1) the broad distribution of relaxation times which can fit $\exp(-t/\tau)^{\beta}$ is apparent even when the perturbation is small, i.e. the curves designated by the initial temperatures of 34 and 36°C, and (2) the variable δ is in itself a structural variable, hence the relaxation time depends on it and results in a pair of nonlinear relaxation behaviors, designated by the initial temperatures of 30 and 40°C that are not symmtrical against the abscissa

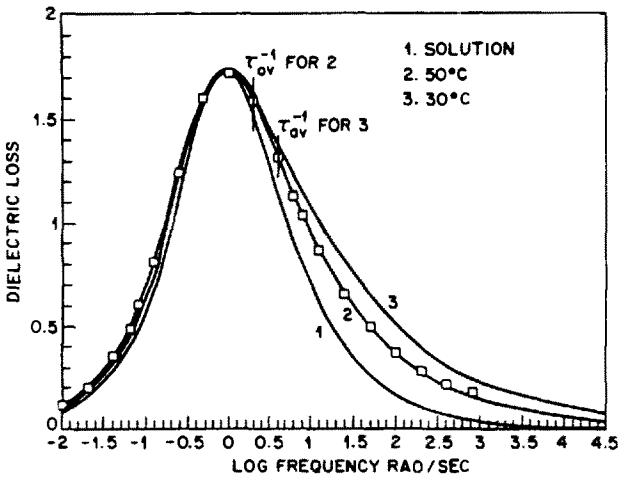

Fig. 3. Data by Mashimo et al. [27] which indicate that the relaxation spectrum broadens in the order: 1. in solution, 2. at 50°C, and 3. at 30°C for polyvinyl acetate. The curves have been normalized to coincide at the loss peak, by scaling vertically and horizontally. The points are our data at 50°C

and below the equilibrium state would appear more and more of the mirror image of each other as the magnitude of perturbation is reduced as shown in Fig. 2; at $\pm 1^{\circ}C$, the two curves are apparently symmetrical about the abcissa (the log time axis), and this apparently linear response function fits the same Kohlrausch-Williams-Watt formula [4], $\exp[-(t/\tau)^{\beta}]$, obtained from the dielectric data for polyvinyl acetate.

3. Equation for the Relaxation/Recovery Time near the Equilibrium State

The distribution of relaxation times for liquids in the equilibrium state is usually treated as being independent of the temperature. Some dielectric data exhibit a slight broadening at lower temperatures, still in equilibrium, as shown in Fig. 3, but the effect is not pronounced and is frequently ignored by analysts. If the distribution of relaxation times can be assumed as constant over a range of temperatures and aging histories, then any one arbitrary definition of a characteristic relaxation time can be used meaningfully, since its position with respect to the relaxation spectrum remains fixed.

The temperature dependence of the relaxation time in the equilibrium state follows the Vogel-Fulcher formula [5]:

$$\ln\tau = C + H/R(T-T_2) \qquad (2)$$

where δ is the characteristic relaxation time, C a constant, H another constant in the unit of heat or enthalpy, R the gas constant, T the temperature in Kelvin, and T_2 is the well-known divergence temperature [6,7,8]; the equilibrium state at $T = T_2$ is never reached in the laboratory because the relaxation time will become too long before that state can be reached.

Doolittle's free volume formula [9] is another parametric form of the Vogel-Fulcher formula. If the free volume fraction, $f = (V-V_o)/V_o$, is assumed to exhibit a constant rate of thermal expansion α_f, and also to vanish at the above-mentioned divergence temperature , T_2, where V is the specific volume and V_o is the "occupied volume", then we obtain

$$f = \alpha_f(T-T_2) \ldots\ldots \tag{3}$$

or

$$\ln(\tau/\tau_o) = 1/\alpha_f(T-T_2) - 1/\alpha_f(T_o-T_2) \ldots\ldots \tag{4}$$

where the subscript $_o$ is referred to a reference temperature. The above equation can be rewritten in the form:

$$\ln(\tau/\tau_o) = -C_1(T-T_o)/(C_2+T-T_o) \ldots \tag{5}$$

by letting $C_1 = 1/\alpha_f(T_o-T_2)$ and $C_2 = (T_o-T_2)$. This is the well-known Williams-Landel-Ferry (WLF) equation [10]. When the reference temperature, T_o, is chosen to be near the laboratory T_g for a particular liquid, e.g. at 1k Hz, 1 minute, 20^oC/minute, etc., the "universal" values of $C_1 \approx 17$, and $C_2 \approx 50^oC$ are often found, whence the universal values of the fractional free volume at T_g, $f_g \approx 0.02$, and its thermal expansion coefficient, $\alpha_f \approx 4.8\ 10^{-4\,o}C^{-1}$, are cited. The universality for these constants implies that H in the Vogel-Fulcher formula should also be universal, ca. 4.2 k calories per mole, since it is numerically equal to R/α_f.

While the free volume equation is widely used by polymer theorists, and its physical significance has been explored by Cohen and Turnbull [11], and by Simha [12] particularly for polymers, Adam and Gibbs [6] have shown that their equation could also be reduced to the form of the Vogel-Fulcher formula in equilibrium. According to the Adam-Gibbs theory, the temperature dependence of relaxation behavior is explained in terms of the variation in the size of the cooperatively rearranging region. The configurational entropy, S, of the system is compared with the configurational entropy, s^*, of the smallest unit capable of rearrangement, or

$$\ln = \frac{\Delta\mu s^*}{RTS} \ldots. \tag{6}$$

where $\Delta\mu$ is the free energy barrier hindering such rearrangement. Adam and Gibbs have shown that this equation practically coincides with the Vogel-Fulcher equation. Thus, both the free volume theory and the theory based on the configurational entropy can describe the observed temperature dependence of the relaxation times <u>in equilibrium</u>.

4. Relaxation Behavior in teh Nonequilibrium State

Although the predictions by the Adam-Gibbs and the free volume theories are indistinguishable in the equilibrium state, the two theories predict different behaviors in the nonequilibrium state. The Doolittle equation predicts that the relaxation time is totally determined by the structural parameter, f, or the free volume fraction. According to this model, the temperature effect is derived entirely from the change in the fractional free volume and, therefore, the glassy state with a given free volume should exhibit a relaxation or recovery behavior that is independent of temperature. Evidence can be cited to point out that this is not true. A glass with a given fictive temperature is observed to age at a faster rate at a higher temperature [13]. (The definition of the fictive temperature will be discussed subsequently. It is a structural parameter.) Diffusion of gas molecules through glassy polymers at constant fictive temperature is faster at an elevated temperature also. In fact, the viscoelastic relaxatipn behavior of glassy polymers [13], as well as the physical aging behavior [3,14], is of an Arrhenius type at fixed fictive temperature, with the apparent activation energy of 30 to 50 k calories per mole. The Adam-Gibbs formula, which predicts the apparently Arrhenius behavior for the glass with a fixed configurational entropy, S, emerges as a clear winner over the free volume theory when the nonequilibrium state is considered. The "universal" values of H mentioned earlier might be rationalized as the consequence of the "universality" of s^*/S_g where S_g is the entropy at T_g, in a fast cooled state for many different materials.

Hodge [15] has pointed out that, in order for the Adam-Gibbs formula to agree with the Vogel-Fulcher formula in equilibrium, the entropy, S, must depend on the temperature according to the equation:

$$S = C(1-T_2/T) \ldots\ldots . \tag{7}$$

Since the configurational entropy is a structural variable, the temperature in the above formula should be replaced by the fictive temperature T_f, to represent the general (nonequilibrium and equilibrium) case [24], i.e.,

$$S = C(1-T_2/T_f) \ldots\ldots . \tag{8}$$

The fictive temperature is defined as the temperature at which the extended curve (usually a straight line) for the volume, entropy or enthalpy of the glassy state plotted against the temperature intersects the equilibrium liquidus line. Thus, the equilibrium case where $T_f = T$ is a special case. From Eqs. (6) and (8) together, it can be shown that when the ratio T_2/T_f is equal to 7/8 the apparent activation energy of 30 k calories per mole is obtained. In this case, if T_2 is -15^oC, as it

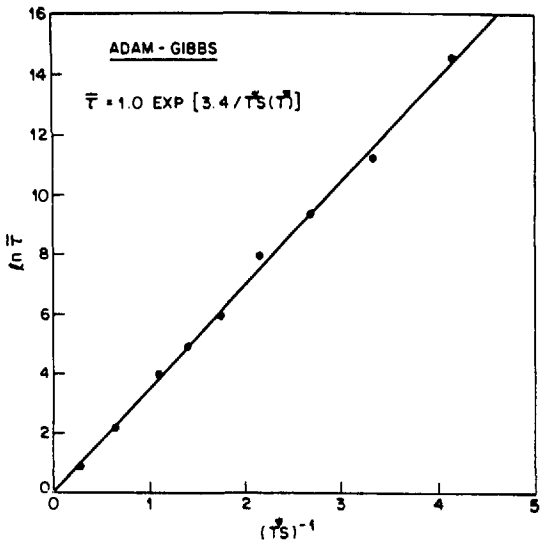

Fig. 4. The points have been generated from the Fredrickson-Andersen model by a Monte Carlo simulation. The straight line is drawn through them to indicate how well the model agrees with the Adam-Gibbs formula, Eq. (6)

is for one of the polyvinyl acetate samples studied, T_f is 22°C. Similarly, T_2/T_f of 10/11, which corresponds to T_f of 11°C for the same polymer, will obtain the apparent activation energy of 50 k calories per mole. To describe a glassy state with one parameter, T_f, presents a number of problem, as is well-known to the most workers in this area of study, but we shall continue this discussion assuming that these problems are of secondary importance for the present purpose. According to Eq. (7), the equilibrium entropy is not proportional to the temperature; instead, the product of the temperature and the entropy is. A recently published kinetic Ising model of cooperative relaxation in dense fluids by Fredrickson and Andersen [16]

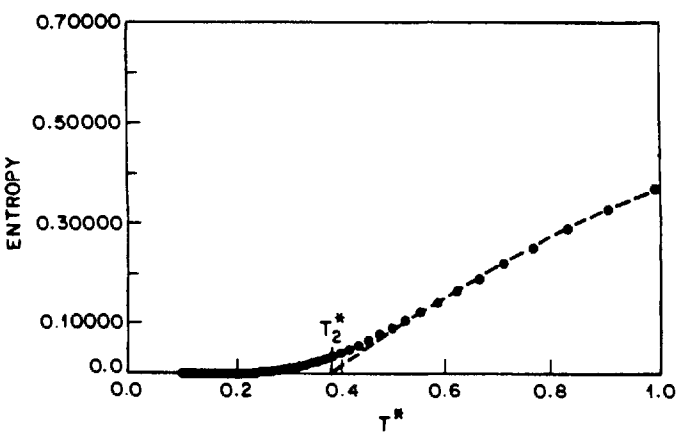

Fig. 5. Entropy vs. reduced temperature at equilibrium, according to the Frederickson-Andersen model. The broken line is fitted using Eq. (7) with an adjustable parameter C

predicts that the relaxation time is in fact proportional to the exponent of C/TS [25,26], as shown in Fig. 4.

As we shall demonstrate below, the Fredrickson-Andersen model is helpful for understanding how the relaxation/recovery phenomena are related to the configurational entropy and, perhaps coincidentally, with the free volume. According to this model, the entropy will not reach zero at T_2, but will persist with a reduced slope well below T_2 as shown in Fig. 5. However, above the (reduced) temperature T^* of 0.6, the curve can be fitted with Eq. (7), which would imply that the product of this entropy and the temperature should follow the Vogel-Fulcher formula, Eq. (2). Thus, above a certain temperature near T_g, the model agrees both with the Adam-Gibbs formula and the Vogel-Fulcher formula.

In this kinetic Ising model two species are involved, one designated as the up spin that represents the high energy state and the other designated as the down spin that represents the low energy state. The model suggests a possible density difference between the two species, and different thermal expansion coefficients. The relative concentration of the high energy species, or the up spins, is predicted to depend linearly on temperature over the range $0.6 < T^* < 1.0$ as shown in Fig. 6. We will

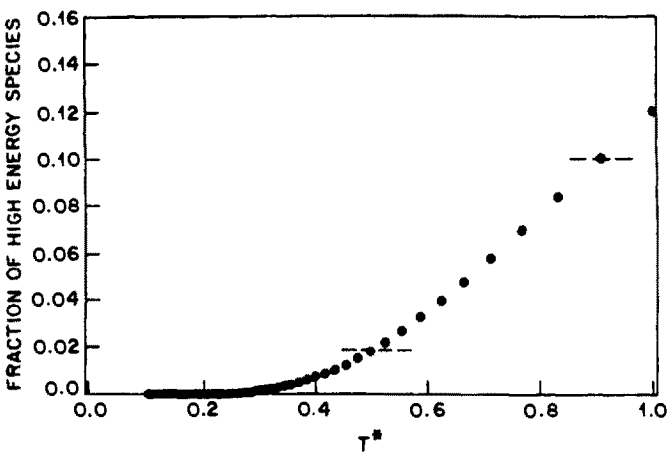

Fig. 6. Fraction of the high energy species, or up spins, increases linearly with temperature in the limited range of temperature chosen here. The range of our interest is estimated to be between 0.02 to 0.10 for the ordinate. This translates to $0.5 < T^* < 0.9$

now equate the concentration of the up species, with the (assumed) higher thermal expansion coefficient, to the fractional free volume as defined by Doolittle. From experience the range of the fractional free volume of interest is from 0.02 to 0.10, which corresponds to the real temperature range from T_g to T_g plus 100°C. From Fig. 6 it is apparent that this range corresponds to the range in the reduced

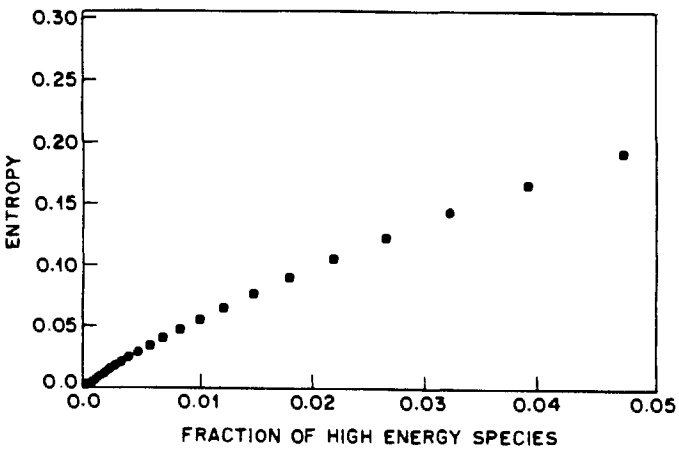

Fig. 7. The plot of entropy vs. fraction of up spins according to the Frederickson-Andersen model

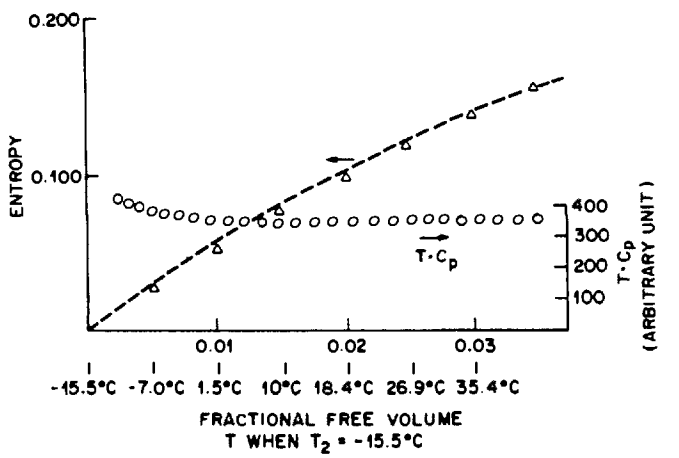

Fig. 8. The dotted line: the entropy of mixing of fractional free volume and the occupied volume following the formula, $S = -R[f \ln f+(1-f)\ln(1-f)]$. Triangles: points calculated from Eq. (7) with an adjustable parameter C. Circles: the product of the temperature and C_p; the latter is the product of temperature and the derivative of entropy

temperature of $0.55 < T^* < 0.85$. It can be seen from Fig. 5 that this temperature range is indeed where the model agreed with both Vogel-Fulcher and the Adam-Gibbs formulae, and it appears that below this range equilibrium is not likely to be attained in the laboratory. The relationship between the entropy for the spin model and the up spin fractions is shown in Fig. 7. For comparison, we have shown in Fig. 8 the plot for the fractional free volume (as abscissa) and the mixing entropy (for

polymers it is Flory-Huggins' conformational entropy). The quantitative similarity between Figs. 7 and 8 is very interesting. From the entropy curve in Fig. 8, the parameter C for Eq. (7) was evaluated, as shown by the triangle points. From these results, the temperature dependence of the specific heat can be deduced. The product of the absolute temperature and the specific heat is plotted against the temperature in Fig. 8, which is nearly constant in the range that the fractional free volume of greater than 0.02 or the temperature above 18.4^{o}C for polyvinyl acetate. What is most illuminating about the Fredrickson-Andersen model is that its range of prediction for the linear relationship between $\ln \tau$ and $1/TS$ exceeds by far the range of practically attainable data.

For the prediction of the recovery process, recognizing that the process in fact depends both on the structural variable and on the temperature independently, Narayanaswamy [17] introduced the empirical formula:

$$\ln \tau = C + xH/RT + (1-x)H/RT_f \quad \ldots\ldots \qquad (9)$$

which has been adopted by Moynihan et al. [18], Kovacs et al. [19] with an approximated form, and other authors [20,21]. This equation becomes an Arrhenius equation at equilibrium, where $T_f = T$, with frequently an unconvincingly large value for the activation energy, H. Others such as Mazurin [22], Scherer [23] and we ourselves [3] found Narayanaswamy's expression inadequate for fitting the data precisely. We find

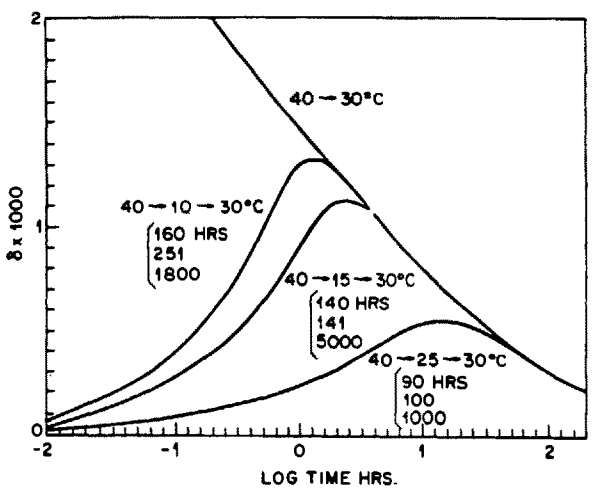

Fig. 9. The memory effect refers to the phenomenon that if an initially quenched glass is quickly heated to $T = T_f$, its volume would not remain at the new equilibrium value but typically first increases and then slowly returns to the equilibrium value. The magnitude of such excursion depends on the extent of physical aging. The three excursion curves are shown with the initial-> aging-> final temperatures as indicated. The 3 numbers in the brackets are, from the top, experimental, Adam-Gibbs, and modified Narayanaswamy [3] values calculated to obtain these curves for the duration of aging

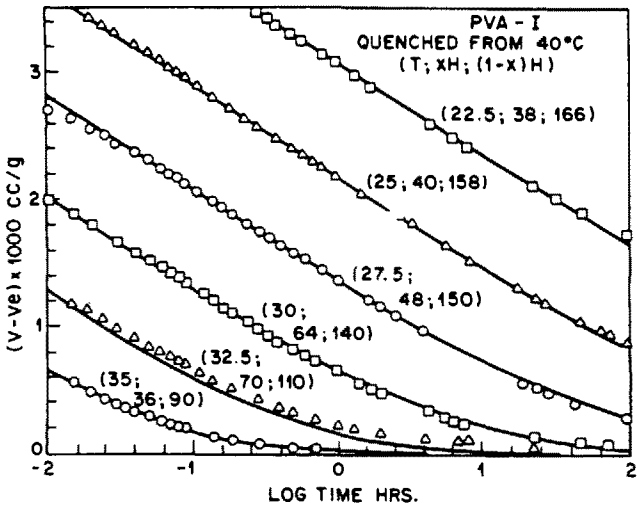

Fig. 10. Isothermal volumetric relaxation following quenching. The numbers in the brackets are (final temperature ^{o}C; activation energy for T; ditto for T_f using Narayanaswamy's formula, Eq. (9)

that the parameter x must increase as either T or T_f increased. We found that by replacing the last term, $(1-x)H/RT_f$, with $H/R(T_f - T_2)$, an excellent fit to data was obtained and, moreover, that the values for H and T_2 thus determined from the kinetic recovery data agree precisely with the values determined from the dielectric relaxation data for the same material, polyvinyl acetate. A critical examination of the temperature dependence at constant T_f is more difficult because of the narrow temperature range that good isothermal data can be found. We had tentatively concluded [3] that a constant xH with the value of 50 k cal per mole could fit some isothermal data [2]. However, this value fails if it is used in predicting the time taken for the memory effect [2,3], and a smaller ad hoc value, ca. 25 k cal per mole, had to be assigned. This discrepancy was resolved when we realized that the value for xH was to be inversely proportional to $T_f - T_2$, in conformity with the Adam-Gibbs formula with the entropy which depends on T_f according to Eq. (8). This is illustrated in Fig. 9. The inadequacy of the Narayanaswamy form in separating the temperature and the structure terms as the sum of two Arrhenius terms is further demonstrated in Fig. 10, where either of the constants could not be kept constant in order to obtain a good fit with the set of data published by Kovacs [24]. Thus we have satisfied ourselves by concluding that the Narayanaswamy equation should be replaced by the Adam-Gibbs equation, and by so doing we find that the dielectric relaxation and thermodynamic recovery processes are brought together with the same distribution and shift factor for the common relaxation times, as summarized in Fig. 11.

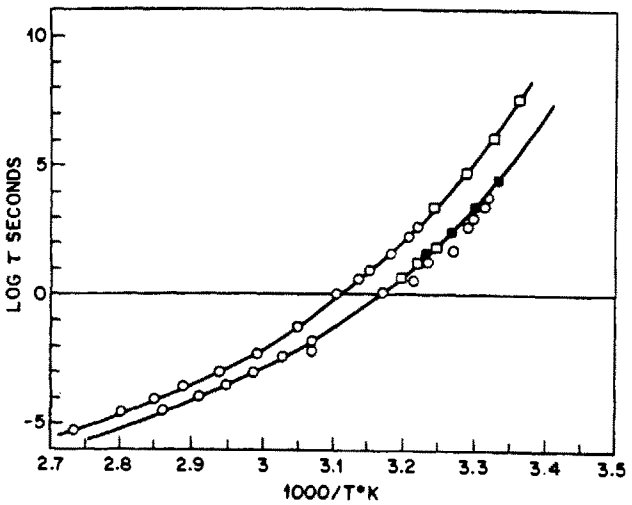

Fig. 11. Relaxation and recovery time vs. $1000/T^{o}K$ for 2 kinds of polyvinyl acetate [3]; circles are dielectric data at equilibrium, squares are the nonequilibrium recovery time extrapolated to the equilibrium state, and the curves are the Adam-Gibbs formula

Earlier we alluded to the fact that the relaxation spectrum would depend on temperature, but the effect was not nearly as pronounced as for the average relaxation time itself. The Fredrickson-Andersen model actually predicts the relaxation spectra to become broader as the degree of cooperativity is increased at a lower temperature as shown in Fig. 12. In Fig. 13, the experimental relaxation modulus is plotted against the logarithm for time for poystyrene obtained at $58^{o}C$, $70^{o}C$, and $90^{o}C$, all

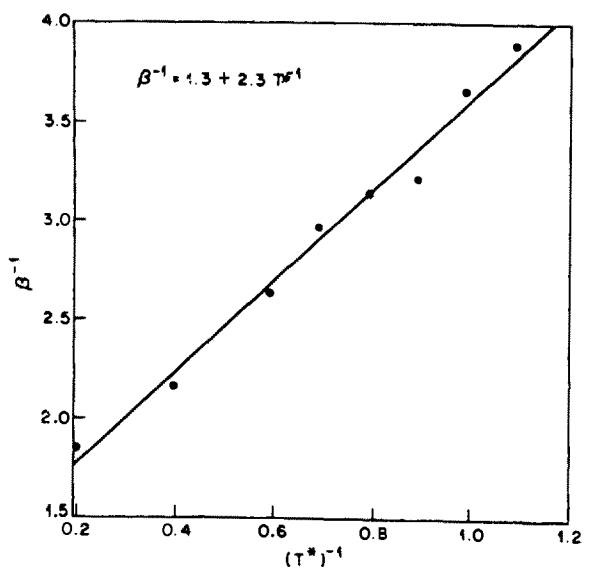

Fig. 12. Monte Carlo simulation of the Fredrickson-Andersen model ban be approximated by the formula: $\beta^{-1} = 1.3 + 2.37^{-1}$, where is the KWW parameter [4], i.e., β decreases as the temperature is lowered, and the spectrum becomes broader

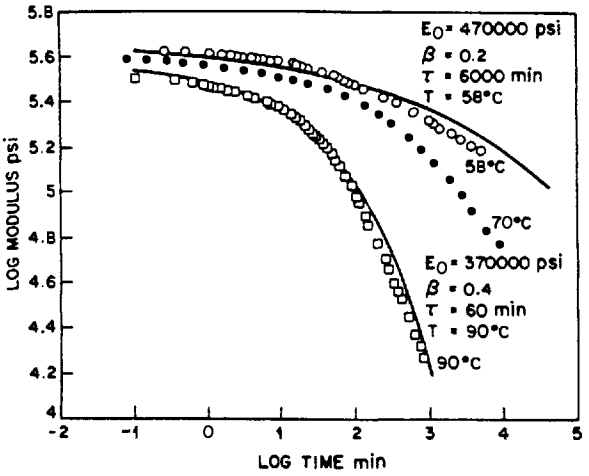

Fig. 13. Relaxation modulus of polystyrene at .5% tensile strain, at 50, 70, and 90°C all following 15 hours of aging at the respective temperatures. The curves are KWW functions to give the best fit to the data, and the parameters are as indicated

after waiting for 15 hours at the respective temperatures. These curves demonstrate the dependence of relaxation spectra on temperature, as expressed by the variation in the KWW parameter β. Similarly, we have shown in Fig. 14 the relaxation stress curves for polystyrene after the different aging conditions but all at 70°C, showing also the variation in β. The Fredrickson-Andersen model predicts that the plot of β^{-1} vs. t^{-1} to be a straight line as illustrated in Fig. 12. Fig. 15 is the plot

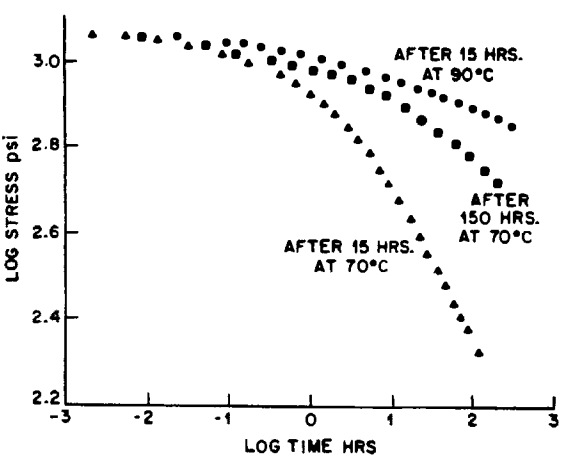

Fig. 14. Relaxation modulus of polystyrene at 70°C at 0.5% tensile strain, following different degrees of aging as indicated

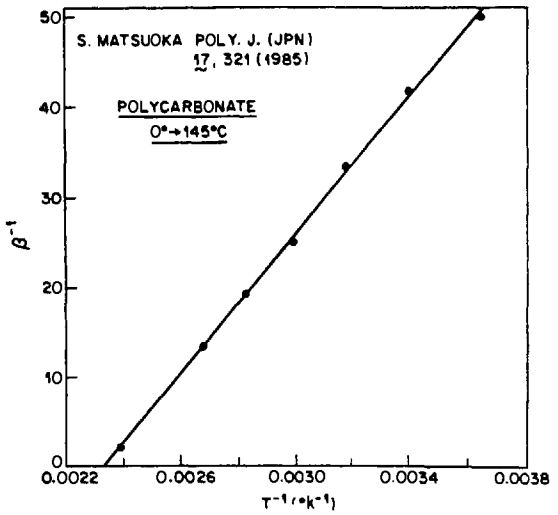

Fig. 15. Experimental β^{-1} for creep data on polycarbonate is plotted against T^{-1} in order to compare with the predicted straight line shown in Fig. 12

of the experimentally obtained β for polycarbonate plotted in this manner, and it is exactly on a straight line.

The jump in the specific heat at the glass transition, Δc_p, is obtained from the equation

$$\Delta c_p = T \frac{dS}{dT} = T \frac{dS}{dT_f} \frac{dT_f}{dT} = T \frac{T_2}{T_f^2} \frac{dT_f}{dT} \quad \ldots\ldots \quad . \tag{10}$$

The value of dT_f/dT, or really dT_f/dt, if for a constant rate of heating or cooling where t is time dependent on the rate of heating/cooling and the aging time/temperature, as well as on the distribution of them, as there should be such a distribution of dT_f/dT. Only if $dT_f/dT = T_f/T$, the relationship $\Delta c_p = cT_2/T_f$ is obtained, which would lead to Eq. (7) for the entropy. The experimental value of Δc_p is in fact observed to decrease with the increasing T_f, either by increasing the rate of heating or by aging, but it is not certain that Δc_p is inversely proportional to T_f, as inferred from the plot in Fig. 9. When we apply the kinetic equation of thermodynamic recovery process to the prediction of the Δc_p vs. temperature relationship (ignoring the distribution of dT_f/dt), we find a good agreement in the areas under the curves, i.e. the enthalpy and the entropy, but the calculated peaks are sharper and narrower than the experimental data, This is an area which will require a further study.

References

[1] Robertson, R.E., Chem. Phys. 44, No. 10, 3950 (1966)

[2] Kovacs, A.J., Fortschr. Hochpolymer. Forsch. 3. 394 (1963)

[3] Matsuoka, S., G. Williams, G.E. Johnson, E.W. Anderson, T. Furukawa, Macromolecules 18, 2652 (1985)

[4] Williams, G., and D.C. Watts, Trans. Faraday Soc. 66, 80 (1970)

[5] Fulcher, G.A., J. Am. Ceram. Soc. 8, 339 (1925)

[6] Adam, G., and J.H. Gibbs, J. Chem. Phys. 43, 139 (1965)

[7] Kauzmann, W., Chem. Rev. 43, 219 (1948)

[8] Gibbs, J.H. and E.A. DiMarzio, J. Chem. Phys. 28, 373 (1958)

[9] Doolittle, A.K., J. Appl. Phys. 22, 1471 (1951)

[10] Williams, M.L., R.F. Landel, and J.D. Ferry, J. Am. Chem. Soc. 77, 3701 (1955)

[11] Cohen, M.H. and D. Turnbull, J. Chem. Phys. 31, 1164 (1959), ibid. 34, 120 (1961)

12 Simha, R., Polymer Eng. and Sci., 20, No. 1, 82 (1980)

13 Matsuoka, S., et al., Polymer Eng. and Sci., 18, No. 14, 1073 (1978)

14 Matsuoka, S., Polymer Eng., and Sci., 21, No. 14, 907 (1981)

15 Hodge, I.M., Macromol. 19, 936 (1986)

16 Fredrickson, G.H. and H.C. Andersen, Phys. Rev. Lett. 53, 1244 (1984)

17 Narayanaswamy, O.S., J. Am. Ceram. Soc. 34. 491 (1971)

18 Moynihan, C.T., et al., Ann. N.Y. Cad. Sci. 279, 15 (1976)

19 Kovacs, A.J., J. Polymer Sci. 30, 131 (1958)

20 Chow, T.S. and W.M. Prest, Jr., J. Appl. Phys. 53 (10), 6568 (1982)

21 Hodge, I.M., Macromol 16, 898 (1983)

22 Mazurin, O.V., J. Non-Cryst. Solids, 25, 130 (1977)

23 Scherer, G.W., J. Am. Ceram. Soc. 67, 504 (1984)

24 Ferry, J.D., "Viscoelastic Properties of Polymers", Wiley, N.Y., 1970

25 Fredrickson, G.H. and S.A. Brawer, J. Chem. Phys. in press

26 Fredrickson, G.H., Annals N.Y. Acad. of Sci., in press

27 Mashimo, S., R. Nozaki, D. Yagihara, S. Takeishi, J. Chem. Phys. 77 (12), 6259 (1982)

PHOTON CORRELATION SPECTROSCOPY TO STUDY THE DYNAMICS OF α- AND β-RELAXATION IN AMORPHOUS POLY(ALKYLMETHACRYLATES) ABOVE Tg

Gerhard Meier
Institut für physikalische Chemie
Universität Mainz
Mainz, FRG

Abstract

A short survey of the underlying principles of isotropic light scattering from amorphous bulk polymers is given. The interrelation between the time dependent longitudinal compliance and the autocorrelation function of density fluctuations is briefly reviewed and a comparison with poly(vinylacetate) PVAc is presented. For four poly(alkylmethacrylates) - poly(methylmethacrylate) PMMA, poly(ethylmethacrylate) PEMA, poly(n-butylmethacrylate) PBMA and poly(n-hexylmethacrylate) PHMA - the results of photon spectroscopic studies are given and discussed in terms of the occurrence of primary and secondary relaxation processes within the accessible time range of the experiment.

Introduction

In recent years, photon correlation spectroscopy (PCS) has become a powerful tool to study dynamic processes in bulk polymers [1]. Most of the studies were performed above the glass transition temperature of the material under consideration and the results showed that the autocorrelation function of the density fluctuations is dominated by the primary or α-relaxation process measured in mechanical or dielectric relaxation measurements. This was found to be true of all those polymers whose temperature difference for the maxima of dielectric or mechanical loss at constant low frequency is quite high. So, at some moderate temperatures above T_g (i.e. the temperatures of measurement) there will be no interference between primary and secondary relaxation processes. Those polymers are i.e.: PPG [2], PEA [3], PMA [4], PVAc [5].

The same feature can also be found for non-polymeric glass forming liquids like o-terphenyl [6] or some hydrogen bonded alcohols [7].

The situation changes for methacrylate polymers. Here it is known from other methods [8,9], that the secondary relaxation will considerably contribute to the time correlation function of density fluctuations if one looks upon dynamic processes in a temperature range $T_g + 15^oC$ to $T_g + 50^oC$ (approximate values) and a time response

of 10 to 10^{-6} sec accessible to a photon correlation experiment. So far those experiments have been performed for four different methacrylate polymers PMMA [10], PEMA [11], P nBMA [12] and P nHMA [13].

The main purpose of this paper will be to demonstrate the extent of the contribution of the secondary relaxation and the experimental conditions necessary to account for the detection and resolution of these relaxations in the net autocorrelation function of density fluctuations.

Theory

Fluctuations in the dielectric tensor of a material are responsible for the scattering of light. These are primarily due to fluctuations of the density if we deal with polymers whose depolarisation ratio is very small.

The field autocorrelation function

$$g^{(1)}(\underset{\sim}{q},t) = \frac{\langle E(\underset{\sim}{q},t)E^{*}(\underset{\sim}{q},0)\rangle}{\langle |E(\underset{\sim}{q},0)|^{2}\rangle} \tag{1}$$

, with $\underset{\sim}{q}$ being the wave vector $|\underset{\sim}{q}| = \frac{4\pi n}{\lambda} \sin\frac{\theta}{2}$, is the desired quantity in a PCS experiment. It depends on the polarisation of the scattered light relative to the incident beam. In the VV-geometry the scattered light includes both isotropic I_{iso} and anisotropic I_{VH} contributions (V and H denote perpendicular and parallel polarisation to the scattering plane, respectively). For the polymers measured here the I_{VH} contribution is very low, so the VV intensity is almost equal to the isotropic component. The spectral density of the scattered field (cf. Eq. (1)) from an assembly of N polymers is determined by the autocorrelation function of

$$\delta\alpha(\underset{\sim}{q},t) = \sum_{j} \alpha_{j}(t) \exp i\,\underset{\sim}{q}\,\underset{\sim}{r}_{j}(t) \tag{2}$$

which is given by [14]

$$g^{(1)}(\underset{\sim}{q},t) = A \left\langle \sum_{\ell,m} \sum_{j,k} \alpha_{j}(t)\alpha_{k}(0) \exp\{i\underset{\sim}{q}[\underset{\sim}{r}_{j}^{\ell}(t) - \underset{\sim}{r}_{k}^{m}(0)]\} \right\rangle . \tag{3}$$

A is the amplitude; ℓ,m is a summation over chains; j,k is summed over segments on a chain, and $a_j(t)$ is the polarizability of a scattering segment j. So, $\underset{\sim}{r}_j(t)$ is the position of the center of mass of the segment j on chain ℓ at the time t. One finds that on the time scale of a photon correlation experiment the quantity $|\underset{\sim}{q}| \cdot |\underset{\sim}{r}_{j}^{\ell}(t) - \underset{\sim}{r}_{k}^{m}(0)| \ll 1$ and therefore the exponential term in Eq. (3) is almost one. What is left is the local fluctuation of polarizability which has no $|\underset{\sim}{q}|$-dependence that is strongly confirmed by the experiment [2]. Oue to intra- and inter-chain contributions to the segmental fluctuation there is no rigorous analytical expression known for this correlation function.

Note here that the situation will change dramatically if we deal with concentration fluctuations. In this case, the exponent in Eq. (3) will be approximately one. By applying reasonable models for diffusive motion the commonly known $|\underset{\sim}{q}|^2$ dependence of the phase factor comes in.

With regard to segmental fluctuations it is important to state that the dynamics of density fluctuations of polymers should be the same for polymers with different molecular weights. This is true only if the glass transition temperature of the material is no longer molecular weight-dependent.

Experimental evidence for this was obtained by an extensive PCS study on polystyrene with different molecular weights [15].

As stated above, an analytical expression for the correlation function due to mutual diffusion of a dissolved polymer chain is known. The situation is different if we consider viscoelastic one-component systems. For the high frequency limit the theory of Lin and Wang [16] has given an analytical expression for the Rayleigh-Brillouin spectrum $I(\underset{\sim}{q},\omega)$ of viscoelastic fluids starting from a generalized hydrodynamic theory.

In the low frequency limit we have to deal with a time-dependent quantity $g^{(1)}(\underset{\sim}{q},t)$ rather than a spectrum. On the other hand, it is known from statistical mechanics that in the so-called thermodynamic limit the total static density fluctuations are given by

$$\lim_{q\to 0} \frac{\overline{(N-\bar{N})^2}}{\bar{N}} = k\,T\rho\varkappa_T \tag{4}$$

where N is the number of particles, ρ is the number density and $\varkappa_T$ is the isothermal compressibility. Using generalized viscoelastic theory Wang and Fischer [17] were able to derive an expression which accounts for the time dependence of the compressibility in the limit of vanishing $\underset{\sim}{q}$. The result of the theory relates the time-dependent longitudinal compliance $D(t)$ with the autocorrelation function of density fluctuations via

$$D_0 - D(t) = \frac{D_\infty}{\langle|\delta\rho(0)|^2\rangle} \langle\delta\rho(t)\delta\rho^*(0)\rangle \tag{5}$$

where D_0 and D_∞ are the limiting compliances with respect to $\omega \to 0$ and $\omega \to \infty$, respectively. $D(t)$ is the relaxing quantity and $\frac{\langle\delta\rho(t)\delta\rho^*(0)\rangle}{\langle|\delta\rho(0)|^2\rangle}$ is the normalized autocorrelation function of density fluctuations. So $\langle\delta\rho(t)\delta\rho^*(0)\rangle$ is the part of density fluctuations related to the time window of correlator consequently. If we deal with polymers above T_g, usually the bulk compliance is much smaller than the shear compliance, so one may set $D(t)$ equal to the time-dependent bulk compressional

compliance B(t) [18]. A comparison of available data on $B^*(\omega)$ with light scattering data was successfully performed. Data on PVAc of $B^*(\omega)$ by McKinney and Belcher [19] have been processed by means of

$$B(t) = \frac{2}{\pi} \int_0^\infty \frac{B'(\omega)}{\omega} \sin\omega t \, d\omega \qquad (6)$$

to relate B(t) with a measured density autocorrelation function at $T = 50^oC$ for the same material, Fig. 1 [20,21]. The result is shown in Fig. 2. One notes a slight

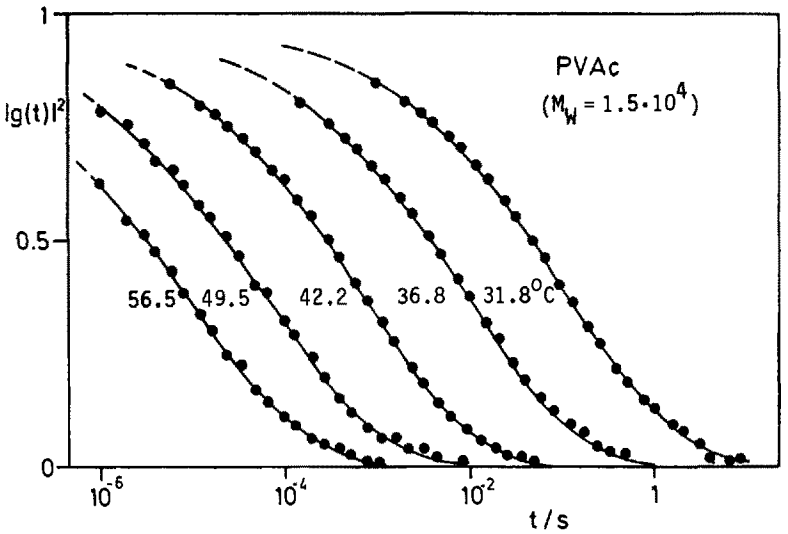

Fig. 1: $|g^{(1)}(t)|^2$ vs. log t for bulk PVAc. Temperatures of measurement as indicated

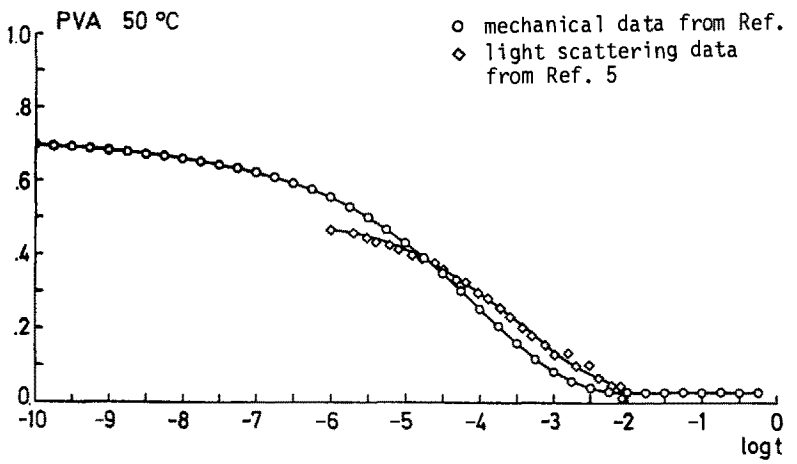

Fig. 2: Comparison of mechanical data from Ref. [19] computed via Eq. (6) with light scattering data from Ref. [5]

discrepancy towards higher frequencies which is probably due to the fact that the theoretical expression is exactly valid for $O(t)$ rather than for $B(t)$. Since light scattering is strongly monitoring $O(t)$, shear contribution will cause differences between the two curves only for high frequencies where one may expect $O(t)$ and $B(t)$ to be different [22].

Unfortunately, there are no mechanical data available on shear and bulk compliances together. Those data should be compared with light scattering results of specimen which give rise to fluctuations in anisotropy. The appropriate theory is still missing.

Experimental

In the section on theory we have seen that the desired quantity is $g_k^{(1)}(t)$, if we neglect the $\tilde{q}$-dependence. What one actually measures is the intensity autocorrelation $G_k^{(2)}(t)$. Both functions are related to the Siegert Relation which has the form

$$G_k^{(2)}(t) = A\left(1 + \frac{1+k}{1+<n>} f(\Omega,\tau)\alpha_r^2 |g^{(1)}(t)|^2\right) \tag{7}$$

for a single clipped homodyne experiment. Here A is the baseline, k is the clip-level, $<n>$ is the number of counts per delay time, $f(\Omega,\tau)$ is the spatial coherence factor which can be calibrated [2], and α_r^2 is the relaxation strength of density fluctuations within the time window of the experiment. Usually $\frac{1+k}{1+<n>} f(\Omega,\tau)\alpha_r^2 = b$ where b is treated as a parameter in a fitting procedure.

The photon correlation spectra shown in this paper were obtained with an apparatus described elsewhere [3], [20]. The light source was an argon ion laser operating at 515.5 nm with a power up to 400 mw. The incident light was polarized perpendicular to the scattering plane and since there was only very little depolarized intensity no polarizer in the scattered light was used. The single clipped photocount autocorrelation function $G_k^{(2)}(t)$ was measured either with a linear 96 channel Malvern correlator or with a 28 channel Malvern correlator with a logarithmic spanning of delay times, so that 3.7 decades in time could be achieved in one run. The method of matching sections with different delay times together with a composite correlation function has been described elsewhere [2]. The polymers used in this study came from industrial sources (Röhm AG, Darmstadt, FRG) and were used to prepare clear, optically homogeneous, dust-free and strain-free samples following a procedure described elsewhere [12].

Data Analysis

The highly non-exponential time correlation functions of bulk polymers can be represented by a so-called Kohlrausch-Williams-Watts (KWW) function

$$g^{(1)}(t) = \exp\left[-\left(\frac{t}{\tau_0}\right)^{\beta}\right] . \tag{8}$$

Here β is a distribution parameter in the range of $0 < \beta \leq 1$. For bulk polymers β was found to be in the order of 0.4 [3], [4], [20], insensitive to T and P, provided that a single relaxation process dominates $g^{(1)}(t)$.

For this case one has to fit the following expression to the correlation function

$$\left(\frac{G_k^{(2)}(t) - A}{A}\right)^{1/2} = b^{1/2} \exp\left[-\left(\frac{t}{\tau_0}\right)^{\beta}\right] . \tag{9}$$

For alkylmethacrylate polymers the situation is more complicated because one has to take into account the influence of the secondary relaxation besides the main chain rubber relaxation. Former attempts to fit a single KWW function to those correlation functions led to temperature-sensitive β-parameters and are probably in error [23] If one has to deal with two relaxation processes within the time window of the experiment, the following expression can successfully be fitted to the correlation function

$$\left(\frac{G_k^{(2)}(t) - A}{A}\right)^{1/2} = a_1 \exp\left[-\left(\frac{t}{\tau_{01}}\right)^{\beta_1}\right] + a_2 \exp\left[-\left(\frac{t}{\tau_{02}}\right)^{\beta_2}\right] . \tag{10}$$

Here the index 1 refers to the fast and the index 2 to the slow relaxation process, respectively [10,11,12].

From those KWW fits the mean relaxation time can be deduced by

$$\bar{\tau} = \int_0^{\infty} g^{(1)}(t)dt = \frac{\tau_0}{\beta} \Gamma(\beta^{-1}) . \tag{11}$$

Another way of processing the data is to try to get the distribution of retardation times (retardation times, because we deal with a compliance rather than with a module, compare Sec. Theory) by using the inverse Laplace transformation technique [24]. In this scheme $g^{(1)}(t)$ is represented by

$$g^{(1)}(t) = \int_0^{\infty} e^{-\frac{t}{\tau}} L(\ln\tau)d\ln\tau . \tag{12}$$

The amplitude $b^{1/2}$ (cf. Eq. (9)) is given by

$$b^{1/2} = \int_0^{\infty} L(\ln\tau)d\ln\tau \tag{13}$$

and the mean relaxation time is given by

$$\bar{\tau} = \frac{\int_0^{\infty} \tau L(\ln\tau)d\ln\tau}{\int_0^{\infty} L(\ln\tau)d\ln\tau} . \tag{14}$$

This representation is actually more straightforward because it avoids the assumption of a model i.e. for the β-parameter of the KWW function. On the other hand, it is interesting to note that recently some models for the KWW parameters [25,26] have been published and that the representation of dynamic processes by the superposition of discrete single relaxation phenomena is in doubt.

No experiment is known so far which may clarify this point in order to decide for the one or the other representation. What can be done is using the exact integral solution of the KWW function as kernel of a Laplace integral [27]

$$\lambda(x,\beta) = \frac{1}{\pi} \int_0^\infty e^{-xu}\, e^{-u^\beta \cos\pi\beta}\, \sin(u^\beta \sin\pi\beta)\, du \qquad (15)$$

where the distribution of retardation times is given by

$$L(\ln\tau) = \frac{\tau_0}{\tau}\lambda(x,\beta) \quad \text{with} \quad x = \frac{\tau}{\tau_0} \ . \qquad (16)$$

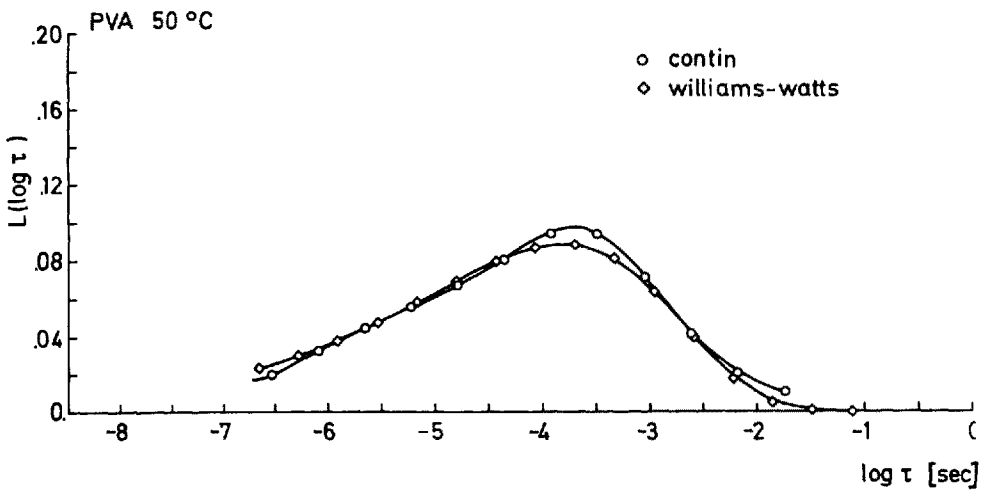

Fig. 3: $L(\lg\tau)$ vs. $\lg\tau$ for PVAc at $T = 50^{\circ}C$. Comparison of Eq. (12) (Contin) with Eq. (16) (Williams-Watts)

In Fig. 3 we show a comparison of both types of analysis. It clearly shows that within the error of computation there is no difference at all at least for a one-relaxation process. Further analysis of more complex correlation functions shows, however, that there is a slight superiority towards the Laplace transformation technique [28].

Results and Oiscussion

In the Introduction it has already been mentioned that for polyalkylmethacrylates one will see the occurrence of the secondary relaxation besides the primary relaxation when performing a dynamic experiment at temperatures up to $T_g + 50^oC$ and within a time-window $10\text{-}10^{-6}$ sec accessible to a PCS experiment. An excellent representation of the conditions based upon mechanical measurements by Heijboer [29] is given in Fig. 4.

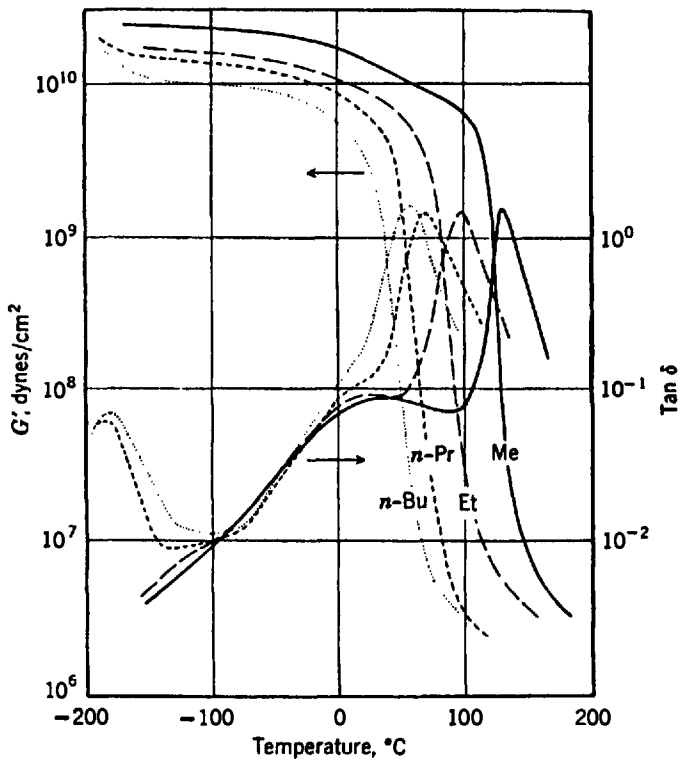

Fig. 4: Logarithms of storage shear modules and loss tangent at 1 Hz plotted against T for four methacrylate polymers

If one concentrates on the mechanical loss tangent at 1 Hz it becomes evident that the temperature difference for the maxima of mechanical loss for primary and secondary relaxation is increased while the side chain length of the alkylmethacrylate polymer is decreased. An extensive discussion of that point is beyond the scope of this article but it is generally believed that the enhancement of mobility with increasing side group length is primarily due to the increase in free volume. A detailed discussion of this point is given by Fujita and Kishimoto [30]. The next step would be to apply the results of Fig. 4 to the situation one has to deal with in a PCS experiment. Here, measurements in the time domain are performed and parameters changed were temperature, pressure and molecular weight of the sample under measurement. Results on

the pressure dependence of dynamic processes will not be discussed here, because due to the difficulty of such an experiment only few data are available [4].

The measurements reported in Fig. 4 were done at a frequency of 1 Hz. By changing frequency and plotting the locus of the loss maximum of the different processes vs. 1/T one will get an activation plot from which activation parameters can be deduced. Schematically this is shown in Fig. 5. Here, $\log f_m$ is plotted vs. 1/T, or $-\log \bar{\tau}$, $\bar{\tau}$ being defined by Eq. (11) or Eq. (14), instead of $\log f_m$. In this representation the straight line is assigned to the secondary relaxation which is an Arrhenius activated process and a bended curve assigned to the α-process. Usually a WLF-type of equation is used to account for its temperature dependence.

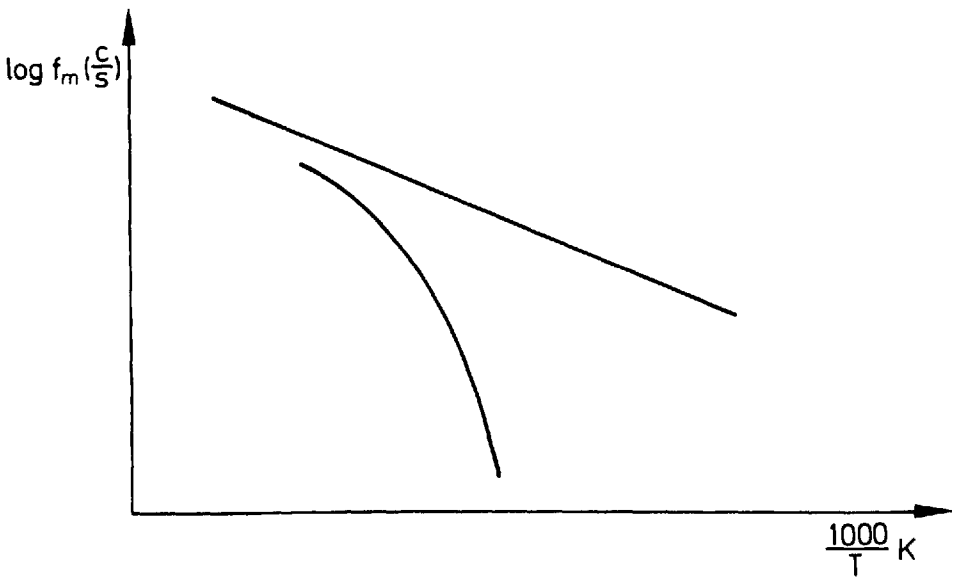

Fig. 5: Scheme of transition map

Let us consider now one kind of PCS experiment performed at a series of different temperatures. According to Fig. 5 one would expect the shape of the correlation function to change from a broad distribution of retardation times close to T_g to a less broad distribution when the two processes are close together at higher temperatures.

This was nicely shown for PBMA [12], where the composite correlation function, Fig. 6, at $T = 39{,}5^{\circ}C$ was fitted to Eq. (10) and at $T = 65{,}5^{\circ}C$ was fitted to Eq. (9). In Fig. 7, the temperature dependence of the mean relaxation time $\bar{\tau}$ is given, which shows that at temperatures $T > 55^{\circ}C$ have merged in accordance with the findings from dielectric relaxation [31]. In Fig. 7, the dots are results of fitting Eq. (10) to the correlation function. The triangles correspond to a fit of Eq. (9) to the correlation function.

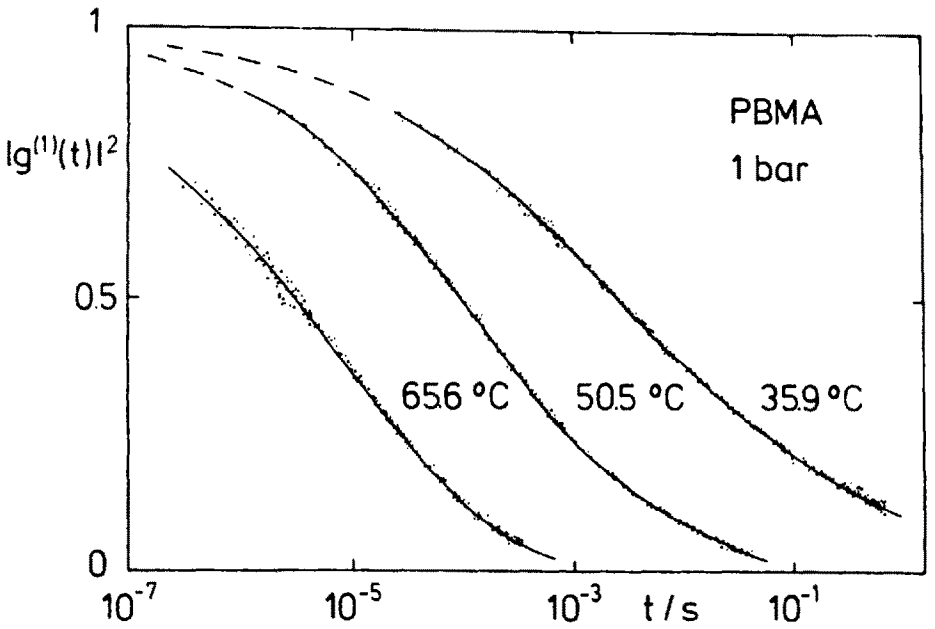

Fig. 6: Normalized composite correlation function for bulk PBMA vs. log t. Temperature of measurement as indicated

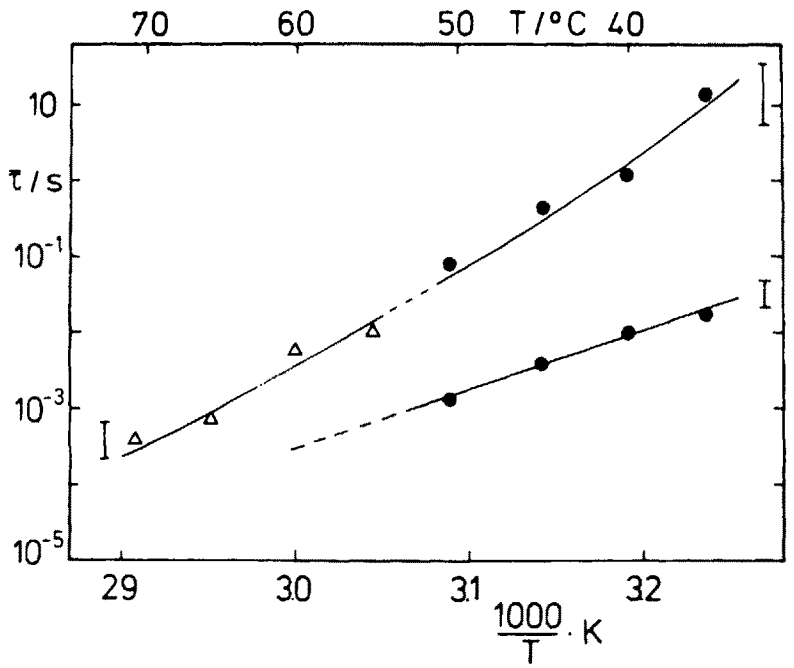

Fig. 7: Mean relaxation time vs. 1/T for bulk PBMA. For different symbols see text

Returning to Fig. 5 we would like to discuss the influence of the molecular weight of the sample. The locus of the secondary relaxation will not be affected at all, because it is understood in terms of localized reorientation of side chain units and due to its noncooperativity the temperature dependence can be successfully described by an Arrhenius-type of activation energy [8,9]. The main chain rubber relaxation is influenced by changing molecular weight to the extent of the molecular weight dependence of the local friction coefficient ξ as given from a modified Rouse-theory [8] applicable to polymer melts. Unless the plateau value in a ξ vs. M plot is reached, the glass transition temperature will decrease with decreasing molecular weight. Phenomenologically great differences for this limiting M can be found. For PPG it is extremely low [2], for PS it seems to be the opposite case [15]. The alkylmethacrylate polymers take some intermediate values. This information can in principle be deduced from steady flow viscosity data [32].

In Fig. 5 the same polymers with different molecular weights will therefore have different α-branches. The one with the lower M will have the α-branch shifted to lower temperatures. If one performs a PCS experiment at a constant temperature there will be a change of shape in the correlation function of the two specimen accordingly. At a given temperature T the α- and β-processes have merged for a low molecular weight sample whereas for a high molecular weight sample that is not the case. For PEMA the correlation function at $T = 85.5^{\circ}C$ for $M = 1.6 \cdot 10^4 D$ can be fitted to

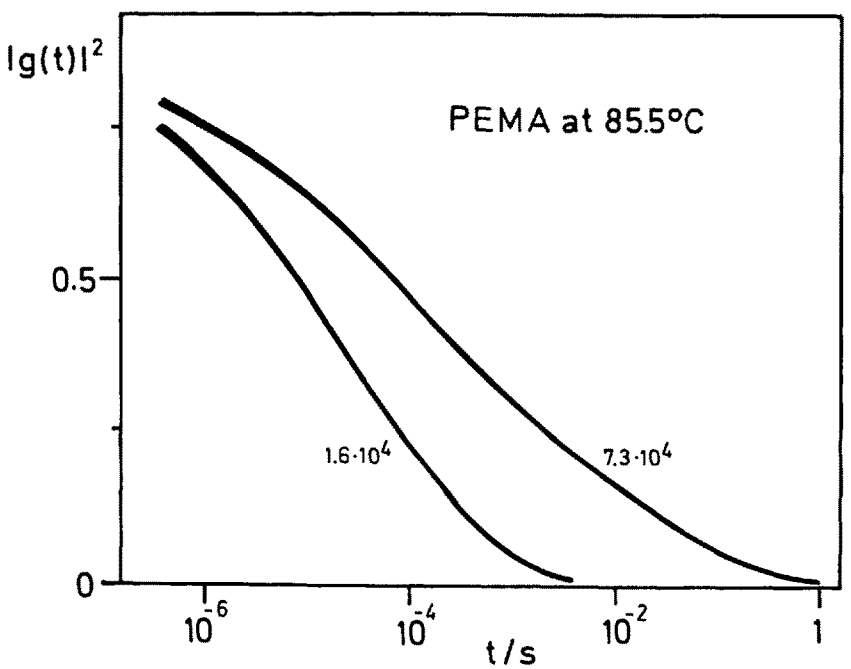

Fig. 8: $|g^{(1)}(t)|^2$ vs. log t for bulk PEMA at $T = 85.5^{\circ}C$. Two different molecular weights are shown

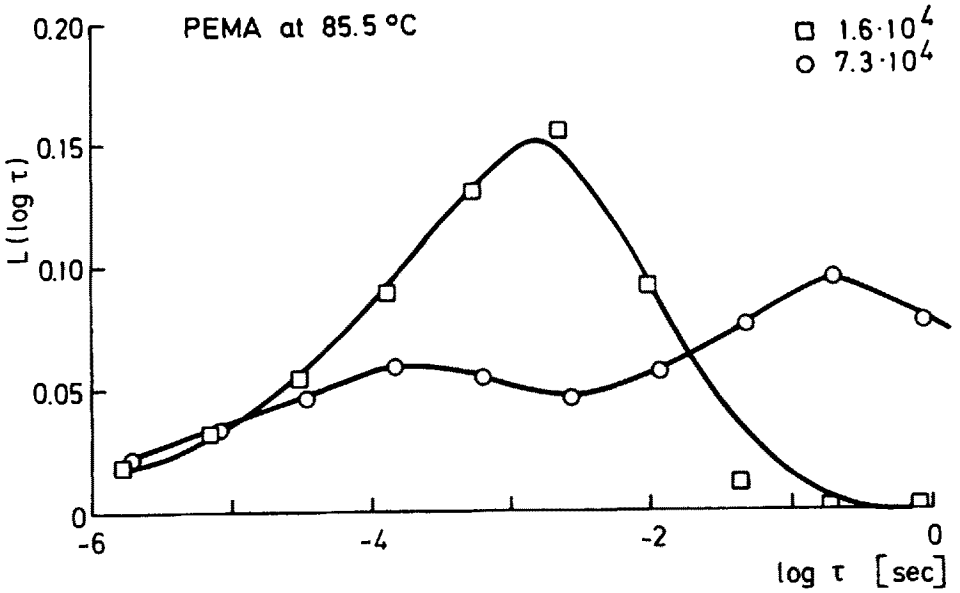

Fig. 9: The use of Eq. (12) on the data of Fig. 8. Plotted is L(lgτ) vs. lgτ

Eq. (9) and for $M = 7.3 \cdot 10^4 D$ can be fitted to Eq. (10) [11], see Fig. 8, as was the case of PMBA mentioned previously.

As was clearly demonstrated in the section on Data Analysis, the description of the measured density autocorrelation function by means of inverse Laplace transformation technique is entirely equivalent to the description by means of KWW functions. In Fig. 9 the result of the application of Eq. (12) to the data in Fig. 8 is given. The advantage of this representation is that it is more straightforward to see whether the processes have already merged or not.

As it is nicely shown by Heijboer's data (cf. Fig. 3) the separation of both processes is enlarged for a smaller side chain length. Thus the best separation is to be expected for PMMA and should be easily detectable if one looks at the shape of the correlation function itself. For a high molecular weight PMMA sample this is demonstrated for 3 different temperatures of measurement in Fig. 10. One can see the bump in the correlation function for $T = 123^{\circ}C$. In this respect PMMA differs from PEMA (cf. Fig. 8) and PBMA (cf. Fig. 6) where the differences in fitting either to Eq. (9) or to Eq. (10) were by no means as striking as in the case of PMMA.

This situation is changed drastically if one tries to analyse the correlation function of PnHMA. In Fig. 11 the composite correlation function for $T = -5^{\circ}C$ and $T = 15^{\circ}C$ is shown. A preliminary analysis of these data shows that the shape of the correlation function can be fitted to Eq. (9) besides, however, the onset of a

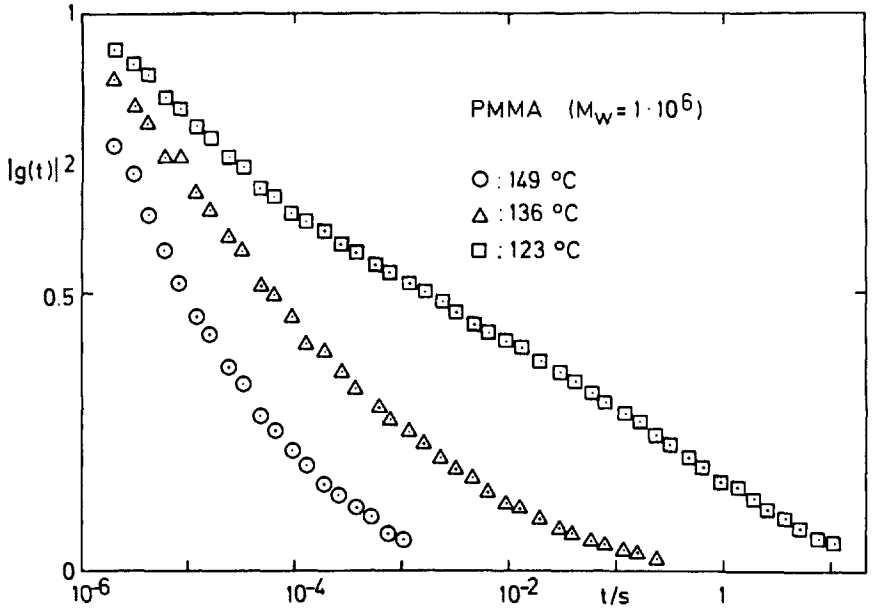

Fig. 10: $|g^{(1)}(t)|^2$ vs. t for bulk PMMA. Temperature of measurement as incidacted

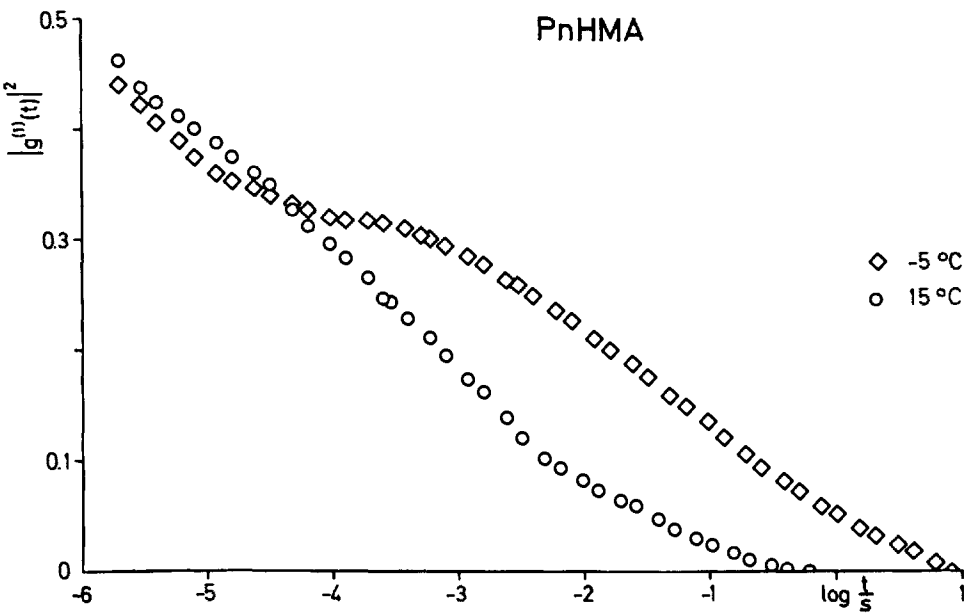

Fig. 11: $|g^{(1)}(t)|^2$ vs. log t for bulk PnHMA. Two temperatures are shown as indicated

further relaxation process towards shorter times. A further analysis of the given results in terms of the inverse Laplace transformation technique will show whether a fine structure can be resolved in order to account for the occurrence of two processes in PnHMA [13].

We assume that the tail end of the process seen at short times is due to a relaxation in the hypersonic region. Consequently, Rayleigh-Brillouin spectra were taken [33]. Usually the Brillouin line-width plotted vs. T will show a maximum at about 100°C higher than the glass transition temperature of the material [34]. For the material under study the situation is different inasmuch as it does not show a maximum at all but the line-width reaches a plateau value and remains on it even up to very high temperatures. One first qualitative interpretation is given in terms of a decoupled motion of the long side chain from the other modes and it is interesting to note that on a further increase of the side chain length of a polyakylmethacrylate this side chain may have a temperature dependence of the dynamic response which can no longer be described by an Arrhenius equation [35]. Further studies on a poly-n-nonylmethacrylate are in progress.

The results of the four polymers under consideration are summarized in Fig. 12. Only representative values are plotted. The data were taken from Ref. [10-13]. The locus

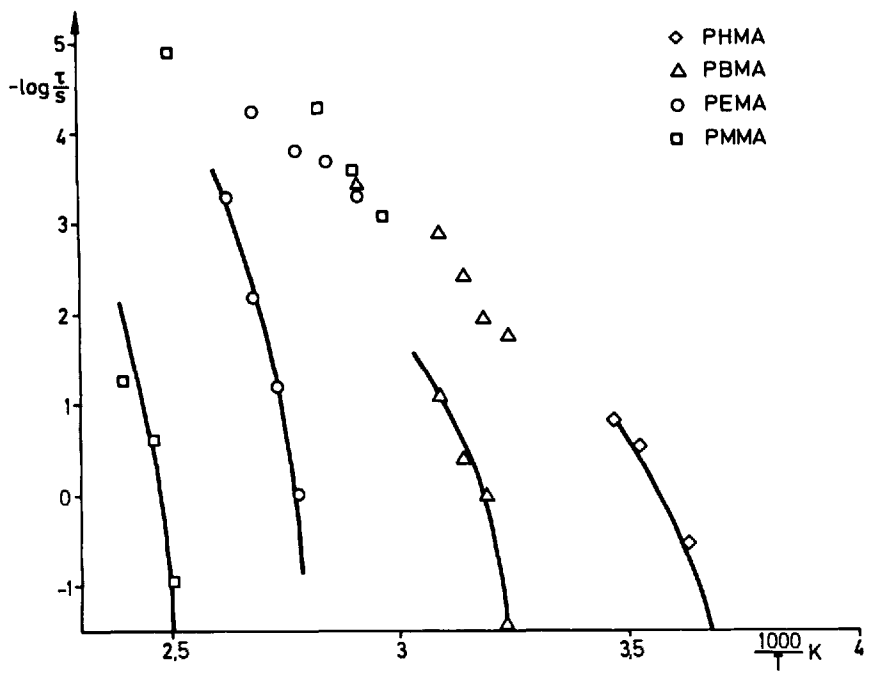

Fig. 12: Plot of $-\log \bar{\tau}$ vs. 1/T for PMMA, PEMA, PnBMA and PnHMA. For further assignment, see text

of the secondary relaxations will fall on one line although one has to bear in mind the difficulties of data evaluation. The solid lines are results from a fit of a WLF equation to the data points characterizing the main chain rubber relaxation. Due to the limited temperature range of a PCS experiment only the C_1 parameter in the WLF equation can successfully be calculated; the C_2 parameter is generally taken from literature.

Actually, the activation parameters deduced from the PCS experiment correspond quite well with those obtained from other methods (cf. Ref. given in Section Introduction).

From the plot it is obvious that PnHMA encounters the greatest difficulties regarding an analysis in terms of α- and β-relaxation separation. If one extrapolates the line of the secondary relaxation to the temperatures where PnHMA exhibits relaxation, the temperature of the two processes that have merged is already very close to the thermal glass transition temperature of the material (T_g from DSC is -7°C). Consequently, the β-distribution parameter according to Eq. (9) for PnHMA is insensitive to T and is found to be considerably lower ($\beta = 0{,}28 \pm 0.03$) than that for the other 3 methacrylate polymers characterizing either the α- or β-process. Very careful analysis of the correlation function in the vicinity of T_g may elucidate this problem especially by means of the inverse Laplace transformation technique.

Acknowledgement

The author is greatly indepted to Professor E.W. Fischer for his valuable advice.

References

[1] Patterson, G.D., Adv. Polym. Sci. 48 (1983) 125

[2] Wang, C.H., Fytas, G., Lilge, D. and Dorfmüller, Th., Macromolecules 14 (1981) 1363

[3] Fytas, G., Patkowski, A., Meier, G. and Dorfmüller, Th., Macromolecules 15 (1982) 870

[4] Fytas, G., Patkowski, A., Meier, G. and Dorfmüller, Th., J. Chem. Phys. 8D (1984) 2214

[5] Fytas, G., Wang, C.H., Meier, G. and Fischer, E.W., Macromolecules 18 (1985) 2214

[6] Fytas, G., Wang, C.H., Lilge, D. and Dorfmüller, Th., J. Chem. Phys. 75 (1985)

[7] Dorfmüller, Th., Dux, H., Fytas, G. and Mersch, W., J. Chem. Phys. 71 (1979) 366

[8] Ferry, J.D., 'Viscoelastic Properties of Polymers', Wiley, New York, 1980

[9] McCrum, N.G., Read, B.E. and Williams, G., 'Anelastic and Dielectric Effects in Polymeric Solids', Wiley, London, 1967

[10] Fytas, G., Wang, C.H., Fischer, E.W. and Mehler, K., J. Polym. Sci., Phys. Ed. 00 (1986) 0000

[11] Fytas, G., Physical Optics and Dynamic Phenomena on Processes in Macromolecular Systems, B. Sedlacek (Ed.), W. de Gruyter, 1985

[12] Meier, G., Fytas, G. and Dorfmüller, Th., Macromolecules 17 (1984) 952

[13] Giebel, L., Meier, G., Fytas, G. and Fischer, E.W., to be published

[14] Berne, B.J. and Pecora, R., 'Dynamic Light Scattering', Wiley, New York, 1976

[15] Mittag, U., Diplom Thesis, Bielefeld, 1983

[16] Lin, Y.H. and Wang, C.H., J. Chem. Phys. 70 (1979) 681

[17] Wang, C.H. and Fischer, E.W., J. Chem. Phys. 82 (1985) 632

[18] Wang, C.H., Fytas, G. and Fischer, E.W., J. Chem. Phys. 82 (1985) 4332

[19] McKinney, J.E. and Belcher, H.V., J. Res. Natl. Bur. Stand. (US) 67 (1963) 43

[20] Fytas, G., Wang, C.H., Meier, G. and Fischer, E.W., Macromolecules 18 (1983) 1492

[21] Meier, G., Hagenah, J.-U., Wang, C.H., Fytas, G. and Fischer, E.W., to be published

[22] Donth, E. and Schneider, K., Acta Polymerica 36 (1985) 273 and refs. cited therein

[23] Patterson, G.D., Stevens, J.R. and Lindsey, L.P., J. Macromol. Sci., Phys. Ed. 18 (1980) 641

[24] Provencher, S.W., Comput. Phys. Commun. 27 (1982) 213, ibid. 27 (1982) 229

[25] Ngai, K.L., Fytas, G., Plazek, D.L. and Plazek, D.J., to appear

[26] Blumen, A., Zumofen, G. and Klafter, J., J. Phys. A (1986) 0000, accepted

[27] Pollard, H., Bull. Amer. Math. Soc. 52 (1946) 908

[28] Hagenah, J.-U., Fytas, G., Meier, G., Wang, C.H. and Fischer, E.W., to be published

[29] Heijboer, J., Proc. Intern. Conf. on Physics of Non-Crystalline Solids, J.A. Prins (Ed.), North Holland Publishing, Amsterdam, 1965

[30] Fujita, H. and Kishimoto, A., J. Colloid Sci. 13 (1958) 418

[31] Williams, G. and Edwards, D.A., Trans. Faraday Soc. 62 (1966) 1329

[32] Berry, B.C. and Fox, T.G., Adv. Polym. Sci. 5 (1968) 261

[33] Wang, C.H. and Fytas, G., unpublished results

[34] Patterson, G.D., Ann. Rev. Mater. Sci. 13 (1983)

[35] Williams, G. and Watts, D.C., Trans. Faraday Soc. 67 (1971) 2793

Lecture Notes in Physics

Vol. 237: Nearby Molecular Clouds. Proceedings, 1984. Edited by G. Serra. IX, 242 pages. 1985.

Vol. 238: The Free-Lagrange Method. Proceedings, 1985. Edited by M.J. Fritts, W.P. Crowley and H. Trease. IX, 313 pages. 1985.

Vol. 239: Geometrics Aspects of the Einstein Equations and Integrable Systems. Proceedings, 1984. Edited by R. Martini. V, 344 pages. 1985.

Vol. 240: Monte-Carlo Methods and Applications in Neutronics, Photonics and Statistical Physics. Proceedings, 1985. Edited by R. Alcouffe, R. Dautray, A. Forster, G. Ledanois and B. Mercier. VIII, 483 pages. 1985.

Vol. 241: Numerical Simulation of Combustion Phenomena. Proceedings, 1985. Edited by R. Glowinski, B. Larrouturou and R. Temam. IX, 404 pages. 1985.

Vol. 242: Exactly Solvable Problems in Condensed Matter and Relativistic Field Theory. Proceedings, 1985. Edited by B.S. Shastry, S.S. Jha and V. Singh. V, 318 pages. 1985.

Vol. 243: Medium Energy Nucleon and Antinucleon Scattering. Proceedings, 1985. Edited by H.V. von Geramb. IX, 576 pages. 1985.

Vol. 244: W. Dittrich, M. Reuter, Selected Topics in Gauge Theories. V, 315 pages. 1986.

Vol. 245: R.Kh. Zeytounian, Les Modèles Asymptotiques de la Mécanique des Fluides I. IX, 260 pages. 1986.

Vol. 246: Field Theory, Quantum Gravity and Strings. Proceedings, 1984/85. Edited by H.J. de Vega and N. Sánchez. VI, 381 pages. 1986.

Vol. 247: Nonlinear Dynamics Aspects of Particle Accelerators. Proceedings, 1985. Edited by J.M. Jowett, M. Month and S. Turner. VIII, 583 pages. 1986.

Vol. 248: Quarks and Leptons. Proceedings, 1985. Edited by C.A. Engelbrecht. X, 417 pages. 1986.

Vol. 249: Trends in Applications of Pure Mathematics to Mechanics. Proceedings, 1985. Edited by E. Kröner and K. Kirchgässner. VIII, 523 pages. 1986.

Vol. 250: Lie Methods in Optics. Proceedings 1985. Edited by J. Sánchez Mondragón and K.B. Wolf. XIV, 249 pages. 1986.

Vol. 251: R. Liebmann, Statistical Mechanics of Periodic Frustrated Ising Systems. VII, 142 pages. 1986.

Vol. 252: Local and Global Methods of Nonlinear Dynamics. Proceedings, 1984. Edited by A.W. Sáenz, W.W. Zachary and R. Cawley. VII, 263 pages. 1986.

Vol. 253: Recent Developments in Nonequilibrium Thermodynamics Fluids and Related Topics. Proceedings, 1985. Edited by J. Casas-Vázquez, D. Jou and J.M. Rubí. X, 392 pages. 1986.

Vol. 254: Cool Stars, Stellar Systems, and the Sun. Proceedings, 1985. Edited by M. Zeilik and D.M. Gibson. XI, 501 pages. 1986.

Vol. 255: Radiation Hydrodynamics in Stars and Compact Objects. Proceedings, 1985. Edited by D. Mihalas and K.-H. A. Winkler. VI, 454 pages. 1986.

Vol. 256: Dynamics of Wave Packets in Molecular and Nuclear Physics. Proceedings, 1985. Edited by J. Broeckhove, L. Lathouwers and P. van Leuven. VIII, 187 pages. 1986.

Vol. 257: Statistical Mechanics and Field Theory: Mathematical Aspects. Proceedings, 1985. Edited by T.C. Dorlas, N.M. Hugenholtz and M. Winnink. VII, 328 pages. 1986.

Vol. 258: Wm. G. Hoover, Molecular Dynamics. VI, 138 pages. 1986.

Vol. 259: R.F. Alvarez-Estrada, F. Fernández, J.L. Sánchez-Gómez, V. Vento, Models of Hadron Structure Based on Quantum Chromodynamics. VI, 294 pages. 1986.

Vol. 260: The Three-Body Force in the Three-Nucleon System. Proceedings, 1986. Edited by B.L. Berman and B.F. Gibson. XI, 530 pages. 1986.

Vol. 261: Conformal Groups and Related Symmetries – Physical Results and Mathematical Background. Proceedings, 1985. Edited by A.O. Barut and H.-D. Doebner. VI, 443 pages. 1986.

Vol. 262: Stochastic Processes in Classical and Quantum Systems. Proceedings, 1985. Edited by S. Albeverio, G. Casati and D. Merlini. XI, 551 pages. 1986.

Vol. 263: Quantum Chaos and Statistical Nuclear Physics. Proceedings, 1986. Edited by T.H. Seligman and H. Nishioka. IX, 382 pages. 1986.

Vol. 264: Tenth International Conference on Numerical Methods in Fluid Dynamics. Proceedings, 1986. Edited by F.G. Zhuang and Y.L. Zhu. XII, 724 pages. 1986.

Vol. 265: N. Straumann, Thermodymamik. VI, 140 Seiten. 1986.

Vol. 266: The Physics of Accretion onto Compact Objects. Proceedings, 1986. Edited by K.O. Mason, M.G. Watson and N.E. White. VIII, 421 pages. 1986.

Vol. 267: The Use of Supercomputers in Stellar Dynamics. Proceedings, 1986. Edited by P. Hut and S. McMillan. VI, 240 pages. 1986.

Vol. 268: Fluctuations and Stochastic Phenomena in Condensed Matter. Proceedings, 1986. Edited by L. Garrido. VIII, 413 pages. 1987.

Vol. 269: PDMS and Clusters. Proceedings, 1986. Edited by E.R. Hilf, F. Kammer and K. Wien. VIII, 261 pages. 1987.

Vol. 270: B.G. Konopelchenko, Nonlinear Integrable Equations. VIII, 361 pages. 1987.

Vol. 271: Nonlinear Hydrodynamic Modeling: A Mathematical Introduction. Edited by Hampton N. Shirer. XVI, 546 pages. 1987.

Vol. 272: Homogenization Techniques for Composite Media. Proceedings, 1985. Edited by E. Sanchez-Palencia and A. Zaoui. IX, 397 pages. 1987.

Vol. 273: Models and Methods in Few-Body Physics. Proceedings, 1986. Edited by L.S. Ferreira, A.C. Fonseca and L. Streit. XIX, 674 pages. 1987.

Vol. 274: Stellar Pulsation. Proceedings, 1986. Edited by A.N. Cox, W.M. Sparks and S.G. Starrfield. XII, 422 pages. 1987.

Vol. 275: Heidelberg Colloquium on Glassy Dynamics. Proceedings, 1986. Edited by J.L. van Hemmen and I. Morgenstern. VIII, 577 pages. 1987.

Vol. 276: R.Kh. Zeytounian, Les Modèles Asymptotiques de la Mécanique des Fluides II. XII, 315 pages. 1987

Vol. 277: Molecular Dynamics and Relaxation Phenomena in Glasses. Proceedings, 1985. Edited by Th. Dorfmüller and G. Williams. VII, 218 pages. 1987.